

© Copyright 2006

Philip A. Sullivan

Theory Guided Design and Molecular Engineering of Organic Materials for Enhanced Second-Order Nonlinear Optical Properties

Philip A. Sullivan

A dissertation
submitted in partial fulfillment of the
requirements for the degree of

Doctor of Philosophy

University of Washington

2006

Program Authorized to Offer Degree:

Department of Chemistry

UMI Number: 3224299

Copyright 2006 by
Sullivan, Philip A.

All rights reserved.

INFORMATION TO USERS

The quality of this reproduction is dependent upon the quality of the copy submitted. Broken or indistinct print, colored or poor quality illustrations and photographs, print bleed-through, substandard margins, and improper alignment can adversely affect reproduction.

In the unlikely event that the author did not send a complete manuscript and there are missing pages, these will be noted. Also, if unauthorized copyright material had to be removed, a note will indicate the deletion.

UMI[®]

UMI Microform 3224299

Copyright 2006 by ProQuest Information and Learning Company.

All rights reserved. This microform edition is protected against
unauthorized copying under Title 17, United States Code.

ProQuest Information and Learning Company
300 North Zeeb Road
P.O. Box 1346
Ann Arbor, MI 48106-1346

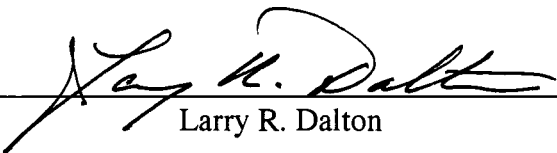
University of Washington
Graduate School

This is to certify that I have examined this copy of a doctoral dissertation by

Philip A. Sullivan

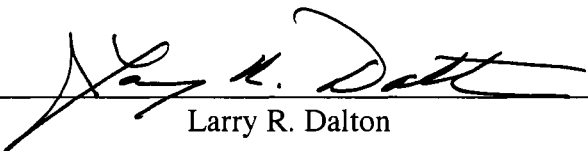
and have found that it is complete and satisfactory in all respects,
and that any and all revisions required by the final
examining committee have been made.

Chair of the Supervisory Committee:




Larry R. Dalton

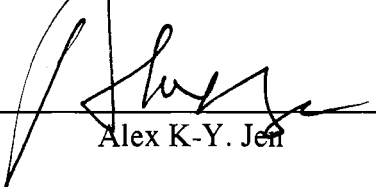
Reading Committee:



Larry R. Dalton



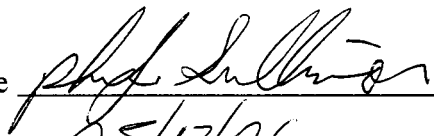
Bruce H. Robinson



Alex K-Y. Jen

Date: 05/15/06

In presenting this dissertation in partial fulfillment of the requirements for the doctoral degree at the University of Washington, I agree that the Library shall make its copies freely available for inspection. I further agree that extensive copying of the dissertation is allowable only for scholarly purposes, consistent with "fair use" as prescribed in the U.S. Copyright Law. Requests for copying or reproduction of this dissertation may be referred to Proquest Information and Learning, 300 North Zeeb Road, Ann Arbor, MI 48106-1346, 1-800-521-0600 to whom the author has granted "the right to reproduce and sell (a) copies of the manuscript in microform and/or (b) printed copies of the manuscript made from microform."

Signature 
Date 05/17/06

University of Washington

Abstract

Theory Guided Design and Molecular Engineering of Organic Materials for Enhanced
Second-Order Nonlinear Optical Properties

Philip A. Sullivan

Chairperson of the Supervisory Committee:
Professor Larry R. Dalton
Department of Chemistry

The last two decades of research in the field of organic 2nd-order nonlinear optical (electro-optic) materials have led to a deeper understanding of salient fundamental processes. Detailed definitions of critical structure-property relationships have led to the realization of new materials displaying dramatically enhanced properties. Despite the many recent advances, some critical problems remain unsolved. Although molecular nonlinearities (β) have increased dramatically, bulk nonlinearity values (r_{33}) have not increased in proportion. The major impediment to the resolution of this shortcoming is the difficulty faced in overcoming limited electric field induced molecular ordering caused by inter-molecular electrostatic interactions. Through the use of sophisticated statistical and quantum mechanical modeling, materials were designed which circumvented such detrimental molecular interactions. In the case of chromophore doped multichromophore dendrimers, these interactions were actually harnessed to enhance electric field induced dipolar order. As a result of this rational, theory guided design approach to novel electro-optic materials, unprecedented r_{33} (> 300 pm/V) was demonstrated. Design, synthesis, and detailed characterization of these new materials is presented within this dissertation. Fundamental research toward molecular structure engineering as well as a new approach to optimization of molecular hyperpolarizability is presented as well.

TABLE OF CONTENTS

	page
List of Figures	iii
List of Schemes	vi
List of Tables	vii
Chapter 1: Introduction to Organic Materials for 2 nd -Order Nonlinear Optics	1
1.1 Introduction	1
1.1 Physical Origin of Nonlinear Optical Effects	2
1.1 $\chi^{(2)}$ and r_{33} in Electric Field Poled Organic EO Materials	5
1.1 Optimizing Chromophore β	8
1.1 Translating β into r_{33}	14
1.1 Optimizing $N\langle\cos^3\theta\rangle$ in Electric Field Poled Organics	18
Notes to Chapter 1	23
Chapter 2: in-situ Pole-and-Probe Polarization Interferometry Reflection Apparatus; a Real-Time Method for Evaluating EO Properties of Poled Organic Thin-Films	33
2.1 Introduction	33
2.1 Experimental Setup	34
2.1 Theory of Static, Ambient Temperature, r_{33} Determination	37
2.1 Real-Time Poling Behavior Analysis Through <i>in-situ</i> Monitoring	40
2.1 Study of Dipolar Orientational Dynamics in EO Thin-Films	42
2.1 Conclusions	44
2.1 Experimental Section	45
Notes to Chapter 2	51
Chapter 3: Novel Dendritic Chromophores for Electro-Optics; Influence of Binding Mode and Attachment Flexibility on EO Behavior	52
3.1 Introduction	52
3.2 Evaluation of EO Behavior as Dendrimer APC Composite Films	54
3.3 Physical and Photophysical Properties of Succinic Ester Tether Based Multichromophore Dendrimers	56
3.4 Physical and Photophysical Properties of Hexanoic Acid Ester Tether Based Multichromophore Dendrimers	64
3.4 Conclusions	70
3.4 Experimental Section	72
Notes to Chapter 3	93
Chapter 4: 2 nd order NLO Properties of Amorphous Organic Glasses and Composites Based on Multichromophore Dendrimers	96
4.1 Introduction	96

4.2 Chromophore Shape Effects; Theory Guided Design	98
4.3 MultiChromophore Dendrimers; Material Design and Synthesis.....	101
4.4 Evaluation of Physical and Photophysical Properties of Multichromophore Dendrimer based Amorphous Glasses.....	105
4.5 Multichromophore Containing Dendrimers as Active Host Matrices.....	113
4.6 Preliminary exploration of poling induced order in PSLD_41 / YLD_124 and PSLD_41 / YLD_130 composite films	124
4.7 Device Testing of PSLD_41 / YLD_124 Composites.....	127
4.8 Photo-Stability of Dendrimer / Guest Composites.....	129
4.9 Thermal Stability of r_{33} in PSLD_41 / YLD_124 Composites.....	131
4.10 Conclusions	133
4.11 Experimental Section.....	134
Notes to Chapter 4	146
Chapter 5: Exploration of A Series Type Multifunctionalized NLO Chromophore Concept.....	150
5.1. Introduction	150
5.2. Theory of Multiple Charge Transfer Chromophore Design	150
5.3. Density Functional Theory (DFT) based Molecular Modeling Results	153
5.4 Synthesis of Multiple Charge Transfer Chromophores and Linear Analogs.....	161
5.5 Photophysical Characterization.....	168
5.6 Conclusions	172
5.7 Experimental Section.....	173
Notes to Chapter 5	184
List of References	186

LIST OF FIGURES

Figure Number	Page
1.2.1 The real and imaginary parts of the complex refractive index of a pure dendrimer organic EO material	3
1.3.1 Depiction of a typical organic EO chromophore / polymer composite material under an applied poling field.....	6
1.4.1 PAS 38, a classical linear charge-transfer EO chromophore	8
1.4.2 Graphical representation of electron density for chromophore HOMO and LUMO created using density functional theory quantum mechanical calculations	9
1.4.3 Electron donating moieties recently investigated for use in EO chromophore structures	11
1.4.4 Examples of high β Chromophore structures based on FTC and CLD type bridges.....	12
1.4.5 Heterocyclic ring based electron acceptor groups.....	14
1.6.1 Three-arm multichromophore dendrimer PS LD_41.....	21
2.2.1 Schematic representation of <i>in-situ</i> reflection ellipsometry setup.....	33
2.2.2 Propagation path for optical probe beam in the <i>in-situ</i> TMT.....	34
2.3.1 Ψ_{sp} scan plot showing AC and DC detector response for a poled sample of EO dendrimer created by a full SB compensator actuation cycle	37
2.4.1 Real-time plot of the poling behavior of an EO dendrimer sample.....	39
2.5.1 Dynamic thermal stability experiment performed on crosslinked (d4pas69) and uncrosslinked (41_124 25%) samples	41
2.5.2 Isothermal r33 stability study performed at 65 °C over 4 hrs on pure dendrimer (PS LD_41) and doped dendrimer (41_124 15%) samples	42
2.7.1 Bandpass filter circuit allowing DC bias of the modulation waveform.....	45
2.7.2 Schematic diagram of heating stage for sample attachment	46
3.3.1 Free chromophore FTC (I), side-on dendritic chromophore (PS LD-138, II), and end-on dendritic chromophore (AALD-1062, III).....	56
3.3.2 Aromatic region of ¹ H NMR spectra of dendritic chromophores II and III.....	59
3.3.3 Thermally induced EO signal decay transitions for APC films containing side-on (II), and end-on (III) dendritic chromophores, as well as FTC (I)	62
3.3.4 Isothermal EO stability data for APC films containing, FTC (I), succinic acid tether based side-on (II), and end-on (III) *Temperature: 105 °C.....	63
3.4.1 Thermally induced EO signal decay transitions for APC samples containing hexanoic acid tether based dendritic chromophores IV and V heated at a ramp rate of 10 °C/min	67
3.4.2 Data plots depicting EO decay of poled APC samples containing dendritic chromophores IV and V heated at constant temperatures of 109, 114 and 118 °C..	69

3.6.1 UV-Vis absorption spectra for FTC (I), and dendritic chromophores II and III.....	85
4.2.1 Analytical model of point-dipole response to a poling field, left; solve neglecting dipole-dipole interactions (W), right; solve including W	99
4.2.2 Monte-Carlo analysis of $N\langle\cos^3\theta\rangle$ with respect to chromophore number density	100
4.3.1 Multichromophore EO dendrimers PSLD_33 and PSLD_41 accompanied by small molecule chromophore CF ₃ -FTC	102
4.4.1 UV-Vis-NIR absorption spectra of dendrimer PSLD_33 (pure film) and CF ₃ -FTC (25% by wt. In APC) on glass	106
4.4.2 r_{33} data for CF ₃ -FTC (25% in APC) and PSLD_33 and PSLD_41 pure films as a function of applied poling voltage.....	108
4.4.3 Representation of PSLD_41 dendrimer showing atom labels, correct Van der Waals radii, and fixed spheroid pi-segments.....	110
4.4.4 Simulation of poling induced order in a multiple dendrimer ensemble.....	111
4.5.1 Guest chromophores YLD_124 and YLD_130.....	113
4.5.2 UV-Visible absorption spectra for YLD_124, YLD_130, compared against CF ₃ -FTC in CHCl ₃ solution.....	114
4.5.3 UV-Vis-NIR absorption spectra for films of PSLD_41 loaded increasingly with YLD_124 ($\times 10^{20}$ molec./cc, corrected for film thickness).....	115
4.5.4 Refractive index (n) and extinction coefficient (k) as a function of wavelength for PSLD_41 pure films and PSLD_41 / YLD_124 25%.....	118
4.5.5 Poling efficiency vs. chromophore N for CF ₃ -FTC in APC, pure dendrimers PSLD_41 and PSLD_33, and a sample series containing increased loading of guest YLD_124 in PSLD_41 host.....	120
4.5.6 ρ vs. N plots for YLD_124 / APC and ((YLD_124 / PSLD_41) – (PSLD_41)) ...	121
4.6.1 Biaxial optical constants for 25% by wt. YLD_130 in PSLD_41, A: unpoled sample, B: sample poled by corona field	126
4.7.1 Panel a: model of device cross-section displaying optical mode, panel b: electrode contact structure for applying poling and modulating fields, panel c: full device view showing electrical and optical inputs, panel d: resonator structure.....	128
4.9.1 Thermally stimulated current experiments for determination of T_{tr} of pure PSLD_41 films and PSLD_41 / YLD_124 (25% by wt).....	132
4.9.2 Dynamic thermal stability experiments performed for PSLD_41 and 25% by weight YLD_124 in PSLD_41 (10 °C/min).....	133
4.11.1 Experimental data for PSLD_41 film, and YLD_124 in APC, components PC1 and PC2 are the two base components from the mathematical decomposition of figure 4.5.3	144
4.11.2 Mathematical reproduction of figure 4.5.3 spectra resulting from linear combination of PSLD_41 and YLD_124 spectra.....	145
5.2.1 Examples of typical donor-bridge-acceptor, linear chromophores.....	151

5.2.2 Schematic representation of parallel and series concepts	151
5.2.3 Examples of three series-type structures, 2-donors & 1-acceptor, 1, 1-donor & 2-acceptors, 2, 2-donors & 2-acceptors, 3.....	152
5.2.4 Example of a 1D linear control, 4, and a parallel substituted multifunctional NLO-phore, 5	152
5.3.1 Representation of the DFT-calculated HOMO and LUMO for linear NLO_phore FTTC.....	154
5.3.2 Representation of the DFT-calculated HOMO and LUMO for parallel-type structure 5	155
5.3.3 Representation of the DFT-calculated HOMO and LUMO for series-type structure, 1	157
5.3.4 Representation of the DFT-calculated HOMO and LUMO for series-type structure, 2	158
5.3.5 Representation of the DFT-calculated HOMO and LUMO for series-type structure, 3	159
5.4.1 ORTEP representation of single crystal x-ray diffraction data for double donor, 8	162
5.4.2 MALDI-TOF data showing 956.4 m/z molecular cation of Molecule 3	166
5.5.1 HRS data corresponding to PAS 25, linear control PAS 38, and two similar three-ring examples for comparison	169
5.5.2 Extinction coefficients vs. wavelegth comparison	171
5.5.3 UV-Vis spectra of dialdehyde bridge precursor and PAS 25.....	172

LIST OF SCHEMES

Scheme Number	Page
1.5.1 Layer-by-layer acentric chromophore deposition through siloxane based sequential synthesis.....	16
3.3.1 Synthesis of side-on dendritic chromophore PSLD-138 (II)	57
3.4.1 Synthetic scheme for hexanoic acid ester based dendritic chromophores IV and V	64
3.6.1 Synthesis of succinic acid ester tether based end-on type dendritic chromophore III (AALD-1062)	79
4.3.1 Synthesis of CF ₃ -FTC type chromophore unit 7	103
4.3.2 Synthesis of three-arm dendrimers PSLD_33 and PSLD_41	104
5.4.1 Outline of synthetic scheme for molecule 3 (PAS 25)	161
5.4.2 Synthetic scheme for linear control chromophore PAS 38 (FTTC).....	167

LIST OF TABLES

Table Number	Page
3.4.1 Average and maximum r_{33} values for Succinate dendritic chromophores II and III, and hexanoic-acid ester dendritic chromophores (IV and V), and free chromophore FTC, doped into APC	66
3.4.2 Isothermal decay data: relaxation time (τ), average relaxation time ($\langle\tau\rangle$), stretching parameters (β), activation energies (E_a), for dendritic chromophores IV, and V	70
3.6.1 UV-Vis absorption and cyclic voltammetry data for FTC and dendritic chromophores II and III	86
4.4.1 Thermal and UV-Vis Absorption data for EO compounds.....	107
4.4.2 Comparison of N and ρ for chromophore / APC composite and dendrimer materials	109
4.5.1 Electrochemical and spectroscopic analysis of I_p (HOMO) and E_a (LUMO) levels of YLD_124, YLD_130, and PSLD_41	117
4.5.2 β_{HRS} , calculated μ , and ρ/N values for free chromophores, dendrimers and composites thereof	123
4.8.1 Photostability FOM for EO materials in air $\lambda = 1550$ nm	130
5.3.1 Calculated electronic data for compounds discussed	160
5.5.1 HRS values of several chromophores for comparison (given relative to chloroform).....	170

ACKNOWLEDGEMENTS

The author would like to extend sincere thanks to all those who assisted along the way. Without my fiancée, Kristy, with whom I have shared my graduate education experience, I would not be where I am today. Thanks also to Professor Larry R. Dalton who has supported my efforts even when skeptical, and given me the great gift of his mentoring. Professor Dong Hoon Choi has also given much of his time and his knowledge to further my education and enhance my overall Ph.D. experience. The Dalton, Jen, Robinson, and Reid research groups have been invaluable to my success as well. The faculty and group members have created a stimulating and exciting environment in which to work and learn.

Financial support for the research detailed herein was provided by: The NSF Science and Technology Center MDITR-(DMR0120967) and NSF-(DMR-0092380), US Air Force AFOSR-(F49620-03-1-0110-P000), and the Darpa MORPH Program (N)) 14-04-10094).

DEDICATION

I would like to dedicate this dissertation to my parents, Dr. Harvey and Mrs. Betty Sullivan, who have steadfastly supported my continued educational endeavors.

Chapter 1

Introduction To Organic Materials for 2nd-order Nonlinear Optics

1.1 Introduction

Organic materials for use in 2nd-order nonlinear optical (electro-optic) applications have received much attention in recent years. These materials hold great promise for performance and cost improvements in areas such as telecommunications, computing, phased array radar, THz generation, as well as numerous other new applications.¹⁻⁶ The major opportunity for implementation of electro-optic (EO) materials is in the area of electrical-to-optical signal transduction. An electrical-to-optical signal transducer, also known as an EO modulator, is basically an optical intensity controller or optical switch. Such a switch can translate digital or analog electrical signals directly into the optical domain and back. While the potential bandwidth of optical data transmission is almost unlimited, transduction between electrical and optical domains remains a critical bottleneck. Organic materials hold the key to removal of this limitation. Devices that incorporate organic materials extend the promise of much higher operational bandwidth when compared to analogous inorganic based devices.⁷⁻¹² Organic EO active materials have many advantages over inorganic EO active materials such as lithium niobate. These advantages include lower cost, improved processing and ease of device integration,

and better overall performance figures of merit. Unlike crystalline inorganic materials, synthetic materials can be “made-to-order”. Physical as well as photophysical properties can be tuned to fit specific requirements.

1.2 Physical Origin of Nonlinear Optical Effects

Nonlinear optical effects alter the way electromagnetic radiation interacts with matter, effectively changing its properties. The material property that is of greatest interest for the current discussion is index of refraction. All nonlinear optical effects are essentially described by electric field induced refractive index modulation. At optical frequencies (ω), the linear polarizability, dielectric constant, and index of refraction of a material are all directly related. For this discussion of linear and nonlinear optical effects, the focus will be on optical susceptibility ($\chi^{(n)}$). Optical susceptibility is a definition of the propagation medium polarization in response to an incident oscillating optical field of a given ω . In the case of linear electric field response, polarization (P) is given by

$$P = \chi^{(1)} \cdot E \quad (1.2.1)$$

where $\chi^{(1)}$ is the linear optical susceptibility and E denotes the amplitude of the optical field. Practically, $\chi^{(1)}$ is a second rank tensor relating polarization vector components to electric field vector components. In order to simplify the included discussion, an anisotropic medium is assumed and all quantities are treated as scalar. A more in-depth discussion and more precise notation can be found elsewhere.¹³ Index of refraction (n_c) is related to $\chi^{(1)}$ by

$$n_c^{(2)}(\omega) = 1 + 4\pi\chi^{(1)}(\omega) \quad (1.2.2)$$

when E is weak and $\chi^{(1)}$ is field independent. Here, index of refraction is actually a frequency dependant complex quantity. Nuclear and electronic resonances associated with molecular structure are coupled with optical field as described by a harmonic oscillator model. This resonance coupling leads to frequency dependance of n and k (refraction and absorption). Complex refractive index is described by

$$n_c = n + ik \quad (1.2.3)$$

in which the real part, n, describes refraction and imaginary, ik, describes absorption.¹³

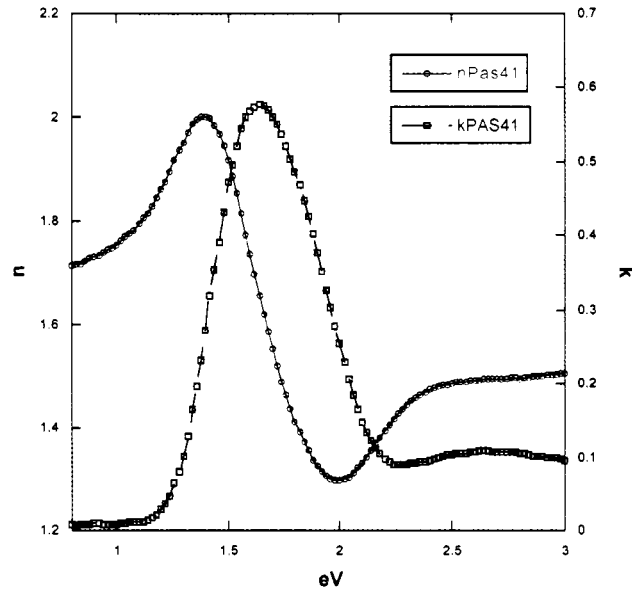


Figure 1.2.1: The real and imaginary parts of the complex refractive index of a pure dendrimer organic EO material (PSLD_41)

Typical frequency dependence of n and k is illustrated in Figure 1.2.1. A given Lorentz oscillator exhibits a natural resonance frequency. When electromagnetic radiation propagating in the medium is of a frequency near to this natural resonance, the oscillator is strongly coupled with the radiation. Because of increased coupling, P and $\chi^{(n)}$ with respect to E , are strongly enhanced. Similar frequency dispersion behavior is displayed by linear as well as higher order (nonlinear) terms, leading to ω dependant EO effects. This will become important in later chapters.

Up to this point, $\chi^{(n)}$ has been considered as independent of the magnitude of E . In the case of high intensity laser radiation, Equation 1.2.1 must be modified to include higher order polarization response.¹³ When $\chi^{(n)}$ terms where $n > 1$ are included, the appropriate description becomes the power series expansion

$$P = \chi^{(1)} \cdot E + \chi^{(2)} : EE + \chi^{(3)} : EEE + \dots \quad (1.2.4)$$

in which quadratic, $\chi^{(2)}$, and cubic, $\chi^{(3)}$, nonlinear optical susceptibilities are also described. When these nonlinear terms are accounted for, Equation 1.2.1 becomes

$$P = \chi_{eff} \cdot E \quad (1.2.5)$$

in which χ_{eff} is the sum of linear and nonlinear terms, and is now E dependant. Substituting χ_{eff} into equation 1.2.2 in place of E independent $\chi^{(1)}$, yields a description of refractive index that is both field and frequency dependent.¹³ It is this E field dependence of n that gives rise to nonlinear optical behavior.¹³

Second order or quadratic susceptibility, $\chi^{(2)}$, is termed first nonlinear optical susceptibility, cubic, $\chi^{(3)}$, represents the second nonlinear optical susceptibility.

Third-order nonlinear optical or Kerr effects lead to an optical intensity dependent refractive index. Kerr effects are important in applications such as all-optical transistors, third harmonic generation, and optical limiting devices. Second-order nonlinear optical effects are important because they give rise to the linear Pockels effect (EO effect). The Pockels effect is defined as a linear refractive index change with respect to a DC or low frequency (RF-THz) as compared to optical ω , external electric field. Unlike $\chi^{(3)}$ effects, $\chi^{(2)}$ dependant processes require bulk material anisotropy.¹³ In order to retain mathematical consistency, the description of nonzero quadratic susceptibility with respect to a sinusoidal optical E field requires a net medium polarizability asymmetry. Dissimilar material polarization response must accompany positive and negative E field vector components.¹³ In the case of organic materials, such polarizability anisotropy is realized through net dipolar order of molecular active constituents. Some crystalline materials display inherent structural anisotropy, but amorphous organic materials must be engineered toward this goal.

1.3 $\chi^{(2)}$ and r_{33} in Electric Field Poled Organic EO Materials

Organic materials designed to display high $\chi^{(2)}$ are generally elaborated by the dispersion of a “NLO dye” or chromophore, into a transparent host material. This chromophore must be highly dipolar and display high π electron polarizability. The resulting composite material is then heated near its glass transition (T_g) under the application of a powerful DC poling field (Figure 1.3.1). Through molecular dipole orientational response to the poling field, the acentric order necessary for $\chi^{(2)}$ is

obtained. This poling-induced dipolar order is expressed using the order parameter, $\langle \cos^3 \theta \rangle$, where the angle between the poling axis and the chromophore dipole vector is denoted as θ .

In an ideal situation in which dipolar units do not interact with one-another or with their surroundings, dipolar order imparted by electric field poling may be enumerated using the relation

$$\langle \cos^3 \theta \rangle = \frac{\mu E}{5kT} \quad (1.3.1)$$

in which the quantity μ represents the ground state dipole moment of individual chromophores. The term kT represents thermally imparted kinetic energy where k is the Boltzman constant, and T represents temperature.

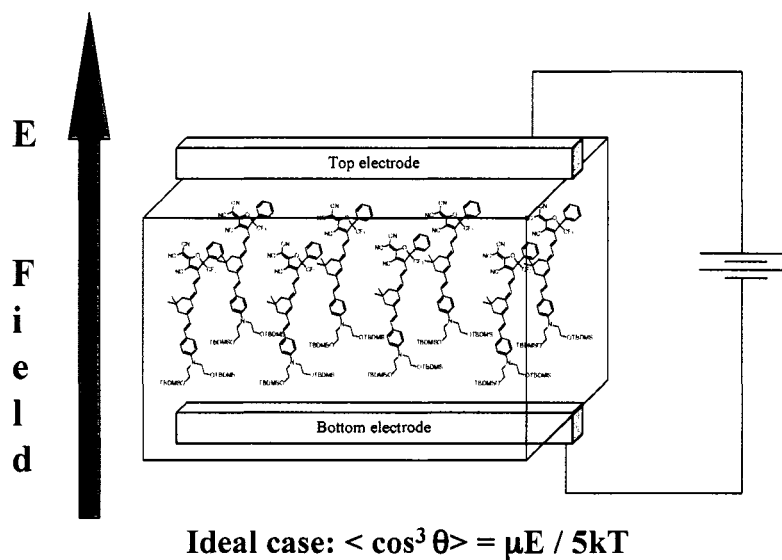


Figure 1.3.1: Depiction of a typical organic EO chromophore / polymer composite material under an applied poling field

For individual chromophore molecules, a polarization power series expansion similar to Equation 1.2.4 can be written. Like the previous expression, first-order and higher order terms can be expressed as a function of E shown by

$$p = \alpha E + \beta EE + \gamma EEE + \dots \quad (1.3.2)$$

as before, α , β , and γ represent first, second and third-order polarization response to E respectively. Again, these terms are second, third and fourth rank tensors that relate molecular electron density polarization vector components to the vector components of propagating radiation as well as those of externally applied potentials. The second-order term, β , denotes the molecular first hyperpolarizability for an individual chromophore. The component of β along the dipolar axis of the chromophore is given as β_{zzz} . Assuming bulk material response arises simply from the combination of constituent chromophore response, β_{zzz} is related to $\chi_{zzz}^{(2)}$ by

$$\chi_{zzz}^{(2)} = NF\beta_{zzz} \langle \cos^3 \theta \rangle \quad (1.3.3)$$

where N represents the chromophore number density per unit volume of composite EO material. The term, F, represents a local field factor that is dependant on the overall dielectric properties of the complex medium.

For second order nonlinear optical materials, the EO coefficient is defined as r_{33} and is given in pm/volt. This coefficient denotes the magnitude of refractive index change with respect to applied E (volts) and is expressed as

$$r_{33} = -2\chi_{zzz}^{(2)} / (n_z)^4 \quad (1.3.4)$$

Therefore, it follows from the discussion that in order to achieve high r_{33} , a large $\chi_{zzz}^{(2)}$ must be achieved. To have high $\chi_{zzz}^{(2)}$, there must exist a large concentration of

high β chromophores that are aligned with a high degree of acentric order within the bulk material.¹⁴⁻¹⁶

1.4 Optimizing Chromophore β

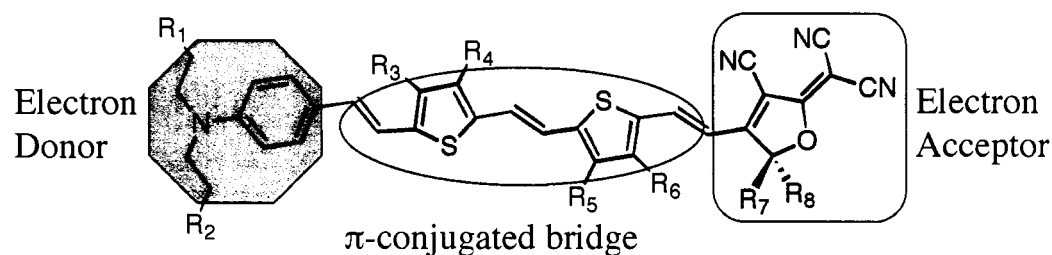


Figure 1.4.1: PAS 38, a classical linear charge-transfer EO chromophore

Typical EO chromophore design is exemplified by the structure shown in Figure 1.4.1 (PAS 38). A π -conjugated bridge is functionalized at either terminus by an electron-donating moiety and an electron-accepting moiety. This asymmetric substitution results in a high, substituent-induced, ground state electron density asymmetry. The π -conjugated nature of the chromophore bridge allows for very effective communication between donor and acceptor. This communication facilitates electron density polarization along the dipolar axis of the chromophore. Electric field determined polarization is energetically favored directionally from donor to acceptor. Such asymmetric, dipole modified polarizability, is required to produce a nonzero β_{zzz} value. This symmetry requirement is analogous to that necessary to realize a nonzero $\chi^{(2)}$, as described in previous sections.

The β value of a specific chromophore structure depends on the individual donor, acceptor and bridge used. The overall combination of these components is also important. Application of the heuristic two-state model yields some insight into the mechanistic details of β . The two-state model was developed by Oudar and Chemla in 1977.^{17,18} From the model, it can be written that

$$\beta \propto \Delta\mu(\mu_{eg})^2 / \Delta E_{eg} \quad (1.4.4)$$

$\Delta\mu$ represents the difference in dipole moment between ground and excited state. The term, μ_{eg} , represents transition dipole moment, and ΔE_{eg} denotes the energy gap between molecular HOMO and LUMO. The two-state model considers that the largest contribution to the electric field polarized state of a chromophore comes from frontier orbitals. Graphical representation of typical chromophore HOMO and LUMO electron density is presented in Figure 1.4.2.

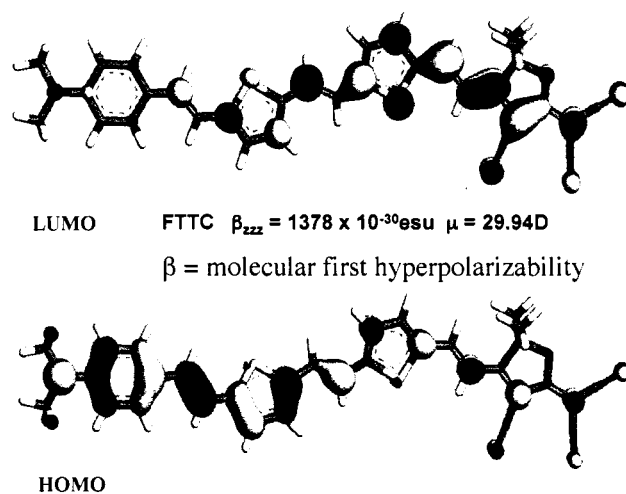


Figure 1.4.2: Graphical representation of electron density for chromophore HOMO and LUMO created using density functional theory quantum mechanical modeling¹⁹

When polarized by an electric field, the admixing of the chromophore HOMO and LUMO is altered, creating a new ground state. This new ground or preferred state represents the lowest energy configuration with respect to electron density localization under the applied field. For evaluation purposes, μ_{eg} and ΔE_{eg} can be probed spectroscopically. Oscillator strength (extinction coefficient, ϵ) is a good measure for μ_{eg} , and ΔE_{eg} (bandgap) can be estimated from red-edge absorption onset or probed electrochemically.²⁰ Typically, a bathochromic shift in λ_{max} and increase in ϵ accompanies increased β within a structurally comparable chromophore series.²¹ It is important to note that continually decreasing ΔE_{eg} will eventually result in high electronic absorption and optical loss at operational wavelengths. This fact leads to a well-known nonlinearity / transparency tradeoff. This tradeoff makes simultaneous optimization of all molecular parameters imperative for continued chromophore improvement.

In recent years much effort has been devoted to the optimization of donor, bridge and acceptor components. Many electron donors have been explored. Some of the most notable examples are illustrated in Figure 1.4.3. Some recent studies have evaluated ferrocenyl (Figure 1.4.3a),²³⁻²⁶ guanidyl (Figure 1.4.3b),²⁷ azaphosphane (Figure 1.4.3c),¹⁰ porphyrin (Figure 1.4.3d),²⁸ cycloheptimidazole (Figure 1.4.3e),²⁹ 1,3-dithiol-rings (Figure 1.4.3f),^{26, 30, 31} tetrathiafulvalene (TTF, Figure 1.4.3g),^{32, 33} carbazole (Figure 1.4.3h),^{12, 34} and aryl-amine (Figure 1.4.3i,j,k) electron donor structures. The amine-based systems were found to be most practical

overall and are still the most widely utilized.^{12, 35-37} The relatively high-energy nitrogen nonbonding lone pair of the tertiary amines is particularly well-suited for the role of electron donor. The lone pair energy is well matched to π^* of the chromophore conjugated network. Alkyl-substituted tertiary amines have typically shown lower thermal and chemical stability relative to the analogous aryl substituted counterparts. Therefore, donor modification through aryl substitution provides a convenient route to improve important qualities associated with donor structure.

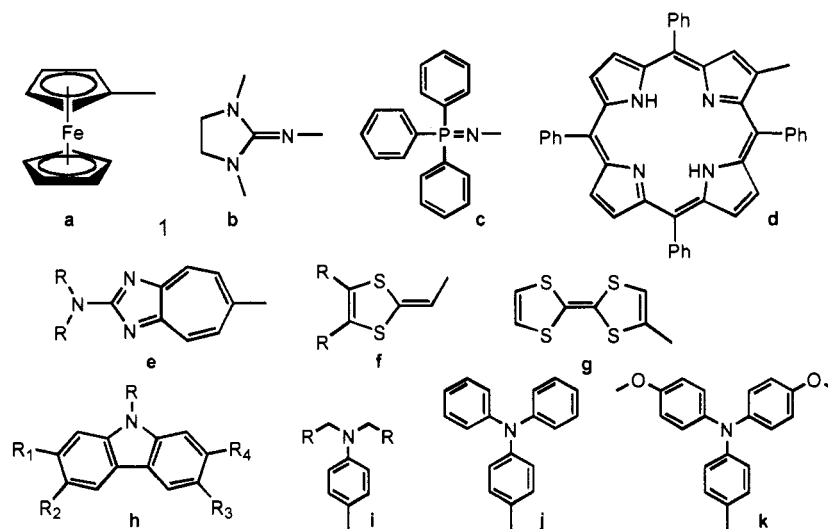


Figure 1.4.3: Electron donating moieties recently investigated for use in EO chromophore structures²²

Many different bridge structures have been investigated over the past decade. A large percentage of the most successful chromophoric materials have been based on either a CLD ({4-[2-(3-Allylidene-5, 5-dimethyl-cyclohex-1-enyl)-vinyl]}-

phenyl}-(dialkyl or diaryl)-amine) polyene-type bridge, or a low ΔE_{eg} aromatic bridge, usually the thienyl-vinylene FTC-type bridge. A number of variations can be seen in Figure 1.4.4. Elongation of these bridging units provides a straightforward approach to increased β values, but at the price of reduced optical transparency. Recent modifications to the CLD type bridge include molecules such as a, b, and c.^{3, 14, 38} Variations of thiophene-based molecules such as d, e, f, and g have been widely studied as well.³⁹⁻⁴²

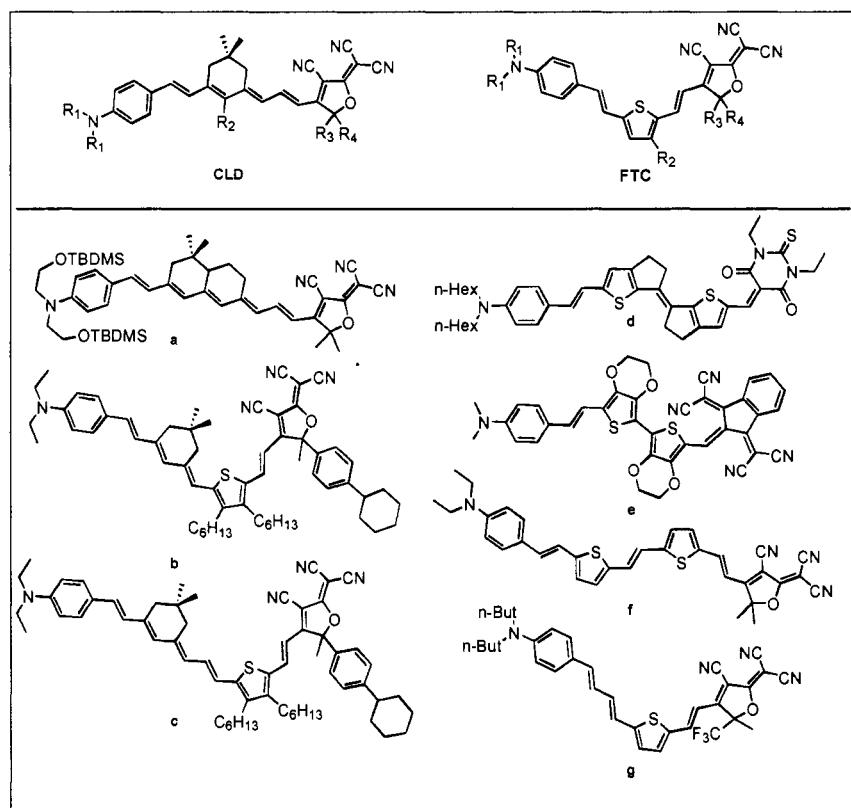


Figure 1.4.4: Examples of high β Chromophore structures based FTC and CLD type bridges²²

Arguably, the π -conjugated bridge class of the most current importance is that of the ring-locked tetraenes (CLD) due to their proven superior β and r_{33} performance.³⁶ However, the FTC bridge has also seen widespread application. Even though the thienyl-vinylene based FTC bridge offers somewhat smaller β values than CLD based chromophores, versatility in secondary functionalization, high thermal and photostability, and ease of synthesis keep FTC very popular.⁴³

In addition to electron donor groups and conjugated bridges, electron acceptor groups have also been heavily explored. Many diverse molecular structures can be envisioned for use as electron acceptors. This structural diversity presents many research opportunities. However, the development of both highly active and sufficiently stable materials is a very challenging endeavor. Many easily synthesized, highly stable materials exhibit poor electron affinity. Many of the compounds exhibiting high electron affinity are chemically and thermally unstable. Ionic acceptors such as pyridinium and diazonium salts, can be incorporated into crystalline or layer-by-layer, sequentially deposited EO materials.^{44, 45} Unfortunately, charged acceptors are of little or no use in electric field poled materials because of high conductivity caused by mobility of ionic species. Exceedingly high conductivity limits the application of electric field during poling resulting in significantly reduced r_{33} . Much research into uncharged electron deficient materials has focused heterocyclic ring based compounds. A wide variety of these structures has been explored, including barbituric and thiobarbituric acid derivatives (Figure 1.4.5a,b),⁴⁶⁻⁴⁹ isoxazolones (Figure 1.4.5c),^{46, 50, 51} and oxazolones (Figure 1.4.5d).⁵²

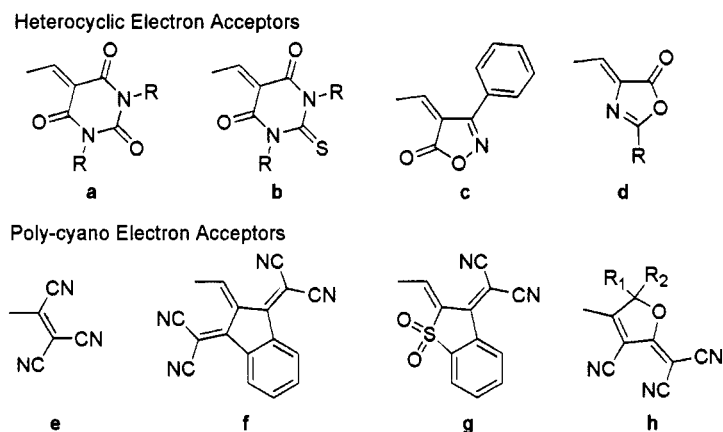


Figure 1.4.5: Heterocyclic ring based electron acceptor groups²²

Nitrile substituent containing acceptor groups have proven to be very electron deficient as well as stable. Neutral acceptors based on the tricyanovinyl moiety (Figure 1.4.5e) have proven stronger than many more complicated heterocyclic compounds.⁵³ The acceptors shown in Figure 1.4.5f and 1.4.5g represent modified nitrile-based compounds and are quite strong acceptors.⁵⁴⁻⁵⁶ Recently, the most successful and widely applied acceptor class has been based on the 2-cyanomethylene-3-cyano-4,5,5-trimethyl-2,5-dihydrofuran (TCF) structure and its derivatives (figure 1.4.5h).^{38, 42, 57-59} The TCF structure can be modified to include various substituents (CF_3) that further augment its performance.

1.5 Translating β into r_{33}

As detailed in Section 1.3, high β is not the only criteria for high material $\chi^{(2)}$ and r_{33} . It follows from Equations 1.3.3 and 1.3.4 that r_{33} is directly proportional to

the chromophore dipolar order within the material. From these relations it also necessary that EO effects are proportional to the number of chromophores encountered by propagating radiation over a given distance. Therefore, not only chromophore β , but also the product of $N\langle\cos^3\theta\rangle$ must be considered when designing organic EO materials. In order to induce long-range acentric (dipolar) molecular order, molecular assembly, crystallization, electric field poling, or other physical alignment techniques must be employed. Nearly perfect alignment is very difficult to achieve. For this reason, bulk material r_{33} has not improved proportionally to the recent dramatic improvements in chromophore β values.

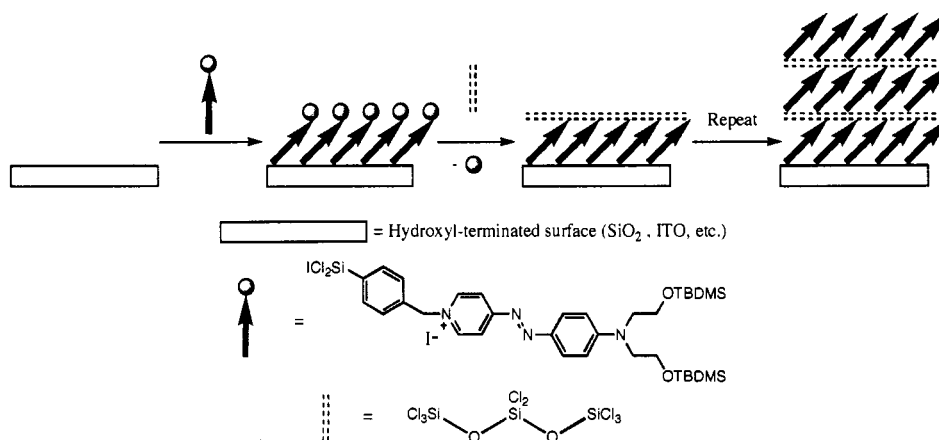
Some examples of organic EO crystals exist such as DAST.⁶⁰ The DAST chromophore (trans-4-[4-Dimethylamino]styryl]-1-methylpyridinium p-toluenesulfonate) is crystallized in a noncentrosymmetric orientation using a specific counterion.^{61, 62} EO crystals present a seemingly ideal situation where the $N\langle\cos^3\theta\rangle$ product is maximized, leading to large r_{33} values. Unfortunately, acentric organic EO crystals still present similar problems to inorganic EO materials. They are tedious and time consuming to grow and are also difficult and expensive to process into working photonic devices.

Like noncentrosymmetric crystallization, self-assembly techniques make use of the complex interplay among intermolecular or inter-surface potentials to drive acentric chromophore ordering. Self-assembly eliminates or reduces the need for application of external forces. Various assembly schemes have been recently employed toward this goal. Langmuir-Blodgett films employ hydrophobic and

hydrophilic interactions at layer surfaces to drive acentric ordering.⁶³⁻⁶⁵ Films produced using Langmuir-Blodgett techniques are generally too thin for practical application and also are thermally and mechanically unstable. Alternatively, the use of hydrogen bonding to direct chromophore assembly has been explored with some success as well.^{66, 67}

One of the most notable examples of organic EO material self-assembly is that of layer-by-layer siloxane-chemistry-based EO chromophore surface deposition. To achieve ordered chromophore layer deposition, a glass substrate is functionalized with a monolayer of an alkyl-halide terminated silane (Scheme 1.5.1).^{11, 68} A pyridinium acceptor-based dipolar chromophore, which is hydroxyl functionalized at the donor terminus, is then covalently linked with the monolayer. After a chromophore layer is attached, a capping layer of alkyl-halide terminated silane is introduced. The process is then repeated through multiple cycles, allowing the growth of many layers.

Scheme 1.5.1: Layer-by-layer acentric chromophore deposition through siloxane based sequential synthesis¹¹



Using this sequential synthesis technique, r_{33} values as high as 120 pm/V have been achieved.⁶⁹ The major drawback to this technique is, again, that of limited thickness. At a high numbers of layers, error propagation and interchromophore electrostatic interactions lead to a roll-off in EO effects. The use of two-dimensional, “large- footprint” chromophore structures has been explored as a method to combat these problems.⁷⁰

Electric field poling of organic materials is probably the most convenient and certainly the most common method employed to induce acentric EO chromophore ordering. A large electric field is applied to the chromophore-containing material while it is heated at a temperature near its T_g . The material is then cooled under continued application of the E field. When an organic material is heated near T_g , molecular motion rates can be expected to increase by roughly 10 orders of magnitude relative to ambient temperature.⁷¹ At such high rates of motion, chromophore dipoles can respond quickly to an applied field. When the material is cooled again, motion rates slow dramatically and the poled orientation is retained. There are two primary E field poling configurations: corona and contact poling. Contact poling requires a capacitor-like sample configuration in which the EO material is physically bound between the top and bottom poling electrodes. Corona poling only requires a directly attached bottom electrode. The top electrode consists of a needle held a short distance from the top of the EO material. When a high voltage is applied between the bottom electrode and needle, a corona field is produced. Contact poling requires lower electric fields and is more controllable and

reproducible.⁷² Therefore, contact poling has been the most commonly employed method for general experiments and device fabrication.

Simple chromophore-polymer guest-host composites are some of the most common EO materials used in both device and experimental configurations. The guest-host approach provides a facile and affordable way to gain insight into the performance characteristics of newly synthesized chromophores. However, many fundamental drawbacks plague polymer-chromophore guest-host composites. Such drawbacks will be addressed in the following section.

1.6 Optimizing $N\langle\cos^3\theta\rangle$ in Electric Field Poled Organics

When considering polymer-chromophore, guest-host composite materials, there are several obvious difficulties to be addressed. Material inhomogeneity and low thermal stability of EO effects are two of the most pronounced problems. In order to achieve high chromophore loading while maintaining optical quality thin films, the highly polar chromophore must be highly soluble in the polymer host. If this condition is not met, aggregation and phase separation lead to poor material properties. Interchromophore electrostatic interactions also counteract the applied poling field at high N . Extensive theoretical work performed by Dalton and Robinson, *et al.* has implicated these dipole-dipole interactions as one of the most severe impediments to high poling induced acentric order.^{15, 73} As chromophore dipole moments are increased and interchromophore distance is decreased, dipole-dipole electrostatic interactions energetically disfavor acentric chromophore

ordering.

Much research has focused on improving material compatibility and increasing poling response. Some of the earliest work focused on main-chain and side-chain polymer architectures. Main-chain polymers incorporate the chromophore units directly into the material backbone as monomeric units.⁷⁴⁻⁷⁶ In side-chain polymers the chromophores do not participate directly in the physical structure of the polymer, but are attached as pendant groups.⁷⁷⁻⁸¹ Polymers in which chromophores are covalently incorporated help to address the problem of guest-host phase separation. Higher loading densities can be achieved, but chromophore mobility is inherently limited by covalent tethering. Intuitively, chromophore mobility is more limited by the use of a main-chain polymer approach compared to a side-chain design. Limited mobility leads to lower poling response per chromophore. Therefore, even though loading density is increased in these systems, r_{33} is not necessarily increased proportionally. The side chain approach yields much better r_{33} values, but is generally somewhat less thermally stable. It is important to note, with some important exceptions, that higher chromophore mobility is associated with lower thermal stability.

Though somewhat less pronounced, side-chain polymers still suffer from high interchromophore electrostatic interactions. Such detrimental electrostatic interactions can be reduced by limiting minimum interchromophore distance using steric bulk. One approach to increasing steric bulk involves encasing the chromophore in a full dendrimer periphery, or alternatively, bulk may be added to

individual polymer pendants creating dendronized polymer systems. Dendronized polymers are synthetically less rigorous to produce than discrete multichromophore dendrimers. They can be realized using polymer post functionalization techniques, or through a more direct block-copolymer approach.⁸²⁻⁸⁴ In some studies a factor of 2 times enhancement in r_{33} has been noted through the use of side chain dendronized polymers.⁸²

Discrete Multichromophore dendrimers are more difficult to synthesize than post-functionalized, dendronized polymers. However, they still represent an attractive material class (figure 1.6.1). Dendrimers display some unique characteristics such as high control over chromophore geometry, and potential for increased chemical and thermal stability of the chromophore units.^{6, 85} Multichromophore dendrimers are also monodisperse, which is attractive for comparative studies due to low batch-to-batch variation. Dendrimers retain many of the best attributes of polymers while allowing further flexibility in the engineering of characteristics displayed by individual chromophore molecules.⁸⁶ Chromophore and host material molecular architecture can play a major role in determining the extent to which chromophores align with poling. Recent results show that chromophore shape and specific supramolecular interactions represent extremely important material design considerations. Theory guided, bottom-up design of chromophore-chromophore and chromophore-host interaction can be used to create materials in which electrostatic interaction now favors acentric rather than centric order.⁸⁷⁻⁸⁹ Such nanoscale material design is the major focus of this dissertation.

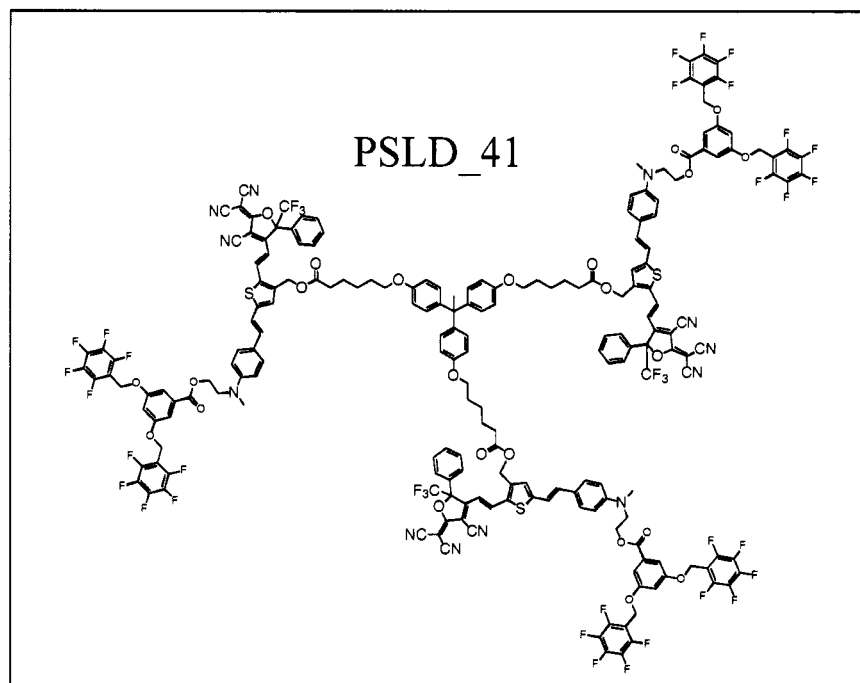


Figure 1.6.1: Three-arm multichromophore dendrimer PS LD_41

The thermal stability of the EO effects is also a very important point to consider when designing materials for practical application. In order to be useful as the active components in photonic micro-devices, poled materials must retain their r_{33} over an extended period of time at elevated operational temperatures. As was mentioned earlier, materials that display high chromophore mobility generally display relatively low glass transition temperatures. Crosslinking chemistry can be employed to improve thermal stability without decreasing initial chromophore mobility and reducing poling induced r_{33} . It is desirable for a material to display relatively low T_g and high chromophore mobility during poling. The material is then

crosslinked during and after poling resulting in high thermal stability of the poling induced order. Of the crosslinking (also called lattice hardening) chemistry explored to date, urethane condensations, trifluorovinyl ether cycloaddition, and Diels-Alder based methods have been the most successful. Although urethane condensation chemistry is relatively straightforward, such condensation reactions are undesirable for use in optical films. Reproducible results are difficult to obtain and by-products from the crosslinking reaction (water) can be detrimental to film quality.^{90, 91} Trifluoro-vinyl ether cycloaddition chemistry represents an improvement over urethane condensation.^{1, 86, 92, 93} A difficulty faced by this and all thermal crosslinking schemes is overlap of the curing and poling processes. During poling, a narrow temperature range exists between optimum poling conditions and dielectric breakdown. If temperatures required for thermal crosslinking do not coincide precisely with optimum poling temperature, r_{33} will be reduced during the crosslinking process. Diels-Alder based crosslinking chemistry was introduced by the Jen Research Group to combat this problem. Crosslinking schemes based on the thermally reversible Diels-Alder (4+2) cycloaddition reaction have the advantages of thermal reversibility and facile temperature tunability.^{94, 95} Unlike urethane condensation schemes, Diels-Alder crosslinking is by-product free.

Notes to Chapter 1

1. Dalton, L. D., Nonlinear optical polymeric materials: from chromophore design to commercial applications. *Advances in Polymer Science* **2002**, 158, (Polymers for Photonics Applications I), 1-86.
2. Dalton, L. R.; Harper, A. W.; Ghosn, R.; Steier, W. H.; Ziari, M.; Fetterman, H.; Shi, Y.; Mustacich, R. V.; Jen, A. K.-Y.; Shea, K. J., Synthesis and processing of improved organic second-order nonlinear optical materials for applications in photonics. *Chem. Mater.* **1995**, 7, (6), 1060-1081.
3. Shi, Y.; Zhang, C.; Zhang, H.; Bechtel, J. H.; Dalton, L. R.; Robinson, B.; Steier, W. H., Low (Sub-1-Volt) Halfwave Voltage Polymeric Electro-optic Modulators Achieved by Controlling Chromophore Shape. *Science* **2000**, 288, 119-122.
4. Sinyukov, A. M.; Leahy, M. R.; Hayden, L. M.; Haller, M.; Luo, J.; Jen, A. K. Y.; Dalton, L. R., Resonance enhanced THz generation in electro-optic polymers near the absorption maximum. *Applied Physics Letters* **2004**, 85, (24), 5827-5829.
5. Rabiei, P.; Steier, W. H.; Zhang, C.; Dalton, L. R., Polymer Micro-Ring Filter and Modulators. *J. Lightwave, Technol.* **2002**, 20, (11), 1968-1975.
6. Sullivan, P. A.; Akelaitis, A. J. P.; K., L. S.; McGrew, G.; Lee, S. K.; Choi, D. H.; Dalton, L. R., Novel Dendritic Chromophores for Electro-optics: Influence of Binding Mode and Attachment Flexibility on Electro-Optic Behavior. *Chem. Mater.* **2006**, 18, 344-351.
7. Dalton, L., Nonlinear Optical Polymeric Materials: From Chromophore Design to Commercial Applications. *Adv. Polym. Sci.* **2001**, 158, 1-86.
8. Chen, D.; Fetterman, H. R.; Chen, A.; Steier, W. H.; Dalton, L. R.; Wang, W.; Shi, Y., Demonstration of 110 GHz electro-optic polymer modulators. *App. Phys. Lett.* **1997**, 70, (25), 3335-3337.
9. Chen, A.; Dalton, L.; Sherwood, T.; Jen, A. K.-Y.; Rabiei, P.; Steier, W.; Huang, Y.; Palocz, G. T.; Poon, J. K. S.; Scherer, A.; Yariv, A., All-organic and organic-silicon photonic ring micro-resonators. *Proceedings of SPIE-The International Society for Optical Engineering* **2005**, 5708, (Laser Resonators and Beam Control VIII), 187-197.
10. Katti, K. V.; Raghuraman, K.; Pillarsetty, N.; Karra, S. R.; Gulotty, R. J.; Chartier, M. A.; Langhoff, C. A., First Examples of Azaphosphanes as Efficient

Electron Donors in the Chemical Architecture of Thermally Stable New Nonlinear Optical Materials. *Chem. Mater.* **2002**, 14, (6), 2436-2438.

11. Facchetti, A.; Abboto, A.; Beverina, L.; van der Boom, M. E.; Dutta, P.; Evmenenko, G.; Pagani, G. A.; Marks, T. J., Layer-by-layer self-assembled pyrrole-based donor-acceptor chromophores as electro-optic materials. *Chem. Mater.* **2003**, 15, (5), 1064-1072.
12. Diaz, J. L.; Dobarro, A.; Villacampa, B.; Velasco, D., Structure and Optical Properties of 2,3,7,9-Polysubstituted Carbazole Derivatives. Experimental and Theoretical Studies. *Chem. Mater.* **2001**, 13, (8), 2528-2536.
13. Prasad, P. N.; Williams, D. J., *Introduction to Nonlinear Optical Effects in Molecules and Polymers*. John Wiley and Sons: New York, 1991.
14. Dalton, L. R., Polymeric electro-optic materials: optimization of electro-optic activity, minimization of optical loss, and fine-tuning of device performance. *Opt. Eng.* **2000**, 39, (3), 589-595.
15. Dalton, L. R.; Harper, A. W.; Robinson, B. H., The role of London Forces in Defining Noncentrosymmetric Order of High Dipole Moment-High Hyperpolarizability Chromophores in Electrically Poled Polymeric Thin Films. *Proc. Natl. Acad. Sci. USA* **1997**, 94, (10), 4842-4847.
16. Luo, J.; Ma, H.; Haller, M.; Jen, A. K.-Y.; Barto, R. R., Large electro-optic activity and low optical loss derived from a highly fluorinated dendritic nonlinear optical chromophore. *Chem. Commun.* **2002**, (8), 888-889.
17. Oudar, J., Optical nonlinearities of conjugated molecules. Stilbene derivatives and highly polar aromatic compounds. *J. Chem. Phys.* **1977**, 67, (2), 446-657.
18. Oudar, J. L.; Chemla, D. S., Hyperpolarizabilities of the nitroanilines and their relations to the excited state dipole moment. *J. Chem. Phys.* **1977**, 66, (6), 2664-2668.
19. Kinnibrugh, T.; Bhattacharjee, S.; Sullivan, P. A.; Isborn, C.; Robinson, B.; Eichinger, B. E., Influence of Isomerism on Nonlinear Optical Properties of Molecules. *submitted* **2006**.
20. Janietz, S.; Bradley, D. D. C.; Grell, M.; Giebeler, C.; Inbasekaran, M.; Woo, E. P., Electrochemical determination of the ionization potential and electron affinity of poly(9,9-dioctylfluorene). *Applied Physics Letters* **1998**, 73, (17), 2453-2455.
21. Liao, Y.; Eichinger, B. E.; Firestone, K. A.; Haller, M.; Luo, J.; Kaminsky, W.; Benedict, J. B.; Reid, P. J.; Jen, A. K. Y.; Dalton, L. R.; Robinson, B. H.,

Systematic study of the structure-property relationship of a series of ferrocenyl nonlinear optical chromophores. *Journal of the American Chemical Society* **2005**, 127, (8), 2758-2766.

22. Sullivan, P. A.; Akelaitis, A. J. P.; Hammond, S.; Sinnes, J.; Dalton, L., Synthetic Approaches to Nanoscale Engineering of Organic Materials for Photonics Applications. *Accounts of Chemical Research* **2006**, in preperation, invited paper.

23. Liao, Y.; Eichinger, B. E.; Firestone, K. A.; Haller, M.; Luo, J.; Kaminsky, W.; Benedict, J. B.; Reid, P. J.; Jen, A. K.-Y.; Dalton, L. R.; Robinson, B. H., Systematic study of the structure-property relationship of a series of ferrocenyl nonlinear optical chromophores. *J. Am. Chem. Soc.* **2005**, 127, (8), 2758-2766.

24. Janowska, I.; Zakrzewski, J.; Nakatani, K.; Delaire, J. A.; Palusiak, M.; Walak, M.; Scholl, H., Ferrocenyl D-p-A chromophores containing 3-dicyanomethylidene-1-indanone and 1,3-bis(dicyanomethylidene)indane acceptor groups. *J. Organomet. Chem.* **2003**, 675, (1-2), 35-41.

25. Farrell, T.; Manning, A. R.; Murphy, T. C.; Meyer-Friedrichsen, T.; Heck, J.; Asselberghs, I.; Persoons, A., Structure-property dependence of the first hyperpolarizabilities of organometallic merocyanines based on the m-vinylcarbynediiron acceptor and ferrocene donor. *Eur. J. Inorg. Chem.* **2001**, (9), 2365-2375.

26. Moore, A. J.; Chesney, A.; Bryce, M. R.; Batsanov, A. S.; Kelly, J. F.; Howard, J. A. K.; Perepichka, I. F.; Perepichka, D. F.; Meshulam, G.; Berkovic, G.; Kotler, Z.; Mazor, R.; Khodorkovsky, V., Synthesis, structures and nonlinear optical properties of novel D-p-A chromophores: intramolecular charge transfer from 1,3-dithiole or ferrocene moieties to polynitrofluorene or dicyanomethylene moieties through conjugated linkers. *Eur. J. Org. Chem.* **2001**, (14), 2671-2687.

27. Boldt, P.; Eisentraeger, T.; Glania, C.; Goeldenitz, J.; Kraemer, P.; Matschiner, R.; Rase, J.; Schwesinger, R.; Wichern, J.; Wortmann, R., Guanidyl and phosphoraniminyl substituents. New electron donors in second-order nonlinear optical chromophores. *Adv. Mater.* **1996**, 8, (8), 672-675.

28. Annoni, E.; Pizzotti, M.; Ugo, R.; Quici, S.; Morotti, T.; Bruschi, M.; Mussini, P., Synthesis, electronic characterisation and significant second-order non-linear optical responses of meso-tetraphenylporphyrins and their ZnII complexes carrying a push or pull group in the b pyrrolic position. *Eur. J. Inorg. Chem.* **2005**, (19), 3857-3874.

29. Zhang, S.; Zhou, G.; Yang, Z.; Qin, A.; Wang, P.; Ye, C., Design and synthesis of low dipole moment chromophores: 2,6-disubstituted cycloheptimidazoles. *Synth. Met.* **2003**, 137, (1-3), 1545-1546.

30. Nguyen, T. T.; Salle, M.; Delaunay, J.; Riou, A.; Richomme, P.; Raimundo, J. M.; Gorgues, A.; Ledoux, I.; Dhenaut, C.; Zyss, J.; Orduna, J.; Garin, J., Functionalized polyolefinic nonlinear optic chromophores incorporating the 1,3-dithiol-2-ylidene moiety as the electron-donating part. *J. Mater. Chem.* **1998**, 8, (5), 1185-1192.
31. Batsanov, A. S.; Bryce, M. R.; Coffin, M. A.; Green, A.; Hester, R. E.; Howard, J. A. K.; Lednev, I. K.; Martin, N.; Moore, A. J.; Moore, J. N.; Orti, E.; Sanchez, L.; Saviron, M.; Viruela, P. M.; Viruela, R.; Ye, T.-Q., Donor-p-acceptor species derived from functionalized 1,3-dithiol-2-ylidene anthracene donor units exhibiting photoinduced electron transfer properties: spectroscopic, electrochemical, x-ray crystallographic and theoretical studies. *Chem. Eur. J.* **1998**, 4, (12), 2580-2592.
32. Gonzalez, M.; Segura, J. L.; Seoane, C.; Martin, N.; Garin, J.; Orduna, J.; Alcala, R.; Villacampa, B.; Hernandez, V.; Lopez Navarrete, J. T., Tetrathiafulvalene derivatives as NLO-phores: synthesis, electrochemistry, Raman spectroscopy, theoretical calculations, and NLO properties of novel TTF-derived donor-p-acceptor dyads. *J. Org. Chem.* **2001**, 66, (26), 8872-8882.
33. Garin, J.; Orduna, J.; Andreu, R., Tetrathiafulvalene and 1,3-dithiole-based chromophores with second-order nonlinear optical properties. *Recent Research Developments in Organic Chemistry* **2001**, 5, (Pt. 1), 77-87.
34. Kuo, W.-J.; Hsiue, G.-H.; Jeng, R.-J., Novel Guest-Host NLO Poly(ether imide) Based on a Two-Dimensional Carbazole Chromophore with Sulfonyl Acceptors. *Macromolecules* **2001**, 34, (7), 2373-2384.
35. Do, J. Y.; Park, S. K.; Ju, J.-J.; Park, S.; Lee, M.-H., Electro-optic materials: hyperbranched chromophores attached linear polyimide and dendritic polyesters. *Polym. Adv. Technol.* **2005**, 16, (2-3), 221-226.
36. Suresh, S.; Zengin, H.; Spraul, B. K.; Sassa, T.; Wada, T.; Smith, D. W., Synthesis and hyperpolarizabilities of high temperature triarylamine-polyene chromophores. *Tetrahedron Lett.* **2005**, 46, (22), 3913-3916.
37. Pan, Q.; Fang, C.; Zhang, Z.; Qin, Z.; Li, F.; Gu, Q.; Wu, X.; Yu, J., Synthesis and characterization of nonlinear optical chromophores containing a-cyan with thermal stability. *Opt. Mater.* **2003**, 22, (1), 45-49.
38. He, M.; Leslie, T. M.; Sinicropi, J. A.; Garner, S. M.; Reed, L. D., Synthesis of Chromophores with Extremely High Electro-optic Activities. 2. Isophorone- and Combined Isophorone-Thiophene-Based Chromophores. *Chem. Mater.* **2002**, 14, (11), 4669-4675.

39. Raimundo, J.-M.; Blanchard, P.; Frere, P.; Mercier, N.; Ledoux-Rack, I.; Hierle, R.; Roncali, J., Push-pull Chromophores based on 2,2'-bi(3,4-ethylenedioxythiophene) (BEDOT) pi-conjugating spacer. *Tetrahedron Lett.* **2001**, 42, 1507-1510.
40. Raimundo, J.-M.; Blanchard, P.; Gallego-Planas, N.; Mercier, N.; Ledoux-Rack, I.; Hierle, R.; Roncali, J., Design and synthesis of push-pull chromophores for second-order nonlinear optics derived from rigidified thiophene-based p-conjugating spacers. *J. Org. Chem.* **2002**, 67, (1), 205-218.
41. Briers, D.; Koeckelberghs, G.; Picard, I.; Verbiest, T.; Persoons, A.; Samyn, C., Novel Chromophore-Functionalized Poly[2-(trifluoromethyl) adamantyl acrylate-methyl vinyl urethane]s with High Poling Stabilities of the Nonlinear Optical Effect. *Macromol. Rapid Commun.* **2003**, 24, 841-846.
42. Liu, S.; Haller, M. A.; Ma, H.; Dalton, L. R.; Jang, S.-H.; Jen, A. K.-Y., Focused microwave-assisted synthesis of 2,5-dihydrofuran derivatives as electron acceptors for highly efficient nonlinear optical chromophores. *Adv. Mater.* **2003**, 15, (7-8), 603-607.
43. Zhang, C.; Wang, C. W.; Dalton, L. R.; Zhang, H.; Steier, W. H., Progress toward Device-Quality Second-Order Nonlinear Optical Materials. 4. A Trilink High mu-Beta NLO Chromophore in Thermoset Polyurethane: A "Guest-Host" Approach to Larger Electrooptic Coefficients. *Macromolecules* **2001**, 34, 253-261.
44. Facchetti, A.; Abbotto, A.; Beverina, L.; van der Boom, M. E.; Dutta, P.; Evmenenko, G.; Marks, T. J.; Pagani, G. A., Azinium-(p-Bridge)-Pyrrole NLO-Phores: Influence of Heterocycle Acceptors on Chromophoric and Self-Assembled Thin-Film Properties. *Chem. Mater.* **2002**, 14, (12), 4996-5005.
45. Ashwell, G. J., Langmuir-Blodgett films: molecular engineering of non-centrosymmetric structures for second-order nonlinear optical applications. *J. Mater. Chem.* **1999**, 9, (9), 1991-2003.
46. Marder, S. R.; Cheng, L.-T.; Tiemann, B. G.; Friedli, A. C.; Blanchard-Desce, M.; Perry, J. W.; Skindhoj, J., Large First Hyperpolarizabilities in Push-Pull Polyenes by Tuning of the Bond Length Alternation and Aromaticity. *Science* **1994**, 263, (5146), 511-514.
47. Cao, Y. W.; Chai, X. D.; Chen, S. G.; Jiang, Y. S.; Yang, W. S.; Ren, Y. Z.; Blanchard-Desce, M.; Li, T. J.; Lehn, J. M., A new series of nonlinear optical organic materials with molecular receptor: design and synthesis. *Synth. Met.* **1995**, 71, (1-3), 1733-4.

48. Garin, J.; Orduna, J.; Ruperez, J. I.; Alcala, R.; Villacampa, B.; Sanchez, C.; Martin, N.; Segura, J. L.; Gonzalez, M., Second-order nonlinear optical properties of tetrathiafulvalene-p-(thio)barbituric acid chromophores. *Tetrahedron Lett.* **1998**, 39, (21), 3577-3580.
49. Zheng, Q.; Yao, Z.; Cheng, J.; Shen, Y.; Lu, Z., Synthesis and nonlinear optical properties of p-(dimethylamino)benzylidene dyes containing different acceptors. *Chem. Lett.* **2000**, (12), 1426-1427.
50. Lu, D.; Marten, B.; Cao, Y.; Ringnalda, M. N.; Friesner, R. A.; Goddard, W. A., III, Ab initio predictions of large hyperpolarizability push-pull polymers: Julolidinyl-n-isoxazolone and julolidinyl-n-N,N'-diethylthiobarbituric acid. *Chem. Phys. Lett.* **1995**, 242, (6), 543-7.
51. Wang, F.; Harper, A. W.; Lee, M. S.; Dalton, L. R.; Zhang, H.; Chen, A.; Steier, W. H.; Marder, S. R., Progress toward Device-Quality Second-Order NLO Materials: 3. Electrooptic Activity of Polymers Containing E,E,E-[4-(N,N-Dialkylamino)-phenyl]pentadienylidene-3-phenyl-5-isoxazolone Chromophores. *Chem. Mater.* **1999**, 11, (9), 2285-2288.
52. Diaz, J. L.; Villacampa, B.; Lopez-Calahorra, F.; Velasco, D., Experimental and Theoretical Study of a New Class of Acceptor Group in Chromophores for Nonlinear Optics: 2-Substituted 4-Methylene-4H-oxazol-5-ones. *Chem. Mater.* **2002**, 14, (5), 2240-2251.
53. Dalton, L. R.; Harper, A. W.; Ghosn, R.; Steier, W. H.; Ziari, M.; Fetterman, H.; Shi, Y.; Mustacich, R. V.; Jen, A. K. Y.; Shea, K. J., Synthesis and Processing of Improved Organic Second-Order Nonlinear Optical Materials for Applications in Photonics. *Chem. Mater.* **1995**, 7, (6), 1060-81.
54. Dalton, L.; Harper, A.; Ren, A.; Wang, F.; Todorova, G.; Chen, J.; Zhang, C.; Lee, M., Polymeric Electro-optic Modulators: From Chromophore Design to Integration with Semiconductor Very Large Scale Integration Electronics and Silica Fiber Optics. *Ind. Eng. Chem. Res.* **1999**, 38, (1), 8-33.
55. Sun, S.-S.; Zhang, C.; Dalton, L. R.; Garner, S. M.; Chen, A.; Steier, W. H., 1,3-Bis(dicyanomethylidene)indane-Based Second-Order NLO Materials. *Chem. Mater.* **1996**, 8, (11), 2539-2541.
56. Alain, V.; Fort, A.; Barzoukas, M.; Chen, C.-T.; Blanchard-Desce, M.; Marder, S. R.; Perry, J. W., The linear and non-linear optical properties of some conjugated ferrocene compounds with potent heterocyclic acceptors. *Inorg. Chim. Acta* **1996**, 242, (1-2), 43-9.

57. He, M.; Leslie, T. M.; Sinicropi, J. A., Synthesis of Chromophores with Extremely High Electro-optic Activity. 1. Thiophene-Bridge-Based Chromophores. *Chem. Mater.* **2002**, 14, (11), 4662-4668.
58. Villemin, D.; Liao, L., Rapid and efficient synthesis of 2-[3-cyano-4-(2-arylidene)-5,5-dimethyl-5H-furan-2-ylidene]-malononitrile under focused microwave irradiation. *Synth. Commun.* **2001**, 31, (11), 1771-1780.
59. Melikian, G.; Rouessac, F. P.; Alexandre, C., Synthesis of substituted dicyanomethylendihydrofurans. *Synth. Commun.* **1995**, 25, (19), 3045-51.
60. Pan, F.; Knoepfle, G.; Bosshard, C.; Follonier, S.; Spreiter, R.; Wong, M. S.; Guenter, P., Electro-optic properties of the organic salt 4-N,N-dimethylamino-4',N'-methyl-stilbazolium tosylate. *Appl. Phys. Lett.* **1996**, 69, (1), 13-15.
61. Marder, S. R.; Perry, J. W.; Schaefer, W. P., Synthesis of Organic Salts with large Second-Order Optical Nonlinearities. *Science* **1989**, 245, (4918), 626-628.
62. Yang, Z.; Aravazhi, S.; Schneider, A.; Seiler, P.; Jazbinsek, M.; Guenter, P., Synthesis and crystal growth of stilbazolium derivatives for second-order nonlinear optics. *Adv. Funct. Mater.* **2005**, 15, (7), 1072-1076.
63. Ashwell, G. J.; Jackson, P. D.; Crossland, W. A., Non-centrosymmetry and second-harmonic generation in Z-type Langmuir-Blodgett films. *Nature* **1994**, 368, (6470), 438-40.
64. Ashwell, G. J.; Maxwell, A. A.; Green, A., Unconventional Langmuir-Blodgett films: alignment of an optically nonlinear dye where the donor and p-electron bridge are hydrophobic and the acceptor is hydrophilic. *J. Mater. Chem.* **2002**, 12, (8), 2192-2196.
65. Schwartz, H.; Mazor, R.; Khodorkovsky, V.; Shapiro, L.; Klug, J. T.; Kovalev, E.; Meshulam, G.; Berkovic, G.; Kotler, Z.; Efrima, S., Langmuir and Langmuir-Blodgett Films of NLO Active 2-(p-N-Alkyl-N-methylamino)benzylidene-1,3-indandione - π /A Curves, UV-Vis Spectra and SHG behavior. *J. Phys. Chem.* **2001**, 105, (25), 5914-5921.
66. Facchetti, A.; Annoni, E.; Beverina, L.; Morone, M.; Zhu, P.; Marks, T. J.; Pagani, G. A., Very large electro-optic responses in H-bonded heteroaromatic films grown by physical vapor deposition. *Nature Materials* **2004**, 3, (12), 910-917.
67. Rashid, A. N.; Erny, C.; Gunter, P., Hydrogen-bond-directed orientation in nonlinear optical thin films. *Adv. Mater.* **2003**, 15, (23), 2024-2027.
68. Facchetti, A.; van der Boom, M. E.; Abbotto, A.; Beverina, L.; Marks, T. J.; Pagani, G. A., Design and Preparation of Zwitterionic Organic Thin Films: Self-

Assembled Siloxane-Based, Thiophene-Spaced N-Benzylpyridinium Dicyanomethanides as Nonlinear Optical Materials. *Langmuir* **2001**, 17, (19), 5939-5942.

69. van der Boom, M. E.; Zhu, P.; Evmenenko, G.; Malinsky, J. E.; Lin, W.; Dutta, P.; Marks, T. J., Nanoscale Consecutive Self-Assembly of Thin-Film Molecular Materials for Electrooptic Switching. Chemical Streamlining and Ultrahigh Response Chromophores. *Langmuir* **2002**, 18, (9), 3704-3707.

70. Kang, H.; Zhu, P.; Yang, Y.; Facchetti, A.; Marks, T. J., Self-assembled electrooptic thin films with remarkably blue-shifted optical absorption based on an x-shaped chromophore. *Journal of the American Chemical Society* **2004**, 126, (49), 15974-15975.

71. Ediger, M. D., Spatially heterogeneous dynamics in supercooled liquids. *Annual Review of Physical Chemistry* **2000**, 51, 99-128.

72. Yitzchaik, S.; Di Bella, S.; Lundquist, P. M.; Wong, G. K.; Marks, T. J., Anomalous Second-Order Nonlinear Optical Response of In-Plane Poled Glassy Polymers. Spectroscopic and Theoretical Support for the Importance of Charged Chromophore Aggregates. *J. Am. Chem. Soc.* **1997**, 119, (13), 2995-3002.

73. Harper, A. W.; Sun, S.; Dalton, L. R.; Garner, S. M.; Chen, A.; Kalluri, S.; Steier, W. H.; Robinson, B. H., Translating microscopic optical nonlinearity into macroscopic optical nonlinearity: The role of chromophore-chromophore electrostatic interactions. *J. Opt. Soc. Am. B* **1998**, 15, (1), 329-337.

74. Huang, D.; Zhang, C.; Dalton, L. R.; Weber, W. P., Synthesis and Characterization of Main-Chain NLO Oligomers and Polymer that Contain 4-Dialkylamino-4'(alkylsulfonyl)azobenzene Chromophores. *J. Polym. Sci. Part A: Polym. Chem.* **2000**, 38, 546-559.

75. Stenger-Smith, J. D.; Zarras, P.; Hollins, R. A.; Chafin, A. P.; Merwin, L. H.; Yee, R.; Lindsay, G. A.; Herman, W. N.; Gratz, R. F.; Nickel, E. G., Main-Chain Syndioregic Nonlinear Optical Polymers. II. Extended Pi Conjugated and Improved Thermal Properties. *J. Pol. Sci. Part A: Polym. Chem.* **2000**, 38, (2824-2839).

76. Tsutsumi, N.; Morishima, M.; Sakai, W., Nonlinear Optical (NLO) Polymers. 3. NLO Polyimide with Dipole Moments Aligned Transverse to the Imide Linkage. *Macromolecules* **1998**, 31, (22), 7764-7769.

77. Huang, D.; Chen, B. Polymers having pendant nonlinear optical chromophores and electro-optic devices made from them. 2003-625371 2004132960, 20030723., 2004.

78. Park, K. H.; Yeon, K. M.; Lee, M. Y.; Lee, S. D.; Shin, D. H.; Lee, C. J.; Kim, N., Synthesis and nonlinear optical properties of PMMA copolymers having novel benzoxazole chromophores attached with various electron-withdrawing groups. *Polymer* **1998**, 39, (26), 7061-7066.
79. Gubbelmans, E.; Verbiest, T.; Picard, I.; Persoons, A.; Samyn, C., Poly(phenylquinoxalines) for second-order nonlinear optical applications. *Polymer* **2005**, 46, (6), 1784-1795.
80. Van den Broeck, K.; Verbiest, T.; Degryse, J.; Van Beylen, M.; Persoons, A.; Samyn, C., High glass transition chromophore functionalized polyimides for second-order nonlinear optical applications. *Polymer* **2001**, 42, (8), 3315-3322.
81. Saadeh, H.; Wang, L.; Yu, L., A New Synthetic Approach to Novel Polymers Exhibiting Large Electrooptic Coefficients and High Thermal Stability. *Macromolecules* **2000**, 33, (5), 1570-1576.
82. Luo, J.; Liu, S.; Haller, M.; Liu, L.; Ma, H.; Jen, A. K.-Y., Design, synthesis, and properties of highly efficient side-chain dendronized nonlinear optical polymers for electro-optics. *Adv. Mater.* **2002**, 14, (23), 1763-1768.
83. Ma, H.; Jen, A. K.-Y.; Wu, J.; Wu, X.; Liu, S., A Convenient Modular Approach of Functionalizing Aromatic Polyquinolines for Electrooptic Devices. *Chem. Mater.* **1999**, 11, (8), 2218-2225.
84. Liao, Y.; Anderson, C. A.; Sullivan, P. A.; Akelaitis, A. J. P.; Robinson, B. H.; Dalton, L. R., Electro-Optical Properties of Polymers Containing Alternating Nonlinear Optical Chromophores and Bulky Spacers. *Chemistry of Materials* **2006**, 18, (4), 1062-1067.
85. Ma, H.; Liu, S.; Luo, J.; Suresh, S.; Liu, L.; Kang, S.-H.; Haller, M.; Sassa, T.; Dalton, L. R.; Jen, A. K.-Y., Highly efficient and thermally stable electro-optical dendrimers for photonics. *Adv. Funct. Mater.* **2002**, 12, (9), 565-574.
86. Ma, H.; Chen, B.; Sassa, T.; Dalton, L. R.; Jen, A. K.-Y., Highly Efficient and Thermally Stable Nonlinear Optical Dendrimer for Electrooptics. *J. Am. Chem. Soc.* **2001**, 123, (5), 986-987.
87. Dalton, L.; Robinson, B. H.; Jen, A.-K.; Ried, P.; Eichinger, B.; Sullivan, P. A.; Akelaitis, A. J. P.; Bale, D.; Haller, M.; Luo, J.; Liu, S.; Liao, Y.; Firestone, K. A.; Bhatambekar, N.; Bhattacharjee, S.; Sinness, J.; Hammond, S.; Buker, N.; Snoeberger, R.; Lingwood, M.; Rommel, H.; Amend, J.; Jang, S.-H.; Chen, A.; Steier, W. H., Electro-optic coefficients of 500 pm/V and beyond for organic materials. *Proceedings of SPIE-The International Society for Optical Engineering*

2005, 5935, (Linear and Nonlinear Optics of Organic Materials V), 593502/1-593502/12.

88. Nielsen, R. D.; Rommel, H. L.; Robinson, B. H., Simulation of the Loading Parameter in Organic Nonlinear Optical Materials. *J. Phys. Chem. B* **2004**, 108, (25), 8659-8667.

89. Pereverzev, Y. V.; Prezhdo, O. V.; Dalton, L. R., Structural origin of the enhanced electro-optic response of dendrimer systems. *Chem. Phys. Lett.* **2003**, 373, (1,2), 207-212.

90. Liang, Z.; Yang, Z.; Sun, S.-S.; Wu, B.; Dalton, L. R.; Garner, S. M.; Kalluri, S.; Chen, A.; Steier, W. H., Processible and thermally stable heterocyclic polymers for second-order nonlinear optical studies. *Chem. Mater.* **1996**, 8, (11), 2681-2685.

91. Mao, S. S. H.; Ra, Y.; Guo, L.; Zhang, C.; Dalton, L. R.; Chen, A.; Garner, S. M.; Steier, W. H., Progress toward Device-Quality Second-Order Nonlinear Optical Materials. 1. Influence of Composition and Processing Conditions on Nonlinearity, Temporal Stability, and Optical Loss. *Chem. Mater.* **1998**, 10, (1), 146-155.

92. Ma, H.; Wu, J.; Herguth, P.; Chen, B.; Jen Alex, K.-Y., A Novel Class of High-Performance Perfluorocyclobutane-Containing Polymers for Second-Order Nonlinear Optics. *Chem. Mater.* **2000**, 12, (5), 1187-1189.

93. Wong, S.; Ma, H.; Jen, A. K.-Y.; Barto, R.; Frank, C. W., Highly Fluorinated Trifluorovinyl Aryl Ether Monomers and Perfluorocyclobutane Aromatic Ether Polymers for Optical Waveguide Applications. *Macromolecules* **2003**, 36, (21), 8001-8007.

94. Luo, J.; Haller, M.; Li, H.; Kim, T.-D.; Jen, A. K.-Y., Highly efficient and thermally stable electro-optic polymer from a smartly controlled crosslinking process. *Adv. Mater.* **2003**, 15, (19), 1635-1638.

95. Haller, M.; Luo, J.; Li, H.; Kim, T.-D.; Liao, Y.; Robinson, B. H.; Dalton, L. R.; Jen, A. K.-Y., A Novel Lattice-Hardening Process To Achieve Highly Efficient and Thermally Stable Nonlinear Optical Polymers. *Macromolecules* **2004**, 37, (3), 688-690.

Chapter 2

In-situ Pole-and-Probe Polarization Interferometry Reflection Apparatus; a Real-Time Method for Evaluating EO Properties of Poled Organic Thin-Films

2.1 Introduction

Recent interest in organic materials for 2nd-order nonlinear optical (electro-optic) applications has created the need for simple and efficient material characterization methods. The most widely accepted method for determination of r_{33} is based on a single beam reflection ellipsometry apparatus. This is referred to as the “Teng-Man” technique (TMT). The basis for the TMT was introduced independently by Teng and Man, and also Schildkraut in 1990.^{1, 2} The TMT has since been widely adopted for the determination of electro-optic (EO) coefficients in electric field poled organic materials. The TMT is popular because of its cost-effective, relatively simple setup, and high throughput material screening capability. The TMT also holds the advantage of non-contact, non-destructive sample measurement over complementary prism coupling techniques. Modifications to this technique allow *in-situ* monitoring of EO behavior during the poling process.³ Such real-time monitoring can be exploited for the study of electric field influenced dipolar orientational dynamics. Poling behavior may be observed in real-time by direct measurement of Pockels coefficients, allowing optimization of material processing conditions.⁴ Thermal stability of the EO effects induced can be studied in detail, allowing comparison of

the activation energy required to initiate abrupt dipolar randomization.^{5, 6} These data are particularly interesting for exploration of the mechanistic details of bulk material EO effects, and their relationship to temporal behavior.⁷

2.2 Experimental Setup

The experimental setup of the *in-situ* pole-and-probe polarization interferometry reflection apparatus has been schematically depicted in Figure 2.2.1. Samples were fabricated by spin coating EO active materials onto ITO-coated (transparent electrode) glass slides. Gold top electrodes were then fabricated through ion coating or vapor deposition. The gold layer served as both an electrode and reflector for the incident probe beam. The capacitor-like, electrode-sandwiched sample was mounted on a heating stage along with a similar blank sample attached to a thermocouple. The temperature of the assembly was controlled through computer interface by an electronic thermal controller. The cooling rate of the system was controlled manually. Slow, controlled cooling was effected by means of a small fan mounted inside the argon-filled sample chamber. Fan speed control allowed fine-tuning of the slow-cooling process. Fast cooling was initiated by means of a circulating chiller attached to the heating stage. The incident probe beam ($\lambda = 1310$ nm) was produced by a small diode laser. This probe beam passed through a polarizer in order to set the initial polarization to 45° with respect to the laboratory axis. This initial polarization was optimized to ensure an equal amplitude contribution from s and p polarizations at the sample. The polarized beam was then passed through a Soleil-Babinet (SB) compensator that was also computer controlled

using a linear actuator, allowing adjustment of the s and p wave relative phase angle (Ψ_{sp}).

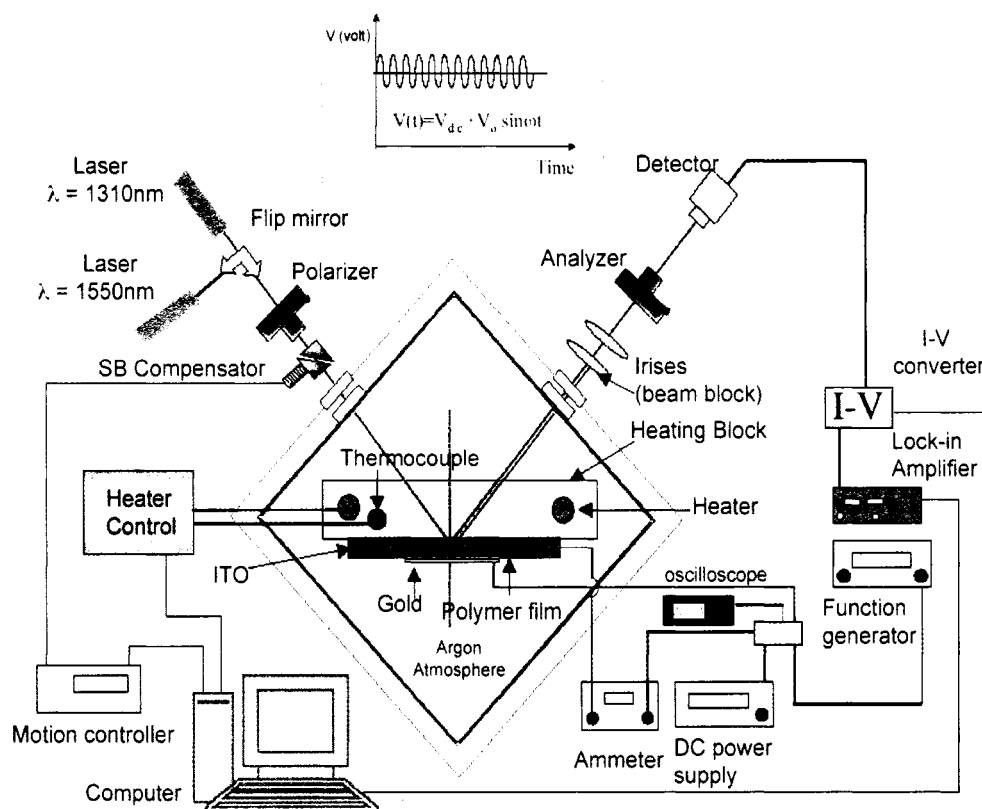


Figure 2.2.1 Schematic representation of *in-situ* reflection ellipsometry setup

The probe beam propagated through the sample at an incident angle θ (Figure 2.2.2) and was reflected from the gold electrode back through the material to exit the sample.¹ Multiple reflected beams arising from hetero-interface reflection were separated by a series of two irises. Last, the isolated beam was passed through a second polarizer or “analyzer” that was set 90° with respect to the first polarizer. The beam was collected by a photodetector.

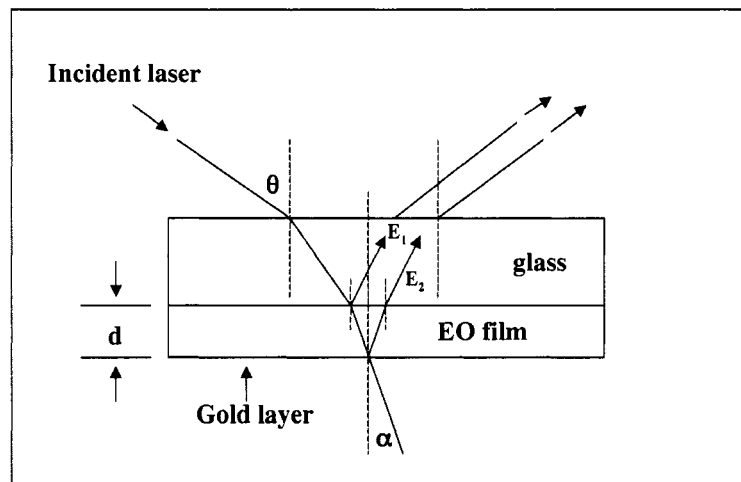


Figure 2.2.2: Propagation path for optical probe beam in the *in-situ* TMT

The detector output was amplified using a low-noise preamplifier. The amplifier output was then split: one output was routed directly to the computer interface, the other was sent to a lock-in-amplifier. The lock-in output was also transmitted to the computer interface. A sine-wave generator was connected across the sample electrodes and a reference signal directed to the lock-in-amplifier for synchronization. A capacitor-based bandpass filter was constructed to allow DC bias of the AC measurement waveform. A high voltage power supply was routed through a low-noise, low-impedance picoammeter, and also to the sample electrodes in order to measure current flow during application of the poling field. All components were computer interfaced using PCI-GPIB (IEE-488) or RS232 ports. Two LabVIEW-based virtual instrument programs, written in-house, allowed manual parameter determination and subsequent measurement automation.

2.3 Theory of Static, Ambient Temperature r_{33} Determination

In order to determine the static r_{33} of a poled sample, a LabVIEW program was employed to create and plot a scan of AC (lock-in) and DC (detector) signals with respect to Ψ_{sp} . The Ψ_{sp} scan was created by moving the linear actuator connected the (SB) compensator through its full range (Figure 2.3.1). The detector could be expected to respond linearly with incident light intensity as controlled by bias voltage. Therefore, by measuring detector response, converted from current to voltage, output light intensity, I_o , was determined from the DC signal.

This relationship is explained below. I_o with respect to Ψ_{sp} can be written as

$$I_o = 2I_c \sin^2(\psi_{sp}/2) \quad (2.3.1)$$

where I_c is the half maximum intensity. The amplitude of the resulting I_c vs. Ψ_{sp} wave is dependent only on the input intensity and the quality of the optical components. Corresponding to the magnitude of the linear electro-optic effect displayed by the poled sample, an AC or modulated signal is superimposed on the DC output. This AC signal carries the frequency signature given by ω_m from the relation

$$V = V_m \sin \omega_m t \quad (2.3.2)$$

where V_m represents the amplitude of the modulation waveform created by the function generator. This signal can be isolated by the lock-in-amplifier and its amplitude measured. The amplitude of the AC signal (ΔI) is linearly dependent on the magnitude of V_m . ΔI , where I_m is the half maximum intensity, is proportional to the r_{33} displayed by the poled sample. Specifically, the AC signal is related to s and p polarization differential refractive index change as a function of applied electric

field. Such a differential refractive index change results in a shift in Ψ_{sp} , and an accompanying increase in intensity at the detector. Strict derivation of the relationship of Ψ_{sp} to I_m/I_c has been described by other authors.^{1, 2, 8} A truncated version is presented here for explanatory purposes.

The EO induced refractive index change under application of the electric field E_z , for the p polarization, can be written as

$$\delta n_e = -n_e^3 r_{33} E_z / 2 \quad (2.3.2)$$

the s wave index change can likewise be written

$$\delta n_o = -n_o^3 r_{13} E_z / 2 \quad (2.3.3)$$

Using the relationship⁸

$$\psi_{sp} = (4\pi d / \lambda) \left[(n_o^2 - \sin^2 \theta)^{1/2} - (n_o / n_e) (n_e^2 - \sin^2 \theta)^{1/2} \right] \quad (2.3.4)$$

taking into account refraction angle (α), and path length changes, it follows that

$$\delta \psi_{sp} = \frac{\delta \psi_{sp}}{\delta n_o} \delta n_o + \frac{\delta \psi_{sp}}{\delta n_e} \delta n_e \quad (2.3.5)$$

From symmetry considerations, it is assumed that $r_{33} = 3r_{13}$. For cases where linear birefringence is low, e.g. poled polymers, the approximation $n_o \approx n_e \approx n$ can also be made. When these approximations are employed, Equation 2.3.5 is simplified and can be written as

$$\psi_{sp} = \frac{4\pi d r_{33} E_z}{3\lambda} \frac{n^2 \sin^2 \theta}{(n^2 - \sin^2 \theta)^{1/2}} \quad (2.3.6)$$

where d is the sample thickness, and λ is the probe wavelength. When Ψ_{sp} is set at 90° or 270° , then I_o will be at half maximum intensity, I_c . At this Ψ_{sp} , where the

curve is most linear, the ratio between the modulated intensity, I_m , and output intensity, I_c , can be taken as

$$I_m / I_c \approx \delta\psi_{sp} \quad (2.3.7)$$

from this approximation,⁸

$$r_{33} = \frac{3\lambda I_m}{4\pi V_m I_c n^2} \frac{(n^2 - \sin^2 \theta)^{1/2}}{\sin^2 \theta} \propto I_m / I_c \quad (2.3.8)$$

all parameters can be determined directly from the measurement (Figure 2.3.1).

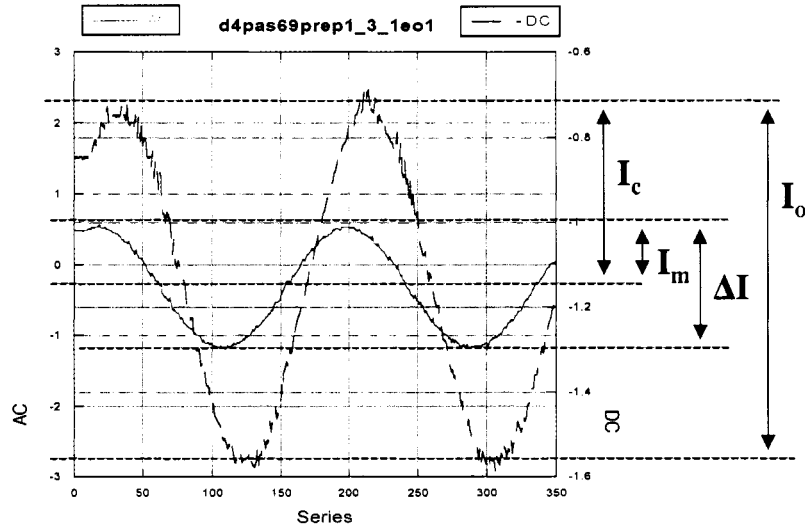


Figure 2.3.1: Ψ_{sp} scan plot showing AC and DC detector response for a poled sample of EO dendrimer created by a full SB compensator actuation cycle

For the calculation of r_{33} , modulated intensity, I_m , and output intensity, I_c , were directly determined from the amplitude of the AC (lock-in-amp), and DC (DAC interface), waves respectively. The two waves were analyzed by curve fitting, using the equation

$$K_0 + K_1 \sin(K_2 x + K_3) \quad (2.3.9)$$

where K_1 is the peak-to-zero sine-wave amplitude, and represents I_c directly for the DC wave. To obtain the correct I_m value, K_1 from the AC wave fit was treated by

$$I_m = K_{lac} \left(\frac{\text{lock_in_sensitivity}}{\text{full_range_voltage}} \right) \quad (2.3.10)$$

in order to correct for amplifier gain factor. The value for V_m was set by the function generator and corrected for sample conductivity by directly monitoring the peak-to-zero voltage applied across the sample electrodes using an oscilloscope.

2.4 Real-Time Poling Behavior Analysis Through *in-situ* Monitoring

Optimization of the poling conditions for each material was performed through *in-situ* monitoring during the poling process. For real-time monitoring of EO film properties, a second LabVIEW program was created. This program allowed the simultaneous control of temperature and applied poling voltage while monitoring the I_m/I_c ratio, time, and current. This monitoring allowed the correlation of poling conditions with changes in approximate r_{33} .

Poling voltage was applied by superimposing a DC bias onto the modulation waveform as shown by

$$V_{(t)} = V_{dc} + V_m \sin \omega_m t \quad (2.4.1)$$

where V_{dc} corresponds to the poling field, E_p , and is reported in units of $V/\mu m$ (inset Figure 2.2.1).

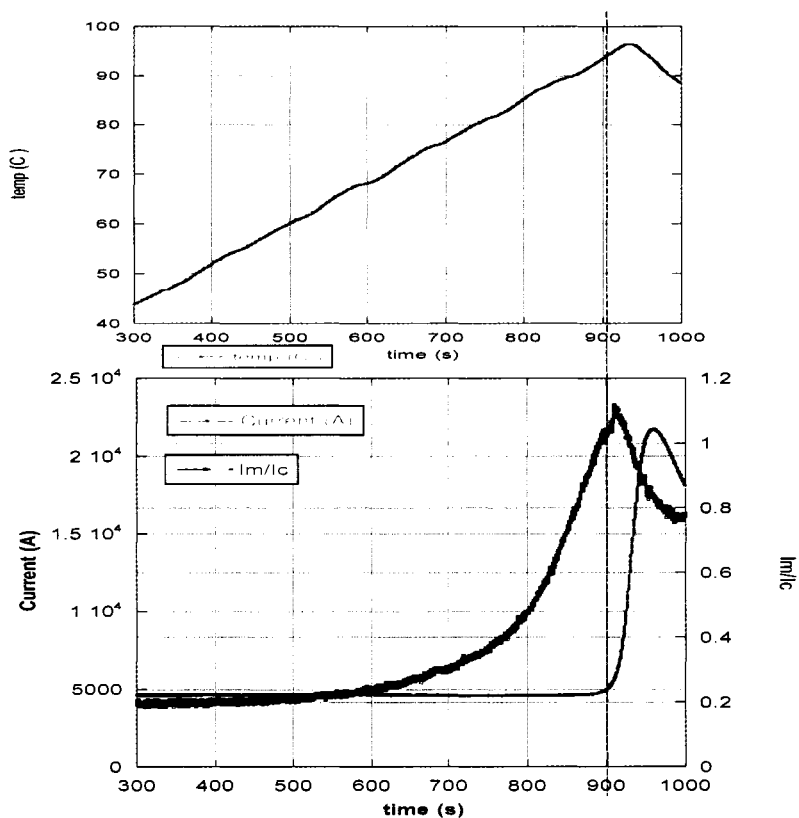


Figure 2.4.1: Real-time plot of the poling behavior of an EO dendrimer sample, $I_m/I_c \propto r_{33}$ is shown in the lower panel plotted with current (nA), the upper panel displays the temperature ramp ($^{\circ}\text{C}$)

Before sample analysis, the output intensity was set to I_c by moving the SB compensator. The I_m/I_c ratio was then monitored while the sample was heated according to a temperature ramp program. The poling voltage was adjusted during the run while limiting the current to an acceptable level (< 0.5 mA). An example of the plotted output is shown in Figure 2.4.1.

From the real-time poling plot, it was evident that an optimum poling temperature existed for each material. By monitoring the current that passed through a sample as a function of temperature, an abrupt transition, or thermally stimulated current (TSC), was observed.⁵ This TSC corresponded very well to the glass transition, T_g , observed for each material by differential scanning calorimetry (DSC). Optimum poling temperature was determined to correspond to the *onset* of the DSC measured glass-transition. Final r_{33} determination for the poled sample was accomplished by Ψ_{sp} scan after cooling to ambient temperature and removal of E_p .

2.5 Study of Dipolar Orientational Dynamics in EO Thin-Films

Thermally-induced randomization of dipolar orientation was also investigated using the *in-situ* TMT. The EO coefficients of poled samples were monitored over time as a function of temperature. Dynamic studies, as well as isothermal studies, were performed. The dynamic thermal stability experiment was performed by monitoring the EO coefficient of a previously poled sample during a temperature ramp. This type of experiment illustrated at what temperature, abrupt dipolar randomization, as measured by loss of r_{33} , occurred. An example of the data obtained is shown in Figure 2.5.1. This experiment was useful for comparison of the thermal stability of EO effects among several materials.

Crosslinking chemistry has recently been given high research priority in the field of organic EO materials.⁹⁻¹¹ Lattice-hardening, or post-poling curing, can greatly improve the thermal and temporal stability of EO effects in organic materials, increasing useful device lifetime. The example shown (Figure 2.5.1) illustrates the

difference in thermal stability between an un-crosslinked dendrimer / chromophore composite sample and a sample that was cured through Diels-Alder “click-chemistry”-based crosslinking. A difference of 48 °C in thermal stability is observed between the two materials. These results illustrate both the utility of the crosslinking technique and the power of the *in-situ* TMT for material property characterization.

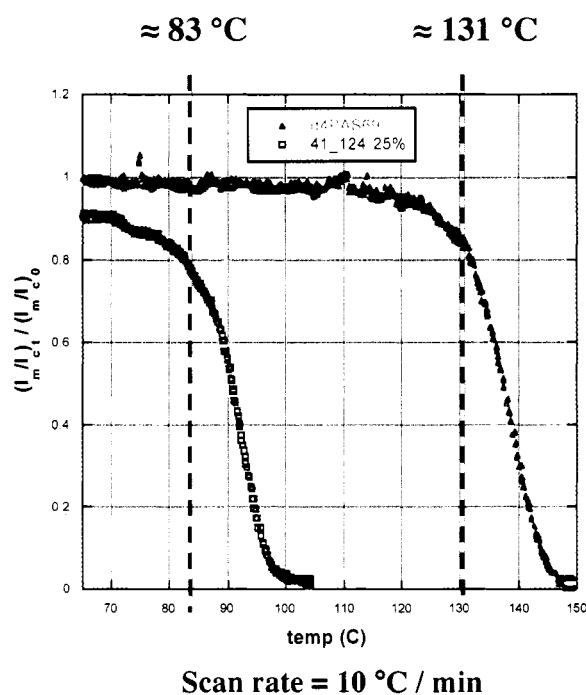


Figure 2.5.1 Dynamic thermal stability experiment performed on crosslinked (d4pas69) and uncrosslinked (41_124 25%) samples

In addition to dynamic thermal stability experiments, isothermal experiments were also very useful. Isothermal EO coefficient stability experiments were somewhat more precise. Similar to DSC experiments, dynamic experiment results varied slightly depending on the temperature ramp rate (10 °C / min is typical).

Isothermal data was also used in accordance with the time-temperature superposition principle for the study of the activation energies of thermal transitions in materials that display significant differences in glass transition behavior.^{5,7}

An isothermal experiment was performed by heating a poled sample at a stable, elevated temperature below its T_g , and monitoring I_m/I_c as a function of time. Data plotted for such an experiment is illustrated in Figure 2.5.2.

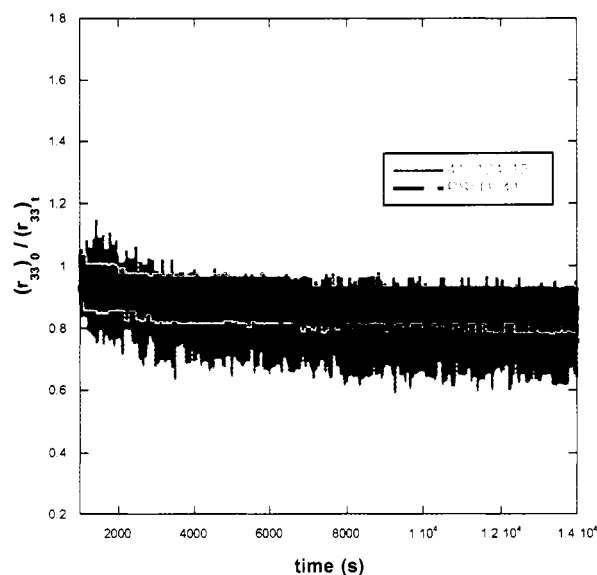


Figure 2.5.2 Isothermal r_{33} stability study performed at 65 °C over 4 hrs on pure dendrimer (PSLD_41) and doped dendrimer (41_124 15%) samples

2.6 Conclusions

The TMT or simple reflection ellipsometry technique represents a powerful and convenient tool for the evaluation of EO properties in electric field poled organic materials. Modification of the standard TMT to include *in-situ*, time-resolved monitoring allows quick optimization of processing conditions and brings about a

deeper understanding of EO mechanisms. Data obtained from isothermal r_{33} decay measurements clearly show Arrhenius decay behavior at temperatures below T_g . This type of behavior is very characteristic of a dipole orientational relaxation behavior.⁷

Unlike SHG experiments, the TMT experiment evaluates Pockels tensor elements directly. This increases the applicability of the findings to expected material behavior when incorporated into a finished photonic device. The *in-situ* TMT is a very powerful and convenient technique both for applied material science as well as fundamental study.

2.7 Experimental Section

Thin Film Fabrication And Spin Coating Procedures: ITO slides were half-masked with vinyl adhesive tape and etched by submersion in a 1:1 conc. HCl : DI-H₂O solution for 2 hours. The masking tape was removed and the slides were cut into 1 x 1 inch squares. Each 1-inch square (now half ITO coated) was individually washed using DI-H₂O and standard glassware detergent. The squares were then placed in a vertical holder and submerged in an ultrasonic bath filled with isopropyl alcohol. The squares were sonicated for 5 minutes. The cleaning bath was then changed to acetone and sonication was continued for an additional 5 minutes. The half-ITO squares were then removed and solvent evaporation was allowed. EO materials were dissolved in their respective spin coating solvents at the desired weight percent in pre-cleaned vials. The solutions were allowed to dissolve for the appropriate amount of time (several hours for APC) and then filtered using a 0.2- μ m

filter. Each slide was placed on the spin coater chuck and the full ITO area and half of the etched side were coated with EO material solution. The coating procedure was accomplished using a half-length Pastuer pipette held slightly above the slide surface. EO material solution was applied by coating in a circular motion from outside in. Samples were spun at appropriate speeds for each material, yielding 1 to 2 μm film thickness. Samples were soft-baked in air on a hotplate for 5 minutes at 75 °C and then cured under full vacuum at 65 – 85 °C for 12 hours. Film thicknesses were determined using a surface profilometer. Gold electrodes were then deposited directly atop the films ($\approx 120\text{ nm}$) by ion (sputter) coating, using a three-electrode mask. Each 1-inch square was then cut into three separate samples. Finally, wire leads were attached to the ITO and gold electrodes using silver paint.

Measurement Component Configuration for In-Situ TMT: The computer interface for the measurement was accomplished using a LabVIEW virtual instrument (vi). This vi controlled all of the various components of the instrument. The J-Kem Scientific Model 210 temperature controller was equipped with a T-type thermocouple and was interfaced using a serial RS232 port. The temperature controller regulated the heating rate of two 1/4 inch 100 watt, 120 volt AC cartridge heaters connected in parallel. The Newport Motion Controller (MM4005) was equipped with a Newport CMA-12pp linear actuator to cycle the SB compensator. The motion controller was computer interfaced using IEE-488 PCI-GPIB. A Keithley 6485 Picoammeter was employed for current measurement also through IEE-488 PCI-GPIB. Poling voltage was supplied by a Stanford Research Systems

PS350 / 5000V-25 W power supply. The sinewave modulation waveform was generated by a (Stanford Research Systems, DS335), 3.1 MHz synthesized function generator. The DC power supply, picoammeter, and function generator were interconnected using the bandpass filter circuit illustrated in Figure 2.7.1.

This filter circuit allowed for the simultaneous application of poling and modulation voltage according to Equation 2.4.1. The circuit contains built-in protection diodes to limit voltage across individual components. The 8.5 mW probe beam was produced by a 1310 nm diode laser (LaserMax, 1300-10). All optics and mounts were purchased through ThorLabs Inc. The output beam was detected using an InGAs photodetector. The detector signal was amplified using a low-noise preamplifier (Stanford Research Systems, SR570).

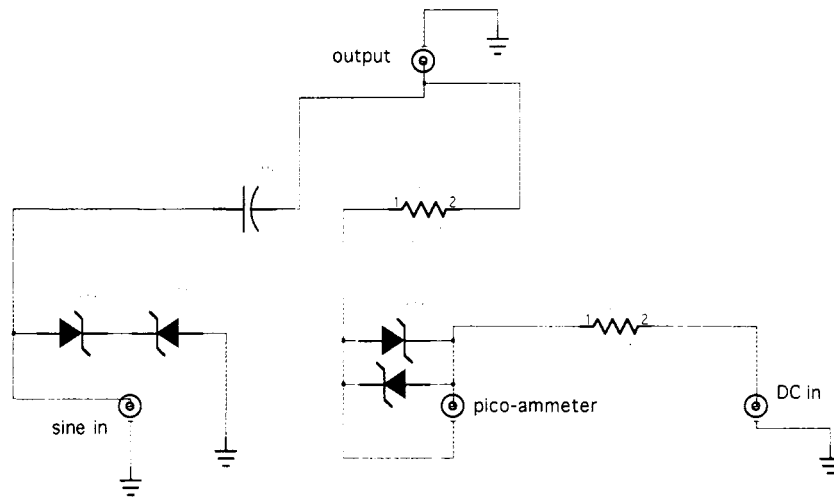


Figure 2.7.1: Bandpass filter circuit allowing DC bias of the modulation waveform

The modulated signal was measured by monitoring the amplifier output using a Lock-in-amplifier (Stanford Research Systems, SR830 DSP) synchronized to 1KHz using the function generator synch output. Outputs from the preamplifier and lock-in-amplifier were routed through a shielded connector block (National Instruments BNC-210) to a DAQ card (National Instruments NI-PCI-6036E). Poling and modulation voltages were monitored directly at the sample electrodes using an oscilloscope (Agilent, 54610B, 500 Mhz) with a 10 M Ω voltage probe.

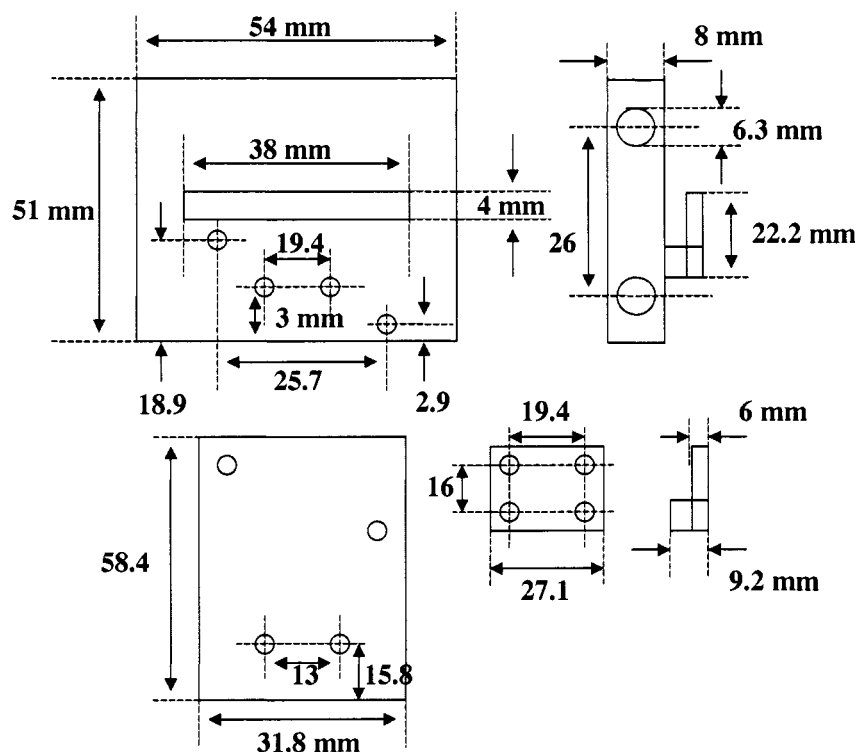


Figure 2.7.2: Schematic diagram of heating stage for sample attachment

Schematics for the sample stage are shown above in Figure 2.7.2. The assembly was mounted on a X – Y translation stage attached to a 360° rotation stage.

The rotation stage was set at 45° with respect to the probe beam. The cartridge heaters were inserted within the heating block and isolated from the mounting assembly by a thin teflon sheet.

In-situ Monitoring of the Poling Process: A sample was mounted onto the heating stage, glass side down, with the gold electrode placed over the horizontal slot. The probe beam was centered on the electrode using a 650 nm alignment beam. The irises were aligned to block the unwanted reflection from the glass surface. Electrode leads were then attached to the power terminals with the gold lead attached to the cathode minimizing charge injection. The sample chamber was then sealed and flushed with argon. A full SB compensator scan was performed in order to determine the position at which Ψ_{sp} led to I_c or half maximum intensity on the I_o curve. The compensator was then set to this position and stopped. A small voltage ($\approx 40 \text{ V}/\mu\text{m}$) was then applied using the DC power supply with the modulation voltage set to 10 volts peak-to-zero. A temperature ramp was then initiated along with LabVIEW data collection. Maximum I_m/I_c was observed just before T_{tr} . At T_{tr} a poling voltage drop was observed corresponding to an abrupt decrease in sample resistance according to Ohm's Law. This voltage drop was accompanied by a decrease in I_m/I_c indicating that optimum poling temperature had been surpassed. The data obtained was then plotted to give a graphical representation similar to Figure 2.3.2. From this plot, optimum poling temperature was determined, and poling conditions were revised accordingly. Following the optimized protocol, samples were treated as before. After poling, the samples were cooled to ambient

temperature, the E_p voltage was removed, leaving only V_m . The SB compensator was then returned to its zero position and scanned through its full range to calculate the resultant r_{33} .

Dynamic Thermal r_{33} Decay Experiment: A sample of EO material was poled as above. After the sample was equilibrated at room temperature and its r_{33} measured, its thermal stability was evaluated. The poling field was removed, and the SB compensator was again set to give an output intensity equal to I_c . The real-time LabVIEW monitor program was initiated and a temperature ramp was begun (10 °C / min). The I_m/I_c output was then recorded until a sharp drop ending in a near-zero value was recorded. The output was then normalized and plotted. The onset of the fast decay transition was noted as the dynamic thermal stability of the material.

Isothermal Elevated Temperature r_{33} Stability Measurement: Each EO material composition was poled as noted previously. A typical sample was poled using an optimized procedure. After optimum EO value was reached and the sample was equilibrated under heating, the thermal controller setpoint was reduced. The sample was allowed to cool to the desired temperature and the poling field was removed. The I_m/I_c ratio was then recorded for a predetermined time period. Thermally-induced decay rates were evaluated at a series of temperatures for each EO material. The data was then analyzed to determine various thermal stability parameters.⁵

Notes to Chapter 2

1. Teng, C. C.; Man, H. T., Simple reflection technique for measuring the electro-optic coefficient of poled polymers. *Applied Physics Letters* **1990**, *56*, (18), 1734-6.
2. Schildkraut, J. S., Determination of the electrooptic coefficient of a poled polymer film. *Applied Optics* **1990**, *29*, (19), 2839-41.
3. Michelotti, F.; Toussaere, E.; Levenson, R.; Liang, J.; Zyss, J., Real-time pole and probe assessment of orientational processes in electro-optic polymers. *Applied Physics Letters* **1995**, *67*, (19), 2765-7.
4. Liao, Y.; Anderson, C. A.; Sullivan, P. A.; Akelaitis, A. J. P.; Robinson, B. H.; Dalton, L. R., Electro-Optical Properties of Polymers Containing Alternating Nonlinear Optical Chromophores and Bulky Spacers. *Chemistry of Materials* **2006**, *18*, (4), 1062-1067.
5. Sullivan, P. A.; Akelaitis, A. J. P.; K., L. S.; McGrew, G.; Lee, S. K.; Choi, D. H.; Dalton, L. R., Novel Dendritic Chromophores for Electro-optics: Influence of Binding Mode and Attachment Flexibility on Electro-Optic Behavior. *Chem. Mater.* **2006**, *18*, 344-351.
6. Michelotti, F.; Nicolao, G.; Tesi, F.; Bertolotti, M., On the measurement of the electro-optic properties of poled side-chain copolymer films with a modified Teng-Man technique. *Chemical Physics* **1999**, *245*, (1-3), 311-326.
7. Michelotti, F.; Toussaere, E.; Levenson, R.; Liang, J.; Zyss, J., Study of the orientational relaxation dynamics in a nonlinear optical copolymer by means of a pole and probe technique. *Journal of Applied Physics* **1996**, *80*, (3), 1773-1778.
8. Shuto, Y.; Amano, M., Reflection measurement technique of electro-optic coefficients in lithium niobate crystals and poled polymer films. *Journal of Applied Physics* **1995**, *77*, (9), 4632-8.
9. Luo, J.; Haller, M.; Li, H.; Kim, T.-D.; Jen, A. K.-Y., Highly efficient and thermally stable electro-optic polymer from a smartly controlled crosslinking process. *Adv. Mater.* **2003**, *15*, (19), 1635-1638.
10. Lu, J.; Yin, J., Synthesis and characterization of photocrosslinkable, side-chain, second-order nonlinear optical poly(ester imide)s with great film-forming ability and long-term dipole orientation stability. *J. Polym. Sci., Part A: Polym. Chem.* **2002**, *41*, (2), 303-312.
11. Ma, H.; Chen, B.; Sassa, T.; Dalton, L. R.; Jen, A. K.-Y., Highly Efficient and Thermally Stable Nonlinear Optical Dendrimer for Electrooptics. *J. Am. Chem. Soc.* **2001**, *123*, (5), 986-987.

Chapter 3

Novel Dendritic Chromophores for Electro-optics; Influence of Binding mode and Attachment Flexibility on EO Behavior

Reproduced in part with permission from *Chem. Mater.* **2006**, 18, 344-351,
Copyright 2006 American Chemical Society

3.1 Introduction

Multichromophore dendritic EO materials were recently introduced as a method for forcing chromophore separation through steric interaction, thus reducing detrimental dipole interactions. These materials consist of EO-active, dipolar chromophores covalently bound to form a dendritic structure. This arrangement acts to site-isolate each active unit within the internal free volume created by the dendrimer.^{1, 2} Site isolation allows each individual chromophore to reorient more independently in response to the external poling field. This reduction of intermolecular electrostatic interactions allows for increased active chromophore number density in the formulation of a composite material, thus enhancing electro-optic response.³⁻⁵ Dendritic encapsulation, as well as the use of dendronized sidechain EO polymers created by post-functionalization, have recently been shown to lead to large EO coefficients and improved material qualities.⁶⁻⁹ EO materials in which active chromophores are covalently bound also present benefits such as reduction of chromophore-polymer phase separation, enhanced thermal stability of EO effects, and the possibility of using covalent attachment to augment external

ordering forces.^{10, 11} Covalent chromophore attachment may also be implemented to introduce initial asymmetry, or to scaffold innovative architectural design in order to facilitate supramolecular self-assembly. The degree of dipolar ordering within a covalently attached chromophore-host matrix, and the resulting macroscale properties, can be expected to be heavily dependant on subtle differences in architectural design.^{9, 12} It is thus necessary to explore such dependences in detail. In particular, in the design of photonic materials based on a dendritic architecture, there exist many fundamentally different possibilities for the covalent attachment of dipolar, high β chromophores to inert matrix building blocks. One important design feature is dipolar orientation with respect to the matrix or dendrimer core.¹³ A second is the nature, especially length, flexibility, and polarity, of the spacer group chosen to facilitate chromophore attachment.

To begin exploration of such fundamental architectural design parameters, four dendritic EO chromophores were designed, prepared, and evaluated. A set of two chromophores was first constructed incorporating a succinate di-ester, chromophore-core tether group. These dendritic chromophores were designed in such a way that they differed only in the dipolar orientation of the active units with respect to the chromophore-core tether group. In one dendritic chromophore the active unit dipoles were oriented normal to the tether group (side-on), and in the other they were oriented parallel to the tether group (end-on). The dendritic chromophores were also compared against the corresponding free chromophore FTC. To investigate the effects of tether group composition, and to more precisely compare thermal relaxation behavior, two additional dendritic chromophores were

then designed using information gathered thus far. These dendritic chromophores were again constructed in side-on and end-on fashion but with a longer, more flexible, mono-ester, chromophore-core tether group derived from a hexanoic acid.

A thiophene containing, FTC type chromophore was chosen as the EO active unit for construction of all dendritic chromophores in this study because of its robustness as well as its relatively large β value.⁵ Thin film composites of the dendritic compounds as well as FTC dispersed into amorphous polycarbonate (APC), were deposited atop ITO-coated glass substrates, and evaluated for differences in EO activity. The dynamic behavior of EO response was observed using an *in-situ* pole-and-probe, single beam polarization interferometry reflection apparatus.^{14, 15} Signal decay times were employed to estimate the activation energies associated with relaxation of the dipolar, chromophore lattice. The effect of binding geometry, and tether group composition on EO behavior was thus investigated.

3.2 Evaluation of EO Behavior as Dendrimer APC Composite Films

Each dendritic chromophore was mixed with solid APC (6.14×10^{19} chromophore active molecules in 0.09g of APC). The solid components were then dissolved into cyclopentanone (8% total solid weight). The solutions were stirred, filtered, and then spin-cast onto ITO coated glass slides. Film thicknesses were measured to be 2.2- 2.5 μm using a surface profilometer (KOSAKA, ET-3000). Gold was then deposited at the surface of the polymer-composite film to create both a reflective surface for measurement and an electrode for application of poling and modulating fields.

The EO measurement method used was a modification of the standard reflection technique used for measuring EO effects in thin films and calculating corresponding r_{33} values.^{16, 17} The experimental setup employed has been described more fully in chapter 2. For standard EO measurement the film was contact poled and an AC voltage (10 V_{rms} at 1 kHz) was applied to the sample.¹⁴ The modulated signal intensity (I_m) was simultaneously monitored. The linear EO coefficient r_{33} is directly proportional to I_m/I_c and was calculated using

$$r_{33} = \frac{3\lambda I_m}{4\pi V_m I_c n^2} \frac{(n^2 - \sin^2 \theta)^{\frac{1}{2}}}{\sin^2 \theta} \propto I_m/I_c \quad (3.2.1)$$

In this equation, n is the refractive index at the probe beam wavelength ($\lambda=1300$ nm), I_m is the amplitude of EO modulation, V_m is the AC voltage applied and I_c is the intensity of incident light where the phase retardation between T_E and T_M is 90°.

DC biased or *in-situ* measurements were performed by mounting the sample on a hot stage and applying a combination of a constant DC poling field (adjustable) and an AC modulating field, as represented by

$$V(t) = V_{DC} + V_0 \sin \omega t \quad (3.2.2)$$

This method allows for simultaneous poling and probing of the sample while monitoring sample temperature and current flow.

3.3 Physical and PhotoPhysical Properties of Succinic Ester Tether Based Multichromophore Dendrimers

The first two dendrimers (figure 3.3.1), were based on a 1,1,1-tris-(succinic acid phenyl ester)ethane core. This core incorporated a relatively short, inflexible, succinic acid ester, chromophore-core tether group.

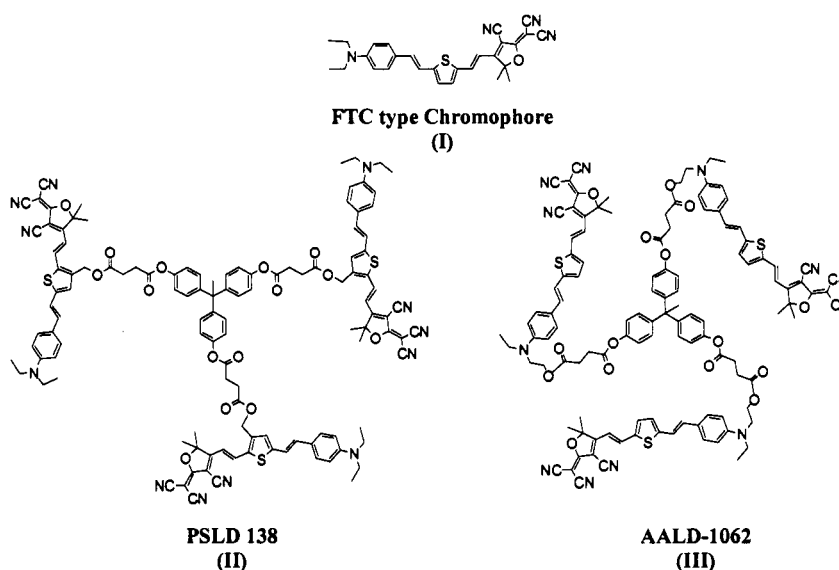
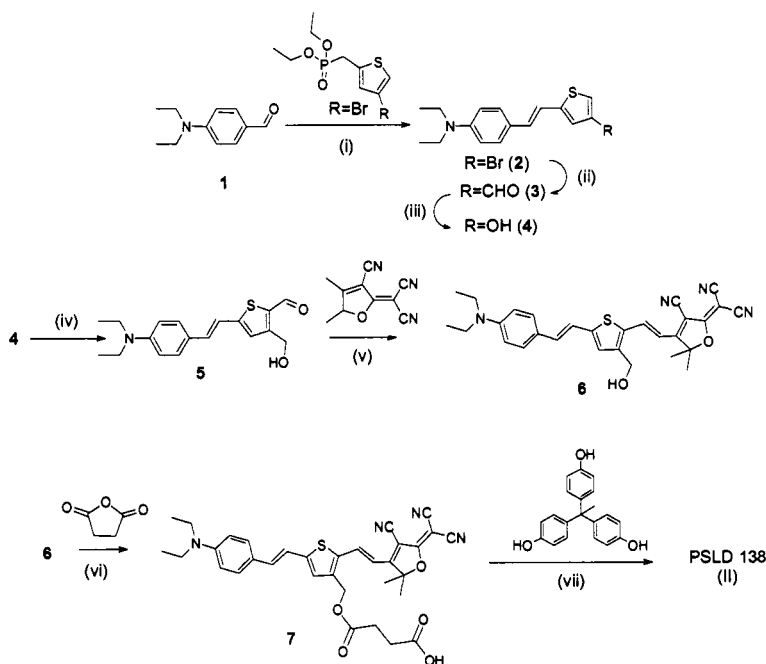


Figure 3.3.1: Free chromophore FTC (I), side-on dendritic chromophore (PSLD-138, II), and end-on dendritic chromophore (AALD-1062, III).

Synthesis of the side-on EO-active moiety (6), began by Horner-Emmons olefination of (4-bromo-2-thienylmethyl)phosphonate with aldehyde 1 to produce donor-bridge 2. In order to create an attachment point, a low temperature kinetic formylation reaction was used to produce aldehyde 3. The aldehyde was reduced quantitatively to give 3-hydroxymethylene substituted donor-bridge 4. Product 4 was then formylated once again to give structure 5. Knoevenagel condensation of the

2-cyanomethylene-3-cyano-4, 5, 5-trimethyl-2, 5-dihydrofuran (TCF) acceptor to aldehyde **5** was performed to yield chromophore **6**, as a copper-like solid.^{18, 19} The 3-hydroxymethylene unit in chromophore **6** was then used to ring-open succinic anhydride. This reaction produced the carboxylic acid functionalized chromophore **7**. Molecule **7** was then attached to 1,1,1-tris(4-hydroxy-phenyl)ethane to create the side-on dendritic chromophore PSLD- 138 (II, Scheme 1).

Scheme 3.3.1. Synthesis of side-on dendritic chromophore PSLD-138 (II)^a



^aConditions: (i) ^tBuOK, THF, RT overnight, 90% (ii) (a) n-BuLi, Et₂O -78 °C, 3hr; (b) DMF, RT, 18hr, 67% (iii) NaBH₄/NaOH, MeOH/THF 0 °C-RT, quant.) (iv) (a) n-BuLi, THF, -78 °C, 3hr (b) DMF, RT, 18hr, 87% (v) NH₄OAc/EtOH, 50 °C, 12hr (80%) (vi) DMAP, Py, DCM, RT, 6hr, 96% (vii) DCC/DPTS, THF/DCM, RT, 24hr, 88%.

Synthesis of the end-on type EO-active moiety (AALD-1062, compound III), proceeded in an analogous manner. The only variation was the creation of an attachment point on the donor side of the molecule rather than the bridge.

UV-visible absorption spectroscopy revealed that side-on compound II had a λ_{max} of 672 nm in chloroform solution and 655 nm in an APC film. This was very similar to FTC (I), which exhibited a λ_{max} of 672 nm in chloroform and 659 nm in APC film. End-on compound III showed a λ_{max} of 635 nm in chloroform and 627 nm in APC. This trend was also observed through cyclic voltametry analysis.²⁰ Free FTC records a HOMO-LUMO energy gap $E_g = 1.529$ eV, while the dendritic chromophores II and III were found to exhibit $E_g = 1.503$ eV, and $E_g = 1.606$ eV respectively. The largest energy gap was displayed by end-on compound III while side-on compound II displayed an energy gap similar to FTC. This difference can be understood by the presence of the electron withdrawing ester group at different sites on the dipolar, conjugated system. Such an explanation was supported by ^1H NMR data (Figure 2). Doublet b ($J_{\text{H-H}} = 15.5\text{Hz}$, trans C=C, 1H), can be assigned to vinylic protons closest to the chromophore electron-accepting moiety. These proton resonances exhibit a substantial downfield shift for side-on compound II. This shift is caused by a reduction of electron density at this site effected by the proximity of the ester tether group. Doublet a ($J_{\text{H-H}} = 8.3\text{Hz}$, phenyl, 2H), was assigned to phenyl ring protons closest to the amine electron-donor portion of the chromophore. Doublet a shows a relative downfield shift for protons in this position on end-on compound III. This shift results from attachment of the ester tether group close to the amine donor, reducing electron density at this site. The end-on attached system can be expected to

be affected to a greater extent due to more effective communication between the nonbonding nitrogen lone pair and π^* of the ester. No other pronounced shift differences were observed in proton resonances between dendritic EO-active moieties. These specific differences in ^1H NMR spectra support the hypothesis that observed differences in optical E_g can be attributed largely to intra-molecular effects rather than differing external interactions.

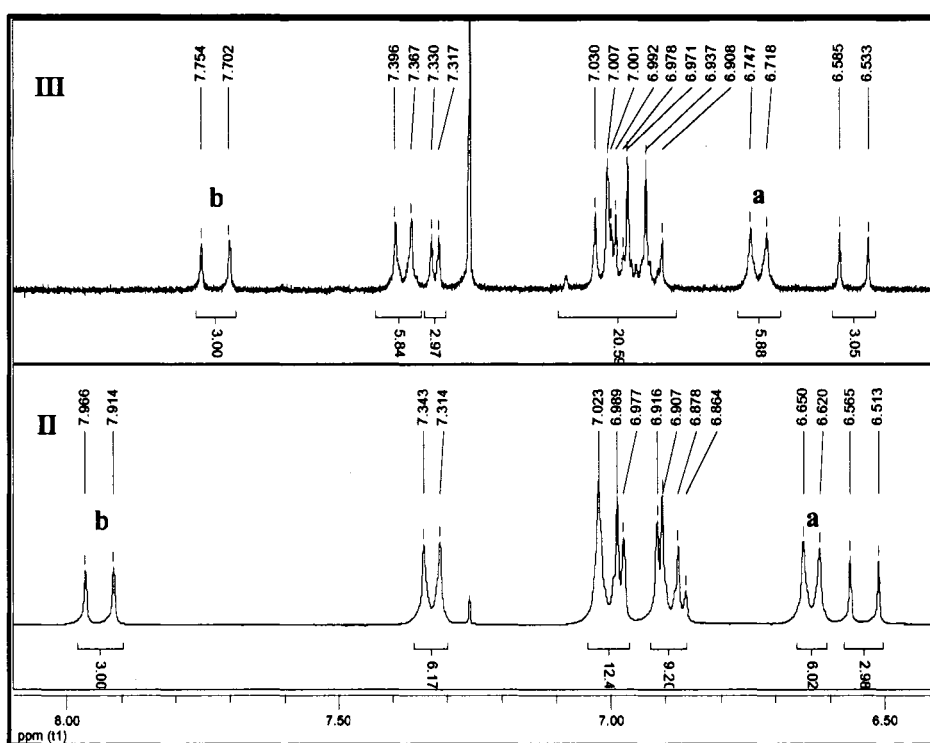


Figure 3.3.2: Aromatic region of ^1H NMR spectra of dendritic chromophores II and III

Variable angle spectroscopic ellipsometry measurements were performed on APC films containing FTC, and dendritic compounds II and III (6.14×10^{19} chromophore active molecules in 0.09 g of APC). These data were used in

combination with the absorption spectra of each film to accurately determine the real and imaginary part of refractive index at 1300 nm. Using consistent measurement conditions these samples containing FTC, side-on compound II, and end-on compound III, displayed refractive indices of 1.68, 1.64, and 1.62, respectively. The larger refractive index displayed by samples containing free chromophore FTC relative to samples containing dendritic compounds II and III, is consistent with a greater dielectric constant and larger 1st-order (linear) susceptibility. Due to a greater freedom of motion, bulk linear polarization is more easily induced in samples containing free chromophore FTC. Consistently, films containing side-on compound II display a higher refractive index than is recorded for samples containing end-on compound III. This refractive index data was then used for calculation of the EO coefficient.

Melting and glass transition temperatures were obtained for pure samples of the EO materials by differential scanning calorimetry. FTC displayed a melting and probable decomposition point at 242 °C, but showed no T_g . Dendritic chromophores II and III displayed almost identical T_g of 110 °C regardless of the difference in the binding mode of the chromophore. Additionally, measurements of a thermally stimulated flowing current were performed using APC films containing comparable loading of the active materials (concentration noted above). This experiment was used to determine the temperature at which an abrupt spike in current was observed under applied dc voltage. This “transition temperature” (T_{tr}), can be used to help determine the optimum poling temperature for the EO experiments. The Values of T_{tr} can be expected to correlate closely with the temperature required for an abrupt

increase in degree of molecular freedom within the host matrix corresponding to energy required to overcome intermolecular interactions such as Van der Waals forces. This T_{tr} is also an indication of proximity to the material dielectric breakdown point for a given temperature and electric field. The lowest temperature transition occurred for the sample containing FTC at 129 °C, followed by sample containing end-on III at 158 °C, then the highest by the sample of side-on II at 163 °C.

For the study of electro-optic activity, an equal number (concentrations noted previously) of active units (EO-active moieties) of pure materials FTC, succinic acid ester tether based dendritic chromophores side-on II, and end-on III were dissolved into amorphous polycarbonate (APC). In order to observe optimized EO coefficients as well as dynamic behavior, a real-time pole and probe modification to the simple reflection setup was used. Under a poling field of 70V/ μ m, FTC demonstrated the highest average r_{33} (≈ 25 pm/V) of the three, while samples containing side-on II and end-on III displayed lower average r_{33} values of ≈ 9 , and ≈ 5 pm/V, respectively.

For the purpose of evaluating the temperature at which dipolar relaxation, or loss of EO signal is initiated, a dynamic, thermally induced relaxation experiment was performed. Fresh films of dendrimers II and III, as well as FTC in APC were poled to reach their respective maximum EO signal as previously described. The samples were cooled with continued application of the DC poling field. The poling field was then removed and a temperature ramp (5 °C / min) was initiated while observing I_m/I_c . The resulting data traces were normalized and plotted against one another. Data corresponding to thin film APC composites of FTC (I), succinic acid based side-on (II), and end-on (III), is shown in figure 3.3.3.

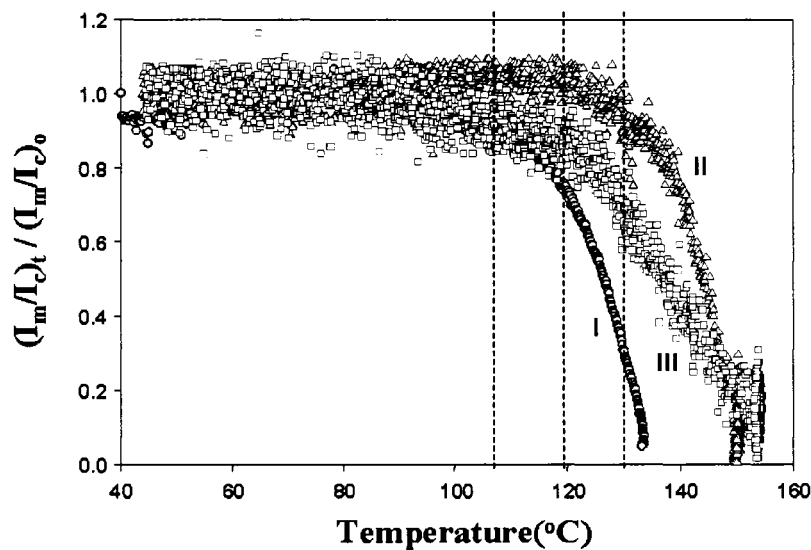


Figure 3.3.3: Thermally induced EO signal decay transitions for APC films containing side-on (II), and end-on (III) dendritic chromophores, as well as FTC (I)

The data shows that the highest temperature was required to initiate abrupt dipolar relaxation in the side-on attached dendritic chromophore II samples (approximately 130 °C). A temperature of approximately 110 °C was required to initiate fast relaxation of a sample containing FTC, and 120 °C was required for samples of end-on III. This suggested that the activation energy required for dipole relaxation and thus randomization was smaller for the end-on than for the side-on dendrimer samples.

An isothermal decay study at 105 °C was also performed using APC samples containing FTC, and each of the two succinic acid based dendritic chromophores (Figure 4).

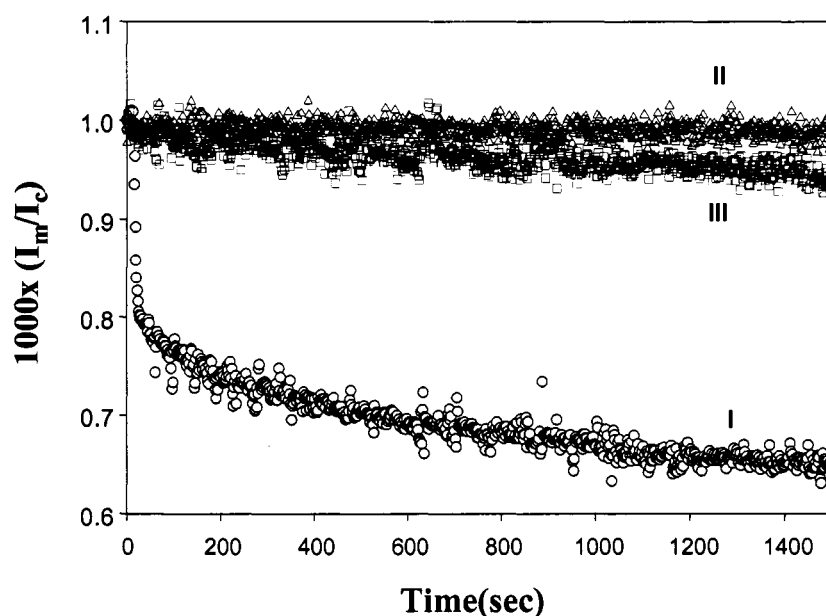


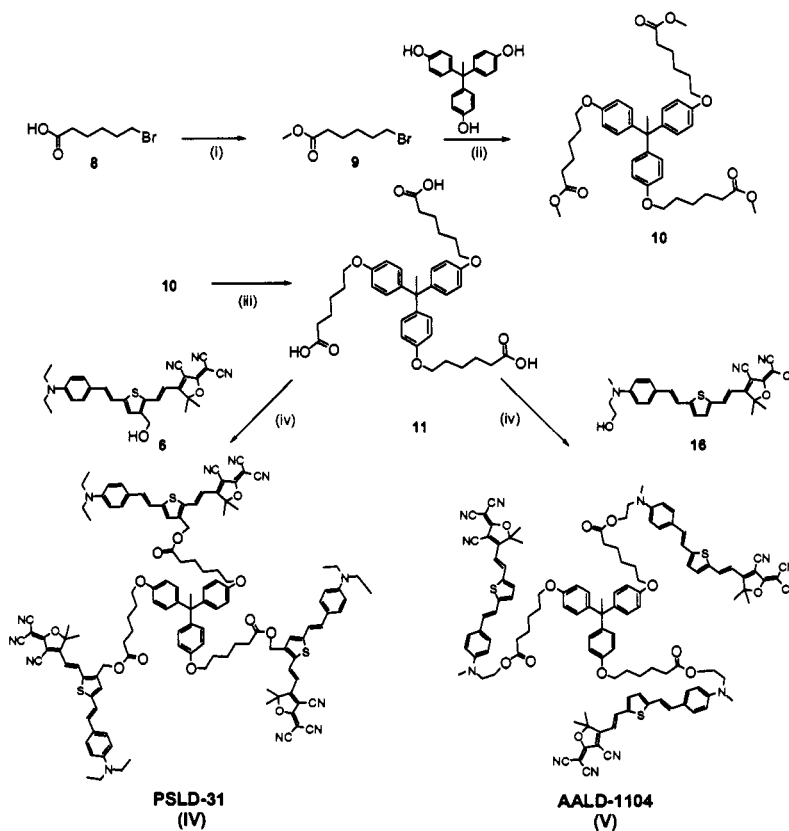
Figure 3.3.4: Isothermal EO stability data for APC films containing, FTC (I), succinic acid tether based side-on (II), and end-on (III) * Temperature : 105 °C

Conditions similar to those that could be encountered by a working EO device were approximated by this experiment. After poling, the samples were cooled to 105 °C, and the EO signal decay was monitored with respect to time. The data obtained shows that the dendrimer systems indeed demonstrate much more thermally stable EO properties than the simple guest-host system exemplified by FTC / APC composites. The sample composed of FTC in APC shows a fast and dramatic decay whereas the decay rate is greatly retarded for samples composed of dendritic chromophores in APC.

3.4 Physical and PhotoPhysical Properties of Hexanoic Acid Ester Tether Based Multichromophore Dendrimers

Noting the greatly lowered EO activity of the succinic acid tether group based dendritic chromophores compared to their free chromophore counterpart, a longer, more flexible, tether unit seemed desirable. In order to realize this idea, two new dendritic chromophores were designed and synthesized based on a 1,1,1-tris-(6-phenoxy-hexanoic acid ester)ethane core.

Scheme 3.4.1: Synthetic scheme for hexanoic acid ester based dendritic chromophores IV and V^a



^aConditions: (i) H₂SO₄, MeOH, overnight, Quant. (ii) NaH, DMF, 90 °C, 12hr, >99% (iii) NaOH, Acetone, 5hr, 89% (iv) DCC, DPTS, CH₂Cl₂, 24hr, RT, 25-68%

Synthesis of PSLD-31 (side-on dendrimer IV), and AALD-1104 (end-on dendrimer V) is illustrated in scheme 3.4.1. Esterification of 6-bromo-1-hexanoic acid (**8**), was performed overnight using methanol and catalytic sulfuric acid to yield 6-bromo-1-hexanoic acid methyl ester (**9**). The standard Frechet-type tri-phenol core, (1,1,1-tris(4-hydroxy-phenyl)ethane), was then tri-functionalized with **9** using sodium hydride under Williamson conditions to produce **10**. This tri-ester core was then saponified to produce 1,1,1- tris(6-phenoxy-hexanoic acid)ethane (**11**), a compound bearing three carboxylic-acid terminated, highly flexible, aliphatic tether groups. Side-on type chromophore (**6**) bearing a center-affixed hydroxyl group, identical to that of the active moiety in side-on compound II, was then attached to each tether group again under mild esterification conditions to yield hexanoic acid ester (HE) tether group based, side-on, 1st generation dendrimer PSLD-31 (IV). A similar procedure was followed in preparation the HE-end-on, 1st generation dendrimer AALD-1104 (V). Both dendritic materials were obtained as metallic blue solids. Side-on IV exhibited a $\lambda_{\text{max}} = 679$ nm in CHCl_3 , somewhat red-shifted relative to a $\lambda_{\text{max}} = 640$ nm for end-on V. This data was consistent with the previous succinate ester based dendrimers. Both side-on IV and end-on V were dissolved into solutions of APC and cyclopentanone so that each formulation contained an equal number of active molecules with respect to weight of APC, in the same concentration as above. Thin film samples were then fabricated using the new dendrimers.

Thermally Stimulated Current (TSC) transition temperatures (T_{tr}) were observed as before. Unlike the previous succinate ester based dendritic chromophores II and III, the new compounds IV and V displayed significantly different T_{tr} values. Samples composed of side-on dendritic chromophore IV in APC show a T_{tr} of approximately 120 °C. End-on V in APC displayed T_{tr} of approximately 110 °C. As before, higher poling temperatures were required for Side-on IV based samples under the same poling field. Thermal analysis by DSC also revealed a lower T_g of 90 °C for pure end-on compound V while pure side-on IV displayed a T_g of 125 °C.

Table 3.4.1: Average and maximum r_{33} values for Succinate dendritic chromophores II and III, and hexanoic-acid ester dendritic chromophores (IV and V), and free chromophore FTC, doped into APC.

Compound	Spacer	$E_p(V/\mu m)$	$T_g(^{\circ}C)$	Time(min)	Max $r_{33}(pm/V)$	Ave. $r_{33}(pm/V)^a$
Side-on II	diester	70	110	15	10	9
End-on III	diester	70	110	15	7	5
Side-on IV	HE	70	125	15	35	27
End-on V	HE	70	90	15	26	20
FTC	-	70	-	15	30	25

^aAverage value of 5 fresh samples poled under identical conditions.

Observation of equilibrium EO values revealed that under identical experimental conditions, differences in r_{33} between side-on and end-on geometries were small, but they were consistent over multiple samples. The average r_{33} value

obtained for samples of side-on IV under a DC poling field of 70 V/ μm was 27 pm/V. The average r_{33} for end-on V was 20 pm/V. EO properties are tabulated in table 3.4.1, a maximum r_{33} value is shown in addition to an average determined from the values of five freshly poled samples in order to illustrate approximate range in r_{33} . The values obtained using hexanoic acid tether based dendritic chromophores IV and V represent a significant improvement over previous succinic acid tether based dendritic chromophores II and III.

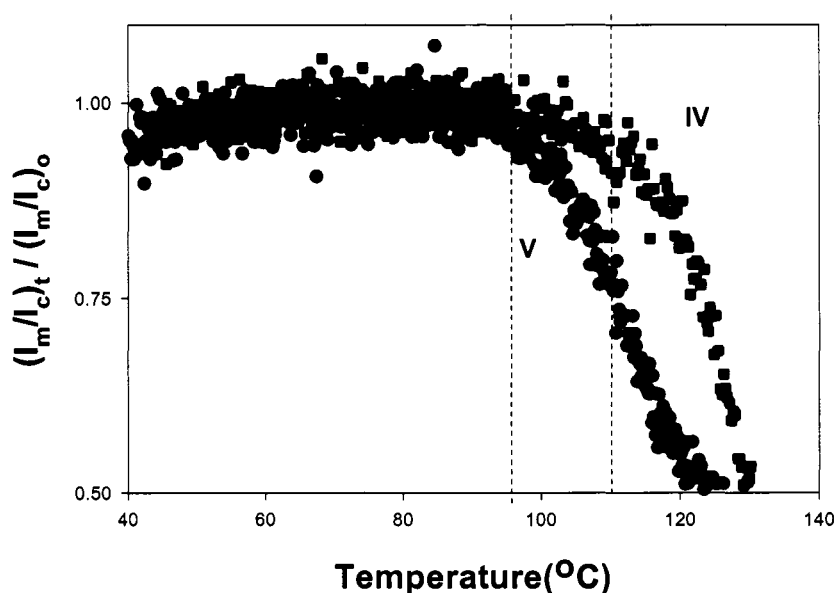


Figure 3.4.1: Thermally induced EO signal decay transitions for APC samples containing hexanoic acid tether based dendritic chromophores IV and V heated at a ramp rate of 10 °C/min

Dynamic thermal decay experiments were again performed using samples of the new materials. The resulting data shows that a higher temperature was again required to initiate abrupt dipolar relaxation in the side-on attached dendrimer IV

samples. Somewhat lower temperatures were required to initiate fast decay in samples of dendrimers IV and V than in samples containing dendrimers II and III. This behavior was expected due to the more aliphatic nature (longer chain length and increased flexibility) of the hexanoic acid ester tether in IV and V. A temperature of approximately 108 °C was required to initiate fast relaxation of a sample containing end-on V, and 114 °C was required for samples of side-on IV. Again the side-on type compound consistently displayed a more thermally stable EO signal (figure 3.4.1).

In order to more precisely compare average activation energies for initiation of dipolar relaxation between the side-on and end-on binding geometries, EO decay curves of the two new hexanoic acid tether group based compounds were recorded at various elevated temperatures, normalized, and plotted. Data was gathered for samples containing dendritic chromophores IV and V at experimental temperatures of 109, 114, 119 °C. These data were then analyzed by curve fitting, using the Kohlrausch-Williams-Watts (KWW) stretched exponential function.

$$(I_m / I_c)_t = (I_m / I_c)_\infty + \Delta(I_m / I_c) \exp(-t / \tau)^\beta \quad (3.4.1)$$

Where τ represents relaxation time, and β represents a stretching parameter.

The KWW function yields an average relaxation time $\langle \tau \rangle$ given by^{21, 22}

$$\langle \tau \rangle = (\tau / \beta) \Gamma(1 / \beta) \quad (3.4.2)$$

Activation energies (Kcal/mol) for dipolar relaxation were then estimated from a linear plot of $\log \langle \tau \rangle$ vs. $1/T$. Isothermal decay data for APC samples containing compounds IV and V are depicted in figure 3.4.2.

Comparison of average relaxation times $\langle\tau\rangle$, reveals that side-on IV exhibits much larger average activation energies (303 Kcal/mol compared to 125 Kcal/mol, (table 3.4.2). This data emphasizes the point that the side-on chromophore attachment geometry provides improved thermal EO signal stability when compared with the end-on attached arrangement.

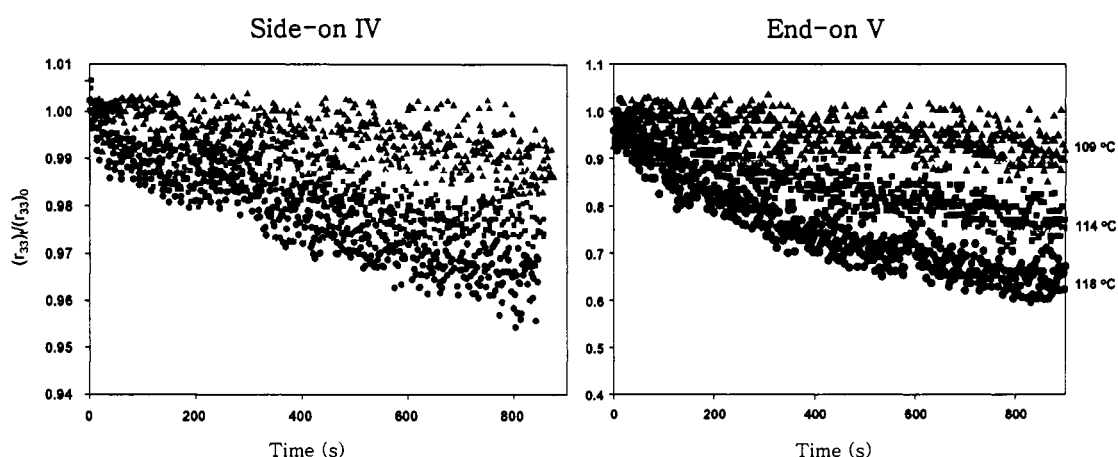


Figure 3.4.2: Data plots depicting EO decay of poled APC samples containing dendritic chromophores IV and V heated at constant temperatures of 109, 114, and 118 °C.

As an amorphous polymeric film is heated near its glass transition, molecular motion rates may be expected to increase abruptly by nearly 10 orders of magnitude.²³ This high rate of molecular motion promotes both ordering in the presence of an electric field, and relaxation to a preferred state without. The energy required to cause this increase in average molecular motion depends on many factors. These factors may include polymer main chain rigidity, degree of branching, free volume, chromophore binding mode, and chromophore electrostatic

interactions.^{23, 24} Upon poling, the dipolar order induced within the guest-host, dipolar chromophore system induces intra- and intermolecular strain. The nature and magnitude of this strain is strongly dependent on chromophore shape, and the nature of the interaction of the dipolar unit with its surroundings.

Table 3.4.2: Isothermal decay data: relaxation time (τ), average relaxation time ($\langle\tau\rangle$), stretching parameters (β), and activation energies (E_a), for dendritic chromophores IV, and V

temperature	end-on V			side-on IV		
	τ (s)	$\langle\tau\rangle$ (s)	b	τ (s)	$\langle\tau\rangle$ (s)	b
118 °C	47.39	817.54	0.337	133.37	666.57	0.3506
114 °C	67.66	1369.50	0.300	454.55	14354.25	0.227
109 °C	409.33	32669.02	0.256	2327.21	6037700.72	0.150
E_a (Kcal/mole)		124.57			302.84	

3.5 Conclusions

Four novel dendritic chromophores were synthesized. These dendritic EO-active materials were dispersed into APC and tested as thin-film composites using a real-time, in-situ pole and probe EO measurement apparatus. The results demonstrate a dependence of EO behavior on chromophore tethering orientation. The side-on type dendritic chromophore showed greater thermal stability (higher activation energy for dipolar randomization), than the end-on. The differences in average r_{33} between side-on and end-on geometries were rather small but consistent. EO behavior was shown to depend heavily on the length and rigidity of the moieties used to covalently anchor the chromophore to the inert host or core. A nearly three-fold enhancement in EO coefficient was noted when the short-diester tether group was replaced by a longer,

more aliphatic system. Changes in tether group rigidity might be expected to also affect the magnitude of the r_{33} difference between side-on and end-on attachment geometry but the data obtained suggest that these effects are small. The major differences are observed in thermal stability data. The hexanoic acid based molecules IV and V displayed r_{33} values that were very comparable to those of FTC while maintaining much improved thermal EO stability. All four dendrimer systems exhibited much slower thermally induced EO signal decay rates as compared to free chromophore FTC. This study demonstrates the importance of seemingly subtle design changes in the nanoscale architecture of dendritic chromophore systems for 2nd-order nonlinear optics. It also suggests intelligently designed dendritic EO chromophores as promising candidates for further development.

In future experiments we seek to further explore the use of these dendritic effects in the rational design of new materials with greatly amplified EO coefficients. Incorporation of chromophores with enhanced hyperpolarizabilities is in progress. In addition, amplification of the dendrimer site-isolation effect can be achieved through the addition of bulky second-generation dendrons to the outer periphery, thereby increasing the degree of chromophore encapsulation. The use of an optically inert host polymer matrix inherently reduces EO material performance through restrictive effects, compatibility problems, and reduced active chromophore content per unit volume. An attractive goal and potential improvement may be found in polymer-free, all dendrimer thin-films. In addition to the high thermal stability of EO effects demonstrated by dendritic chromophore architectures, lattice hardening chemistry can be envisioned to further improve thermal properties.

3.6 Experimental Section

General: All commercially available starting materials were purchased from Aldrich, or ACROS Co. and used without further purification unless otherwise stated. HPLC grade tetrahydrofuran and diethyl ether were purchased from Fisher chemical and distilled from sodium and benzophenone immediately before use. HPLC grade methylene chloride was also purchased from Fisher and distilled from CaH prior to use.

All reactions were performed under an argon atmosphere unless otherwise stated. Alkyl lithium reagents were purchased from ACROS and titrated using 4-biphenylmethanol according to literature method.²⁵ Diethyl (4-bromo-2-thienylmethyl)phosphonate, diethyl (2-thienylmethyl)phosphonate,²⁶ and 2-cyanomethylene-3-cyano-4,5,5-trimethyl-2,5-dihydrofuran (TCF),²⁷ were prepared according to literature procedure.

Synthetic details for Succinate acid ester based dendritic chromophores II and III;

{4-[2-(4-Bromo-thiophen-2-yl)-vinyl]-phenyl}-diethyl-amine (2): An oven dried, mag.-stirred, 250 mL RBF was charged with a solution of diethyl-4-bromo-2-thienylmethylphosphonate (29.0 g, 93.0 mmol), and 4-(*N,N*-

diethylamino)benzaldehyde (11.0 g, 62.1 mmol) in 100 mL freshly distilled THF.

Potassium *tert*-butoxide (105 mL, 1.00 M soln. in THF) was added dropwise over 0.5 hr. The mixture was allowed to stir for 12 hrs and 100 mL NaCl (sat'd) was added. The organic phase was separated and extracted with dichloromethane (DCM). The organics were then combined and dried over MgSO_4 , filtered, and the solvent was removed *in vacuo*. The resulting crude product was then purified by silica gel column chromatography (5% EtOAc/Hexane) to yield 10.0 g (99.0%) of a bright yellow solid. m.p.= 80 °C, ^1H NMR (300.1 MHz, CDCl_3): δ (ppm) 7.36 (d, J = 8.73 Hz, 2H), 7.02 (s, 1H), 6.95 (d, J = 16 Hz, 1H), 6.89 (d, J = 16 Hz, 1H), 6.46 (d, J = 8.73 Hz, 2H), 3.41 (q, J = 6.9 Hz, 4H), 1.22 (t, J = 6.9 Hz, 6H).

^{13}C NMR (75 MHz, CDCl_3): δ (ppm) 147.77, 145.10, 130.11, 127.99, 126.14, 123.55, 119.64, 115.59, 111.33, 110.01, 44.42, 12.68.

HRMS (ESI): exact mass calcd for $\text{C}_{16}\text{H}_{19}\text{BrNS}$ $[\text{M}+\text{H}]^+$, 336.0404. Found, 336.0409.

5-[2-(4-Diethylamino-phenyl)-vinyl]-thiophene-3-carbaldehyde (3): A solution of *n*-BuLi (1.6 M in hexanes) was titrated using 4-biphenyl methanol as the indicator and found to be 1.20 M.¹ An oven dried, mag.-stirred 250 mL RBF was charged with 3-bromo-5-{4-[*N,N*-diethylamino]styryl}thiophene (**2**) (9.10 g, 27.1 mmol). This was dissolved in 100 mL freshly distilled diethyl ether and was then cooled to -78 °C (dry ice/acetone). The *n*-BuLi (22.0 mL, 27.1 mmol) was then added dropwise over 15 min. The reaction temp was raised slightly by addition of more acetone to the bath. The reaction was stirred for 10 min. and then quenched with dry

DMF (20.2 mL, 260 mmol) by dropwise addition. The cooling bath was removed for 10 min. and then NH_4Cl (sat'd, 100 mL) was added. The organics were separated and the aqueous phase was extracted with EtOAc. The organics were then combined, dried of MgSO_4 , and the solvent removed *in vacuo*. The crude product was purified by silica gel column chromatography (5% EtOAc/Hexane) to yield 7.0g (90%) of a non-flourescent, yellow, crystalline solid. m.p. = 84 °C

^1H NMR (300.1 MHz, CDCl_3): δ (ppm) 9.84 (s, 1H), 7.88 (d, J = 9 Hz, 1H), 7.36 (m, 3H), 6.98 (d, J = 16 Hz, 1H), 6.90 (d, J = 16 Hz, 1H), 6.67 (d, J = 9 Hz, 2H), 3.41 (q, J = 6.9 Hz, 4H), 1.21 (t, J = 6.9 Hz, 6).

^{13}C NMR (75 MHz, CDCl_3): δ (ppm) 184.99, 147.87, 146.15, 143.41, 134.54, 131.19, 128.05, 123.34, 120.86, 115.67, 111.61, 44.41, 12.65.

HRMS (ESI): exact mass calcd. for $\text{C}_{17}\text{H}_{20}\text{NOS}$ $[\text{M}+\text{H}]^+$, 286.1266. Found, 286.1255.

{5-[2-(4-Diethylamino-phenyl)-vinyl]-thiophen-3-yl}-methanol (4): A 250 mL, 2-neck, mag.-stirred, RBF was equipped with an addition funnel and charged with NaBH_4 (0.400 g, 10.5 mmol). An aqueous solution of NaOH (8 mL, 0.2N) was then added and the mixture was cooled to 0 °C (ice bath). A solution of 5-[2-(4-diethylamino-phenyl)-vinyl]-thiophene-3-carbaldehyde (3) (7.00 g, 24.6 mmol) dissolved in 1:1 THF/MeOH (40 mL) was then added dropwise. The reaction was stirred for 30 minutes and the cooling bath was removed. After 1 hour the reaction was quenched by the slow addition of NH_4Cl (sat'd). The organics were separated and the aqueous phase was extracted with EtOAc. The organics were then combined,

dried of MgSO₄, and the solvent removed *in vacuo*. The reaction was quantitative by NMR and the product was used without further purification. m.p. = 97 °C

¹H NMR (300.1 MHz, CDCl₃): δ (ppm) 7.36 (d, *J* = 9 Hz, 2H), 6.99 (m, 3H), 6.87 (d, *J* = 16 Hz, 1H), 6.68 (d, *J* = 9 Hz, 2H), 3.91 (q, *J* = 7.2 Hz, 4H), 1.19 (t, *J* = 6.9 Hz, 6H).

¹³C NMR (125.1 MHz, CDCl₃): δ (ppm) 147.5, 145.01, 142.70, 129.05, 127.78, 123.94, 119.41, 116.93, 111.73, 60.88, 44.42, 12.62.

HRMS (ESI): exact mass calcd. for C₁₇H₂₂NOS [M+H]⁺, 288.1422. Found, 288.1408.

5-[2-(4-Diethylamino-phenyl)-vinyl]-3-hydroxymethyl-thiophene-2-

carbaldehyde (5): In a 250mL, oven dried, mag.-stirred RBF, {5-[2-(4-diethylamino-phenyl)-vinyl]-thiophen-3-yl}-methanol (**4**) (5.61 g, 19.5 mmol) was dissolved in freshly distilled THF (30 mL). The solution was then cooled to -78 °C (dry ice/acetone). n-BuLi (40.7 mL, 48.9 mmol, 1.2M sol'n. in hexanes) was then added dropwise over 15 minutes. After addition a light green color was observed. The mixture was allowed to stir for 1 hour and then quenched with dry DMF (7.57 mL, 97.7 mmol). The reaction was allowed to warm to room temperature overnight. A saturated solution of NaCl (100 mL) was then added. The organics were separated and the aqueous phase was extracted with DCM. The organics were combined, dried of MgSO₄, and the solvent removed *in vacuo*. The crude product was purified by silica gel column chromatography (5% EtOAc/DCM) to yield 5.35g (87%) of a red, oily, solid. m.p. = 125 °C

^1H NMR (300.1 MHz, CDCl_3): δ (ppm) 9.82 (s, 1H), 7.39 (d, $J = 9$ Hz, 2H), 7.09 (d, $J = 15.9$ Hz, 1H), 7.04 (s, 1H), 6.92 (d, $J = 15.9$ Hz), 6.65 (d, $J = 9$ Hz, 2H), 4.83 (s, 2H), 3.40 (t, $J = 7.2$ Hz, 4H), 1.21 (t, $J = 6.9$ Hz, 6H).

^{13}C NMR (125.1 MHz, CDCl_3): δ (ppm) 182.27, 154.31, 151.46, 148.39, 133.95, 128.78, 126.42, 122.75, 115.19, 111.53, 59.50, 44.46, 12.66.

HRMS (ESI): exact mass calcd for $\text{C}_{18}\text{H}_{22}\text{NO}_2\text{S}$ $[\text{M}+\text{H}]^+$, 316.1371. Found, 316.1365.

2-[3-Cyano-4-(2-{5-[2-(4-diethylamino-phenyl)-vinyl]-3-hydroxymethyl-thiophen-2-yl}-vinyl)-5,5-dimethyl-5H-furan-2-ylidene]-malononitrile (6): A mag.- stirred, 25mL RBF was charged with 5-[2-(4-diethylamino-phenyl)-vinyl]-3-hydroxymethyl-thiophene-2-carbaldehyde (**5**) (5.00 g, 15.8 mmol), 3-cyano-5,5-dimethyl-2-dicyanomethylene-4-methyl-2,5-dihydrofuran (TCF) (3.48 g, 17.4 mmol), and NH_4OAc (≈ 10 mol%). This mixture was dissolved in 60 mL absolute ethanol. The reaction was heated to 50°C overnight. The ethanol was removed *in vacuo* and the crude product was purified by silica gel column chromatography (10% EtOAc/DCM) to afford 5.30g (67%) pure product. m.p. = 220°C

^1H NMR (500 MHz, CDCl_3): δ (ppm) 8.13 (d, $J = 15.5$ Hz, 1H), 7.45 (d, $J = 9$ Hz, 2H), 7.20 (s, 1H), 7.19 (d, $J = 16$ Hz, 1H), 7.14 (d, $J = 16$ Hz, 1H), 6.67 (d, $J = 9$ Hz, 2H), 6.53 (d, $J = 15.5$ Hz, 1H), 4.66 (s, 2H), 3.39 (q, $J = 7$ Hz, 4H), 1.75 (s, 6H), 1.12 (t, $J = 7\text{Hz}$, 6H).

^{13}C NMR (125.1 MHz, CDCl_3): δ (ppm) 177.28, 174.65, 154.33, 152.87, 148.76, 138.44, 135.14, 132.68, 129.70, 128.79, 123.03, 115.96, 113.59, 112.83, 112.10, 111.87, 111.25, 98.71, 95.25, 58.20, 52.81, 44.27, 26.08, 13.00.

HRMS (ESI): exact mass calcd for $\text{C}_{29}\text{H}_{30}\text{N}_4\text{O}_2\text{S}$ $[\text{M}+\text{H}]^+$, 497.2011. Found, 497.2005.

Succinic acid mono-{2-[3-Cyano-4-(2-{5-[2-(4-diethylamino-phenyl)-vinyl]-3-hydroxymethyl-thiophen-2-yl}-vinyl)-5,5-dimethyl-5H-furan-2-ylidene]-malononitrile }ester (7): An oven dried, mag. stirred, 100 mL RBF was charged with chromophore (6) diethyl-donor functionalized FTC (4.00 g, 8.06 mmol), succinic anhydride (1.21 g, 12.1 mmol), and DMAP (1.00 g, 8.06 mmol). This mixture was then dissolved in 100 mL of freshly distilled methylene chloride. Dry pyridine (2.00 mL, excess) was added dropwise. Pyridine was previously distilled under reduced pressure and stored over solid KOH. The reaction was stirred for 6 hours, followed by TLC (20% EtOAc/DCM), and then diluted with NH_4Cl (sat'd), and the organic phase was separated. The organics were then washed with DI water and the solvent was removed *in vacuo*. The crude product was purified by silica gel column chromatography using a solvent step gradient starting with 10% EtOAc/DCM to remove S.M. and moving to 10% MeOH/DCM to elute product. Purification yielded 5.2 g (100%) of a blue solid. m.p. = 208 °C

^1H NMR (300 MHz, CDCl_3): δ (ppm) 7.94 (d, J = 15.6 Hz, 1H), 7.36 (d, J = 9 Hz, 2H), 7.03 (s, 1H), 7.029 (d, J = 15.6 Hz, 1H), 6.91 (d, J = 15.6 Hz, 1H), 6.66

(d, $J = 9$ Hz, 2H), 6.55 (d, $J = 15.6$ Hz, 1H), 5.18 (s, 2H), 3.42 (q, $J = 7.2$ Hz, 4H), 2.68 (s, 4H), 1.75 (s, 6H), 1.21 (t, $J = 6.9$ Hz, 6H).

^{13}C NMR (75 MHz, CDCl_3): δ (ppm) 175.71, 173.40, 172.28, 152.84, 148.83, 148.19, 144.65, 137.47, 136.73, 135.26, 134.81, 129.22, 128.79, 124.32, 122.63, 114.94, 112.36, 112.19, 111.71, 111.67, 110.99, 97.34, 96.58, 58.34, 55.51, 44.54, 29.16, 26.48.

HRMS (ESI): exact mass calcd for $\text{C}_{33}\text{H}_{33}\text{N}_4\text{O}_5\text{S}$ $[\text{M}+\text{H}]^+$, 597.2171. Found, 597.2169.

1,1,1-Tris-(succinic acid mono-{2-[3-Cyano-4-(2-{5-[2-(4-diethylamino-phenyl)-vinyl]-3-hydroxymethyl-thiophen-2-yl}-vinyl)-5,5-dimethyl-5H-furan-2-ylidene]-malononitrile} ester-phenyl) ethane (PSLD-138, side-on dendritic chromophore II): An oven dried, mag.- stirred, 100mL RBF was charged with (7) (4.88 g, 8.20 mmol), 1,3-dicyclohexylcarbodiimide (1.79 g, 8.66 mmol), DPTS (0.69 g, 2.34 mmol), and 1,1,1-tris(4-hydroxy-phenyl)ethane (0.72 g, 2.34 mmol). This mixture was dissolved in a mixture of freshly distilled THF (75 mL) and DCM (75 mL). The reaction was stirred overnight, washed with NaCl (sat'd) and then DI water. The organic phase was separated and dried over MgSO_4 and concentrated *in vacuo*. The dark blue crude residue was then purified by silica gel column chromatography (5% THF/DCM) to yield 4.21g (88%) of a deep blue solid. $T_g = 110^\circ\text{C}$, $\lambda_{\text{max}} (\text{CHCl}_3) = 672\text{nm}$

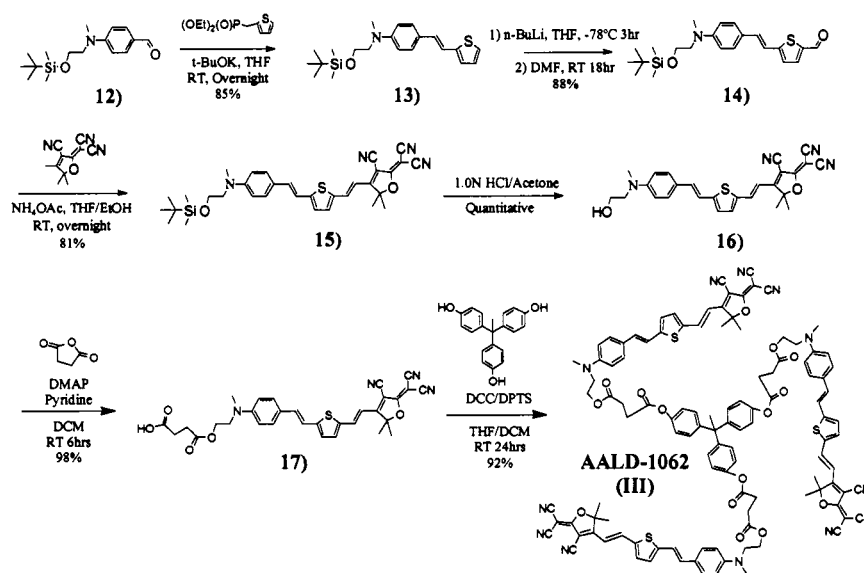
^1H NMR (500 MHz, CDCl_3): δ (ppm) 7.95 (d, $J = 15.5$ Hz, 3H), 7.34 (d, $J = 9$ Hz, 6H), 7.01 (m, 12H), 6.91 (m, 9H), 6.65 (d, $J = 9$ Hz, 6H), 6.53 (d, $J = 15.5$ Hz,

3H), 5.18 (s, 6H), 3.42 (q, $J = 6.5$ Hz, 12H), 2.9 (t, $J = 5.5$ Hz, 6H), 2.79 (t, $J = 7$ Hz, 6H), 2.06 (s, 3H), 1.74 (s, 18H), 1.21 (t, $J = 6.9$ Hz, 18H).

^{13}C NMR (125.1 MHz, CDCl_3): δ (ppm) 175.72, 173.35, 171.87, 171.15, 170.81, 152.88, 148.84, 148.77, 146.12, 144.36, 136.66, 135.33, 134.96, 129.59, 129.28, 128.73, 122.53, 120.80, 114.83, 112.42, 112.25, 111.80, 111.63, 111.06, 97.40, 96.59, 67.99, 60.41, 58.54, 55.48, 51.55, 44.55, 29.25, 29.06, 26.47, 25.64, 12.74.

MALDI-TOF: $[\text{M}+\text{H}]$, 2041.175, $[\text{M}+\text{Na}]$, 2064.231, HRMS (ESI): exact mass calcd for $\text{C}_{119}\text{H}_{110}\text{N}_{12}\text{O}_{15}\text{S}_3$ $[\text{M}+\text{H}]^+$, 2041.7297. Found, 2041.7375. EA (CHN) analysis calcd for $\text{C}_{119}\text{H}_{109}\text{N}_{12}\text{O}_{15}\text{S}_3$; C, 69.98; H, 5.33; N, 8.23%. Found; C, 69.28; H, 5.60; N, 7.97%.

Scheme 3.6.1: Synthesis of succinic acid ester tether based end-on type dendritic chromophore III (AALD-1062)



{4-[2-(thiophen-2-yl)-vinyl]-phenyl}-*N*-Methyl-*N*-(2-*tert*-butyldimethylsiloxy)-ethylamine (13). An oven dried, mag.-stirred, 2000mL RBF was charged with 4-[*N*-methyl-*N*-(2-(*tert*-butyldimethylsiloxy)ethylamino)] benzaldehyde (**12**) (35.58 g, 121.4 mmol), and thiophen-2-ylmethyl-phosphonic acid diethyl ester (64.14 g, 273.8 mmol) in 500 mL freshly dissolved THF. A separate oven dried, mag. stirred, 500 mL RBF was charged with Potassium *tert*-butoxide (32.5 g, 290 mmol) in 350 mL freshly distilled THF. This solution was transferred under argon into the 1000 mL flask. The mixture was allowed to stir overnight at room temperature at which time 125 mL NH₄Cl (sat'd) and 50 mL water were added. The organic phase was separated and the aqueous phase was extracted with diethyl ether. The combined organics were dried over MgSO₄, filtered, and the solvent removed *in vacuo*. The resulting solid was washed with methanol and filtered to yield 18.0 g (40%) of yellow crystals. Compound matches literature characterization.²⁸

2-{4-[*N*-Methyl-*N*-(2-(*tert*-butyldimethylsiloxy)ethylamino)-phenyl]-vinyl}-thiophene-5-carboxaldehyde (14): An oven dried, mag.-stirred, 500 mL RBF was charged with {4-[2-(thiophen-2-yl)-vinyl]-phenyl}-*N*-Methyl-*N*-(2-*tert*-butyldimethylsiloxy)-ethylamine (**13**) (10.0 g, 25.8 mmol). This was dissolved in 150 mL of freshly distilled THF and cooled to -78 °C (dry ice/acetone). Approximately 1.5 equivalents of *n*-BuLi (20.6 mL, 51.6 mmol) was added dropwise over 20 min. Reaction continued at -78°C for 3hr, and then was removed from the

ice bath. Immediately DMF (3.20 mL, 43.9mmol) was added slowly and allowed to stir overnight at room temperature. The reaction was diluted with 200 mL of THF and 200 mL of Brine. Organics were separated and the aqueous phase extracted with dichloromethane. The combined organics were then dried over MgSO_4 , filtered, and the solvent removed *in vacuo*. The resulting solid was washed with methanol and filtered to yield 9.44g (88%) of a orange/red solid. m.p. = 80 °C

^1H NMR (300 MHz, CDCl_3): δ (ppm) 9.833 (s, 1H), 7.648 (d, J = 3 Hz, 1H), 7.396 (d, J = 9 Hz, 2H), 7.06 (m, 3H), 6.700 (d, J = 9 Hz, 2H), 3.806 (t, J = 6 Hz, 2H), 3.536 (t, J = 6 Hz, 2H), 3.062 (s, 3H), 0.901 (s, 9H), 0.039 (s, 6H).

^{13}C NMR (125.1 MHz, CDCl_3): δ (ppm) 182.32, 154.35, 149.73, 140.13, 137.66, 133.65, 128.47, 124.97, 123.57, 115.93, 111.84, 60.52, 54.63, 39.25, 25.92, 18.26, -5.35.

HRMS (ESI): exact mass calcd for $\text{C}_{22}\text{H}_{31}\text{O}_2\text{NSSi}$ $[\text{M}+\text{H}]^+$, 401. 1844. Found, 401.1842.

2-[3-Cyano-4-(2-{5-(4-[*N*-methyl-*N*-(2-(*tert*-butyldimethylsiloxy)ethyl)]-aminophenyl)vinyl}-thiophen-2-yl)-vinyl]-5,5-dimethyl-5H-furan-2-ylidene]-malononitrile (15): A mixture of 2-{4-[*N*-Methyl-*N*-(2-(*tert*-butyldimethylsiloxy)ethylamino)-phenyl]-vinyl}-thiophene-5-carboxaldehyde (14) (3.75 g, 9.35 mmol), 2-cyanomethylene-3-cyano-4, 5, 5-trimethyl -2, 5-dihydrofuran (TCF) (2.14 g, 10.8 mmol), and ammonium acetate (0.72 g, 9.35 mmol) were dissolved in 8mL of dry THF. To this solution was added 50 mL of ethanol, which was stirred for 2 hr. The reaction was stirred for 48 hr, then diluted with 200 mL of

DCM and neutralized with solid ammonium chloride. This mixture was stirred for 30 min, after which sodium bicarbonate was added to neutralize. The mixture separated and the organics dried over MgSO_4 , then condensed *in vacuo*. The mixture was filtered through a short silica gel plug to remove excess salt. The solvent was removed and the dark residue was purified by silica gel column chromatography using DCM ramped to 10% ethyl acetate. The product was further purified via recrystallization from DCM/ethanol to produce a green-copper like powder at 81% yield (4.415g, 7.58mmol). m.p. = 247 °C

^1H NMR (CDCl_3 , 300 MHz): δ (ppm) 7.794 (d, J = 15.6 Hz, 1H), 7.400 (m, 3H), 7.058 (m, 3H), 6.729 (d, J = 9 Hz, 2H), 6.584 (d, J = 15.6 Hz, 1H), 3.820 (t, J = 6 Hz, 2H), 3.559 (t, J = 6 Hz, 2H), 3.088 (s, 3H), 1.771 (s, 6H), 0.902 (s, 9H), 0.042 (s, 6H).

^{13}C NMR (125.1 MHz, CDCl_3): δ (ppm) 176.270, 173.473, 154.980, 150.590, 139.889, 137.847, 135.370, 129.371, 127.421, 123.766, 116.132, 112.799, 112.345, 112.106, 111.568, 97.476, 96.209, 60.955, 56.014, 55.009, 39.764, 39.681, 26.961, 26.335, 26.288, 18.665, -4.931.

HRMS (ESI): exact mass calcd for $\text{C}_{33}\text{H}_{38}\text{O}_2\text{N}_4\text{SSi}$ $[\text{M}+\text{H}]^+$, 582.2484. Found, 582.2467.

2-[3-Cyano-4-(2-{5-(4-[*N*-methyl-*N*-(2-hydroxyethyl)]aminophenyl)vinyl}-thiophen-2-yl)-vinyl]-5,5-dimethyl-5H-furan-2-ylidene]-malononitrile (16): 2-[3-Cyano-4-(2-{5-(4-[*N*-methyl-*N*-(2-(tert-butyl)dimethylsiloxy)ethyl)]-aminophenyl)vinyl}-thiophen-2-yl)-vinyl]-5,5-dimethyl-

5H-furan-2-ylidene]-malononitrile (**15**) (1.52 g, 2.60 mmol) was dissolved in 15 mL acetone and then 1.5 mL 1.0 N HCl (1.8 mmol) was introduced. The reaction was monitored by TLC for 6 hr, at which time triethylamine (0.25 mL, 1.8 mmol) was added to neutralize. To the partially concentrated solution was added 25 mL of water to crystallize the product. Filtration of the product was followed by 24 hr under high vacuum to produce a dark green powder in 98% yield (1.22 g, 2.54 mmol). Compound matches literature characterization.²⁸

Succinic acid mono-{2-[3-Cyano-4-(2-{5-(4-[N-methyl-N-(2-hydroxyethyl)]aminophenyl)vinyl}-thiophen-2-yl)-vinyl]-5,5-dimethyl-5H-furan-2-ylidene]-malononitrile}ester (17**):** To an oven dried round bottom flask equipped with a magnetic stirrer were added 2-[3-Cyano-4-(2-{5-(4-[N-methyl-N-(2-hydroxyethyl)]aminophenyl)vinyl}-thiophen-2-yl)-vinyl]-5,5-dimethyl-5H-furan-2-ylidene]-malononitrile (**16**) (160 mg, 0.341 mmol), succinic anhydride (51.0 mg, 0.512 mmol), and 4-(dimethylamino)-pyridine (DMAP) (42 mg, 0.341 mmol). The solids were dissolved in 8mL of freshly distilled DCM, and then a catalytic amount of dry pyridine (0.15mL) was added dropwise. The reaction was allowed to proceed overnight, at which time the reaction was quenched with saturated ammonium chloride. DCM was added and the organic phase was separated and washed with DI water. The organics were dried over MgSO₄ and the solvent removed *in vacuo*. The residue was purified via silica gel column chromatography starting with a eluent system of 20% ethyl acetate in DCM ramped to 40% to remove unwanted materials.

The product was removed by changing the eluent system to 5% methanol in DCM to produce a blue solid at a 94% yield (182 mg, 321 μ mol) m.p. = 165 °C

^1H NMR (CDCl_3 , 300 MHz): δ (ppm) 7.785 (d, J = 15.9 Hz, 1H), 7.429 (d, J = 9 Hz, 2H), 7.386 (d, J = 3.9 Hz, 1H), 7.069 (m, 3H), 6.765 (d, J = 8.7 Hz, 2H), 6.600 (d, J = 15.6 Hz, 1H), 4.333 (t, J = 6 Hz, 2H), 3.685 (t, J = 5.7 Hz, 2H), 3.069 (s, 3H), 2.640 (m, 4H), 1.771 (s, 6H).

HRMS (ESI): exact mass calcd for $\text{C}_{31}\text{H}_{28}\text{O}_5\text{N}_4\text{S}$ $[\text{M}+\text{H}]^+$, 568.1780, Found, 568.1782.

1,1,1-Tris-(succinic acid mono-{2-[3-Cyano-4-(2-{5-(4-[N-methyl-N-(2-hydroxyethyl)]aminophenyl)vinyl}-thiophen-2-yl)-vinyl]-5,5-dimethyl-5H-furan-2-ylidene]-malononitrile}ester)-phenyl)ethane (AALD-1062, end-on dendritic chromophore III): 4-Succinate-([[(N-[2-ethyl])-N-methyl aminophenyl]-4-vinyl]-thiophen-2-yl)-5-vinyl)-2-dicyanomethylene-3-cyano-5,5-dimethyl-2,5-dihydrofuran (**17**) (94 mg, 0.16 mmol), 1,3-dicyclohexylcarbodiimide (DCC) (39.7 mg, 0.192 mmol), DPTS (13.4 mg, 0.046 mmol), and 1,1,1-tris-(4-hydroxyphenyl)ethane (13.9 mg, 0.046 mmol) were added to an over dried round bottom flask and dissolved in 4 mL of freshly distilled DCM and 2 mL dry THF. Reaction stirred overnight at room temperature, and then washed with saturated NaCl and then water. Organics were dried over MgSO_4 and condensed via rotary evaporation. The residue was purified via silica gel column chromatography using an eluent system 3% THF in DCM to produce a blue solid at 56% yield (51 mg, 0.026 mmol). T_g = 110 °C

^1H NMR (CDCl_3 , 300 MHz): δ (ppm) 7.749 (d, $J = 15.6$ Hz, 3H), 7.403 (d, $J = 9$ Hz, 6H), 7.344 (d, $J = 3.9$ Hz, 3H), 6.999 (m, 19H), 6.754 (d, $J = 9$ Hz, 6H), 6.580 (d, $J = 15.6$ Hz, 3H), 4.350 (t, $J = 6$ Hz, 6H), 3.767 (m, 6H), 3.693 (t, $J = 5.7$ Hz, 6H), 3.058 (s, 9H), 2.809 (t, $J = 6.6$ Hz, 6H), 2.669 (t, $J = 6.6$ Hz, 6H), 2.089 (s, 3H).

^{13}C NMR (CDCl_3 , 75 MHz): δ (ppm) 175.841, 173.167, 171.975, 170.904, 154.077, 149.841, 148.797, 146.053, 139.503, 137.757, 137.623, 134.492, 129.580, 128.879, 127.185, 124.019, 120.843, 116.261, 112.381, 112.234, 111.835, 111.112, 97.182, 96.033, 67.982, 61.784, 55.590, 51.572, 50.720, 38.673, 29.234, 29.077, 26.485.

HRMS (FAB): exact mass calcd for $\text{C}_{113}\text{H}_{96}\text{O}_{15}\text{N}_{12}\text{S}_3$ $[\text{M}+\text{H}]^+$, 1957.63, Found, 1957.7. MALDI-TOF MS $[\text{M}+\text{H}]^+$ found 1957.474. EA (CHN) analysis calcd for $\text{C}_{113}\text{H}_{96}\text{N}_{12}\text{O}_{15}\text{S}_3$; C, 69.31; H, 4.94; N, 8.58%. Found; C, 68.93; H, 5.30; N, 8.30%.

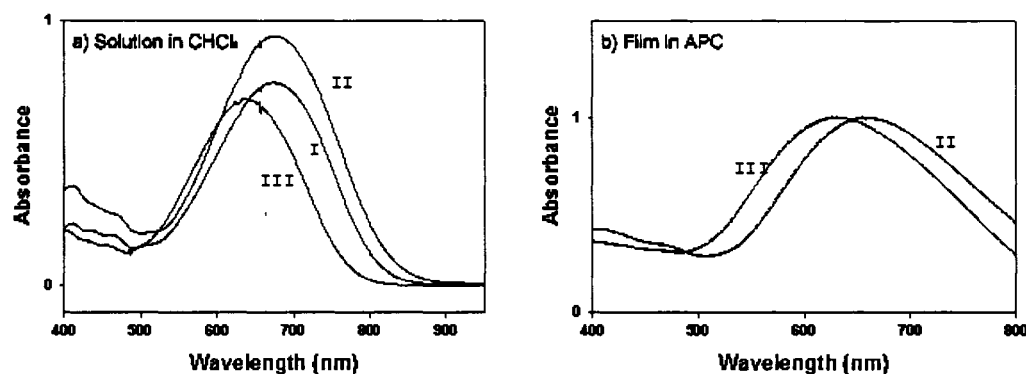


Figure 3.6.1: UV-Vis absorption spectra for FTC (I), and dendritic chromophores II and III.

Table 3.6.1: UV-Vis absorption and cyclic voltametry data for FTC and dendritic chromophores II and III.

	λ_{max} (nm)		Cyclic Voltametry				Absorption Spectroscopic Data	
	CHCl ₃	Film in APC	E ^{1/2} _{ox}	E _{HOMO} (eV)	E _{LUMO} (eV)	ΔE_{CV}	$\lambda_{\text{cut-off}}$ (nm)	E _g (eV)
FTC	672		0.227	-5.027	-3.498	1.529	811	1.609
Side-On	672	655	0.196	-4.996	-3.493	1.503	825	1.628
End-On	635	627	0.276	-5.076	-3.470	1.606	772	1.707

Synthetic details for hexanoic acid ester based dendritic chromophores IV and V;

1,1,1-Tris(6-phenoxy-hexanoic acid methyl ester)ethane (10)- An oven dried, magnetically-stirred, 500 mL 2-neck RBF was charged with 1,1,1-tris(4-hydroxy-phenyl)ethane (3.62g, 12.0mmol), then placed under high vacuum for 30 min. The solid was dissolved in 150 mL dry DMF, and the 6-bromo-hexanoic acid methyl ester (10.0 g, 47.8mmol) was added. After stirring at RT for 10 min NaH (1.91g (60% in oil), 47.8mmol) was added and the mixture heated to 90 °C. The reaction mixture was stirred overnight, diluted with DI water, and extracted with

DCM. The organics were combined, dried over MgSO_4 , and condensed *in vacuo*.

The yellow oil was purified using a short silica gel column (5% EtOAc/Hexanes-20% EtOAc/Hexanes) to yield 6.64g (80%) of a clear liquid.

^1H NMR (300 MHz, CDCl_3): δ (ppm) 6.97 (d, $J = 8.7$ Hz, 6H), 6.75 (d, $J = 8.7$ Hz, 6H), 6.93 (t, $J = 6.6$ Hz, 6H), 3.66 (s, 9H), 2.34 (t, $J = 7.5$ Hz, 6H), 2.09 (s, 3H), 1.76 (m, 6H), 1.70 (m, 6H), 1.51 (m, 6H).

^{13}C NMR (75 MHz, CDCl_3): δ (ppm) 173.91, 157.02, 141.74, 129.56, 113.60, 76.50, 51.39, 50.58, 33.84, 28.99, 25.52, 24.69.

HRMS (ESI): exact mass calcd for $\text{C}_{41}\text{H}_{55}\text{O}_9$ $[\text{M}+\text{H}]^+$, 691.3846. Found, 691.3841.

1,1,1-Tris-(6-phenoxy-hexanoic acid)ethane (11)- A 250ml RBF was charged with 10, and dissolved in 25mL of 1N KOH in EtOH and 10 mL THF. After 24hr at RT, 30 mL of 1N KOH in water was added. After 24hr, a solution of 1N HCl was added until pH ~6. The product was extracted with EtOAc, combined, dried over MgSO_4 , and condensed *in vacuo*. A cream colored solid was purified by rinsing the product with a small amount of DCM, to yield 5.56 g (89%) of an ivory solid.

^1H NMR (300 MHz, CDCl_3): δ (ppm) 6.96 (d, $J = 8.7$ Hz, 6H), 6.76 (d, $J = 8.7$ Hz, 6H), 3.94 (t, $J = 6.3$ Hz, 6H), 2.38 (t, $J = 7.2$ Hz, 6H), 2.09 (s, 3H), 1.78 (m, 6H), 1.70 (m, 6H), 1.52 (m, 6H)

^{13}C NMR (75 MHz, DMSO): δ (ppm) 174.88, 157.06, 141.71, 129.65, 114.04, 67.66, 50.59, 34.12, 30.87, 29.00, 29.70, 24.78

HRMS (ESI): exact mass calcd for $\text{C}_{38}\text{H}_{49}\text{O}_9$ $[\text{M}+\text{H}]^+$, 649.3377. Found, 649.3366.

1,1,1-Tris-(6-phenoxy-hexanoic acid ({2-[3-cyano-4-(2-{5-[2-(4-diethylamino-phenyl)-vinyl]-3-hydroxymethyl-thiophen-2-yl}-vinyl)-5,5-

dimethyl-5*H*-furan-2-ylidene]-malononitrile} ester)ethane (PSLD-31, side-on

dendritic chromophore IV): An oven dried, mag.- stirred, 100 mL RBF was

charged with 1,1,1-tris-(6-hexanoic acid-4-phenyl)ethane (11), (0.15 g, 0.23 mmol),

2-[3-cyano-4-(2-{5-[2-(4-diethylamino-phenyl)-vinyl]-3-hydroxymethyl-thiophen-2-yl}-vinyl)-5,5-dimethyl-5*H*-furan-2-ylidene]-malononitrile, (0.37 g, 0.75mmol), 1,3-

dicyclohexylcarbodiimide (0.17 g, 0.84 mmol), and DPTS (0.67 g, 0.23 mmol). This

solid was then dissolved in a mixture of freshly distilled THF (4 mL) and methylene

chloride (10 mL). The reaction was then stirred overnight, washed with NaCl (sat)

and then DI water. The organic phase was separated and dried over MgSO₄ and

concentrated *in vacuo*. The dark blue crude residue was then purified by silica gel

column chromatography (5% THF/DCM) to yield 0.320g (68%) of a deep blue solid.

$T_g = 125\text{ }^{\circ}\text{C}$, λ_{max} (CHCl₃) = 679 nm

¹H NMR (300 MHz, CDCl₃): δ (ppm) 8.03 (d, $J = 15.5$ Hz, 3H), 7.38 (d, $J = 8.4$ Hz, 6H), 7.14-6.96 (m, 15H), 6.76 (d, $J = 8.4$ Hz, 6H), 6.67 (d, $J = 8.4$ Hz, 6H), 6.59 (d, $J = 15.5$ Hz, 3H), 5.17 (s, 6H), 3.92 (t, $J = 5.7$ Hz, 6H), 3.43 (dd, $J_1 = 6.9$ Hz, $J_2 = 6.3$ Hz, 12H), 2.40, (t, $J = 6.9$ Hz, 6H), 2.08 (br-s, 3H), 1.80 (s, 27H), 1.76-1.66 (m, 6H), 1.53-1.48 (m, 6H), 1.22 (t, $J = 6.9$ Hz, 18H).

¹³C NMR (75 MHz, CDCl₃): δ (ppm) 175.68, 173.29, 173.18, 156.96, 152.91, 148.85, 144.83, 141.76, 136.76, 135.40, 134.81, 129.59, 129.23, 128.73,

122.63, 114.90, 113.58, 112.32, 112.21, 111.65, 110.97, 67.47, 44.54, 33.98, 28.96, 26.54, 25.67, 24.61, 12.70.

MALDI-TOF: [M+H], 2083.71, [M+Na], 2106.71 (m/z).

EA (CHN) analysis calcd for C₁₂₅H₁₂₆N₁₂O₁₂S₃; C, 72.02; H, 6.09; N, 8.06%.

Found; C, 70.67; H, 6.09; N, 7.81%.

1,1,1-Tris-(6-hexanoic acid-4-[(N-[2-ethyl](-N-methyl aminophenyl)-4-vinyl]-thiophen-2-yl)-5-vinyl)-2-dicyanomethylene-3-cyano-5,5-dimethyl-2,5-dihydrofuran]-phenyl)ethane (AALD-1104, End-on dendritic chromophore V):

An oven dried, mag.- stirred, 100 mL two-neck RBF was charged with 1,1,1-tris-(6-hexanoic acid-4-phenyl)ethane (**11**) (0.234g, 0.361mmol), 2-[3-cyano-{5-(4-[N-Methyl-N-(2-hydroxyethyl)]aminophenyl)vinyl}-thiophen-2-yl)-vinyl]-5,5-dimethyl-5H-furan-2-ylidene]-malononitrile (0.600 g, 1.24 mmol), 1,3-dicyclohexylcarbodiimide (0.313 g, 1.52 mmol), and DPTS (0.106 g, 0.361 mmol). The mixture was dissolved in freshly distilled THF (10 mL) and DCM (15 mL). The reaction was stirred for 48hr, washed with NaCl (sat.), and the organic layer collected. The aqueous layer was extracted with DCM, and the combined organics were washed with water, dried over MgSO₄, and condensed *in vacuo*. The dark blue crude solid was purified by silica gel column chromatography (5% THF/ DCM) to yield 0.182 g (25%) of a deep blue solid. T_g = 90 °C, λ_{max} (CHCl₃) = 640 nm

¹H NMR (300 MHz, CDCl₃): δ (ppm) 7.74 (d, *J* = 15.6 Hz, 3H), 7.37 (d, *J* = 9 Hz, 6H), 7.33 (d, *J* = 3.9 Hz, 3H), 6.87 (m, 27H), 6.54 (d, *J* = 15.6 Hz, 3H), 4.27

(t, $J = 6$ Hz, 6H), 3.88 (t, $J = 6$ Hz, 6H), 3.65 (m, 6H), 3.03 (s, 9H), 2.28 (t, $J = 7.2$ Hz, 6H), 2.07 (s, 3H), 1.73 (s, 18H), 1.60 (mm, 24H)

^{13}C NMR (75 MHz, CDCl_3): δ (ppm) 175.79, 173.46, 173.04, 157.02, 154.12, 149.88, 141.74, 139.42, 137.58, 134.57, 129.59, 128.87, 127.10, 124.03, 116.22, 113.61, 112.30, 112.20, 111.84, 111.60, 111.07, 97.076, 96.12, 67.54, 61.198, 55.84, 50.79, 50.60, 38.65, 34.10, 30.08, 29.02, 26.51, 25.69, 24.58.

MALDI-TOF: Exact mass calcd for $\text{C}_{119}\text{H}_{114}\text{N}_{12}\text{O}_{12}\text{S}_3$ $[\text{M}+\text{Na}]^+$, 2023.44.
Found $[\text{M}+\text{Na}]^+$, 2023.209,

EA (CHN) analysis calcd for $\text{C}_{119}\text{H}_{114}\text{N}_{12}\text{O}_{12}\text{S}_3$; C, 71.45; H, 5.74; N, 8.40%.
Found; C, 70.22; H, 5.80; N, 7.78%.

Instruments: Absorption spectra of thin film composite samples as well as those of chromophore solutions (chloroform, conc. 1×10^{-4} mole/L) were obtained using a HP 8453, photodiode array type UV-VIS spectrophotometer at 190-1100 nm. Melting temperatures and glass transition behavior were measured using a Perkin Elmer 7 differential scanning calorimeter (DSC) under nitrogen flow at a temperature ramp rate of 5 °C per minute. ^1H and ^{13}C NMR spectra were recorded using either a 300 or 500 MHz Bruker Avance NMR spectrometer using deuterated chloroform or DMSO purchased from Cambridge Isotope Laboratories, Inc. Spectroscopic ellipsometry measurements were performed on thin films using a Woollam VASE model incorporating an auto reader in the range of 310-1550 nm (0.8-4.0 eV), recording at incidence angles of 65, 70, and 75 degrees. The pseudo-dielectric functions were fit using non-linear Levenberg-Marquardt algorithm using

WVASE32 software. Elemental analysis was performed by Prevalere Life Sciences, Inc., Whitesboro NY. High resolution mass analysis was performed on a thermo-electron carburation Finnigan LTQ-FT electro-spray ionization or a JEOL HX-110 fast atom bombardment (2 point calibration with PEG 600, resolution 10000, matrix; 3-nitrobenzyl alcohol), mass spectrometer as indicated (all samples within 0.5ppm). MALDI-TOF analysis was performed on a Bruker Daltonics Autoflex MADI-TOF (matrix; α -CCA), mass spectrometer.

Thin film fabrication for EO study; Each dendritic chromophore was mixed with solid APC (6.14×10^{19} molecules in 0.09 g of APC). The solid components were then dissolved into cyclopentanone (1:1) with 8% total solid weight. The solutions were stirred, filtered, and then spin-cast onto ITO coated glass slides. Film thicknesses were measured to be 2.2- 2.5 μm using a surface profilometer (KOSAKA, ET-3000). Gold was then deposited at the surface of the polymer-composite film to create both a reflective surface for measurement and an electrode for application of poling and modulating fields.

Thermally stimulated current measurements under applied DC poling field; DC current profiles were examined under applied DC electric field as a function of increasing temperature. The same sample configuration as detailed in the film fabrication section was also used in this experiment. Current was measured using a Keithley 2400 sourcemeter by applying a poling voltage of $E_p = 70 \text{ V}/\mu\text{m}$

while continuously monitoring temperature using a Keithley Digital Multimeter 2000 (k-couple). Current data was integrated using a computer interface.

Isothermal EO signal decay experiment; Each sample was poled to its maximum r_{33} value, and then cooled to 105°C. When the r_{33} value was stable, the dc poling field was removed and the decay curves were observed.

Notes to Chapter 3

1. Chasse, T. L.; Sachdeva, R.; Li, Q.; Li, Z.; Petrie, R. J.; Gorman, C. B., Structural effects on encapsulation as probed in redox-active core dendrimer isomers. *Journal of the American Chemical Society* **2003**, 125, (27), 8250-8254.
2. Furuta, P.; Frechet, J. M. J., Controlling solubility and modulating peripheral function in dendrimer encapsulated dyes. *Journal of the American Chemical Society* **2003**, 125, (43), 13173-13181.
3. Frechet, J. M. J.; Hawker, C. J.; Gitsov, I.; Leon, J. W., Dendrimers and hyperbranched polymers: two families of three-dimensional macromolecules with similar but clearly distinct properties. *Journal of Macromolecular Science, Pure and Applied Chemistry* **1996**, A33, (10), 1399-1425.
4. Gopalan, P.; Katz, H. E.; McGee, D. J.; Erben, C.; Zielinski, T.; Bousquet, D.; Muller, D.; Grazul, J.; Olsson, Y., Star-Shaped Azo-Based Dipolar Chromophores: Design, Synthesis, Matrix Compatibility, and Electro-optic Activity. *J. Am. Chem. Soc.* **2004**, 126, (6), 1741-1747.
5. Breitung, E. M.; Shu, C.-F.; McMahon, R. J., Thiazole and Thiophene Analogues of Donor-Acceptor Stilbenes: Molecular Hyperpolarizabilities and Structure-Property Relationships. *J. Am. Chem. Soc.* **2000**, 122, (6), 1154-1160.
6. He, M.; Leslie, T. M.; Sinicropi, J. A.; Garner, S. M.; Reed, L. D., Synthesis of Chromophores with Extremely High Electro-optic Activities. 2. Isophorone- and Combined Isophorone-Thiophene-Based Chromophores. *Chem. Mater.* **2002**, 14, (11), 4669-4675.
7. Albert, I. D. L.; Marks, T. J.; Ratner, M. A., Optical nonlinearities in the lowest excited triplet state of organic molecules. *Book of Abstracts, 210th ACS National Meeting, Chicago, IL, August 20-24 1995*, (Pt. 2), PHYS-213.
8. Luo, J.; Haller, M.; Li, H.; Tang, H.-Z.; Jen, A. K.-Y.; Jakka, K.; Chou, C.-H.; Shu, C.-F., A Side-Chain Dendronized Nonlinear Optical Polyimide with Large and Thermally Stable Electrooptic Activity. *Macromolecules* **2004**, 37, (2), 248-250.
9. Luo, J.; Haller, M.; Ma, H.; Liu, S.; Kim, T.-D.; Tian, Y.; Chen, B.; Jang, S.-H.; Dalton, L. R.; Jen, A. K.-Y., Nanoscale Architectural Control and Macromolecular Engineering of Nonlinear Optical Dendrimers and Polymers for Electro-Optics. *J. Phys. Chem. B.* **2004**, 108, (25), 8523-8530.
10. Bai, Y.; Song, N.; Gao, J. P.; Sun, X.; Wang, X.; Yu, G.; Wang, Z. Y., A New Approach to Highly Electrooptically Active Materials Using Cross-Linkable, Hyperbranched Chromophore-Containing Oligomers as a Macromolecular Dopant. *J. Am. Chem. Soc.* **2005**, 127, (7), 2060-2061.

11. Pereverzev, Y. V.; Prezhdo, O. V.; Dalton, L. R., Structural origin of the enhanced electro-optic response of dendrimer systems. *Chem. Phys. Lett.* **2003**, 373, (1,2), 207-212.
12. Ma, H.; Luo, J.; Kang, S. H.; Wong, S.; Kang, J. W.; Jen, A. K. Y.; Barto, R.; Frank, C. W., Highly fluorinated and crosslinkable dendritic polymer for photonic applications. *Macromolecular Rapid Communications* **2004**, 25, (19), 1667-1673.
13. Cha, S. W.; Choi, D. H.; Jin, J.-I., Unusually fast optically induced birefringence in polyoxetanes bearing 4-(N,N-diphenyl)amino-4'-nitroazobenzene chromophores. *Advanced Functional Materials* **2001**, 11, (5), 355-360.
14. Michelotti, F.; Toussaere, E.; Levenson, R.; Liang, J.; Zyss, J., Real-time pole and probe assessment of orientational processes in electro-optic polymers. *Applied Physics Letters* **1995**, 67, (19), 2765-7.
15. Sullivan, P. A.; Akelaitis, A. J. P.; K., L. S.; McGrew, G.; Lee, S. K.; Choi, D. H.; Dalton, L. R., Novel Dendritic Chromophores for Electro-optics: Influence of Binding Mode and Attachment Flexibility on Electro-Optic Behavior. *Chem. Mater.* **2006**, 18, 344-351.
16. Teng, C. C.; Man, H. T., Simple reflection technique for measuring the electro-optic coefficient of poling polymers. *Applied Physics Letters* **1990**, 56, (18), 1734-6.
17. Schildkraut, J. S., Determination of the electrooptic coefficient of a poled polymer film. *Applied Optics* **1990**, 29, (19), 2839-41.
18. Briers, D.; Koeckelberghs, G.; Picard, I.; Verbiest, T.; Persoons, A.; Samyn, C., Novel Chromophore-Functionalized Poly[2-(trifluoromethyl) adamantyl acrylate-methyl vinyl urethane]s with High Poling Stabilities of the Nonlinear Optical Effect. *Macromol. Rapid Commun.* **2003**, 24, 841-846.
19. Zhang, C.; Wang, C.; Dalton, L. R.; Zhang, H.; Steier, W. H., Progress toward Device-Quality Second-Order Nonlinear Optical Materials. 4. A Trilink High uB NLO Chromophore in Thermoset Polyurethane: A "Guest-Host" Approach to Larger Electrooptic Coefficients. *Macromol.* **2001**, 34, (2), 253-261.
20. Janietz, S.; Bradley, D. D. C.; Grell, M.; Giebeler, C.; Inbasekaran, M.; Woo, E. P., Electrochemical determination of the ionization potential and electron affinity of poly(9,9-dioctylfluorene). *Applied Physics Letters* **1998**, 73, (17), 2453-2455.
21. Michelotti, F.; Toussaere, E.; Levenson, R.; Liang, J.; Zyss, J., Study of the orientational relaxation dynamics in a nonlinear optical copolymer by means of a pole and probe technique. *Journal of Applied Physics* **1996**, 80, (3), 1773-1778.

22. Lindsey, C. P.; Patterson, G. D., Detailed comparison of the Williams-Watts and Cole-Davidson functions. *Journal of Chemical Physics* **1980**, 73, (7), 3348-57.
23. Ediger, M. D., Spatially heterogeneous dynamics in supercooled liquids. *Annual Review of Physical Chemistry* **2000**, 51, 99-128.
24. Bahar, I.; Erman, B.; Fytas, G.; Steffen, W., Intramolecular Contributions to Stretched-Exponential Relaxation Behavior in Polymers. *Macromolecules* **1994**, 27, (18), 5200-5.
25. Furniss, B. S.; Hannaford, A. J.; Smith, P. W. G.; Tatchell, A. R., *Vogel's Textbook of Practical Organic Chemistry*. fifth edition ed.; Addison Wesley Longman Singapore Pte Limited: 1989.
26. Zhang, C.; Wang, C. W.; Dalton, L. R.; Zhang, H.; Steier, W. H., Progress toward Device-Quality Second-Order Nonlinear Optical Materials. 4. A Trilink High mu-Beta NLO Chromophore in Thermoset Polyurethane: A "Guest-Host" Approach to Larger Electrooptic Coefficients. *Macromolecules* **2001**, 34, 253-261.
27. Melikian, G.; Rouessac, F. P.; Alexandre, C., Synthesis of substituted dicyanomethylendihydrofurans. *Synth. Commun.* **1995**, 25, (19), 3045-51.
28. Briers, D.; Koeckelberghs, G.; Picard, I.; Verbiest, T.; Persoons, A.; Samyn, C., Novel chromophore-functionalized poly[2-(trifluoromethyl)adamantyl acrylate-methyl vinyl urethane]s with high poling stabilities of the nonlinear optical effect. *Macromolecular Rapid Communications* **2003**, 24, (14), 841-846.

Chapter 4

2nd order NLO Properties of Amorphous Organic Glasses and Composites Based on Multichromophore Dendrimers

4.1 Introduction

Materials exhibiting large electric field poling induced nonlinear susceptibilities ($\chi^{(2)}$), and therefore, large electro-optic coefficients (r_{33}) have ordinarily been elaborated through the dispersion of highly dipolar chromophoric materials throughout an optically inert, polymeric host material matrix. Large electro-optic (EO) coefficients require both high chromophore number density and efficient acentric molecular ordering. Extensive experimental as well as theoretical study has implicated interchromophore electrostatic (dipolar) interaction, guest-host incompatibility, and chromophore shape as major factors affecting poling induced order.¹ Increased chromophore number density commonly magnifies the severity of these effects resulting in the appearance of an optimum loading density. Chromophore densities greater than this optimum result in reduced poling induced order, and thus lower r_{33} .²

In order to control these potentially detrimental effects, material systems must be engineered at the molecular level employing first-principals theory guided design. Chromophore shape can be modulated by asymmetric substitution with

specifically designed dendritic units, modifying supramolecular and intramolecular (electrostatic) interactions. Covalent modification may also be used to address compatibility problems by attachment of the chromophore to the host material or by creation of dendritic or hyperbranched molecular structures. Such well-designed molecular architectures have demonstrated significantly enhanced r_{33} as compared to analogous guest-host blends.³

Multichromophore dendrimers are of particular interest due to the opportunities for molecular-scale architectural control. Alteration of chromophore and successive dendrimer generation binding geometry, attachment flexibility, and polarity, can very effectively direct both internal and external molecular interactions.^{4,5-7} Theoretical analysis can be used as a guide in the bottom-up design of materials which exploit this control to achieve greatly increased active chromophore number density with no loss of poling induced ordering efficiency.

In this chapter I have examined the electro-optic properties of such multichromophore dendrimers and demonstrate the effectiveness of theory-guided molecular engineering. Multiple chromophore containing dendritic materials were used to fabricate stand-alone thin films with extremely high chromophore content, which exhibit dramatically enhanced poling efficiency, $\rho(r_{33}/E_p)$. Dramatic improvements were then further augmented by application of these dendritic materials as host matrices for further incorporation of an additional, highly active guest. Employing this principle, massive loading densities were achieved resulting in unprecedented r_{33} values (≈ 300 pm/V).

4.2 Chromophore Shape Effects; Theory Guided Design

The coefficient of the second-order term in the power series expansion describing bulk material polarization response to an externally applied electric field, $\chi^{(2)}$, is given by

$$\chi_{zzz}^{(2)} \propto N\beta_{zzz} \langle \cos^3 \theta \rangle \quad (4.2.1)$$

The term, N , represents number density of active chromophore units each having a molecular first hyperpolarizability tensor with the element β_{zzz} oriented along the dipolar axis of the molecule. The angle of the dipole vector with respect to applied DC poling field is given by θ . Thus, $\langle \cos^3 \theta \rangle$ relates dipole orientation to poling field and incident EM radiation, and represents the overall dipolar order obtained throughout the material during the poling process. Using this relation it is possible to express an electric field induced refractive index change in terms of $\chi^{(2)}$ $(-\omega, \omega, 0)$ and the electro-optic coefficient r_{33} using

$$r_{33} \propto -2\chi_{zzz}^{(2)} / (n_z)^4 \quad (4.2.2)$$

where n_z represents refractive index. Proportionality constants depend on the inherent dielectric properties of each material lattice.

From the above equation it is noted that an increase in N , holding all other parameters constant, results in an accompanying linear increase in $\chi^{(2)}$ and therefore also in r_{33} . However, through previous experimental analysis, this relationship is only obeyed at very low chromophore number density. Analysis using statistical mechanics modeling based on a point-dipole approximation leads to the implication of interchromophore electrostatic interactions as an important factor in determining

such sub-linear behavior.^{8,9} Guest compatibility with the host environment will also play a critical role due to modification of interchromophore interaction through effective solvation.

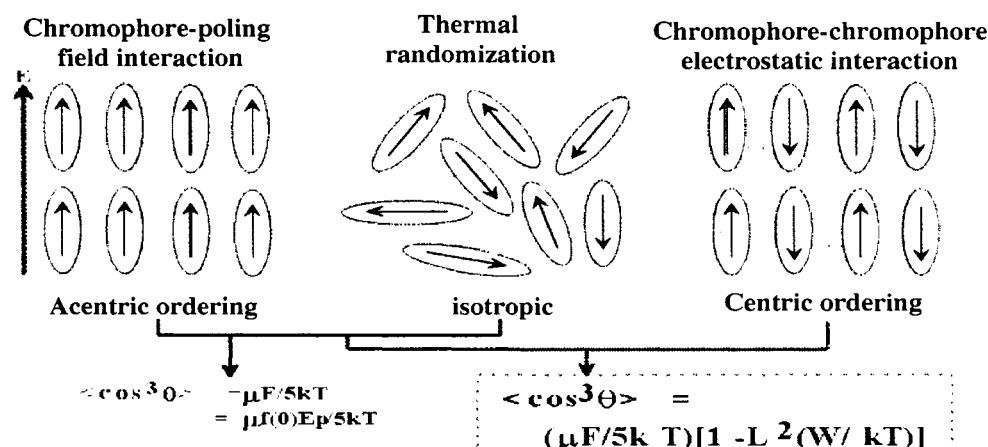


Figure 4.2.1: Analytical model of point-dipole response to a poling field, left; neglecting dipole-dipole interactions (W), right; including W ^{8,9}

From the point-dipole based model (Figure 4.2.1), neglecting dipole-dipole electrostatic potentials (W), it is found that $\langle \cos^3 \theta \rangle$ is independent of chromophore number density. When W is included, the model reveals a $\langle \cos^3 \theta \rangle$ attenuated by a factor proportional to N . Increasing N reduces the average distance between dipolar chromophores, increasing W . When N becomes large, electrostatic potentials begin to drive centric ordering, eventually becoming dominant, ultimately limiting achievable order and attenuating r_{33} . From this simple analysis, correctly accounting for W , it immediately becomes evident that the limiting factor in achieving high r_{33} , is the $N\langle \cos^3 \theta \rangle$ product, designated as the loading parameter.

The point-dipole model does not consider the effects molecular shape may have in determining the nature and magnitude of the various potential functions associated with preferred chromophore orientation. This model is therefore of limited utility. A more detailed, and much more complex approach, requires the use of pseudo-atomistic Monte Carlo molecular dynamics modeling to simulate interactions among many molecules.¹⁰ Pseudo-atomistic molecular modeling of large systems such as dendrimers is computationally intensive. Modeling of this type requires consideration not only of W , but also nuclear repulsive (steric) forces, Van der Waals interactions, and potential functions associated with rotation about covalent bonds.

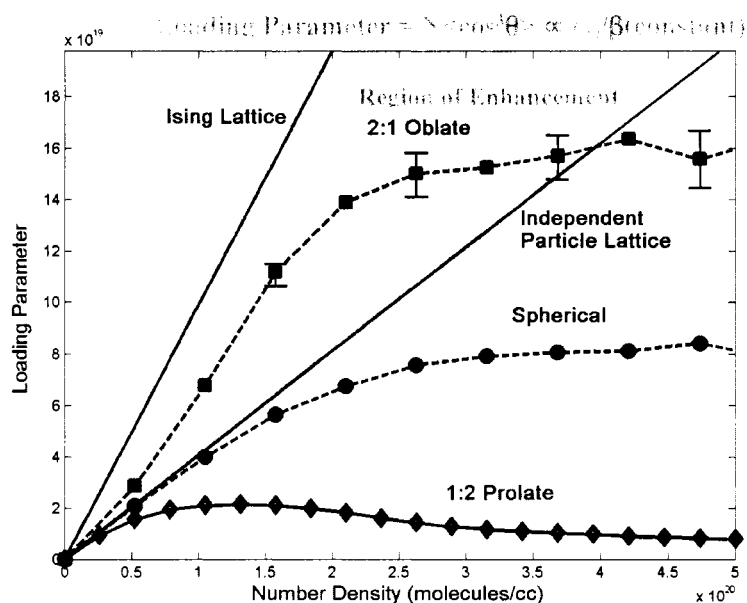


Figure 4.2.2: Monte-Carlo analysis of $\langle \cos^3 \theta \rangle$ with respect to chromophore number density¹¹

Using Monte Carlo simulations to explore the dependence of loading parameter as affected by the chromophore aspect ratio, it has been demonstrated that

molecular shape plays a critical role (Figure 4.2.2).¹² Molecular shape regulates the relative energy contributions from differing electrostatic interactions. These contributions make up the overall potential energy distribution that defines equilibrium dipolar order in molecular ensembles under the influence of an external electric field. A prolate, or rod-like chromophore in which the long aspect corresponds to the dipolar axis, favors side-side intermolecular interaction. The lowest energy arrangement for this type of dipole interaction corresponds to anti-parallel, centric ordering, resulting in reduced $\langle \cos^3\theta \rangle$. A prolate shape therefore displays a low optimum loading parameter. Spherically symmetric shape reduces side-side interactions while maintaining favorable head-tail interactions. An oblate, or center-thick aspect ratio brings about the possibility of enhanced dipolar order resulting from electrostatic interaction.¹¹ Interchromophore side-approach is severely disfavored, allowing head-tail interactions to dominate, driving acentric order and resulting in poling response above the independent particle limit.

4.3 Multichromophore Dendrimers; Material Design and Synthesis

Multi-chromophore dendrimers offer many distinct advantages over analogous polymer or small molecule based molecular designs. Dendrimers display better overall mechanical stability and film forming properties than small molecules yet retain many of their desirable characteristics. Chromophore containing dendrimers are monodisperse and display little batch to-batch variability, providing highly consistent, repeatable results. Dendritic structures also offer unique characteristics such as globular shape, large internal free-volume, and an outer

periphery capable of providing physical isolation of contents within. These attributes not only offer the ability to control molecular structure, solubility and processibility, they can also be employed to enhance photo-stability as well as to minimize optical loss.¹³

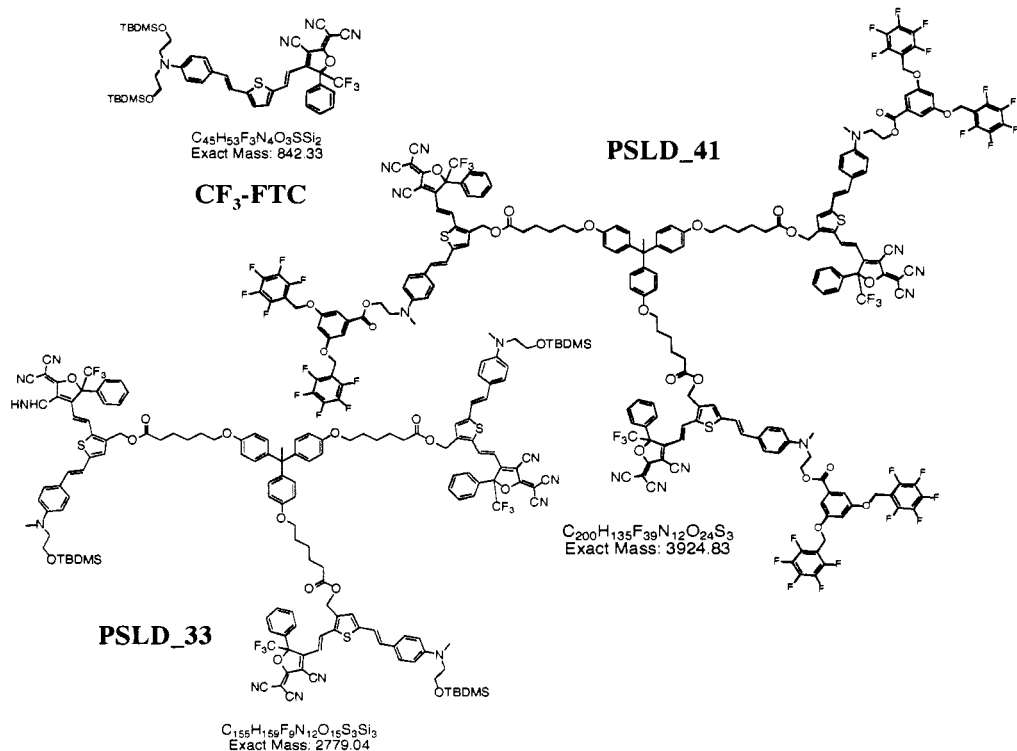
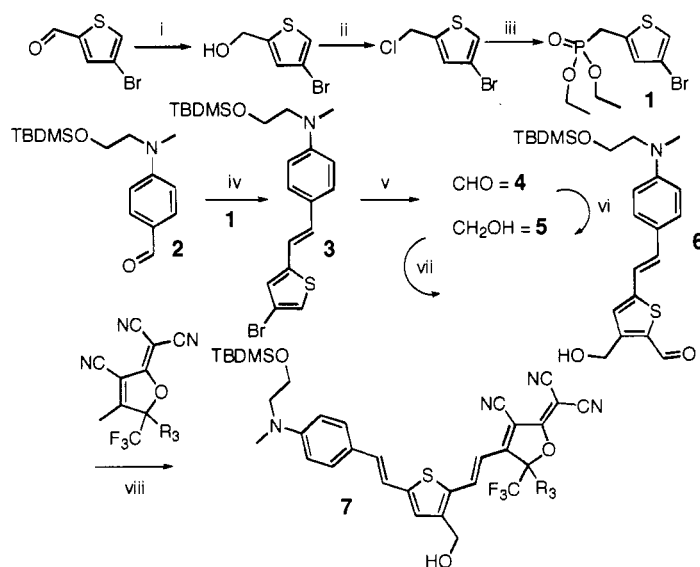


Figure 4.3.1: Multichromophore EO dendrimers PS LD_33 and PS LD_41 accompanied by small molecule chromophore CF₃-FTC

Previous work has focused on the optimization of intramolecular design parameters of three-arm dendritic chromophores.¹⁴ In this report previous findings have been employed in order to guide the design and synthesis of three-arm dendritic structures with extended outer peripheral units. These dendritic materials were designed for use in the fabrication of stand-alone amorphous thin films. Figure 4.3.1

illustrates the structures of the two three-arm dendrimers (PSLD_41 and PSLD_33), considered herein. Also depicted for comparison is the analogous small molecule EO chromophore CF₃-FTC.

Scheme 4.3.1: synthesis of CF₃-FTC type chromophore unit 7^a

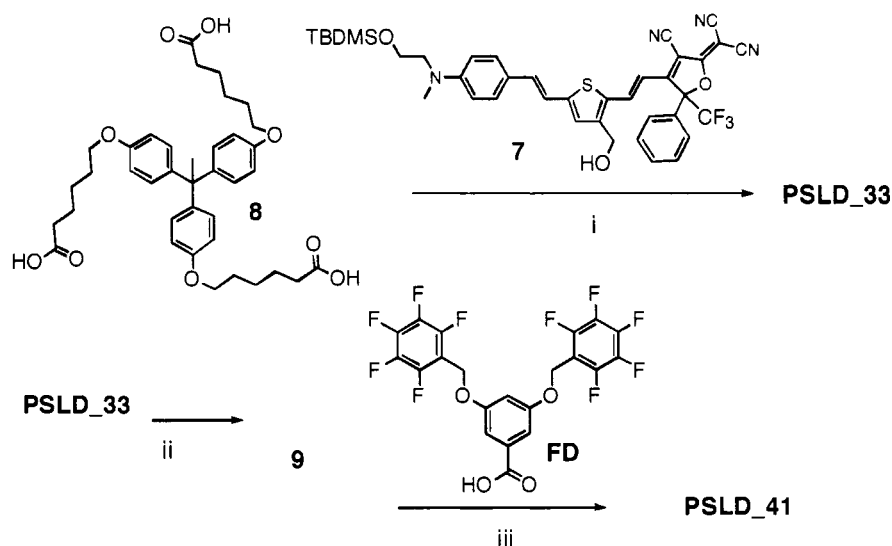


^aConditions: i) NaBH₄, NaOH, MeOH, 0 °C-RT, quant.; ii) HCl (conc.), 0 °C 2 hrs, quant.; iii) P(OEt)₃, 90 °C 36 hrs, quant.; iv) 7, t-BuOK, THF, RT overnight, 90%; v) n-BuLi, DMF, Et₂O, -78 °C, 70%; vi) NaBH₄, NaOH, MeOH/THF, 0 °C 2 hrs, quant.; vii) n-BuLi, DMF, THF, -78 °C 2 hrs, 87%; viii) CF₃-phenyl-TCF, EtOH, RT 24 hrs, 62%

Both PSLD_41 and PSLD_33 incorporate three chromophore units based on the CF₃-FTC design. The aryl-amine terminated thienyl-vinylene donor bridge (FTC-type) was chosen because it is robust, offers facile asymmetric functionalization, and displays large β values.^{15, 16} The electron acceptor moiety, 2-cyanomethylene-3-cyano-4-methyl-5-trifluoromethyl-5-phenyl-2, 5-dihydrofuran (CF₃-Phenyl-TCF), is one of the strongest to date.^{17,18} Scheme 4.3.1 details the

synthesis of the chromophore unit. Synthetic procedures are similar to those reported previously with modifications to include asymmetric functionality.^{14, 19}

Scheme 4.3.2: Synthesis of three-arm dendrimers **PSLD_33** and **PSLD_41**^a



^aConditions: i) DCC / DPTS, DCM : DMF, reflux 48 hrs, 50%; ii) 1N HCl (MeOH soln.), acetone, RT 2.5 hrs, quant.; iii) DCC / DPTS, DCM : DMF, reflux 48 hrs, 62%

Scheme 4.3.2 outlines the synthetic route chosen for the elaboration of dendrimers **PSLD_33** and **PSLD_41**. Synthesis of the tri-hexanoic acid core was reported previously.¹⁴ Use of this core has been shown to lead to materials exhibiting good thermal and mechanical properties while allowing efficient poling. Three equivalents of chromophore **7** were attached to the core by esterification in the presence of DCC and DPTS to produce tri-TBDMS ('Butyl-dimethyl-silyl) functionalized three-arm dendrimer **PSLD_33**. The resulting material was then purified by silica gel column chromatography followed by reprecipitation. The TBDMS groups were then removed under mildly acidic conditions. The resulting

tri-hydroxyl dendrimer was then functionalized with three equivalents of the pentafluoro phenyl containing Frechet-type dendron (FD), to yield PSLD_41, which was again purified by column and reprecipitation. Synthetic material identity and purity was confirmed by ^1H and ^{13}C NMR, MALDI-TOF mass spectrometry, and elemental analysis.

4.4 Evaluation of Physical and Photophysical Properties of Multi-chromophore Dendrimer based Amorphous Glasses

UV-visible absorption spectroscopy performed on the two dendrimers as well as $\text{CF}_3\text{-FTC}$ yielded the results listed in Table 4.4.1. Shown also are thermal data obtained by differential scanning calorimetry (DSC). Dendrimers PSLD_33 and PSLD_41 displayed distinct glass transition temperatures while only a melting point was observed for the small molecule chromophore $\text{CF}_3\text{-FTC}$.

The absorption maxima corresponding to each compound, both from a solution in chloroform and from a thin solid film are shown. Compound $\text{CF}_3\text{-FTC}$ was dispersed into Poly [bisphenol A carbonate-co-4, 4'-(3,3,5-trimethylcyclohexylidene) diphenol carbonate], (APC), at a loading density that delivered optimized r_{33} (25% by weight, 1.78×10^{20} molec. / cc). Both PSLD_33 and PSLD_41 were spin cast on glass slides as solutions of pure compounds. Very comparable absorption maxima were recorded for $\text{CF}_3\text{-FTC}$ and the PSLD_33 dendrimer, both in chloroform and in thin film. The line shape corresponding to chromophore $\pi\text{-}\pi^*$ is somewhat broadened for the PSLD_33 pure film as expected (Figure 4.4.1)

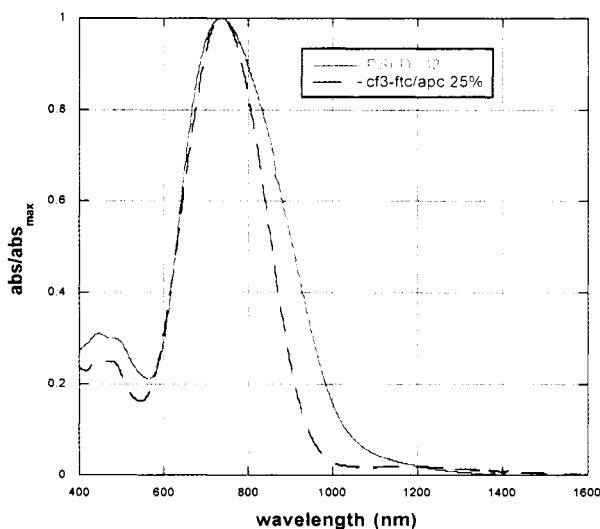


Figure 4.4.1: UV-Vis-NIR absorption spectra of dendrimer PSLD_33 (pure film) and CF₃-FTC (25% by wt. In APC) on glass

Both spectra corresponding to PSLD_33 and CF₃-FTC display a pronounced bathochromic shift in chloroform solution (≈ 20 nm). These solvatochromic shift data suggest that individual chromophore units in CF₃-FTC and PSLD_33 materials are affected by very similar dielectric environments. Similar spectra recorded for both APC and pure dendrimer films suggest that these chromophore environments are comparable as well, which may be surprising given the much higher N corresponding to PSLD_33 pure film. PSLD_41 exhibits a relatively large hypsochromic shift in λ_{max} as compared to CF₃-FTC and PSLD_33. This shift may result from a combination of intermolecular and intramolecular effects.^{14,18} Decreased solvatochromic dependence is apparent for PSLD_41 when changed from solution to film. Attenuated solvatochromic shift implies that the chromophore units comprising

PSLD_41 are effectively shielded from the surrounding environment by the extended peripheral structure.²⁰

Table 4.4.1: Thermal and UV-Vis Absorption data for EO compounds

Compound	T _g (°C)	T _m (°C)	λ_{max} (CHCl ₃) nm	λ_{max} (film) ^a nm
CF ₃ -FTC	---	182	758	738
PSLD_41	103	---	724	720
PSLD_33	85	---	759	734

^afilm data for CF₃-FTC were collected using 25% by wt. chromophore / APC composites

Evaluation of the electro-optic properties of CF₃-FTC / APC composites and pure films of PSLD_33 and PSLD_41 was performed using a modification of the standard single-beam polarization interferometry reflection apparatus. The instrument was modified to simultaneously monitor the modulated signal intensity (I_m), and incident intensity (I_c), in real-time during poling.^{14, 21} Such modification allowed *in-situ* optimization of processing conditions. Samples of each material were prepared by solution spin-casting onto ITO-coated glass slides. Gold electrodes ($d \approx 200$ nm) were then deposited atop the films. EO measurements were performed at $\lambda = 1310$ nm, and r_{33} measurements were recorded after cooling and removal of the poling field. Values were calculated by sine wave fitting of lock-in-amplifier and direct current detector response curves as a function of the relative phase angle (Ψ_{sp}) between T_E and T_M .²²

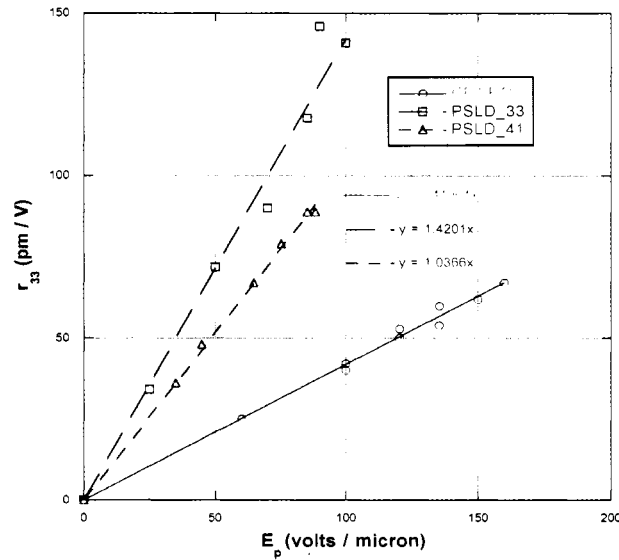


Figure 4.4.2: r_{33} data for $\text{CF}_3\text{-FTC}$ (25% in APC) and PSLD_33 and PSLD_41 pure films as a function of applied poling voltage.

The slope of a linear plot of r_{33} with respect to electric field E_p ($\text{V}/\mu\text{m}$) applied at optimum poling temperature defines the poling efficiency, ρ (r_{33}/E_p , $10^{-18} \text{ m}^2/\text{V}^2$), of a given material. Poling efficiency determines the r_{33} obtained through application of a known poling voltage. However, maximum ρ does not necessarily guarantee maximum EO activity. Secondary material properties such as resistivity often also depend on N and can limit the maximum E_p that can be applied before dielectric breakdown occurs.

Electro-optic activity has been experimentally confirmed as linearly dependant on E_p . The magnitude of the applied field determines $\langle \cos^3 \theta \rangle$. Therefore, by substituting into Equation 4.2.1 it can be written that

$$r_{33} \propto N\beta_{zzz}E_p \mu m \quad (4.4.1)$$

where μ represents chromophore dipole moment, and m is defined as the ordering efficiency of the material and is given by

$$m \propto \langle \cos^3 \theta \rangle / E_p \mu \quad (4.4.2)$$

Ordering efficiency (m) denotes the extent of dipolar order produced within the bulk material in terms of E_p and is proportional to $1/kT$. In the case where m is independent of N , ρ should increase linearly according to increased N , resulting in a high loading parameter.

The ρ values determined for CF₃-FTC in APC, and pure dendrimer films of PSLD_33 and PSLD_41 were determined as 0.42, 1.03, and 1.42 x 10⁻¹⁸ m²/V² respectively (Figure 4.4.2). Using the molecular weight of the active chromophore portion of each material (AMW = 554.58 g/mol) and a density of 1 g/cc, N was determined for all three materials. These values were then normalized against the 25% CF₃-FTC / APC composite samples and are presented below in table 4.4.2

Table 4.4.2: comparison of N and ρ for chromophore / APC composite and dendrimer materials

compound	N (x 10 ²⁰ molec/cc)	$\rho = r_{33}/E_p$	$(\rho_c/\rho_m)/(N_c/N_m)^a$
CF ₃ -FTC/APC	1.78	0.42	---
PSLD_41	4.6	1.03	0.95
PSLD_33	6.8	1.42	0.89

^asubscripts c and m denote CF₃-FTC / APC composite and pure dendrimer material values

The data illustrated that for PSLD_41 films, normalized ρ divided by normalized $N \{(\rho_c/\rho_m)/(N_c/N_m)\}$ was approximately unity. A value of unity suggests that the dendrimer structure very effectively isolated individual chromophore units while allowing highly efficient poling response. Such effective isolation yielded an increase in r_{33} that was linear with high N . The slightly lower than linear value of $(\rho_c/\rho_m)/(N_c/N_m) = 0.89$, determined for PSLD_33 still indicated a dramatic improvement in $N\langle\cos^3\theta\rangle$ as compared to the $\text{CF}_3\text{-FTC}$ composite. Maximum repeatable r_{33} values for PSLD_33, PSLD_41, and $\text{CF}_3\text{-FTC} / \text{APC}$ were found to be approximately 118, 90, and 52 pm/V respectively. From this analysis, the advantages of the dendronized material as compared to the APC composite material were immediately clear. These data illustrated a three-fold enhancement of r_{33} resulting from the molecular engineering of dendrimer encapsulated chromophore architecture.

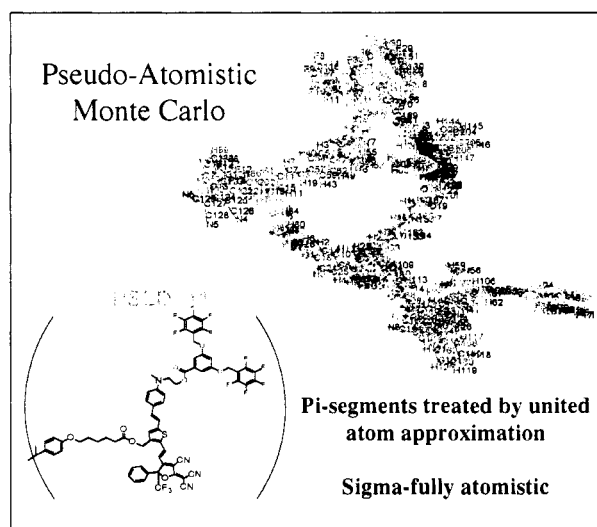


Figure 4.4.3: Representation of PSLD_41 dendrimer showing atom labels, correct Van der Waals radii, and fixed spheroid pi-segments

In order to further our understanding of the enhancement in r_{33} brought about by the highly engineered dendrimer structures, statistical mechanics was again employed. To simulate and examine poling induced order in the mutli-arm dendrimers under consideration, pseudo-atomistic Monte Carlo molecular dynamics simulations were used as before. The pi-conjugated structures of the chromophore units within the dendrimers were approximated as prolate spheroid structures that mimic the chromophore length, aspect ratio, and dipole moment. Sigma segments were treated completely atomistically, using correct bond and rotation potentials. Using this approach, an individual PSLD_41 dendrimer molecule was digitally reproduced (Figure 4.4.3).

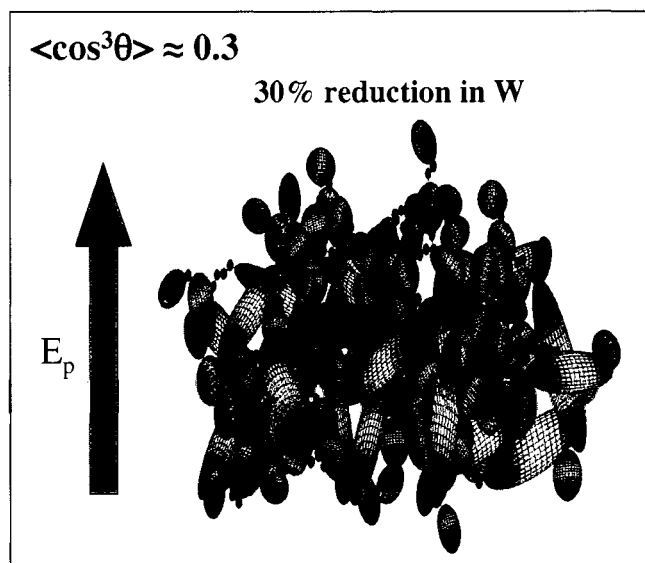


Figure 4.4.4: Simulation of poling induced order in a multiple dendrimer ensemble

After the single dendrimer model was completed, the single molecule structure was then duplicated and simulations were performed considering many such structures interacting with each other as well as the poling field (Figure 4.4.4). Potential functions such as Van der Waals forces, intermolecular as well as intramolecular dipole-dipole electrostatic interactions, and nuclear repulsive (steric) forces were accounted for. Realistic chromophore densities were approximated and kinetic energy corresponding to thermal excitation was introduced. Through such modeling, it was found that $\langle \cos^3 \theta \rangle$ in the range of 0.2-0.3 was expected in electric field poled thin films consisting of the PSLD_41 dendrimer. Order parameters in this range for systems having chromophore density as high as 4.6×10^{20} molecules per cubic centimeter correspond to a reduction in interchromophore electrostatic interaction of more than 30% as compared to analogous guest-host composite materials.

In addition to modified electrostatic potentials, molecular dynamics models also imply that covalent chromophore tethering leads to fundamental changes in the molecular lattice. Covalently bound dipoles can no longer access all available orientation states. Tethering prevents total free rotation and redefines appropriate limits of integration when considering molecular θ , leading to an Ising-like lattice structure. This modified lattice increases the favorability of an overall dipolar, aligned state, allowing further decrease in the dependence of m and thus of $\langle \cos^3 \theta \rangle$ on N .

4.5 Multichromophore Containing Dendrimers as Active Host Matrices

Results outlined in the previous section imply that an intelligently designed nanoscale superstructure allows the introduction of very high chromophore density into organic electro-optic materials without encountering the previously reported r_{33} roll-off behavior. In this section, the potential for applying these dendrimer-based materials as EO-active host matrices was explored. Materials for EO in which the highly dipolar chromophore constituents are covalently bound display reduced phase separation and chromophore-host compatibility problems. It is therefore reasonable to assume that this type of material represents a more homogeneous, more polar environment, as compared to a guest-host material. Improved homogeneity and increased polarity make these materials excellent candidates as EO active host materials.

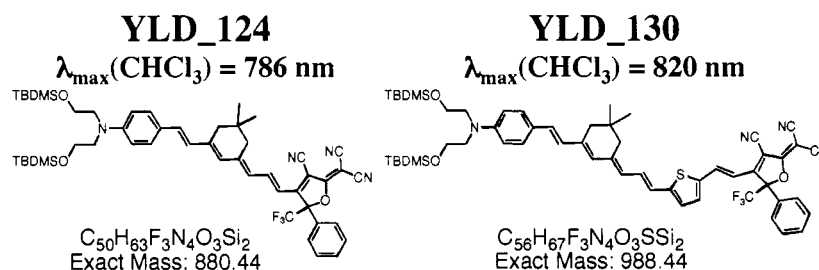


Figure 4.5.1: Guest chromophores YLD_124 and YLD_130

Highly miscible blends of dendrimers and high β EO chromophores have been demonstrated. Effective solvation of the guest chromophore contributes to the shielding of electrostatic interaction. From this solvation, in combination with an

imperfect match in dipole length and magnitude between guest and host chromophores, a reduction in the overall energy of poling induced ordered states within the material is expected.

In order to study the behavior of dendrimer – guest composite materials, two more high β chromophores (YLD_124 and YLD_130) were introduced (figure 4.5.1). Synthesis of these materials has been presented elsewhere.²³⁻²⁵ Both YLD_124 and YLD_130 exhibit substantially red-shifted absorbance maxima as compared to CF₃-FTC (Figure 4.5.2). These materials exhibit higher EO activities than CF₃-FTC when loaded at optimum N in APC. As noted previously, such small molecules do not display glass transition behavior, rather, distinct melting points are observed at 172 °C (YLD_124) and 212 °C (YLD_130).

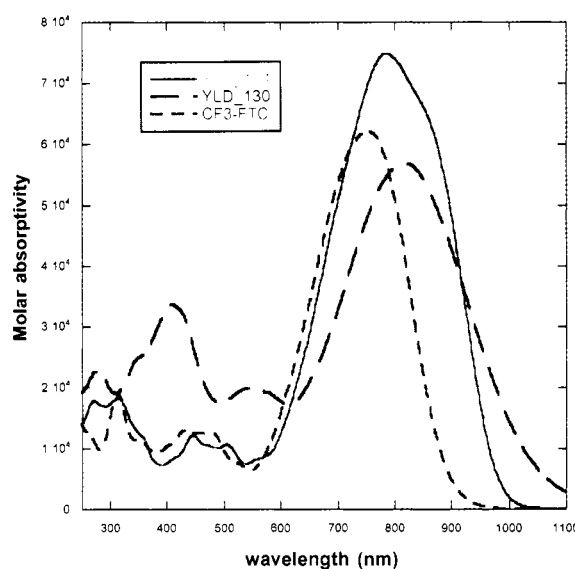


Figure 4.5.2: UV-Visible absorption spectra for YLD_124, YLD_130, compared against CF₃-FTC in CHCl₃ solution

In order to assess EO activity of PSLD_41 / YLD_124 composite films, a series of samples was prepared by systematically increasing the loading percentage of YLD_124 co-dissolved with PSLD_41 in 1,1,2-trichloroethane. The solutions were then spin-cast onto ITO-coated glass slides and top electrodes were fabricated as before. Preliminary examination of the resulting thin films by UV-Visible absorption spectroscopy revealed a bathochromic broadening and moderate spectral distortion as a result of increased loading of YLD_124 (Figure 4.5.3).

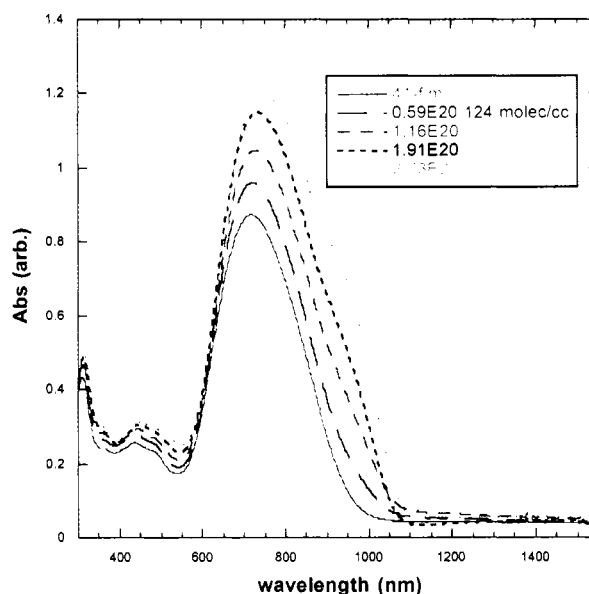


Figure 4.5.3: UV-Vis-NIR absorption spectra for films of PSLD_41 loaded increasingly with YLD_124 ($\times 10^{20}$ molec./cc, corrected for film thickness)

In order to probe the origin of the spectral distortion associated with YLD_124 addition, the spectra obtained were first analyzed mathematically. The spectra were fit and then decomposed into two separate contributions. These contributions were then compared to the spectra arising from YLD_124 in APC, and

pure film spectra of PSLD_41, each normalized by chromophore concentration (see experimental section). It was found that by comparison, the spectral contribution associated with PSLD_41 was almost unchanged by the addition of YLD_124. The spectral contribution resulting from YLD_124 was broadened modestly, but was still relatively unchanged. Linear combination of the normalized spectra of pure PSLD_41 dendrimer and YLD_124 in APC spectra, assuming constant density, resulted in very satisfactory reproduction of the broadening associated with the material blends.

In order to examine the favorability of excited-state charge transfer among guest and host chromophores, electrochemical data were obtained using cyclic voltammetry (Table 4.5.1). Electrochemical data allows comparison of the electron affinity (E_a), ionization potential (I_p), and band-edge offsets of potentially absorptive species.²⁶ These data allow qualitative estimation of the free energy associated with charge transfer that could potentially impact electro-optic properties. Intermolecular charge-transfer and ground or excited state molecular orbital overlap could significantly impact molecular β . Depending on specific aggregate photophysics, absorptive processes and optical transparency at operational wavelengths may also be influenced.

From the data collected it is apparent that ΔE determined from absorption onset is significantly overestimated as compared to electrochemical data. An interesting point to note is that a comparable ΔE is calculated for PSLD_41 and YLD_124 by CV, while UV data shows ΔE to be considerably larger for PSLD_41.

Table 4.5.1: Electrochemical and spectroscopic analysis of I_p (HOMO) and E_a (LUMO) levels of YLD_124, YLD_130, and PSLD_41

compound	Electrochemical analysis ^a			Spectroscopic analysis		
	HOMO (eV)	LUMO (eV)	ΔE	LUMO (eV)	ΔE	Cut-off (nm)
ferrocene	-0.4235	---	---	---	---	---
YLD_124	-5.036	-4.069	0.967	-3.767	1.269	977
YLD_130	-4.834	-4.085	0.749	-3.629	1.205	1029
PSLD_41	-5.182	-4.105	0.958	-3.745	1.437	909

^adata collected from 10^{-3} M soln. in CH_2Cl_2 and referenced against ferrocene standard

The dendrimer structure itself may contribute to the observed deviation from expected trends. The aromatic stabilization of the thienyl-vinylene bridge slightly reduces both HOMO and LUMO energies in PSLD_41 leading to a small band offset as compared to the tetraene bridge-based YLD_124. The longer bridge of YLD_130 leads to a narrowing of the ΔE gap due to both an increase in HOMO and decrease in LUMO energies resulting from increased conjugation length. This is reflected by reduced ΔE demonstrated by both spectroscopic and electrochemical analysis.

Despite small band offsets between PSLD_41 and YLD_124 excited state charge transfer would not be expected to be extremely favorable. Values calculated for HOMO and LUMO offsets are 0.15 eV and 0.04 eV respectively. These electrochemical potentials are not comparable to the 0.3 – 0.4 eV coulombic attraction potential binding photogenerated excitons,²⁷ even if closely associated aggregates exist in the dendrimer / guest thin films, charge separation rates are expected to be retarded. Extremely low extinction coefficients at the measurement wavelengths of 1310 and 1550 nm should also lead to low population of excited states further disfavoring intermolecular excited state charge transfer contributions.

One potential uncertainty that is not completely accounted for by the data presented above is that of aggregate contribution to molecular hyperpolarizability. Intermolecular charge transfer does not seem favorable if molecules are treated under a long-range electronically coupled monomer approximation. However, recent quantum mechanical and experimental analysis obtained from asymmetric porphyrin aggregates suggest that intermolecular orbital overlap may influence β .^{28,29}

After careful analysis of the absorption spectra derived from PSLD_41 / YLD_124 composites, refractive index change as a function of doping was investigated using Variable Angle Spectroscopic Ellipsometry (VASE). Measurements relating refractive index to extinction coefficient were performed on samples of pure PSLD_41 and samples of 25% by weight (1.91×10^{20} molec. / cc) YLD_124 in PSLD_41. The data obtained are plotted in figure 4.5.4.

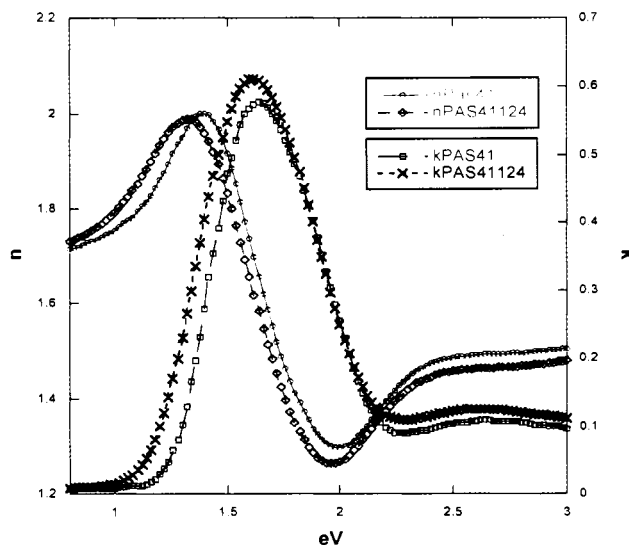


Figure 4.5.4: Refractive index (n) and extinction coefficient (k) as a function of wavelength for PSLD_41 pure films and PSLD_41 / YLD_124 25%

Refractive indices of PSLD_41 at 0.799 eV (1550 nm) and 0.944 eV (1310 nm) were determined to be 1.71 and 1.73 respectively. Indices of the 25% YLD_124 loaded films were calculated to be 1.73 and 1.77. Such index changes are expected to accompany an increase in chromophore loading. The dielectric environment and linear susceptibilities are altered by the increase in density of highly polarizable, highly dipolar chromophores within the material matrix. The index data obtained was then used for calculation of r_{33} .

Measurement of r_{33} was performed as before. Using the *in-situ* reflection apparatus, poling conditions were optimized. The EO behavior of the PSLD_41 / YLD_124 sample range was then systematically characterized with respect to N and E_p . Two series of APC composite samples of CF₃-FTC and YLD_124 were also prepared and evaluated for comparison. Within each series, excluding pure dendrimers, the guest loading density was incrementally increased until ρ values could not be satisfactorily determined. The results are presented in figure 4.5.5. All values presented assume approximately 15% error from film thickness and poling voltage measurements.

The data show that the slopes of ρ vs. N found for PSLD_41 and CF₃-FTC / APC are very comparable at low loading. These data imply that, in the dilute limit, where dipoles are dispersed homogeneously and interact only weakly, β , and μ are unchanged. More importantly, in the dilute limit, ordering efficiency (m , equation 4.4.2) is comparable between the dendrimer structure PSLD_41 and free chromophore composite of CF₃-FTC in APC. However, as N increases to 2.9×10^{20}

molec. /cc, CF₃-FTC reaches a maximum consistent ρ value of 0.63. Optimum r_{33} of 52-55 pm/V is obtained from samples where $\rho = 0.42$ (1.79×10^{20} molec./cc). At higher N, ρ value determination becomes very imprecise and r_{33} is diminished. No such behavior is observed for PSLD_41 or PSLD_33 samples. Due to synthetic limitations, the maximum N investigated for the dendrimer system was 6.8×10^{20} molec. / cc (inherent N of PSLD_33). Here, a ρ value of 1.34 is recorded. This ρ value was only slightly less than linear with respect to increased N. These findings further support the hypothesis that chromophore isolation and nanoscale environment homogeneity are enhanced when dipolar units are incorporated into dendritic structures such as PSLD_41 or PSLD_33.

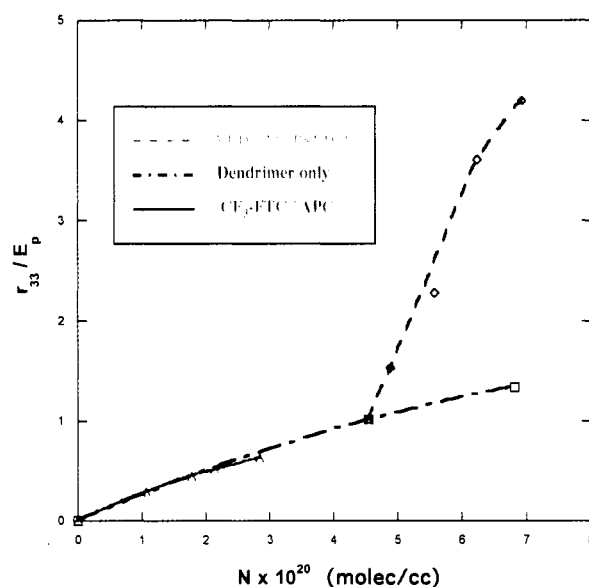


Figure 4.5.5: Poling efficiency vs. chromophore N for CF₃-FTC in APC, pure dendrimers PSLD_41 and PSLD_33, and a sample series containing increased loading of guest YLD_124 in PSLD_41 host

When the PSLD_41 / YLD_124 sample series was examined, striking results were obtained. A very large increase in the slope of ρ vs. N was recorded in addition to an over 3-fold increase in ρ . Maximum r_{33} values reproducibly observed for this sample series were in the range of 245 – 285 pm/V. Barring optical enhancement, an increase in the slope of ρ vs. N must indicate a large increase in the product of $\mu\beta m$ as shown below.

$$r_{33}/E_p N \propto \mu\beta m \quad (4.5.1)$$

In a situation where this increase is due mostly or only to an increase in ordering efficiency, the new slope corresponding to YLD_124 loaded into a PSLD_41 host exceeds that expected for the independent particle limit. A slope greater than the independent particle limit suggests that electrostatic interactions are acting to drive the ordering of the dopant.

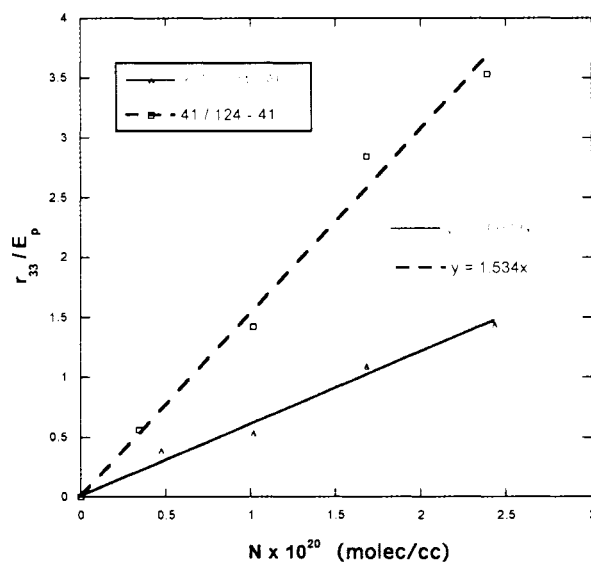


Figure 4.5.6: ρ vs. N plots for YLD_124 / APC and ((YLD_124 / PSLD_41) - (PSLD_41))

For comparison of the inherent $\mu\beta m$ differences between CF₃-FTC and YLD_124, respective ρ vs. N values were compared by examining the poling behavior of the YLD_124 / APC series. In order to evaluate the change in ρ vs. N of YLD_124 in an APC host with respect to a PSLD_41 dendrimer host, the contribution from the dendrimer ρ , normalized for material content percentage, was subtracted from the total. This approximation was made assuming that the PSLD_41 value was unchanged by the dopant. Figure 4.5.6 illustrates the hypothesis of greatly enhanced m of YLD_124 when poled in a PSLD_41 host. An enhancement factor of 2.5 was observed between YLD_124 in APC and in a PSLD_41 composite when the PSLD_41 host contribution was removed.

Table 4.5.2 lists β values that were experimentally determined by spectrally resolved Hyper Raleigh Scattering (HRS) measurements recorded at an excitation wavelength of 1.9 μm . The μ values shown were obtained using Density Functional Theory (DFT) quantum mechanical modeling. Values of ρ / N are included as well. When compared to that of CF₃-FTC in APC, the ρ / N of YLD_124 in APC is enhanced by a factor of 2.64. The $\mu\beta$ product calculated for YLD_124 using tabulated values is a factor of 2.6 greater than that of CF₃-FTC. These differences in $\mu\beta$ account very well for the experimentally determined differences in ρ / N between the two small-molecule / APC composites. However, they do not account for the enhancement factor of 2.5 between YLD_124 in APC and YLD_124 in PSLD_41.

Table 4.5.2: β_{HRS} , calculated μ , and ρ/N values for free chromophores, dendrimers and composites thereof

compound	β_{HRS} ($\times 10^{-30}$ esu) ^a	μ (D) ^b	ρ/N
CF ₃ -FTC	2997	26.1	0.222
YLD_124	7087	28.7	0.585
PSLD_33 and 41	---	---	0.199
41 / 124	---	---	1.378

^a β_{HRS} values are recorded @ $\lambda = 1.9 \mu\text{m}$ using FTC standard

^b μ values are calculated using DFT (Dmol³) in gas phase

Very simple analysis, excluding changes in photophysical properties, supports the hypothesis that when YLD_124 is introduced in to the PSLD_41 host, greatly increased dopant η is observed. This dramatic increase in ordering efficiency is therefore associated with a more favorable electrostatic environment. Improved guest-host compatibility, enhanced chromophore isolation, disfavored side-to-side dipolar interactions and greatly favored head-to-tail interaction, may all contribute to a situation in which intermolecular electrostatic interaction actually favors acentric chromophore order.

However, as mentioned previously, at this time it is extremely difficult to account for resonance effects that may be magnified by solvatochromic shift and line broadening associated with intermolecular interaction. Recent literature reports also suggest that at higher loading, increased intermolecular π -orbital overlap could enhance β values.^{28,29} At small intermolecular distances, contributions from intermolecular orbital overlap associated with H or J aggregation may play a significant role. Anti-parallel or slipped J-aggregates may be expected to induce a red shift in absorbance spectra and an increase in β . It is interesting to note that this type of aggregation may be associated with head-to-tail, donor-to-acceptor and

slipped interactions. Aggregation of this or similar nature can be projected to not only enhance β , but also to contribute to increased order. Previous examination of UV-Vis absorption spectra suggests that such aggregation effects have less of an influence on the molecular orbital picture than they do ordering. The UV data discussed previously also suggest that aggregate molecular orbital overlap contributions are small. Pronounced changes in absorption spectra should accompany any significant intermolecular electron density delocalization.

The possibility also exists that chromophore β values may be influenced by their immediate dielectric environment. As N is increased, the dielectric constant of the composite material can be expected to increase. Changes in external environment will have a direct impact on the relative admixing of chromophore ground and excited states. This altered ground state will also affect the nature of molecular orbital contribution to the electric field polarized state, influencing hyperpolarizability.

4.6 Preliminary exploration of poling induced order in PSLD_41 / YLD_124 and PSLD_41 / YLD_130 composite films

To obtain some preliminary estimation of the poling induced order obtained in PSLD_41 / YLD_124 composite samples a technique based on Attenuated Total Reflection (ATR) was employed. ATR uses the same sample configuration as the reflection technique making sample measurement convenient and comparable. The ATR technique for measuring EO coefficients is a prism coupling technique. The sample is pressed against a high index prism (in this case rutile) by a pneumatic

piston. An AC modulation waveform is then applied to the sample electrodes.

The prism-sample assembly is then rotated to find a coupling angle (critical angle) with respect to the incident laser beam. At this critical angle, incident light is coupled into the EO film and reflected intensity is attenuated. At this angle, a modulation waveform frequency-correlated refractive index dithering can be measured by a lock-in-amplifier. The intensity of the lock-in response can then be compared to the derivative (slope) of the reflected intensity attenuation curve, and based on this ratio, EO coefficients are calculated. ATR has the distinct advantage of independent determination of both r_{13} and r_{33} . The anisotropy between these tensor components can be used as probe of $\langle \cos^3 \theta \rangle$. In the reflection based polarization interferometry technique (Teng-Man), r_{33}/r_{13} is assumed to be 3 based on experimental measurement and order parameters theoretically derived from the isotropic model.³⁰

The tensor component r_{33} represents the EO coefficient in which the electric field of incident light oscillates in a plane parallel to the poling axis (T_M for ATR). In this orientation, the β_{zzz} of chromophores oriented by poling and therefore material $\chi^{(2)}$ is allowed maximum interaction. Likewise, r_{13} represents interaction with polarized light in which the e-field oscillates in a plane perpendicular to the poling axis (T_E for ATR). The ratio of r_{33}/r_{13} should increase in response to increased order parameter. Several samples of PSLD_41 / YLD_130 composite material were measured. A typical example, values were measured for a 25% by wt. (59% of total N), YLD_124 in PSLD_41 sample that was poled at $E_p = 75 \text{ V}/\mu\text{m}$. The r_{33} for this sample measured by reflection was 285 pm/V. Using the ATR method r_{33} and r_{13}

were determined to be 244 pm/V and 79 pm/V respectively, yielding an r_{33}/r_{13} ratio of 3.09. Discrepancy in the absolute value of r_{33} between reflection and ATR can be attributed to increased conductivity when sample is placed under pressure (20 psi) against the prism for ATR measurement. Simply maintaining poling induced order at such increased density represents a rather dramatic improvement in organic EO material performance. An r_{33} / r_{13} ratio of approximately 3 at such high N may suggest a substantially increased dopant ordering efficiency.

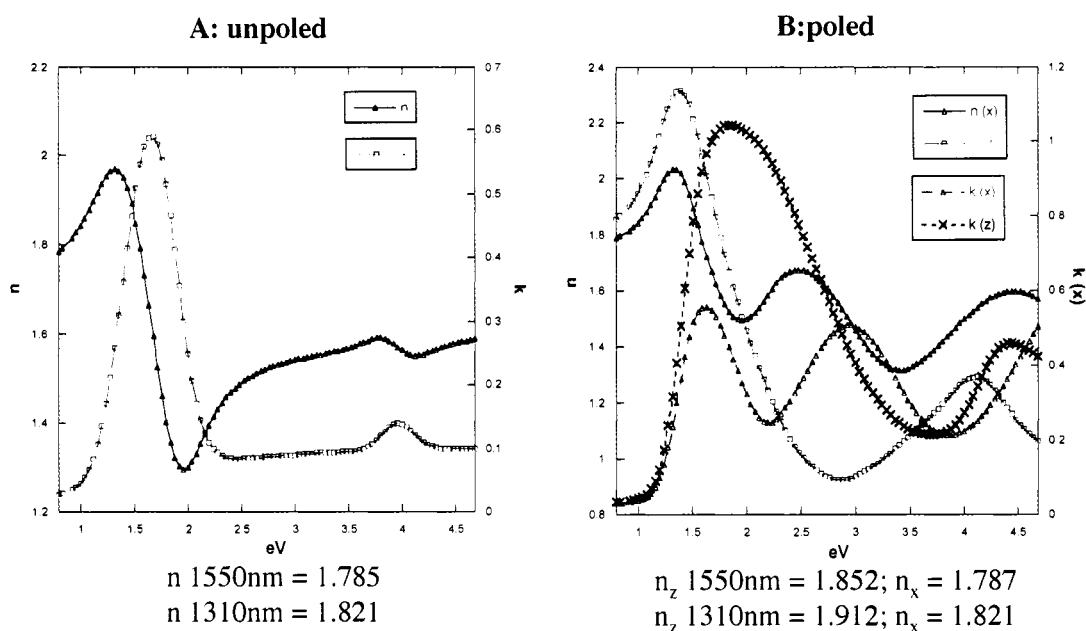


Figure 4.6.1: Biaxial optical constants for 25% by wt. YLD_130 in PSLD_41, A: unpoled sample, B: sample poled by corona field

Composite materials consisting of PSLD_41 and YLD_130 were briefly explored as well. Preliminary HRS data indicated that YLD_130 displayed enhanced hyperpolarizability as compared to YLD_124. Thorough studies were not

performed due to concerns about measurement accuracy caused by increased optical absorption at probe wavelengths. The effects of this absorption on reflection apparatus based r_{33} and HRS derived β measurements are not fully understood. Preliminary r_{33} measurements of a 25% YLD_130 in PSLD_41 composite yielded ρ values of 4.6 and maximum r_{33} of 430 pm/V.

Using VASE the poling induced birefringence of this material was evaluated (Figure 4.6.1). A sample was corona poled and then biaxial optical constants were evaluated using polarized light. The data was then compared to an unpoled sample. The poled sample indeed displayed significant birefringence. Unfortunately, relating linear to nonlinear polarizability is nontrivial. It is therefore difficult to relate this data directly to an order parameter relevant to EO behavior. Nevertheless, further research is currently underway to help understand the problem.

4.7 Device Testing of PSLD_41 / YLD_124 Composites

Large r_{33} values displayed by dendrimer / chromophore composite materials immediately led to interest in photonic microdevice based testing. Preliminary testing was accomplished through a collaborative project involving the research group of professor Axel Scherer at the California Institute of Technology.

The test configuration consisted of a new device design based on a slotted waveguide micro-ring resonator.²⁴ A slotted ring was fabricated in silicon on insulator (SOI). The top silicon layer was doped with 10^{19} phosphorous atoms per cm^3 in order to achieve a resistivity of approximately 0.025 ohm-cm. This layer served as both the waveguide structure as well as the poling and modulating

electrodes (Figure 4.7.1). The slot width was 110nm deep by 100nm wide. After fabrication, the slot was filled with EO material by solution casting. The slotted waveguide design allowed the bulk of the optical intensity to be confined to the low index region between the silicon outer rails. The electric field associated with the optical mode can be magnified to values near 10^6 V/m using this type of configuration.³¹ Inset A in Figure 4.7.1 shows modeling of this mode nanoconfinement.

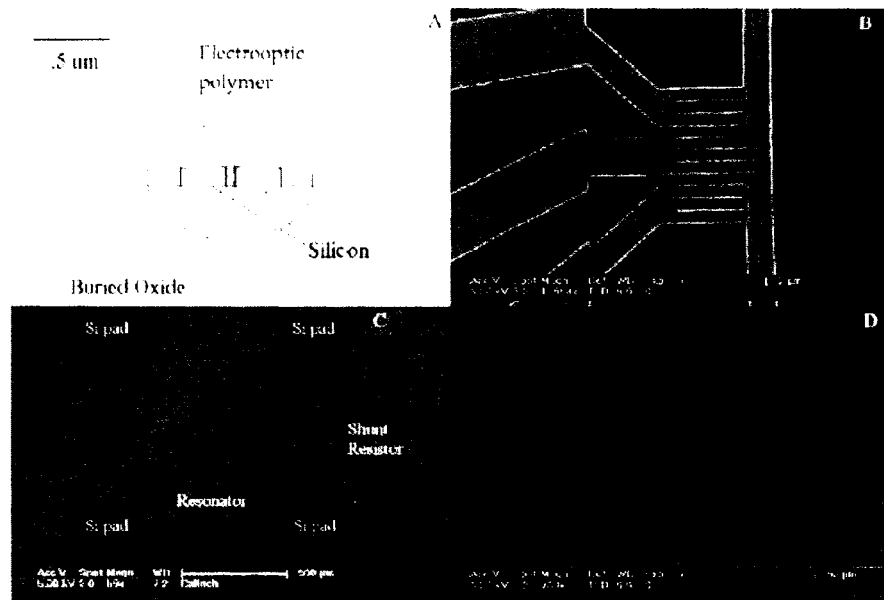


Figure 4.7.1: Panel a: model of device cross-section displaying optical mode, panel b: electrode contact structure for applying poling and modulating fields, panel c: full device view showing electrical and optical inputs, panel d: resonator structure

Samples were tested using YLD_124, 25% in APC as well as YLD_124, 25% in PSLD_41 as EO active material components. Testing revealed optical modulation at high Mhz frequencies (limited by test electronics) corresponding to 33

pm/V for the YLD_124 / APC composite and 79 pm/V for PSLD_41 / YLD_124 composites at a test wavelength of 1550 nm. In addition to pockel's effect modulation, these devices also recorded the first demonstration of nonlinear optical rectification at sub-milliwatt optical power levels. Previous demonstrations of this direct, zero bias, optical detection have required kilowatt power levels from pulsed laser sources.

Nonlinear optical rectification is essentially the reverse process of pockel's effect optical modulation. Modulated optical intensity input is converted to modulated electrical signal output. These results bring about the possibility of optical modulation and detection using the same device configuration, fully integrated on-chip with silicon electronics. Optical detectors based on this configuration could potentially compete with current III-V semiconductor-based devices, allowing increased bandwidth and decreased processing complexity and cost.

4.8 Photo-Stability of Dendrimer / Guest Composites

Telecommunications, computing, and other industrial applications require that photonic devices must display reasonable stability and functionality over many years of continuous operation. Parameters that determine this functionality and ultimately define device lifetime include the photochemical stability of the EO active material.^{32, 33}

The relative photostability of PSLD_41 and PSLD_41 / guest composites fabricated using YLD_124 in PSLD_41 and YLD_130 in PSLD_41 was determined.

Standard figures of merit (FOM) were measured by exposure of the materials to 1550 nm radiation. The FOM of the dendrimer and dendrimer composite materials were then compared to APC composites of CF₃-FTC and YLD_124. Dendrimer PSLD_41 was measured as a pure film. Dendrimer / chromophore composites were measured at 25% loading by weight. Similar concentrations of the analogous chromophores were studied in APC for a baseline comparison. Full experimental details for the pump-probe measurements were presented elsewhere by D. Bale *et al.*³⁴

Table 4.8.1: photostability FOM for EO materials in Air $\lambda = 1550$ nm

sample	FOM: $B/\sigma \times 10^{32} \text{ m}^{-2}$
PSLD_41 (pure film)	37 ± 7
CF ₃ -FTC / APC 21%	8 ± 2
PSLD_41 / YLD_124 25%	28 ± 7
YLD_124 / APC 25%	5 ± 2
PSLD_41 / YLD_130 25%	13 ± 3

Photodecay kinetics were determined using the previously described literature model.³⁵ Following these guidelines, material photodegradation was assessed using the effective lifetime, τ , as defined following

$$N_t / N_0 = \exp(-t / \tau) \quad (4.8.1)$$

here N_t defines chromophore concentration after 1550 nm light exposure, N_0 denotes initial chromophore concentration and t represents time. The photostability FOM, B/σ , is related to effective lifetime by

$$\tau = B / \sigma n \quad (4.8.2)$$

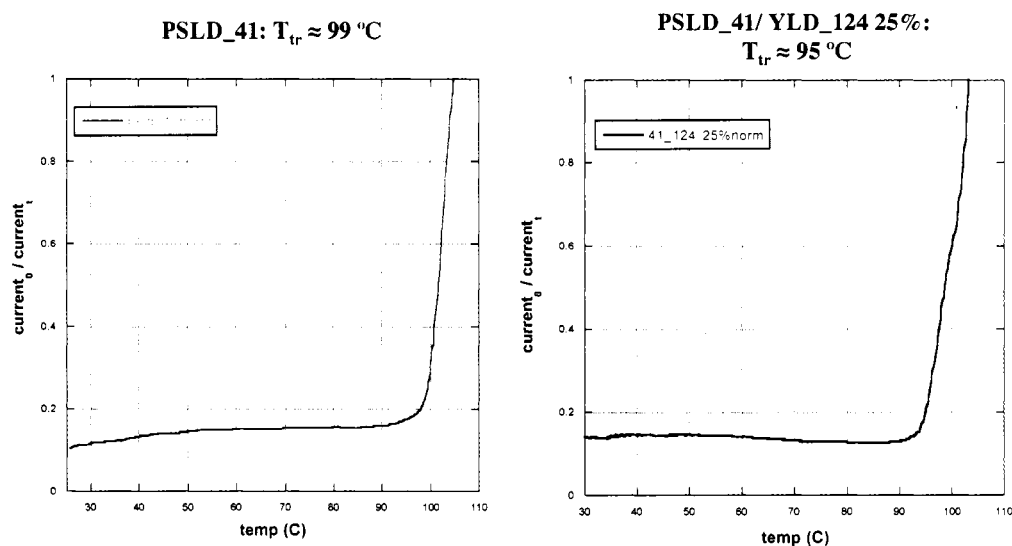
where σ represents chromophore single-photon absorption cross-section, B^{-1} is the quantum yield for photobleaching, and n is photon flux.

Greater B/σ values indicate enhanced photostability.^{35, 36} Data for the systems considered here is presented in table 4.8.1. Photostability FOMs show that the dendrimer based PSLD_41 and composite materials represent a quite substantial improvement as compared to APC composites. Comparison of PSLD_41 with CF₃-FTC shows the most dramatic improvement. Chromophore YLD_124 in APC shows reduced photostability compared to CF₃-FTC in APC. It is therefore reasonable to assume that the reduced photostability demonstrated for dendrimer / chromophore composites as compared to pure dendrimer is a result of the addition of the less stable guest. Increased lattice density as well as dendritic encapsulation may account for enhanced photochemical stability in these materials.

4.9 Thermal Stability of r_{33} in PSLD_41 / YLD_124 Composites

Thermal stability measurement procedures using an *in-situ* r_{33} determination apparatus have been thoroughly discussed in chapters 2 and 3.^{14, 37} The temperature at which an abrupt increase in current is observed during poling (T_{tr}) can be taken as the onset of material glass transition. The value of T_{tr} varies according to the thermal properties of the specific material used, and also on the level of guest chromophore doping. Plasticization effects are generally observed when a guest chromophore is loaded into a host material. Examples of T_{tr} experimental results are illustrated in figure 4.9.1. Values of T_{tr} for pure film samples of PSLD_41 were found to be very comparable with T_{tr} for doped dendrimer samples of 25% by weight YLD_124 in

PSLD_41. Optimum poling temperatures for the two materials were therefore also very similar ($\approx 95^\circ\text{C}$). The data demonstrated that glass transition temperature was not depressed as much as expected from the initial T_g of 103°C of the pure



PSLD_41 material.

Figure 4.9.1: Thermally stimulated current experiments for determination of T_{tr} of pure PSLD_41 films and PSLD_41 / YLD_124 (25% by wt)

Thermal stability was investigated further through dynamic thermal stability experiments performed at a temperature ramp rate of $10^\circ\text{C}/\text{min}$. The results are presented in figure 4.9.2. The onset of abrupt thermally induced dipolar randomization was recorded for pure PSLD_41 at approximately 92°C . A value of 83°C was recorded for a 25% by weight sample of YLD_124 in PSLD_41. Roughly a 10°C difference is observed. The observed plasticization behavior is consistent with expectation for guest host systems.

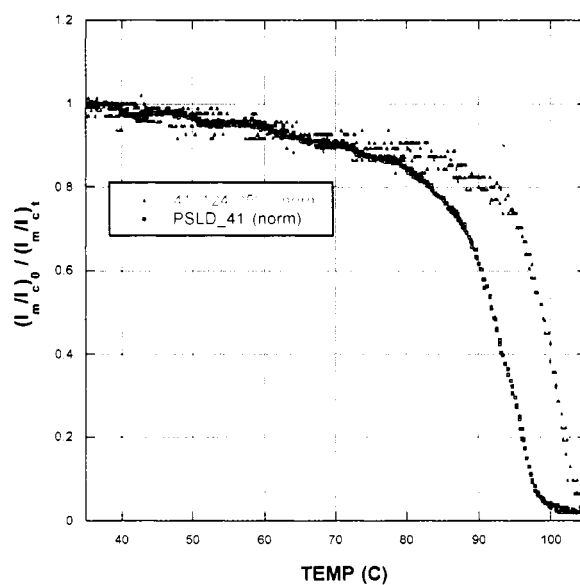


Figure 4.9.2: Dynamic thermal stability experiments performed for PSLD_41 and 25% by weight YLD_124 in PSLD_41 (10 °C/min)

4.10 Conclusions

Multichromophore dendrimer based organic materials for 2nd order nonlinear optical applications offer great insight into fundamental material properties. Excellent agreement with theory demonstrates the power of the rational design process for the creation of materials with tailored photo-physical properties. Dendritic structures containing covalently attached EO chromophores offer good isolation from intermolecular electrostatic interaction while allowing for efficient poling field induced dipolar ordering. These materials exhibit dramatic improvement in the $N\langle\cos^3\theta\rangle$ product through a decoupling of poling efficiency and chromophore number density.

Introduction of a guest chromophore into the dendrimer matrix leads to startling results. Preliminary analysis suggests that an ordered host lattice such as the multichromophore dendrimer PSLD_41 may give rise to guest chromophore ordering efficiency greater than that expected for non-interacting dipoles. This implies that dipolar interaction actually augments acentric dipolar order rather than attenuating it. Future work will be focused on a greater understanding of this phenomenon. Various experiments are currently underway to further probe dopant effects on the molecular lattice as well as lattice effects on the dopant. Experiments such as determination of the concentration dependence of the r_{33}/r_{13} ratio are being performed both experimentally using ATR and theoretically by simulation.

In addition to ordering efficiency studies, probing the effects of chromophore environment on β is also underway. The polarity and nature of the environment surrounding each chromophore can be expected to perturb relative location of ground state electron density as well as the mixing of the various ground and excited states. Intermolecular contributions to hyperpolarizability are also possible. Frequency Agile Hyper Rayleigh Scattering experiments in different solvent environments are currently underway.

4.11 Experimental Section

Pseudo-Atomistic Monte Carlo Simulations. Calculations were performed in collaboration with the Bruce H. Robinson research group and are detailed elsewhere.^{8, 11, 12}

Synthesis General. All solvents were purified by distillation prior to use unless otherwise stated. Commercially available chemicals were used as received unless otherwise stated. All alkyllithium reagents were titrated by literature procedure prior to use. Glassware was base treated and oven or flame dried. All reactions were performed under inert atmosphere.

Diethyl (2-thienylmethyl)phosphonate (1): was prepared according to literature procedure.¹⁹

{4-[2-(4-Bromo-thiophen-2-yl)-vinyl]-phenyl}-[2-(*tert*-butyl-dimethyl-silanyloxy)-ethyl]-methyl-amine (3): An oven dried, mag.-stirred, 250 mL RBF was charged with a solution of p-(N,N-diethylamino)benzaldehyde (**15**), (17.62 g, 56.27 mmol), and Diethyl (4-bromo-2-thienylmethyl)phosphonate (**24**), (11.01 g, 37.51 mmol) in 100 mL freshly distilled THF. Potassium *tert*-butoxide (63.77 mL, 1.0 M soln. in THF) is added dropwise over 0.5 hr. The mixture was allowed to stir for 12hrs and 100mL NaCl (sat) was added. The organic layer was separated and the aqueous layer was extracted with DCM. The Combined organics were dried over MgSO₄, filtered, and the solvent was removed in vacuo. The resulting crude product was then purified by silica gel column chromatography (5% EtOac/Hex) to yield 15.1 g (90%) of a bright yellow solid.

¹H NMR (500 MHz, CDCl₃): δ 7.37 (d, *j* = 9 Hz, 2H), 7.03 (d, *j* = 1 Hz, 1H), 6.96 (d, *j* = 15.5 Hz, 1H), 6.92 (d, *j* = 2 Hz, 1H), 6.90 (d, *j* = 15.5 Hz, 1H), 6.72 (d, *j*

= 9 Hz, 2H), 3.836 (t, j = 6.5 Hz, 2H), 3.55 (t, j = 6.4 Hz, 2H), 3.07 (s, 3H), 0.958 (s, 9 H), 0.092 (s, 6 H)ppm.

^{13}C NMR (500 MHz, CDCl_3): δ 149.17, 145.01, 130.03, 127.84, 126.31, 124.15, 119.78, 115.94, 111.88, 110.03, 60.56, 54.74, 39.27, 25.98, 18.32, -5.29 ppm.

HRMS (ESI): exact mass calcd for $\text{C}_{21}\text{H}_{31}\text{N O Si S}$ $[\text{M}+\text{H}]^+$, 452.1079, Found, 452.1079.

5-[2-(4-{[2-(*tert*-Butyl-dimethyl-silanyloxy)-ethyl]-methyl-amino}-phenyl)-vinyl]-thiophene-3-carbaldehyde (4): A solution of n-BuLi (1.6 M in hexanes) was titrated using 4-biphenyl methanol as the indicator and found to be 1.2 M. An oven dried, mag.-stirred 250 mL RBF was charged with {4-[2-(4-Bromothiophen-2-yl)-vinyl]-phenyl}-[2-(*tert*-butyl-dimethyl-silanyloxy)-ethyl]-methyl-amine (**16**), (5 g, 11.04 mmol). This was dissolved in 100mL freshly distilled diethyl ether. The solution was then cooled to -78°C (dry ice / acetone). Exactly 1 equivalent of n-BuLi (9.3 mL, 11.04 mmol) was added dropwise over 15 minutes. The reaction temp was raised slightly by addition of more acetone to the bath. The reaction was stirred for 10 minutes and then quenched with dry DMF (8.6 mL, 110.4 mmol) by dropwise addition. The cooling bath was removed for 10 minutes and then NH_4Cl (sat, 100 mL) was added. The organics were separated and the aqueous phase was extracted with EtOAc. The organics were then combined, dried of MgSO_4 , and the solvent removed in vacuo. The crude product was purified by silica gel column

chromatography (5% EtOAc/Hex) to yield 3.0 g (7.47 mmol, 67%) of a non-flourescent, yellow, crystalline solid.

^1H NMR (500 MHz, CDCl_3): δ 9.84 (s, 1H), 7.89(s, 1H), 7.36 (d, j = 9 Hz, 2H), 7.35 (s, 1H), 6.98 (d, j = 15.5 Hz, 1H), 6.91 (d, j = 15.5 Hz, 1H), 6.70 (d, j = 9 Hz, 2H), 3.81 (t, j = 6 Hz, 2H), 3.53 (t, j = 6 Hz, 2H), 3.05 (s, 3H), 0.92 (s, 9H), 0.06 (s, 6H) ppm.

^{13}C NMR (500 MHz, CDCl_3): δ 184.99, 149.28, 146.04, 143.40, 134.69, 131.13, 127.89, 123.95, 121.02, 116.03, 111.85, 60.52, 54.69, 39.24, 25.93, 18.28, -5.34 ppm.

HRMS (ESI): exact mass calcd for $\text{C}_{22}\text{H}_{32}\text{N}\text{O}_2\text{SiS}$ $[\text{M}+\text{H}]^+$, 402.1923, Found, 402.1915.

{5-[2-(4-{[2-(*tert*-Butyl-dimethyl-silanyloxy)-ethyl]-methyl-amino}-phenyl)-vinyl]-thiophen-3-yl}-methanol (5): A 250 mL, 2-neck, mag.-stirred, RBF was equipped with an addition funnel and charged with NaBH_4 (0.2 g, 5.28 mmol). An aqueous solution of NaOH (4 mL, 0.2 N) was then added and the mixture was cooled to 0°C (ice bath). A solution of 5-[2-(4-{[2-(*tert*-Butyl-dimethyl-silanyloxy)-ethyl]-methyl-amino}-phenyl)-vinyl]-thiophene-3-carbaldehyde (**17**), (3.0 g, 7.47 mmol) dissolved in 1:1 THF/MeOH (40 mL) was then added dropwise. The reaction was stirred for 30 minutes and the cooling bath was removed. After 1 hour the reaction was quenched by the slow addition of NH_4Cl (sat). The organics were separated and the aqueous phase was extracted with EtOAc. The organics were then

combined, dried of MgSO_4 , and the solvent removed in vacuo. The reaction was quantitative by NMR and the product was used without further purification.

^1H NMR (300 MHz, CDCl_3): δ 7.35 (d, j = 9 Hz, 2H), 6.99 (m, 3H), 6.80 (d, j = 16.2 Hz, 1H), 6.70 (d, j = 9 Hz, 2H), 4.65 (s, 2H), 3.79 (t, j = 6 Hz, 2H), 3.51 (t, j = 6 Hz, 2H), 3.03 (s, 3H), 0.916 (s, 9H), 0.056 (s, 6H) ppm.

^{13}C NMR (500 MHz, CDCl_3): δ 148.91, 144.85, 142.72, 129.02, 127.64, 124.77, 124.07, 119.44, 117.30, 111.96, 60.83, 60.56, 54.76, 39.25, 25.98, 18.32, -5.29 ppm.

HRMS (ESI): exact mass calcd for $\text{C}_{22} \text{H}_{34} \text{N} \text{O}_2 \text{Si} \text{S}$ $[\text{M}+\text{H}]^+$, 404.2080, Found, 404.2069.

5-[2-(4-{[2-(*tert*-Butyl-dimethyl-silanyloxy)-ethyl]-methyl-amino}-phenyl)-vinyl]-3-hydroxymethyl-thiophene-2-carbaldehyde (6): In a 250 mL, oven dried, mag.-stirred RBF, {5-[2-(4-{[2-(*tert*-Butyl-dimethyl-silanyloxy)-ethyl]-methyl-amino}-phenyl)-vinyl]-thiophen-3-yl}-methanol (**18**), (3.0 g, 7.47 mmol) was dissolved in freshly distilled THF (30 mL). The solution was then cooled to -78°C (dry ice/acetone). $n\text{-BuLi}$ (14.44 mL, 2.30 mmol, soln. in hexanes) was then added dropwise over 15 minutes. After addition a light green color was observed. The mixture was allowed to stir for 1 hour and then quenched with dry DMF (1.74 mL, 22.41 mmol). The reaction was then allowed to warm to room temperature overnight. A saturated solution of NaCl (100 mL) was then added. The organics were separated and the aqueous phase was extracted with DCM. The organics were then combined, dried of MgSO_4 , and the solvent removed in vacuo. The crude

product was then purified by silica gel column chromatography (10% EtOAc/Hex) and then repurified, again by column (DCM). To yield 2.76 g (5.26 mmol, 70%) of a red, oily, solid.

^1H NMR (500 MHz, CDCl_3): δ 9.75 (s, 1H), 7.39 (d, j = 9 Hz, 2H), 7.12 (d, j = 15.5 Hz, 1H), 7.08 (s, 1H), 6.97 (d, j = 15.6 Hz, 1H), 6.70 (d, j = 8 Hz, 2H), 4.86 (s, 2H), 3.81 (t, j = 6 Hz, 2H), 3.54 (t, j = 6 Hz, 2H), 3.07 (s, 3H), 0.91 (s, 9H), 0.06 (s, 6H) ppm.

^{13}C NMR (300 MHz, CDCl_3): δ 182.19, 153.97, 151.67, 149.79, 134.01, 133.83, 128.55, 126.45, 123.49, 115.63, 111.86, 60.53, 59.30, 54.60, 39.20, 25.91, 18.24, -4.98, ppm.

HRMS (ESI): exact mass calcd for $\text{C}_{23}\text{H}_{34}\text{N}_3\text{O}_3\text{SiS}$ $[\text{M}+\text{H}]^+$, 432.2029, Found, 432.2019.

2-[4-(2-{5-[2-(4-{[2-(*tert*-Butyl-dimethyl-silanyloxy)-ethyl]-methyl-amino}-phenyl)-vinyl]-3-hydroxymethyl-thiophen-2-yl)-vinyl]-3-cyano-5-phenyl-5-trifluoromethyl-5*H*-furan-2-ylidene]-malononitrile (7): A mag.- stirred, 25 mL RBF was charged with 5-[2-(4-{[2-(*tert*-Butyl-dimethyl-silanyloxy)-ethyl]-methyl-amino}-phenyl)-vinyl]-3-hydroxymethyl-thiophene-2-carbaldehyde (**19**), (2.00 g, 4.64 mmol), and 2-(3-Cyano-4-methyl-5-phenyl-5-trifluoromethyl-5*H*-furan-2-ylidene)-malononitrile; compound with methane (TCF) (1.53, 4.85 mmol). This mixture is then dissolved in 5 mL absolute ethanol. The reaction was heated to 50 °C overnight. The ethanol was removed in *vacuo* and the crude product was purified by

silica gel column chromatography (10% EtOAc/DCM), to yield a metallic blue solid (2.00 g, 2.74 mmol, 60%). $\lambda_{\text{max}} = 757.00 \text{ nm}$,

^1H NMR (300 MHz, CDCl_3): δ 8.16 (d, $J = 15.3 \text{ Hz}$, 1H), 7.56 (br s, 5H), 7.38 (d, $J = 8.7 \text{ Hz}$, 2H), 7.12 (d, $J = 15.9 \text{ Hz}$, 1H), 7.07 (s, 1H), 6.97 (d, $J = 15.9 \text{ Hz}$, 1H), 6.71 (d, $J = 8.7 \text{ Hz}$, 2H), 6.55 (d, $J = 15.3 \text{ Hz}$, 1H), 4.65 (s, 2H), 3.82 (t, $J = 5.4 \text{ Hz}$, 2H), 3.57 (t, $J = 6 \text{ Hz}$, 2H), 3.10 (s, 3H), 0.89 (s, 9H), 0.03 (s, 6H), ppm.

^{13}C NMR (300 MHz, CDCl_3): δ 175.42, 161.23, 156.70, 154.55, 150.87, 138.86, 137.15, 133.55, 131.49, 129.99, 129.65, 128.30, 126.72, 122.94, 120.19, 115.42, 112.22, 111.74, 111.34, 111.02, 110.63, 60.60, 58.86, 56.97, 54.59, 39.32, 25.87, 18.21, -4.89, ppm.

HRMS (ESI): exact mass calcd for $\text{C}_{39}\text{H}_{40}\text{N}_4\text{O}_3\text{F}_3\text{SiS}$ $[\text{M}+\text{H}]^+$, 729.2543, Found, 729.2528.

1,1,1-Tris-(6-hexanoic acid-4-phenyl)ethane (8): Tri-acid dendrimer core was synthesized according to literature procedure.¹⁴

PSLD_33: An oven dried, mag.- stirred, 100mL two-neck RBF was charged with (31) (0.221 g, 0.341 mmol), (d2.pas.27) (0.820 g, 1.13 mmol), 1,3-dicyclohexylcarbodiimide (0.260 g, 1.26 mmol), and DPTS (0.10 g, 0.341mmol). After 1hr of drying under a high vacuum, the mixture was dissolved in freshly distilled THF (10 mL) and DCM (15 mL). The reaction was stirred for 48 hr, washed with NaCl (sat.), and organic layer collected. The aqueous layer was extracted with DCM, and the combined organics were washed with water, dried over MgSO_4 , and

condensed *in vacuo*. The dark blue crude solid was purified by silica gel column chromatography (5% THF/ DCM) to yield 0.182 g (25%) of a deep blue solid. $T_g = 96\text{ }^{\circ}\text{C}$, $\lambda_{\text{max}} = 759\text{ nm}$ (CHCl_3)

^1H NMR (300 MHz, CDCl_3): δ 7.89 (J = 15.3 Hz), 7.58-7.54 (m, 15H), 7.39 (d, J = 9 Hz, 6H), 7.13 (d, J = 15.9 Hz, 3H), 7.03 (s, 3H), 6.98, (d, J = 8.7 Hz, 6H), 6.96 (d, J = 15.9 Hz, 3H), 6.77 (d, J = 8.7 Hz, 6H), 6.68 (d, J = 8.7 Hz, 6H), 6.64 (d, J = 15.3 Hz, 3H), 4.92 (d, J = 3 Hz, 6H), 3.94 (t, J = 6.3 Hz, 6H), 3.81 (t, J = 6 Hz, 6H), 3.56 (t, J = 6 Hz, 6H), 3.10 (s, 9H), 2.35 (t, J = 7.2 Hz, 6H), 2.09 (br-s, 3H), 1.87-1.79 (m, 6H), 1.72-1.67(m, 6H), 1.55-1.49 (m, 6H), 0.89 (s, 27H), 0.03 (s, 18H), ppm.

MALDI-TOF: $[\text{M}+\text{Na}]$, 2804.476 (m/z).

EA (CHN) analysis calcd for $\text{C}_{155}\text{H}_{159}\text{F}_9\text{N}_{12}\text{O}_{15}\text{S}_3\text{Si}_3$; C, 66.93; H, 5.76; N, 6.04%. Found; C, 67.92; H, 5.96; N, 5.89%.

λ_{max} (CHCl_3) = 759 nm ; λ_{max} (flm) = 734 nm

$T_g = 85\text{ }^{\circ}\text{C}$

PSLD_40 (9): A 50mL RBF is charged with d2.pas.33 (0.19 g) and acetone was added to dissolve (4 mL). 1N HCl (0.5 mL) was then added. The reaction was allowed to proceed for 2.5 hr. The mixture was then neutralized with NaHCO_3 and product collected by filtration. The blue solid was obtained in quantitative yield and used without further purification.

PSLD_41: An oven dried, mag.- stirred, 100mL two-neck RBF was charged with (d2.pas.40) (0.10 g, 0.041 mmol), (dendron1) (0.084 g, 0.164 mmol), 1,3-dicyclohexylcarbodiimide (0.038 g, 0.184 mmol), and DPTS (0.030 g, 0.20 mmol). After 1hr of drying under a high vacuum, the mixture was dissolved in freshly distilled THF (10 mL) and DCM (15 mL). The reaction was stirred for 48 hr, washed with NaCl (sat.), and organic layer collected. The aqueous layer was extracted with DCM, and the combined organics were washed with water, dried over MgSO₄, and condensed *in vacuo*. The dark blue crude solid was purified by silica gel column chromatography (2.5% THF/ DCM) to yield 0.1 g (0.025 mmol, 62%), of a deep blue solid.

¹H NMR (500 MHz, CDCl₃): δ 7.93, (d, J = 15.5, 3H), 7.58-7.54 (m, 15H), 7.39 (d, J = 9 Hz, 6H), 7.21 (d, J = 2.5 Hz, 6H), 6.99 (s, 3H), 6.98 (d, J = 7 Hz, 6H), 6.96 (d, J = 15.5 Hz, 3H), 6.87 (d, J = 15.5 Hz, 3H), 6.83 (d, J = 9 Hz, 6H), 6.77 (d, J = 9 Hz, 6H), 6.71 (t, J = 2.5 Hz, 3H), 6.66 (d, J = 15.5 Hz, 3H), 4.99 (s, 12H), 9.86 (dd, J₁ = 13 Hz, J₂ = 6.5 Hz, 6H), 4.54 (t, J = 5.5 Hz, 6H), 3.93 (t, J = 6.5 Hz, 6H), 3.86 (t, J = 5.5 Hz, 6H), 3.13 (s, 9H), 2.36 (t, J = 7.5 Hz, 6H), 2.09 (br-s, 3H), 1.82-1.76 (m, 6H), 1.73-1.67 (m, 6H), 1.53-1.47 (m, 6H), ppm.

EA (CHN) analysis calcd for C₂₀₀H₁₃₅F₃₉N₁₂O₂₄S₃; C, 61.16; H, 3.46; N, 4.28%. Found; C, 60.86; H, 3.25; N, 4.46%.

λ_{max} (CHCl₃) = 726 nm; λ_{max} (flm) = 720 nm

T_g = 103 °C

Chemical Analysis: CHN analysis was performed by Prevalere Life Sciences, Inc., Whitesboro NY. ^1H and ^{13}C NMR, UV-Vis NIR spectroscopy, and thermal analysis were performed as reported previously.¹⁴

Thin Film Fabrication Techniques and EO Measurements: Real time pole and probe r_{33} measurement details have been reported previously.¹⁴ Samples of each material were prepared by solution spin-casting onto ITO-coated glass slides gold electrodes ($d \approx 200$ nm) were then deposited atop the films. EO measurements were performed at $\lambda = 1300$ nm, and r_{33} measurements were recorded after cooling and removal of the poling field. Values were calculated by sine-wave fitting of lock-in-amplifier and direct current detector response curves as a function of the relative phase angle (Ψ_{sp}) between TE and TM. Values for r_{33} were then calculated from I_c and I_m values using

$$r_{33} = \frac{3\lambda I_m}{4\pi V_m I_c n^2} \frac{(n^2 - \sin^2 \theta)^{1/2}}{\sin^2 \theta} \propto I_m / I_c \quad (4.9.1)$$

where V_m is measured directly at the sample electrodes during poling.¹⁷

Variable Angle Spectroscopic Ellipsometry: Index measurements performed using VASE were performed in collaboration with the Dong Hoon Choi research group at Korea University, Seoul Korea. Measurements were performed using a Woollam VASE model with auto reader in the range of 310-1550 nm (0.8-4.0 eV), with incidence angles of 65, 70, and 75 degrees. The pseudo-dielectric

functions were fit using non-linear Levenberg-Marquardt algorithm using WVASE32 software.

Singular Value Decomposition of UV-VIS NIR Spectra: Curve-fitting was performed by Prof. Bruce Robinson.

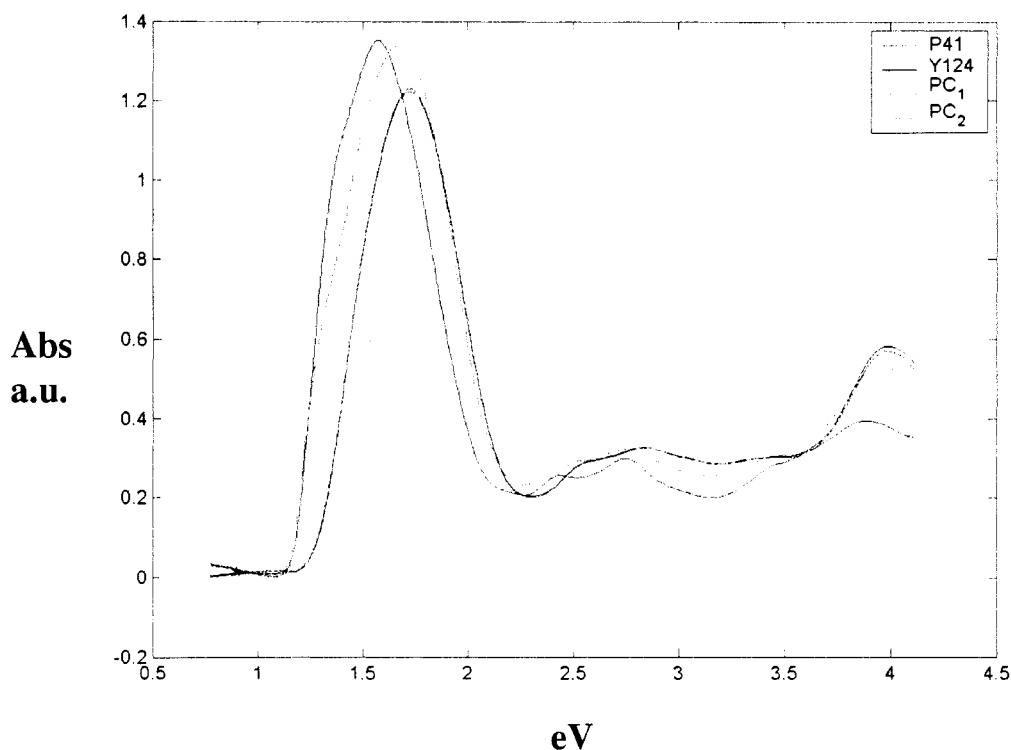


Figure 4.11.1: Experimental data for PSLD_41 film, and YLD_124 in APC, components PC1 and PC2 are the two base components from the mathematical decomposition of Figure 4.5.3.

Shown in Figure 4.8.1 are actual data for a film of PSLD_41 (P41) and YLD_124 (Y124) in APC normalized by chromophore number density. Also shown are spectra of the mathematically decomposed components of the UV-Vis NIR spectra for PSLD_41 / YLD_124 composites (Figure 4.5.3). The spectra for

PSLD_41 and PC1 are identical, YLD_124 in APC and PC2 are very similar in shape, PC 2 is somewhat broadened.

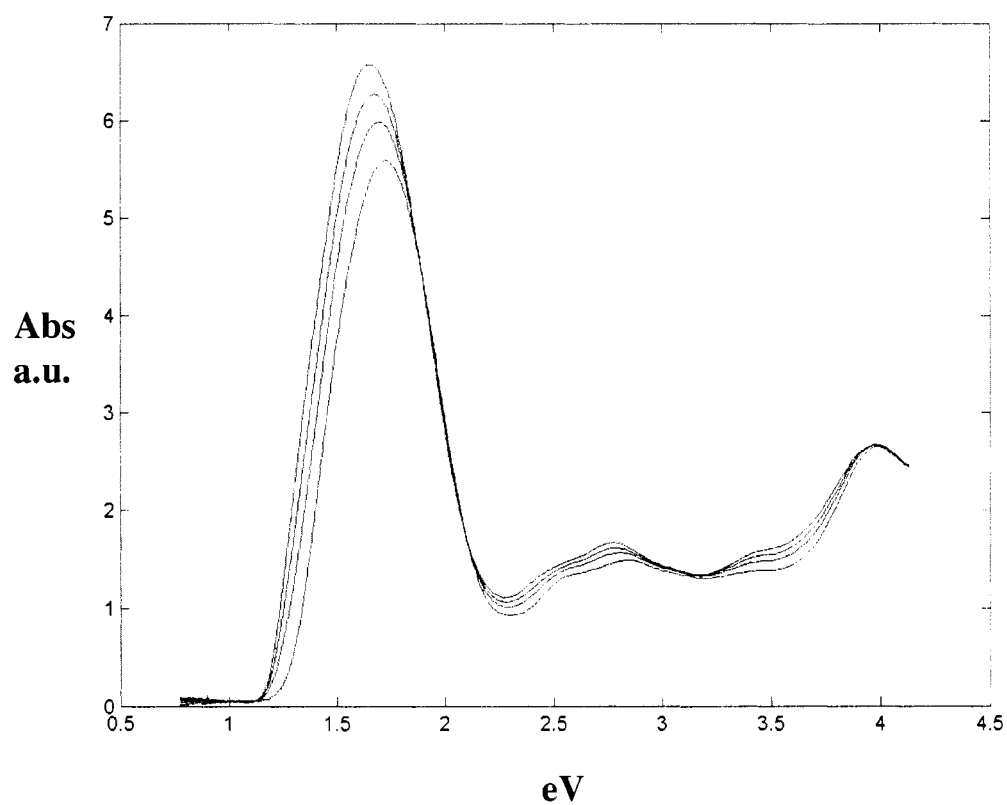


Figure 4.11.2: Mathematical reproduction of figure 4.5.3 spectra resulting from linear combination of PSLD_41 and YLD_124 spectra

Notes to Chapter 4

1. Dalton, L. R., Organic electro-optic materials. *Pure and Applied Chemistry* **2004**, 76, (7-8), 1421-1433.
2. Robinson, B. H.; Dalton, L. R., Monte Carlo statistical mechanical simulations of the competition of intermolecular electrostatic and poling-field interactions in defining macroscopic electro-optic activity for organic chromophore/polymer materials. *J. Phys. Chem. A* **2000**, 104, (20), 4785-4795.
3. Luo, J.; Kim, T.-D.; Ma, H.; Liu, S.; Kang, S. H.; Wong, S.; Haller, M. A.; Jang, S.-H.; Li, H.; Barto, R. R.; Frank, C. W.; Dalton, L. R.; Jen, A. K.-Y., Nanoscale architectural control of organic functional materials for photonics. *Proceedings of SPIE-The International Society for Optical Engineering* **2003**, 5224, (Nanomaterials and Their Optical Applications), 104-112.
4. Pereverzev, Y. V.; Prezhdov, O. V.; Dalton, L. R., Structural origin of the enhanced electro-optic response of dendrimer systems. *Chem. Phys. Lett.* **2003**, 373, (1,2), 207-212.
5. Do, J. Y.; Park, S. K.; Ju, J.-J.; Park, S.; Lee, M.-H., Electro-optic materials: hyperbranched chromophores attached linear polyimide and dendritic polyesters. *Polym. Adv. Technol.* **2005**, 16, (2-3), 221-226.
6. Yokoyama, S.; Nakahama, T.; Otomo, A.; Mashiko, S., Intermolecular Coupling Enhancement of the Molecular Hyperpolarizability in Multichromophoric Dipolar Dendrons. *J. Am. Chem. Soc.* **2000**, 122, 3174-3181.
7. Gopalan, P.; Katz, H. E.; McGee, D. J.; Erben, C.; Zielinski, T.; Bousquet, D.; Muller, D.; Grazul, J.; Olsson, Y., Star-Shaped Azo-Based Dipolar Chromophores: Design, Synthesis, Matrix Compatibility, and Electro-optic Activity. *J. Am. Chem. Soc.* **2004**, 126, (6), 1741-1747.
8. Dalton, L. R.; Harper, A. W.; Robinson, B. H., The role of London forces in defining noncentrosymmetric order of high dipole moment-high hyperpolarizability chromophores in electrically poled polymeric thin films. *Proceedings of the National Academy of Sciences of the United States of America* **1997**, 94, (10), 4842-4847.
9. Dalton, L.; Robinson, B. H.; Jen, A.-K.; Ried, P.; Eichinger, B.; Sullivan, P. A.; Akelaitis, A. J. P.; Bale, D.; Haller, M.; Luo, J.; Liu, S.; Liao, Y.; Firestone, K. A.; Sago, A.; Bhatambekar, N.; Bhattacharjee, S.; Sinness, J.; Hammond, S.; Buker,

- N.; Snoeberger, R.; Lingwood, M.; Rommel, H.; Amend, J.; Jang, S.-H.; Chen, A.; Steier, W. H., Optimizing electro-optic activity in chromophore/polymer composites and in organic chromophore glasses. *Proceedings of SPIE-The International Society for Optical Engineering* **2005**, 5990, 100-109.
10. Dalton, L. R.; Robinson, B. H., Monte Carlo Simulations of the Effect of a Poling Field on the Ordering of High Dipole Moment Organic Chromophores. *J. Phys. Chem.* **2000**, 104, 4785-4795.
 11. Dalton, L.; Robinson, B. H.; Jen, A.-K.; Ried, P.; Eichinger, B.; Sullivan, P. A.; Akelaitis, A. J. P.; Bale, D.; Haller, M.; Luo, J.; Liu, S.; Liao, Y.; Firestone, K. A.; Bhatambrekhar, N.; Bhattacharjee, S.; Sinness, J.; Hammond, S.; Buker, N.; Snoeberger, R.; Lingwood, M.; Rommel, H.; Amend, J.; Jang, S.-H.; Chen, A.; Steier, W. H., Electro-optic coefficients of 500 pm/V and beyond for organic materials. *Proceedings of SPIE-The International Society for Optical Engineering* **2005**, 5935, (Linear and Nonlinear Optics of Organic Materials V), 593502/1-593502/12.
 12. Nielsen, R. D.; Rommel, H. L.; Robinson, B. H., Simulation of the Loading Parameter in Organic Nonlinear Optical Materials. *J. Phys. Chem. B* **2004**, 108, (25), 8659-8667.
 13. Jen, A. K.-Y.; Nielsen, R.; Robinson, B. H.; Steier, W. H.; Dalton, L. R., Rational design of organic electro-optic materials. *Materials Research Society Symposium Proceedings* **2002**, 708, (Organic Optoelectronic Materials, Processing and Devices), 153-160.
 14. Sullivan, P. A.; Akelaitis, A. J. P.; K., L. S.; McGrew, G.; Lee, S. K.; Choi, D. H.; Dalton, L. R., Novel Dendritic Chromophores for Electro-optics: Influence of Binding Mode and Attachment Flexibility on Electro-Optic Behavior. *Chem. Mater.* **2006**, 18, 344-351.
 15. Breitung, E. M.; Shu, C.-F.; McMahon, R. J., Thiazole and Thiophene Analogues of Donor-Acceptor Stilbenes: Molecular Hyperpolarizabilities and Structure-Property Relationships. *Journal of the American Chemical Society* **2000**, 122, (6), 1154-1160.
 16. Rao, V. P.; Jen, A. K. Y.; Chandrasekhar, J.; Namboothiri, I. N. N.; Rathna, A., The Important Role of Heteroaromatics in the Design of Efficient Second-Order Nonlinear Optical Molecules: Theoretical Investigation on Push-Pull Heteroaromatic Stilbenes. *Journal of the American Chemical Society* **1996**, 118, (49), 12443-12448.
 17. Liao, Y.; Anderson, C. A.; Sullivan, P. A.; Akelaitis, A. J. P.; Robinson, B. H.; Dalton, L. R., Electro-Optical Properties of Polymers Containing Alternating Nonlinear Optical Chromophores and Bulky Spacers. *Chemistry of Materials* **2006**, 18, (4), 1062-1067.

18. Liao, Y.; Eichinger, B. E.; Firestone, K. A.; Haller, M.; Luo, J.; Kaminsky, W.; Benedict, J. B.; Reid, P. J.; Jen, A. K.-Y.; Dalton, L. R.; Robinson, B. H., Systematic study of the structure-property relationship of a series of ferrocenyl nonlinear optical chromophores. *J. Am. Chem. Soc.* **2005**, 127, (8), 2758-2766.
19. Zhang, C.; Wang, C.; Dalton, L. R.; Zhang, H.; Steier, W. H., Progress toward Device-Quality Second-Order Nonlinear Optical Materials. 4. A Trilink High mb NLO Chromophore in Thermoset Polyurethane: A \"Guest-Host\" Approach to Larger Electrooptic Coefficients. *Macromolecules* **2001**, 34, (2), 253-261.
20. Ma, H.; Liu, S.; Luo, J.; Suresh, S.; Liu, L.; Kang, S. H.; Haller, M.; Sassa, T.; Dalton, L. R.; Jen, A. K.-Y., Highly efficient and thermally stable electro-optical dendrimers for photonics. *Adv. Funct. Mater.* **2002**, 12, (9), 565-574.
21. Michelotti, F.; Toussaere, E.; Levenson, R.; Liang, J.; Zyss, J., Real-time pole and probe assessment of orientational processes in electro-optic polymers. *Applied Physics Letters* **1995**, 67, (19), 2765-7.
22. Sullivan, P. A. Chapter 2: Theory Guided Design and Molecular Engineering of Organic Materials for Enhanced 2nd-Order Nonlinear Optical Properties University of Washington, Seattle, 2006.
23. Liao, Y.; Sullivan, P. A.; Akelaitis, A., Extended-bridge Polyene-Aromatic hybrid, High Beta Chromophores In Univeristy of Washington: 2006.
24. Baehr-Jones, T.; Hochberg, M.; Wang, G.; Lawson, R.; Liao, Y.; Sullivan, P. A.; Dalton, L.; Jen, A. K. Y.; Scherer, A., Optical modulation and detection in slotted silicon waveguides. *Opt. Express* **2005**, 13, (14), 5216-5226.
25. He, M.; Leslie, T. M.; Sinicropi, J. A.; Garner, S. M.; Reed, L. D., Synthesis of Chromophores with Extremely High Electro-optic Activities. 2. Isophorone- and Combined Isophorone-Thiophene-Based Chromophores. *Chem. Mater.* **2002**, 14, (11), 4669-4675.
26. Janietz, S.; Bradley, D. D. C.; Grell, M.; Giebeler, C.; Inbasekaran, M.; Woo, E. P., Electrochemical determination of the ionization potential and electron affinity of poly(9,9-dioctylfluorene). *Applied Physics Letters* **1998**, 73, (17), 2453-2455.
27. Lemaure, V.; Steel, M.; Beljonne, D.; Bredas, J.-L.; Cornil, J., Photoinduced Charge Generation and Recombination Dynamics in Model Donor/Acceptor Pairs for Organic Solar Cell Applications: A Full Quantum-Chemical Treatment. *Journal of the American Chemical Society* **2005**, 127, (16), 6077-6086.
28. Ray, P. C.; Leszczynski, J., Nonlinear optical properties of highly conjugated push-pull porphyrin aggregates: Role of intermolecular interaction. *Chemical Physics Letters* **2006**, 419, (4-6), 578-583.

29. Zhang, T.-G.; Zhao, Y.; Asselberghs, I.; Persoons, A.; Clays, K.; Therien, M. J., Design, Synthesis, Linear, and Nonlinear Optical Properties of Conjugated (Porphinato)zinc(II)-Based Donor-Acceptor Chromophores Featuring Nitrothiophenyl and Nitrooligothiophenyl Electron-Accepting Moieties. *Journal of the American Chemical Society* **2005**, 127, (27), 9710-9720.
30. Shuto, Y.; Amano, M., Reflection measurement technique of electro-optic coefficients in lithium niobate crystals and poled polymer films. *Journal of Applied Physics* **1995**, 77, (9), 4632-8.
31. Almeida Vilson, R.; Xu, Q.; Barrios Carlos, A.; Lipson, M., Guiding and confining light in void nanostructure. *Optics letters* **2004**, 29, (11), 1209-11.
32. Galvan-Gonzalez, A.; Stegeman, G. I.; Jen, A. K. Y.; Wu, X.; Canva, M.; Kowalczyk, A. C.; Zhang, X. Q.; Lackritz, H. S.; Marder, S.; Thayumanavan, S.; Levina, G., Photostability of electro-optic polymers possessing chromophores with efficient amino donors and cyano-containing acceptors. *J. Opt. Soc. Am. B: Opt. Phys.* **2001**, 18, (12), 1846-1853.
33. Galvan-Gonzalez, A.; Belfield, K. D.; Stegeman, G. I.; Canva, M.; Marder, S. R.; Staub, K.; Levina, G.; Twieg, R. J., Photodegradation of selected p-conjugated electrooptic chromophores. *J. Appl. Phys.* **2003**, 94, (1), 756-763.
34. Bale, D. H.; Liao, Y.; Sullivan, P. A.; Luo, J.; Lao, D., B.; Jen, A. K. Y.; Reid, P. J.; Dalton, L. R., Photodegradation of Polymeric Electro-Optic Materials at Telecommunication C-band Wavelengths. *Polymeric Materials Science and Engineering* **2006**, in press.
35. DeRosa, M. E.; He, M.; Cites, J. S.; Garner, S. M.; Tang, Y. R., Photostability of High mb Electro-Optic Chromophores at 1550 nm. *Journal of Physical Chemistry B* **2004**, 108, (25), 8725-8730.
36. Stegeman, G. I.; Van-Gonzales, A. G.; Canva, M.; Twieg, R.; Kowalczyk, A. C.; Zhang, X. Q.; Lackritz, H. S.; Marder, S.; Thayumanavan, S.; Chan, K. P.; Jen, A. K. Y.; Wu, X., Photodegradation of various electro-optic polymer families. *MCLC S&T, Section B: Nonlinear Optics* **2000**, 25, (1-4), 57-66.
37. Michelotti, F.; Toussaere, E.; Levenson, R.; Liang, J.; Zyss, J., Study of the orientational relaxation dynamics in a nonlinear optical copolymer by means of a pole and probe technique. *Journal of Applied Physics* **1996**, 80, (3), 1773-1778.

Chapter 5

Exploration of a Series-Type Multifunctionalized NLO Chromophore Concept

5.1 Introduction

Multiple charge transfer nonlinear optical chromophores are attractive candidates for NLO active materials because they may show significantly enhanced first hyperpolarizability (β), while still exhibiting only modest increases in ground state dipole moment (μ_0). A small number of non-classical chromophores containing multiple donor and acceptor substituents such as λ -shaped, Y-shaped, and X-shaped two dimensional charge transfer chromophores have been developed. All of these designs show hyperpolarizability contributions from large off-diagonal β -tensorial components.¹ They exhibit an improved nonlinearity-transparency trade-off compared to one-dimensional dipolar chromophores.² Little is known about the effect of adding additional donor or acceptor groups to a system that already exhibits a large hyperpolarizability.

5.2 Theory of Multiple Charge Transfer Chromophore Design

Two examples of one-dimensional dipolar molecules are the chromophores FTC and FTTC (Figure 5.2.1). For this discussion these structures will serve as

controls with which to compare multifunctional molecules that possess the same basic backbone.

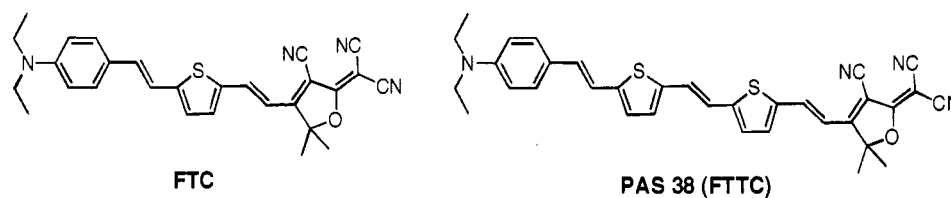


Figure 5.2.1: Examples of typical donor-bridge-acceptor, linear chromophores

An important point to consider when designing a multiple donor/acceptor chromophore is how the donating and accepting substituents communicate with one another. Different substitution patterns may vary the degree to which a particular electron configuration contributes to electric field induced molecular polarization. Two models for substitution patterns that can be envisioned are as shown below (Figure 5.2.2).

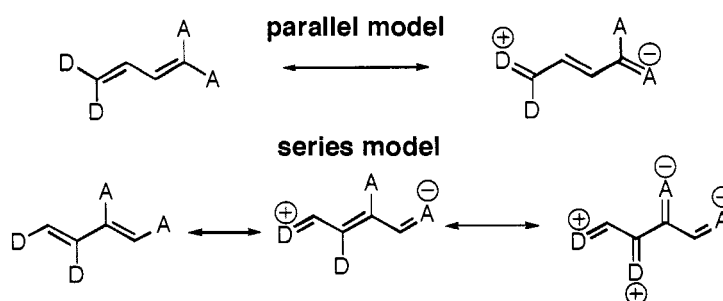


Figure 5.2.2: Schematic representation of parallel and series concepts

A parallel arrangement is one in which both donor and acceptor pairs are in conjugation with each other before charge transfer. A series-type arrangement allows for a larger contribution from a second donor and acceptor pair as the chromophore is polarized in the presence of an external electric field.

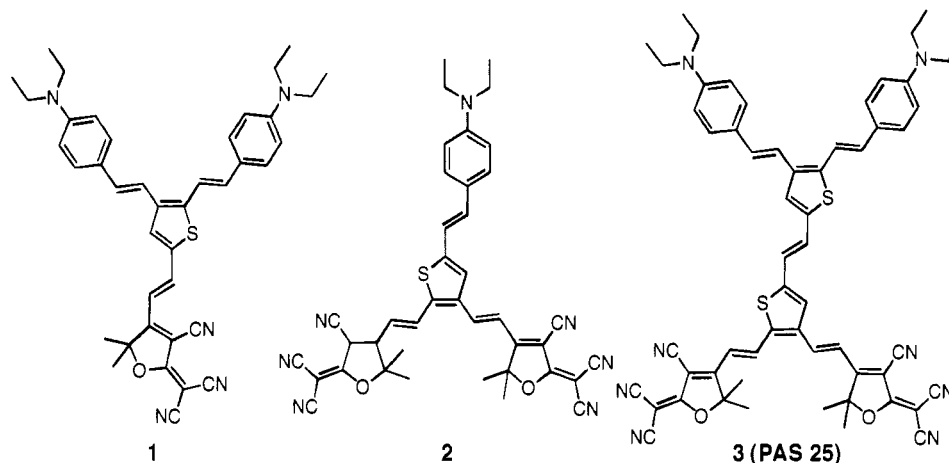


Figure 5.2.3: Examples of three series-type structures, 2-donors & 1-acceptor, 1, 1-donor & 2-acceptors, 2, 2-donors & 2-acceptors, 3

During polarization, the second active substituent or pair that was not in maximum conjugation in the ground state becomes a part of the conjugated system and hence contributes to β .

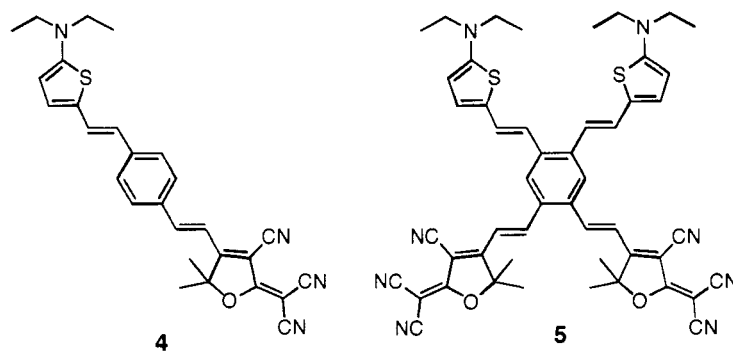


Figure 5.2.4: Example of a 1D linear control, 4, and a parallel substituted multifunctional NLO-phore, 5

Figure 5.2.3 shows three series-type molecular architectures considered herein. Shown for comparison (Figure 5.2.4) is an example of a parallel-type structure and its linear counterpart. Polarization primarily results from the admixing of chromophore ground and excited states. It has been suggested that chromophore

polarization behavior can be viewed from a frontier orbital theory perspective as shown by the two state model (equation 5.2.1).³ This theory suggests that the charge-transfer polarized state can be described by a combination of ground and excited states. Of these occupied and unoccupied molecular orbitals, the highest occupied molecular orbital (HOMO), and lowest unoccupied molecular orbital (LUMO), will contribute most significantly. This idea can be written as

$$\beta \propto \Delta\mu(\mu_{eg})^2 / \Delta E_{eg} \quad (5.2.1)$$

$\Delta\mu$ represents the difference in dipole moment between the ground and polarized states, μ_{eg} is the transition dipole moment and ΔE_{eg} is the difference in energy between the HOMO and the LUMO. Optimizing any of the parameters in Equation 2, increases β . The transition dipole moment can be thought of as a measure of the extent of admixing of HOMO and LUMO levels. $\Delta\mu$ can be viewed as a measure of the change in localization of electron density between ground and polarized states, essentially a measure of the overall polarizability of the chromophore. If μ_{eg} is large, and ΔE_{eg} is small, there exists a relatively small energy difference between ground and polarized states. This small energy difference leads to electron density being less localized on the donor side of the molecule and being more evenly distributed along the dipolar axis from donor to acceptor in the unpolarized state, leading to a reduced $\Delta\mu$.

5.3 Density Functional Theory (DFT) based Molecular Modeling Results

Density functional theory (DFT) quantum mechanical modeling can be used to evaluate ground and excited state electron density localization. From these data a

qualitative picture of molecular orbital contribution to β can be derived. From inspection of Figure 5.3.1, effective ground state electron density delocalization is noted. The HOMO and LUMO representations shown for FTTC exemplify typical one-dimensional donor-bridge-acceptor based chromophore design. The largest amount of electron density is localized on the donor side in the HOMO diagram and on the acceptor side in the LUMO diagram. The donor and acceptor pair is positioned to have maximum communication with each other through the delocalized π -electron system in the ground state. This leads to a significant portion of the total electron density being distributed along the dipolar axis of the molecule in the unpolarized state, resulting in reduced asymmetry. This illustrates the mutually exclusive behavior between μ_{eg} and $\Delta\mu$ in conventional, 1D chromophore design.

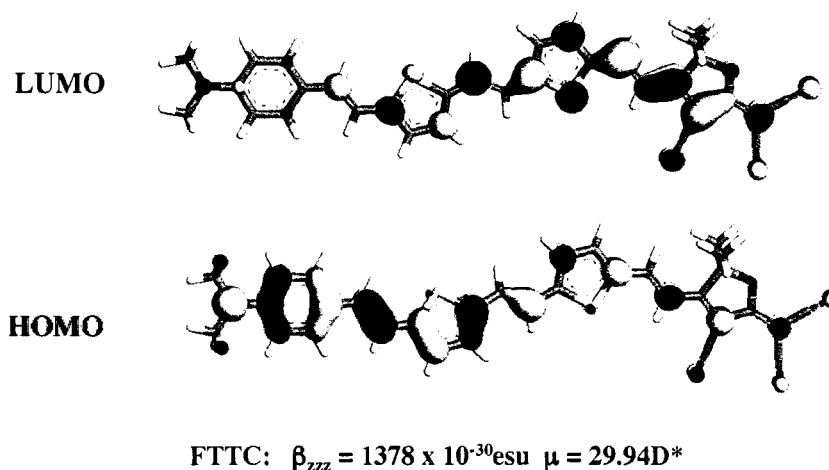


Figure 5.3.1: Representation of the DFT-calculated HOMO and LUMO for linear NLO-phore FTTC

Due to the fact that a linear molecule is of finite length, increased ground state electron density localization can lead to a large shift of electron density upon polarization and thus, a large $\Delta\mu$ and β . Therefore, to realize high β , a balance must be struck between ground state electron density asymmetry and the extent of admixing of ground and excited states. Large ground state electron density localization leads to a large $\Delta\mu$ only if effective charge polarization can be achieved. For effective polarization of electron density, a large μ_{eg} must be simultaneously realized. A series substitution pattern is a novel approach to the simultaneous optimization of μ_{eg} , ΔE_{eg} , and $\Delta\mu$.

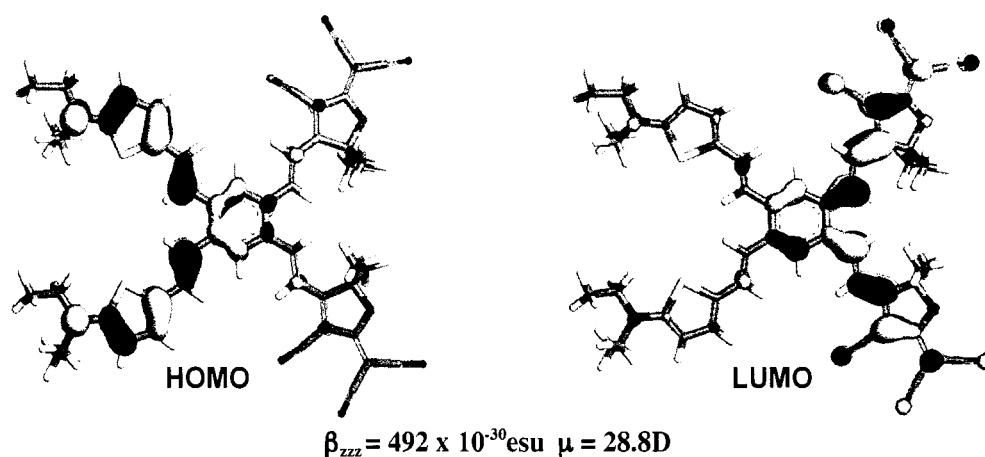


Figure 5.3.2: Representation of the DFT-calculated HOMO and LUMO for parallel-type structure 5

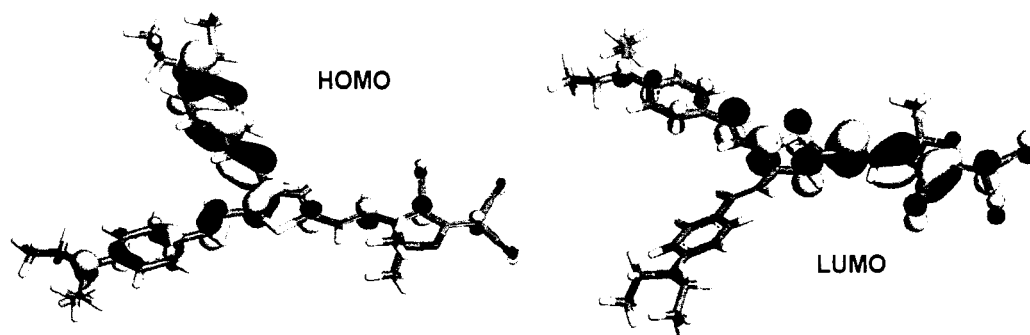
A parallel type multiply-substituted NLO-phore, shown for comparison (figure 5.3.2), shows orbital pictures that are much the same as seen in the linear example. This compound exhibits a relatively modest calculated increase in

hyperpolarizability (20% enhancement in β_{zzz}) compared to its linear control example but the dipole moment is actually decreased.

For all three series-type multiple charge transfer chromophores shown, unlike linear and parallel design, only one pair of donor and acceptor groups is in maximum conjugation in the ground state. During polarization, the second active substituent or pair is brought into a greater degree of conjugation and hence contributes more significantly to the first hyperpolarizability (β). Structure **1** is composed of two N,N-diethylaniline-p-vinylene donors linked in the 2 and 3 positions of a thiophene ring. One tri-cyano-furan (TCF) electron acceptor is placed in the 5 position to compliment the two donors. The single acceptor of **1** is most effectively conjugated with the donor substituent located in the 2 position of thiophene. This is evidenced by the observation that electron density of this donor is less localized and more distributed along the conjugated system as seen in the HOMO diagram (figure 5.3.3). DFT calculations show that all three series chromophores exhibit similar characteristics. One donor, acceptor, or pair is in greater conjugation than the others in the ground state. The LUMO diagram of **1** suggests that upon polarization, electron density from only one of the donor substituents can be highly displaced to the acceptor side of the molecule. Calculations show this molecule to have the smallest hyperpolarizability of the three series type structures. The double donor and single acceptor substitution pattern exemplified by **1** also shows the least enhancement (15% increase in β_{zzz} compared to its 1 dimensional control FTC) of the three series substitution patterns studied. Similar analysis of **2** shows that upon polarization all electron density available can be effectively shifted toward the

double electron acceptor substituted side of the tri-substituted thiophene bridge (figure 5.3.4). This molecule would be expected to possess a much greater $\Delta\mu$ than that of FTC and that of molecule 1. Hyperpolarizability calculations show a 52% increase in β_{zzz} over FTC for 2.

The most dramatic calculated enhancement of hyperpolarizability comes from a series substitution pattern made up of two complete donor acceptor pairs (figure 5.3.5). A calculated 156% increase in hyperpolarizability compared to FTTC is observed for molecule 3. The HOMO energies of chromophores containing aromatic bridge components are reduced by the aromatic stabilization within each component. If the polarized state is to resemble the charge separated (quinoidal) resonance structure that can be drawn for the molecule, this aromatic stabilization must be overcome upon polarization. This stabilization must therefore be seen to reduce μ_{eg} and increase ΔE_{eg} , thus reducing the hyperpolarizability.



Molecule 1: $\beta_{zzz} = 444 \times 10^{-30} \text{esu}$ $\mu = 26.72 \text{D}$

Figure 5.3.3: Representation of the DFT-calculated HOMO and LUMO for series type structure, 1

In series type multifunctionalized chromophores the electron donor and acceptor pair that is in maximum communication in the ground state should aid in overcoming aromatic stabilization energy, thus increasing μ_{eg} . The most effective series type chromophore is therefore one that can take advantage of this reduced energy polarizable state by donating as well as accepting more electron density. This combination will maximize μ_{eg} helping in the optimization of β . Steric strain in these multiple charge transfer chromophores may also contribute towards decreasing the HOMO-LUMO energy gap as compared to the coplanar linear chromophores.

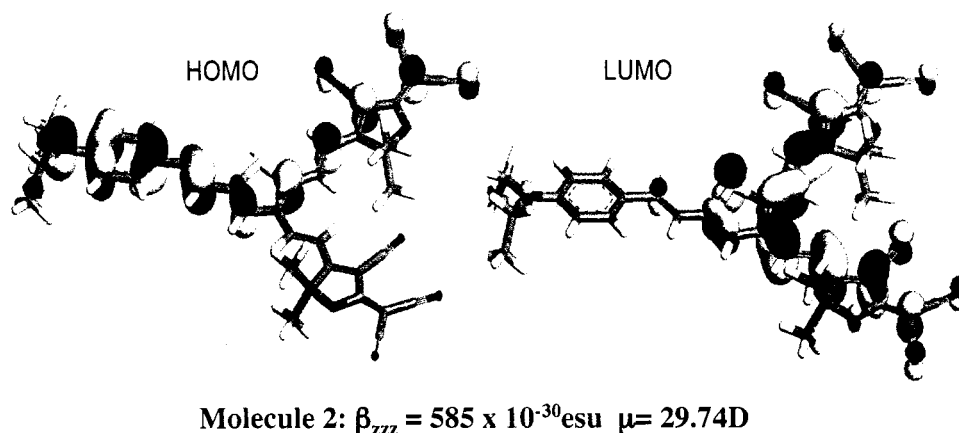


Figure 5.3.4: Representation of the DFT-calculated HOMO and LUMO for series type structure, 2

The slightly reduced coplanarity of the molecules may decrease the efficiency of the π -orbital overlap and increase the HOMO energy increasing ΔE_{eg} . However reduced planarity may also reduce the electronic communication between the donor and the acceptor that may lead to a decrease in first hyperpolarizability (β).

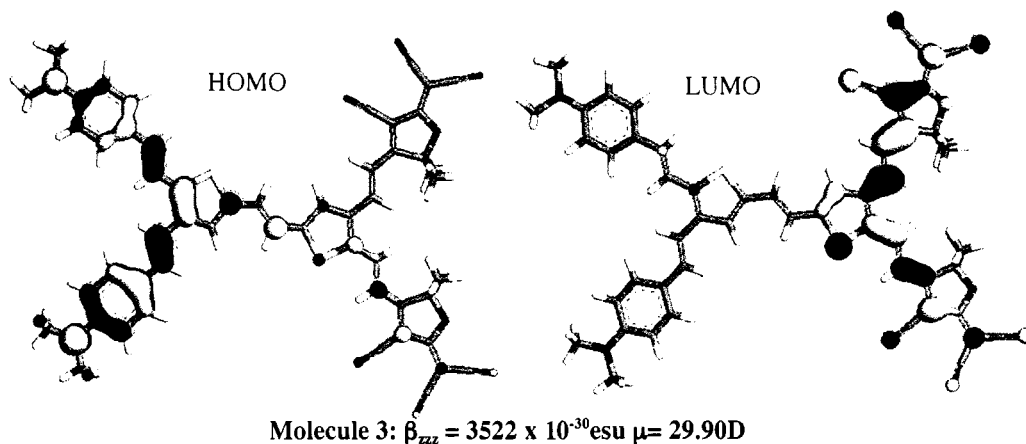


Figure 5.3.5: Representation of the DFT-calculated HOMO and LUMO for series type structure, 3

The difference between the dipole moments and the hyperpolarizabilities of molecules 1, 2, 3 and 4, are substantial. Series-type designs incorporating two pairs of electron donor/acceptor substituents show the largest enhancement among the designs studied. The series molecule, 3, displays the highest calculated first hyperpolarizability. Chromophore 3 shows almost 3 times enhancement in β_{zzz} in comparison to the linear FTTC chromophore constructed from the same donor, bridge and acceptor. Calculated values are tabulated below (Table 1). All of the multifunctional molecules possess ground state dipole moments that are lowered or only modestly enhanced by the addition of active substituents.

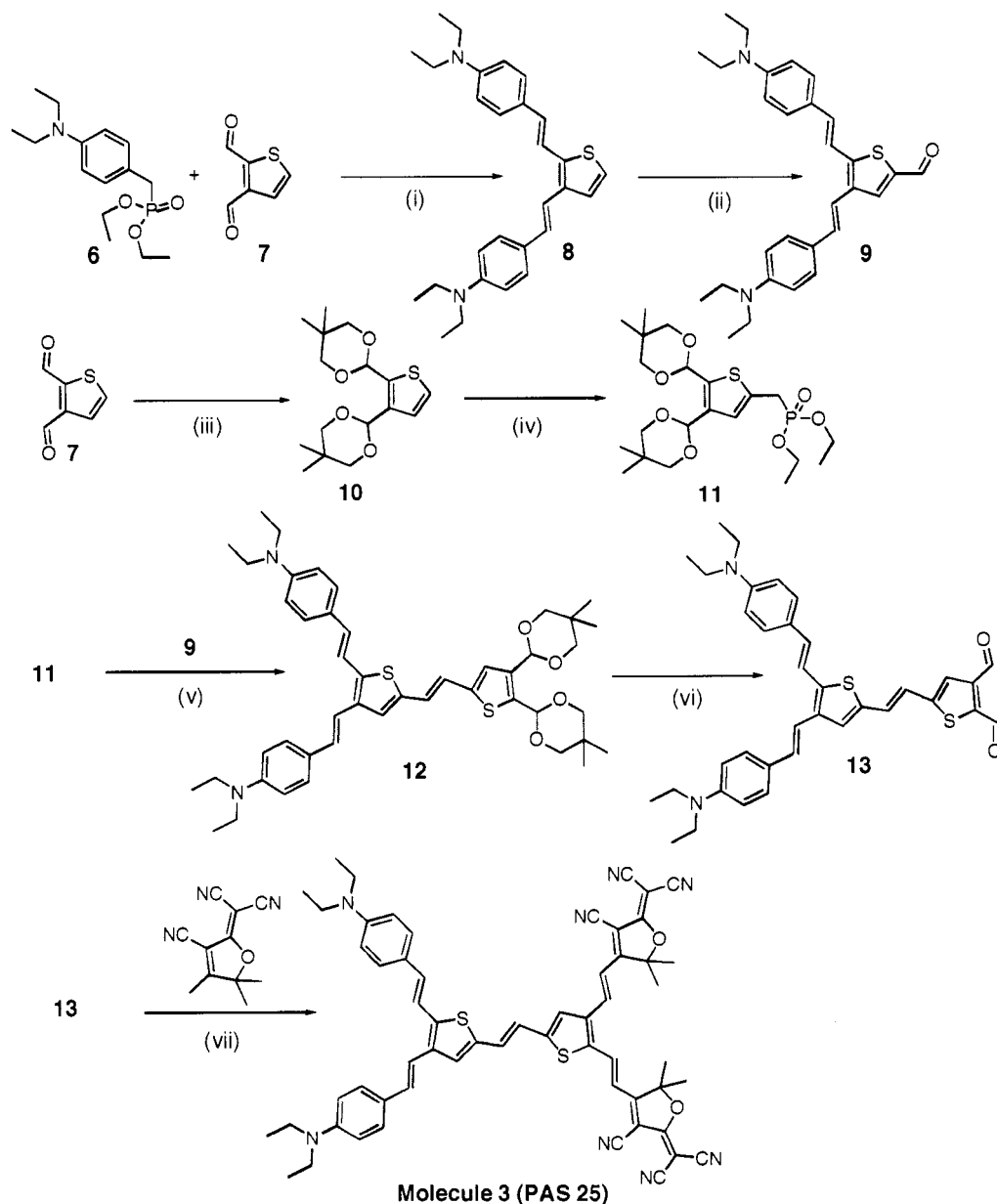
Table 5.3.1: Calculated electronic data for compounds discussed above

Molecule	Dipole Moment (μ)(Calc.) (D)	Hyperpolarizability (calc)	
		β_{HRS}	β_{ZZZ}
FTC	25.97	175	386
FTTC	29.94	605	1378
1	26.72	199	444
2	29.74	258	585
3	29.90	1789	3522
4	25.3	114	411
5	28.8	163	492

Geometries were optimized using DFT calculations, and the structures shown are optimized geometries. Geometries were optimized to an accuracy of 10^{-4} Ha using DMol^{4, 5}, a density functional program, utilizing a numerical basis set familiar in Hartree-Fock theory. Geometry optimization and all subsequent calculations were performed with the RPBE⁵ Hamiltonian. The hyperpolarizability was calculated by applying external fields with magnitudes 0.001 au and 0.002 au along the $\pm X$, $\pm Y$, and $\pm Z$ coordinate axes. In all, 13 calculations were performed for each molecule in its fixed optimized geometry. The resulting dipole vectors were analyzed using the method of Sim, et al.⁶, and the hyper-Rayleigh scattering value of the hyperpolarizability was calculated from the β tensor using the equations of Cyvin, Rauch, and Decius.⁷ Both molecules 1 and 2 are slightly twisted owing to the steric hindrance in the ortho positions of thiophene.

5.4 Synthesis of Multiple Charge Transfer Chromophores and Linear Analogs

Scheme 5.4.1: Outline of synthetic scheme for molecule **3** (PAS 25)^a



^aConditions: (i) ^tBuOK, THF, 0 °C – RT 12 h, 30%; (ii) (a) *n*-BuLi, THF, -78 °C 1 h; (b) DMF, RT 12h, >95%; (iii) neopentyl glycol, TsOH, C₆H₆, reflux 12 h, quant; (iv) (a) *n*-BuLi, THF, -78 °C 1 h; (b) CuI, THF -20 °C; (c) iodo-methyl phosphonate, -20 °C 12 h, 72%; (v) ^tBuOK, THF, 0 °C – RT 12 h, 99%; (vi) H₂SO₄ (1N), THF, reflux 2 h, 80%; (vii) Et₃N, CHCl₃, reflux 12 h, 30%

The synthesis of Molecule **3** (PAS 25) is outlined in Scheme 5.4.1. This particular molecular design was used because of facile synthetic access. Noting the selection of commercially available starting materials and drawing on prior synthetic knowledge, the 2,3-thienyl vinylene linkage used for both double donor and double acceptor portions of PAS-25 (**3**) was thus envisioned. Synthetic access to molecules **1** and **2** was also explored but will not be discussed here.

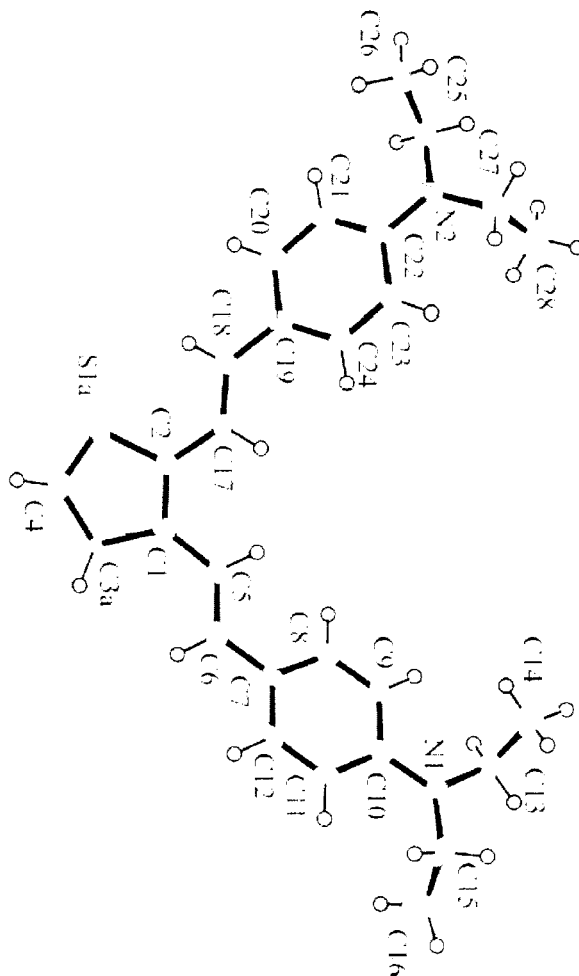


Figure 5.4.1: ORTEP representation of single crystal x-ray diffraction data for double donor, **8**

The starting material 2,3-thiophene dicarboxaldehyde **7** was purchased from Sigma Aldrich, but can be prepared in three steps from 3-thiophene bromide. Tandem olefination by Horner-Waddsworth-Emmons modification of the Wittig reaction using 4-diethylamino-benzyl-diethyl phosphonate affords the double electron donor substituted thiophene divinylene moiety in 18 – 30% yield. Figure 5.4.1 shows a representation of single crystal x-ray diffraction data for double donor **8**. From this data atomic distances and torsion angles can be calculated. This data is in good agreement with optimized geometries obtained from DFT calculations. From inspection of the crystal structure, it is apparent that double bond portions of the molecule do not display a high degree of twist with respect to the thiophene ring, as might be expected due to steric constraints. The two phenyl rings are somewhat out of planarity. However, they do not exhibit higher torsion angles than would be seen in a similar linear chromophore.

Although the final structure does not seem highly crowded, low yields obtained from the Horner-Emmons reaction in the synthesis of **8** may be due to steric hindrance during formation of the 4-member oxyphosphetane ring familiar in Wittig type chemistry. Excess unreacted phosphonate is recovered from the reaction mixture even when excess base is used. Some preliminary test results suggest that the yield of this reaction may be somewhat improved by the use of 4-diethylamino-benzyltriphenylphosphonium bromide. This compound is the Wittig salt analog of the Horner-Emmons phosphonate initially used for the reaction. The reason for this improved yield may stem from a difference between the two reactions in the rate-determining step. The electrophilicity of the phosphonium anion of the Horner-

Emmons phosphonate compared to the Wittig-salt is reduced. Causing the formation of the O-P bond between the ylide phosphonium and carbonyl oxygen to become the rate-determining step in the Horner-Emmons reaction. This means that before the formation of the 4-member oxyphosphetane ring, the Horner-Emmons reaction is reversible and equilibrium dependant. In contrast, the formation of the C-C bond between ylide carbon and carbonyl carbon is the rate-determining step in the analogous, classic Wittig reaction. This means that compared to the formation of the C-C bond, the O-P bond formation in the Wittig case is very fast and thus addition to the aldehyde carbonyl is irreversible.⁸

In the second step of the synthesis, the 5 position of double donor thiophene **8** is lithiated at low temperature using *n*-butyl lithium. This lithiated species is then quenched with anhydrous dimethyl formamide and hydrolyzed to produce the 5-formyl double donor species **9**. In order to create two functional aldehydes for future Knoevenagel addition of electron accepting groups, protected phosphonate **11** is synthesized, again starting from dialdehyde **7**. The dialdehyde is protected using neopentyl glycol under dehydrating conditions to form the diacetal derivative **10**. This product is then lithiated and added to a slightly warmer, air free, solution of copper iodide in THF to form the cuprate of the protected thiophene aldehyde. This cuprate is then used to displace iodine in an S_N2 fashion from Iodo-methyl phosphonate to form the phosphonate **11** according to a modified literature procedure.⁹ Phosphonate **11** can then be used to couple with aldehyde **9**, again through Horner-Emmons chemistry. The removal of the protecting groups from structure **12** can be effected by multiple procedures. Cleavage can be promoted via a one-pot method by addition of

3N sulfuric acid directly to the reaction mixture, or **12** can be first purified and then deprotected. The one-pot method gives only 46% yield. If product **12** is isolated it is found that the Horner-Emmons olefination is very high yielding and **12** can be deprotected to give **13** in improved yield. A deprotection procedure using pyridinium tosylate as the catalyst¹⁰ was also investigated and found to remove one protecting group quickly (18hrs) and quantitatively (as confirmed by ¹H NMR), but the other is left intact over several days at reflux. The last step in the synthesis of molecule **3** involves a tandem Knoevenagel condensation between **13** and two equivalents of 3-cyano-5,5-dimethyl-2-dicyanomethylene-4-methyl-2,5-dihydrofuran (TCF) electron acceptor moiety. This reaction is typically carried out in chloroform using a catalytic amount of a tertiary amine base while the solvent is dehydrated by passage through a soxhlet extractor filled with activated 4 angstrom molecular sieves. By TLC, a very polar, dark colored product is produced which can be purified by silica gel column chromatography to yield molecule **3** (PAS 25) as evidenced by MALDI-TOF mass spectrometry (Figure 5.4.2).

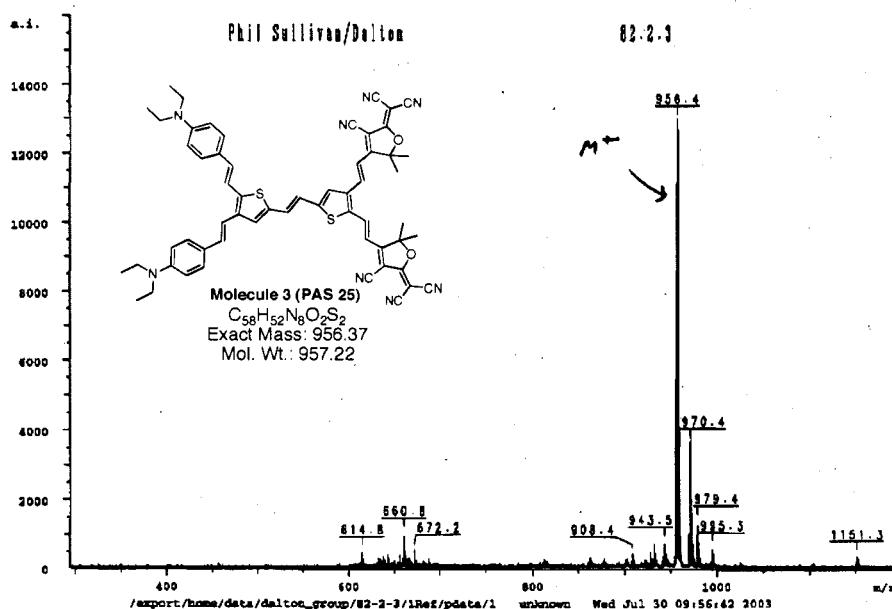
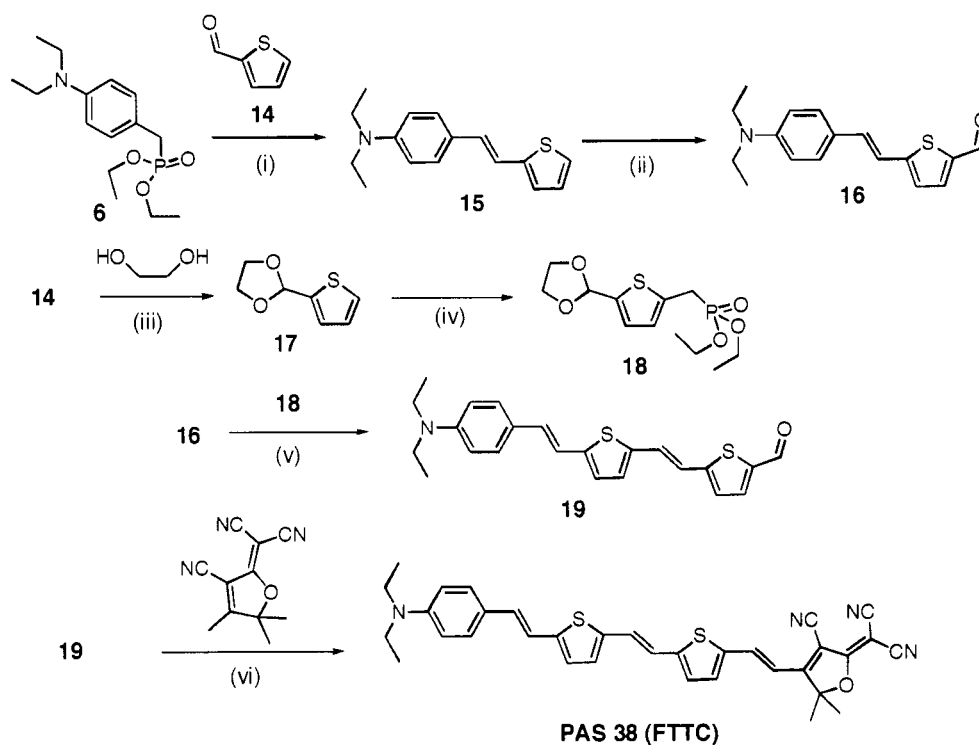


Figure 5.4.2: MALDI-TOF data showing 956.4 m/z molecular cation of Molecule 3

The synthesis of PAS 38 (FTTC) is more straightforward (Scheme 5.4.2). Olefination of 2-thiophene carboxaldehyde **14** is effected as before under Horner-Emmons conditions using phosphonate **6**. Carbonylation of donor-bridge **15** proceeds in high yield under standard conditions to produce **16**. In order to extend the system by one thienyl vinylene carboxaldehyde unit via a one-pot method, **18** is synthesized starting from 2-thiophene carboxaldehyde. The aldehyde is protected in quantitative yield with ethylene glycol using p-toluenesulfonic acid monohydrate as a catalyst and dehydrating by azeotropic distillation in benzene to produce **17**. This product is then converted to the corresponding Horner-Emmons phosphonate in an analogous manner to that used in synthesis of **11**. Low yields of **18** are obtained due to the deprotection of the aldehyde during purification on silica gel or neutral alumina. The deprotected product can be isolated and reprotected using analogous

conditions to the original protection with either a large excess of ethylene glycol or a lesser excess of neopentyl glycol. Either phosphonate can then be used to effect olefination of **16** with *in situ* deprotection of the aldehyde to produce **19**. The neopentyl protecting group requires more stringent conditions to remove and removal results in some decomposition of product. Removal of the ethylene glycol protecting group *in situ* proceeds quickly and cleanly. Final product chromophore PAS 38 is produced by Knoevenagel condensation with the TCF acceptor.

Scheme 5.4.2: Synthetic scheme for linear control chromophore PAS 38 (FTTC)^a



^aConditions: (i) ^tBuOK, THF, 0 °C – RT 12 h, 90%; (ii) (a) *n*-BuLi, THF, -78 °C 1 h; (b) DMF, RT 12h, >95%; (iii) TsOH, C₆H₆, reflux 12 h, quant; (iv) (a) *n*-BuLi, THF, -78 °C 1 h; (b) CuI, THF -20 °C; (c) iodo-methyl phosphonate, -20 °C 12 h, 50%; (v) (a) ^tBuOK, THF, 0 °C – RT 12 h; (b) H₂SO₄ (1N), THF, 99%; (vi) Et₃N, CHCl₃, reflux 12 h,

5.5 Photophysical Characterization

After completion of the synthesis of PAS 25 and PAS 38 the two chromophores were analyzed using a femtosecond Hyper-Rayleigh Scattering (HRS) system with excitation wavelength of 780nm and 1300nm. HRS is a technique used to measure molecular first hyperpolarizability (β) by observing the intensity of the frequency-doubled signal relative to a standard. This technique is a solution measurement that does not require orientation of the chromophores. HRS gives β via equation 5.5.1 where I is the signal intensity and N represents number density. Using HRS, β is measured directly, unlike Electric Field Induced Second Harmonic Generation (EFISH) which gives a value roughly proportional to the product of hyperpolarizability and dipole moment ($\mu\beta$).

$$\frac{I_{sample}}{I_{solvent}} = \frac{N_{sample} \langle \beta^2_{sample} \rangle + N_{solvent} \langle \beta^2_{solvent} \rangle}{N_{solvent} \langle \beta^2_{solvent} \rangle} \quad (5.5.1)$$

Some phenomena that must be considered when interpreting HRS data are multi-photon fluorescence (MPF) and dispersion processes. MPF can be reasonably subtracted from spectrally-resolved HRS signals. Dispersion processes that lead to resonance enhancement are much more difficult to correct for mathematically. Resonant enhancement effects occur most severely when the frequency doubled signal falls near the chromophore λ_{max} . The contribution of this enhancement to observed HRS signal is best understood by taking measurements using different excitation wavelengths that lead to a frequency doubled signal that differs in relation to chromophore λ_{max} . Figure 5.5.1 shows PAS 38, PAS 25, their λ_{max} in chloroform,

and HRS data. Also shown for comparison are two other similar three-ring systems DMC3-97, and PAS 54. For PAS 38, data is shown for measurement at 780nm and at 1300nm. Excitation at 780nm and 1300nm correspond to frequency-doubled signals at 390nm and 650nm respectively.

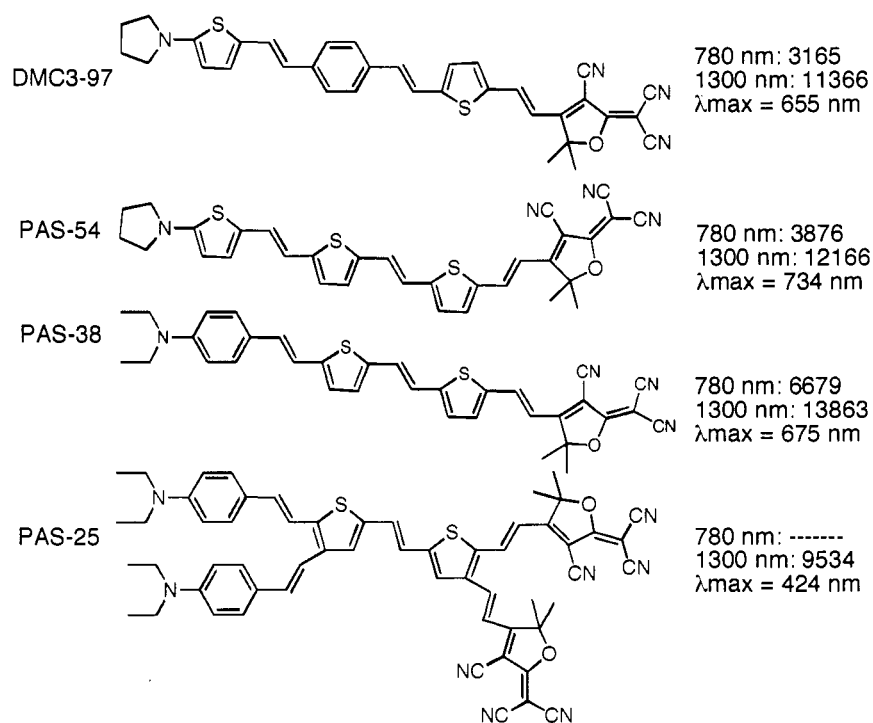


Figure 5.5.1: HRS data corresponding to PAS 25, linear control PAS 38, and two similar three-ring examples for comparison

All β values are reported relative to chloroform. Using a 780nm excitation beam the value for PAS 38 is 6679 times that of chloroform (solvent), using 1300nm, the value doubles to 13863. At 1300nm the HRS signal (650nm) falls almost exactly on the λ_{max} (675nm) of PAS 38. This signal doubling illustrates the problem of resonance enhancement. Currently there is only HRS data for PAS 25

using 1300nm. Here the value of β is 9534 times that of chloroform with a λ_{\max} of 424nm. The 650nm HRS signal falls much farther away from λ_{\max} of PAS 25. This implies that the value for this chromophore is not significantly enhanced and not easily compared to PAS 38 at this wavelength. Observing a blue shifted maximum absorbance and a strong HRS signal for PAS 25 is an encouraging result. In house, this is by far the highest β value reported for a chromophore with a similar λ_{\max} . Table 5.5.1 shows HRS data for comparison with PAS 25

Table 5.5.1: HRS values of several chromophores for comparison (given relative to chloroform).

Chromophore	$\lambda_{\max}(\text{nm})$	$\beta(780\text{nm})$	$\beta(1300\text{nm})$
pNA	348	303	66
DR1	479	1292	783
PAS -25	424	-----	9534
PAS-38	675	6679	13863
OLD-1	754	12943	17312
EZ-FTC	674	9929	15607

PAS 25 exhibits a λ_{\max} that is blue shifted relative to DR1 but shows a hyperpolarizability more than ten times greater. Data at 780nm would probably show an enhanced hyperpolarizability for PAS 25.

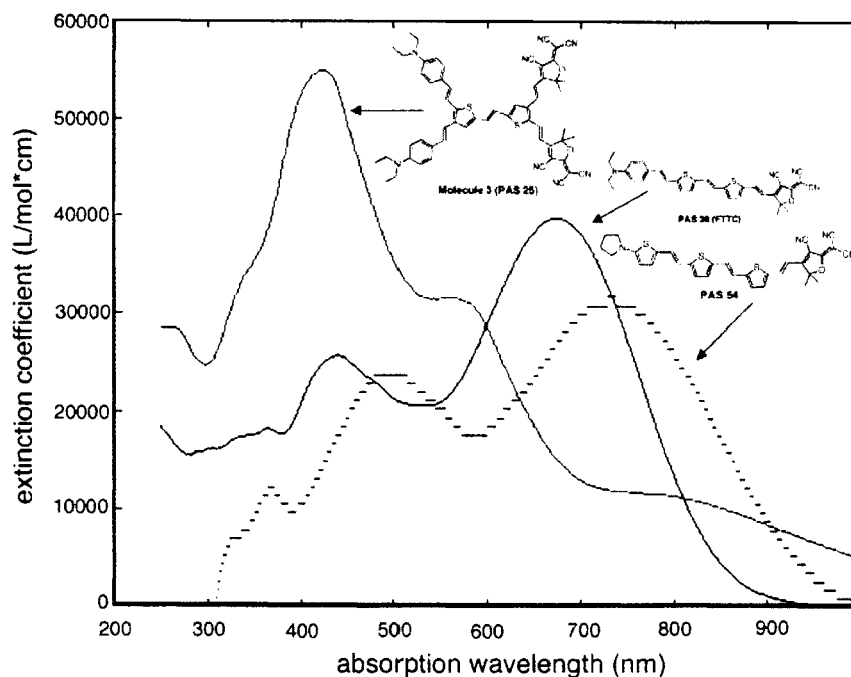


Figure 5.5.2: Extinction coefficients vs. wavelength comparison

Extinction coefficients corresponding to PAS 25, and linear control chromophores PAS 38 and PAS 54 are shown in figure 5.5.2. The largest is observed for x-shaped PAS 25.

Three absorption bands are displayed in the absorption spectra of x-shaped chromophore PAS 25. Figure 5.5.4 compares the absorption spectrum of PAS 25 with that of the dialdehyde precursor. A bathochromic shift is observed in all absorption bands corresponding to the addition of the acceptor moieties. The broad peak at approximately $\lambda = 800$ nm may be associated with molecular aggregation.¹ An attempt to test this hypothesis was made through dilution of a standard solution in chloroform. At low concentrations, signal-to-noise ratios for the UV-Vis

spectrophotometer available was rather poor. In addition, the low solubility of PAS 25 may cause aggregation to extend into the very high dilution regime.

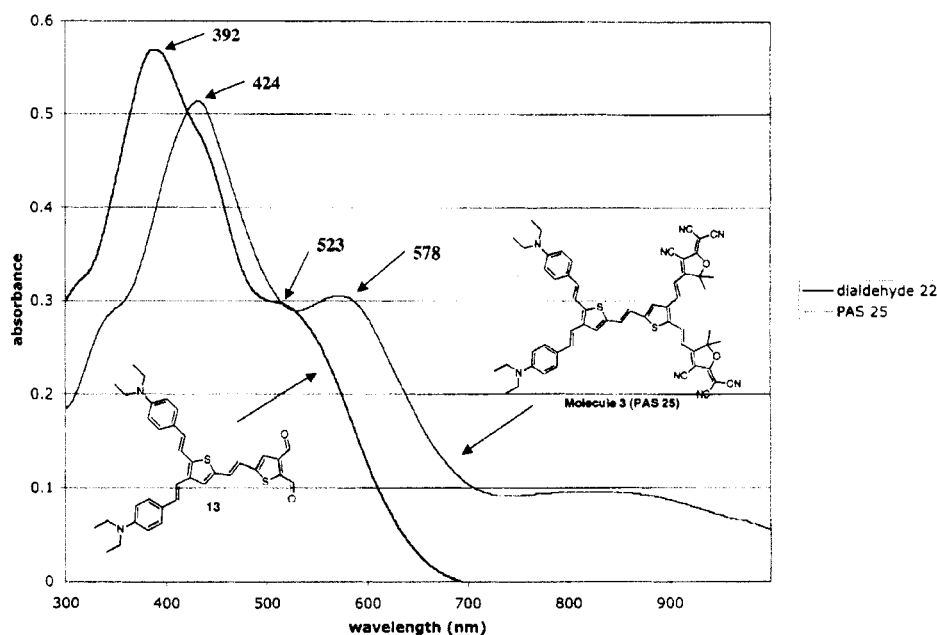


Figure 5.5.4: UV-Vis spectra of dialdehyde bridge precursor and PAS 25

5.6 Conclusions

Two-dimensional Multiple charge transfer chromophores represent a novel approach to the optimization of β without correspondingly increasing dipole moment. Optical nonlinearity may also be improved without the corresponding bathochromic shift in λ_{max} that is typically observed in conventional linear chromophores. These advantages hold the promise of simultaneously improved r_{33} and optical loss. In order to adequately explore these possibilities more work must be done toward materials with sufficient solubility and stability for more detailed characterization.

The novel x-shaped, series type, multiple charge transfer chromophore was designed using quantum mechanical modeling. The compound was then synthesized and characterized along with analogous linear control compound, PAS 38. Although the maximum absorbance of PAS 25 was blue-shifted as compared with that of PAS 38, β_{HRS} was not dramatically reduced. Unfortunately, PAS 25 displayed poor solubility and an extremely complicated UV-Vis absorption spectrum. These two complications prevented unambiguous analysis of photophysical properties. However, the results obtained as well as recent independent reports show promise. This concept is therefore attractive for continued research.¹

5.7 Experimental Section

General: All starting materials were purchased from Aldrich, or Alfa Aesar and used without further purification unless otherwise specified. All NMR data was obtained using Bruker Avance 300, 301, or 500Mhz, nuclear magnetic resonance spectrometers.

2,3-((N,N-diethyl amino)styryl)thiophene (8): An oven dried, mag stirred, 500mL round bottomed flask (RBF) was charged with p-(N,N-diethyl amino)benzyl ethylphosphonate **6** (9.4g, 31.372mmol), and 2,3-thiophene dicarboxaldehyde **7** (2.0g, 14.26mmol). This mixture was then dissolved in freshly distilled THF (60mL). While stirring, a 1.0M solution of Kot-bu in THF (32.8mL, 32.8mmol), was added dropwise over 0.5hrs. The mixture was allowed to stir overnight and then quenched

with a saturated solution of NaCl. The organic layer was separated and the aqueous layer extracted with DCM (2x30mL). The organics were then combined, dried over magnesium sulfate, and the solvent removed *in vacuo*. The crude red/brown oil was then purified by silica gel column chromatography (10% EtOac/Hex), to yield 1.13 g (18%) of a fluorescent yellow, crystalline solid.

^1H NMR (200 MHz, CDCl_3): δ 7.36 (dd, $J_1 = 1.8$ Hz, $J_2 = 7$ Hz, 4 H), 7.23 (d, $J = 14.4$ Hz, 1H), 7.21 (d, $J = 5.4$ Hz, 1H), 7.09 (d, $J = 16.2$ Hz, 1H), 7.02 (d, $J = 5.4$, 1H), 6.82 (d, $J = 15.8$ Hz, 1H), 6.79 (d, $J = 15.8$ Hz, 1H), 6.64 (dd, $J_1 = 1.6$, $J_2 = 7$ Hz, 4H), 3.36 (q, $J = 7.6$ Hz, 8H), 1.17 (t, $J = 6.8$ Hz, 12H), ppm.

E.A. Calcd for $\text{C}_{28}\text{H}_{34}\text{N}_2\text{S}$: C, 78.09; H, 7.96; N, 6.50. Found: C, 78.10; H, 7.65; N, 6.53. Single crystal X-ray diffraction data available.

2,3-((N,N-diethyl amino)styryl)thiophene-5-carboxaldehyd (9): An oven dried, mag. Stirred, 100mL RBF was charged with **8** (1.13g, 2.63mmol). Freshly distilled THF (25mL) was added to dissolve the solid. The reaction vessel was cooled to -78°C (dry ice/acetone). A 2.5M solution of n-butyl lithium in pentane (1.15mL, 2.89mmol), was added dropwise over 0.5hrs. The reaction was then stirred for 1.5hrs and anhydrous DMF (0.405mL, 3.42mmol) was added. The solution was then allowed to warm to RT overnight, and quenched with aqueous NaCl. The organic layer was separated, and the aqueous phase was extracted with DCM. The organics were combined and dried over magnesium sulfate and the solvent removed

in vacuo. The red, solid, crude product was then purified by silica gel column chromatography (DCM), to yield 1.19g, 99% of **9**.

^1H NMR (500 MHz, CDCl_3): δ 9.8 (s, 1H), 7.88 (s, 1H), 7.43 (dd, $J_1 = 5$ Hz, $J_2 = 1.6$ Hz, 4H), 7.23 (d, $J = 6.4$ Hz), 7.09 (d, $J = 16$ Hz, 1H), 7.04 (d, $J = 16$ Hz), 6.94 (d, $J = 16$ Hz, 1H), 6.70 (t, $J = 10$ Hz, 4H), 3.42 (q, 5Hz, 8H), 1.27 (t, $J = 6.7$ Hz, 12H), ppm.

^{13}C NMR (500Hz, CDCl_3): δ 182.68, 148.19, 147.67, 147.25, 138.73, 137.08, 135.70, 133.25, 130.77, 128.68, 127.94, 124.25, 123.54, 115.17, 114.02, 111.70, 111.58, 44.48, 29.75, 12.69, ppm.

2,3-thiophene di-neopentyl acetal (10): A mag. Stirred 250mL RBF, was equipped with a Dean-Stark trap and charged with 2,3-thiophene dicarboxaldehyde **7** (1g, 7.13mmol), and neopentyl glycol (1.63g, 15.69mmol). The mixture was dissolved in benzene (50mL), a catalytic amount of p-toluenesulfonic acid monohydrate (0.0136g, 0.0713mmol) was added, and the mixture was heated at reflux overnight (140°C). After cooling to RT, the reaction mixture was washed with NaHCO_3 (SAT). The organics were then separated and dried over MgSO_4 , and the solvent removed *in vacuo* to yield analytically pure, white crystals of **10** in quantitative yield.

^1H NMR (200 MHz, CDCl_3): δ 7.14 (a-b q, $J_1 = 5.6$ Hz, $J_2 = 7.1$ Hz, 2H), 5.82 (s, 1H), 5.56 (s, 1H), 3.70 (m, 4H), 3.50 (m, 4H), 1.24 (s, 6H), 0.742 (s, 6H), ppm.

E.A. Calcd for $\text{C}_{16}\text{H}_{24}\text{O}_4\text{S}$: C, 61.51; H, 7.74. Found; C, 61.60; H, 7.71

(2,3-di-noepentyl acetal)-thiopene-5-methylphosphonate (11): A flame dried, mag. Stirred, 100mL RBF was charged with **10** (0.93g, 2.9mmol), freshly distilled THF (20mL), was then added to dissolve. The solution was then cooled to -78°C (dry ice/acetone). A solution of n-BuLi (1.16mL, 2.9mmol, 2.5M in Hex), was then added dropwise over 0.5hrs. A yellow color was observed upon addition. A second RBF, treated as above was charged with CuI (0.55g, 2.9mmol), evacuated, and backfilled with nitrogen. Dry THF (20mL) was again added to dissolve. The second flask was then cooled to -20°C (ethylene glycol/dry ice). After 1hr, the contents of flask 1 were transferred via cannula to flask 2. The mixture was then stirred for 2 hours at which time N,N-diethyl-methyliodophosphonate was added in one portion. The cooling bath was then removed and reaction was allowed to proceed overnight. The reaction was then quenched with NaHCO_3 (SAT), the organics were separated, and successively washed with H_2O and Brine. The organics were then dried over magnesium sulfate and the solvent was removed *in vacuo*. The crude oil product was then purified on a short silica gel plug (1) 20% EtOAc/Hex, 2) EtOAc) to yield 0.96g (71%) of **11**.

^1H NMR (500 MHz, CDCl_3): δ 6.94 (s, 1H), 5.743 (s, 1H), 5.46 (s, 1H), 4.0 (t, $J = 8\text{Hz}$, 4H), 3.66 (m, 4H), 3.52 (m, 4H), 3.2 (d, $J = 21.5\text{Hz}$, 2H), 1.21 (m, 12H), 0.71 (s, 6H), ppm.

(trans)-5-[2,3-({N,N-diethylamino styrl}thiophen-2-yl)-vinyl]-

thiophene-2,3-di-neopentyl acetal (12): A 250mL RBF, flame dried, magnetically stirred, was charged with 9 (0.8g, 1.74mmol), and 11 (1.22g, 2.61mmol). This mixture was dissolved in freshly distilled THF (50mL). A solution of Kot-bu (2.8mL, 2.8mmol, 1M soln. in THF) was then added dropwise over a period of 20min. The reaction was followed by TLC (20% EtOAc/Hex) The product is fluorescent orange and lower rf than S.M. After 2hrs organics were separated and aqueous layer extracted with DCM. The organics were then combined and dried over MgSO₄ and solvent removed *in vacuo*. Crude product was pure by ¹H NMR and used without further purification.

¹H NMR (200MHz, CDCl₃): δ 7.36 (dd, J₁ = 1.8Hz, J₂ = 7Hz, 4H), 7.2 (d, J = 16Hz, 1H), 7.14 (d, J = 15.5Hz, 1H), 7.13 (s, 1H), 7.0 (d, J = 16Hz, 1H), 6.99 (d, J = 16.1Hz, 1H), 6.92 (d, J = 16Hz, 1H), 6.89 (d, J = 16Hz, 1H), 6.81 (d, J = 5Hz, 1H), 6.71 (dd, J₁ = 2.2Hz, J₂ = 8.8Hz, 4H), 5.88 (s, 1H), 5.58 (s, 1H), 3.70 (m, 4H), 3.50 (m, 4H), 3.42 (q, J = 7Hz, 8H), 1.26 (m, 18H), 0.837 (s, 6H), ppm.

(trans)-5-[2,3-({N,N-diethylamino styrl}thiophen-2-yl)-vinyl]-thiophene-

2,3-di-carboxaldehyde (13): A 200mL RBF, mag. Stirred, equipped with a reflux condenser, was charged with 12 (0.8g, 1.04mmol) and THF (10mL) was added to dissolve. DI H₂O (2mL), and H₂SO₄ (2mL, 6N), were then added. The mixture was heated to reflux and followed by ¹H NMR. After 2hrs the reaction mixture was cooled to RT and neutralized with NaHCO₃ (SAT). The organics were separated and the aqueous phase extracted with DCM. The organics were then recombined and

dried over magnesium sulfate, and the solvent was removed *in vacuo*. The dark red/brown crude product was then purified by silica gel column chromatography (10% EtOAc/DCM) to yield 0.5g (80%), of a deep red solid.

^1H NMR (200MHz, CDCl_3): δ 10.46 (s, 1H), 10.36 (s, 1H), 7.51 (s, 1H), 7.43 (d, $J = 8.8\text{Hz}$, 4H), 7.35 (s, 1H), 7.27 (d, $J = 15.8\text{Hz}$, 1H), 7.25 (d, $J = 16\text{Hz}$, 1H), 7.07 (d, $J = 16\text{Hz}$, 1H), 6.93 (d, $J = 15.6\text{Hz}$, 1H), 6.90 (d, $J = 15.6\text{Hz}$, 1H), 6.87 (d, $J = 15.6\text{Hz}$, 1H), 6.71 (dd, $J_1 = 2.4\text{Hz}$, $J_2 = 9\text{Hz}$, 4H), 3.43 (q, $J = 7\text{Hz}$, 8H), 1.24 (t, $J = 7\text{Hz}$, 12H), ppm.

(trans)-5-[2,3-({N,N-diethylamino styrl}thiophen-2-yl)-vinyl]-thiophene-2,3-vinyl- (2-dicyanomethylene-3-cyano-4,5,5-trimethyl-2,5-dihydrofuran) (PAS-25): A 100mL, mag stirred RBF was equipped with a soxhlet extractor filled with 4 angstrom molecular sieves, and then charged with **13** (0.160g, 0.27mmol). Chloroform was then added (20mL) to this solution was then added 2-dicyanomethylene-3-cyano-4,5,5-trimethyl-2,5-dihydrofuran (0.118g, 0.592mmol). A catalytic amount of triethylamine was introduced into the reaction mixture and the system was allowed to reflux overnight. The system was then cooled to RT and washed with NaHCO_3 (SAT). The organic layer was separated and the aqueous phase was extracted with DCM. The organics were dried over magnesium sulfate and the solvent removed *in vacuo*. The crude product was then purified by silica gel column chromatography (20% EtOAc/DCM), and then by precipitation from hot

DCM by slow addition of MeOH to yield 0.080g (30%) of a dark brown solid.

MALDI-TOF analysis: m/z = 956.4 (m+), 957.4 (m+H).

λ_{max} (shimadzu UV- 1601 UV-visible spectrophotometer) = 424nm

β_{relative} to chloroform (1300nm) = 9534

(trans)-5-[2-(5-Pryolidin-1-yl-phenyl-2-yl)-vinyl]- 2-[(2-thiophen-2-yl)-vinyl-2-vinyl-2-(2-dicyanomethylene-3-cyano-4,5,5-trimethyl-2,5-dihydrofuran)]- thiophene (PAS-38, FTTC): A 100ml RBF, mag stirred is equipped with a small soxhlet extractor apparatus filled with activated 4 angstrom molecular sieves. The apparatus is then charged with (trans)-5-[2-(5-Pryolidin-1-yl-phenyl-2-yl)-vinyl]- 2-[(2-thiophen-2-yl)-vinyl-2-vinyl-2-(2-dicyanomethylene-3-cyano-4,5,5-trimethyl-2,5-dihydrofuran)]- thiophene 5.8g (14.74mmol), and 2-dicyanomethylene-3-cyano-4,5,5-trimethyl-2,5-dihydrofuran 3.5g (17.68mmol). To this mixture is added 40mL chloroform and triethylamine 0.5mL (3.54mmol). The mixture is then heated at reflux for 24hrs. The chloroform is then removed *in vacuo* and the product purified by silica gel column chromatography (50% EtOac/DCM). .

^1H NMR (DMSO_3 , 500 MHz) 8.95 (d, J = 15.5Hz, 1H), 8.61 (d, J = 4Hz), 8.3 (d, J = 16Hz), 8.22 (s, 2H), 7.902-8.110 (m, 4H), 7.69 (d, J = 15.5Hz, 1H), 7.54 (d, J = 15.6Hz, 1H), 7.5 (m, 2H), 3.36 (m, 4H), 1.799 (s, 6H), 1.103 (t, 6H),

LRMS m/z found = 576.2

λ_{max} (shimadzu UV- 1601 UV-visible spectrophotometer) = 673nm

β_{relative} to chloroform = 6679 (+/- 418)

(1300nm) = 13863

β_{HRS} (esu) P. Kaatz and D.P. Shelton = $1069(+/-67) \times 10^{-30}$

β_{HRS} (esu) K. Clays and A. Persoons = $3273 (+/- 204) \times 10^{-30}$

(trans)-1-[5-(2-thiophen-2-yl-vinyl)-thiophen-2-yl]-pyrrolidine¹¹ A 250mL, 2 neck RBF, flame dried, mag stirred, is equipped with an addition funnel and charged with 4.0g (22.07mmol) of 5-pyrrolidin-1-yl-thiophene-2-carboxaldehyde. 150mL dry THF is added and mixture is stirred to dissolve. 10.86g (46.34mmol) diethyl(2-thienylmethyl)phosphonate is added to the solution. Potassium tert-butoxide (48.554mL, 1.0M soln. in THF) is then added dropwise through the addition funnel over a 30min period. The reaction is allowed to stir overnight, quenched with brine, and extracted with diethyl ether. The organics are separated and dried over mag sulfate. Solvent is removed by rotovap. Crude product is recrystallized from cyclohexane to afford 4.22g, (74% yield) of yellow/brown crystals.

¹H NMR (CDCl₃, 500 MHz), 7.036 (d, 1H, J = 4.8 Hz), 6.92 (m, 2H), 6.85 (m, 2H), 6.71 (d, 1H, J = 3.3 Hz), 6.68 (d, 1H, 16 Hz), 5.58 (d, 1H, J = 3.5 Hz), 3.28 (t, 4H, J = 5 Hz), 2.01 (m, 4H)

(trans)-5-[2-(5-Pyrrolidin-1-yl-thiophen-2-yl)-vinyl]-thiophene-2-carbaldehyde¹¹ A vacuum dried, mag stirred, 250mL RBF, is charged with 4.2g

(16.2mmol) of (trans)-1-[5-(2-thiophen-2-yl-vinyl)-thiophen-2-yl]-pyrrolidine.

150mL freshly distilled THF is added and stirred to dissolve. Solution is cooled to -78 C (dry-ice/acetone). n-buLi (22.7mL, 1.6M soln. In hexane), is added dropwise over a 10min period. The reaction mixture is then stirred for 2 hours. DMF (3.78mL, 48.6mmol) is added in 1 portion. Reaction is allowed to warm to RT overnight (12hrs), then quenched with brine and extracted with diethyl ether. Organics are dried over magnesium sulfate and solvent is removed in vacuo. Crude product is purified on silica gel column (DCM mobile phase) to yield 4.5g (96%) of bright red product.

¹H NMR (CDCl₃, 500 MHz), 9.8 (s, 1H), 7.59 (d, 1H, J = 4.0 Hz), 7.14 (d, 1H, J = 15.6 Hz), 6.97 (d, 1H, J = 4.0 Hz), 6.85 (d, 1H, J = 4.2 Hz), 6.60 (d, 1H, J = 15.6 Hz), 5.93 (d, 1H, J = 4.0 Hz), 3.28 (t, 4H, J = 5 Hz), 2.01 (m, 4H

(trans)-5-[2-(5-Pyrrolidin-1-yl-thiophen-2-yl)-vinyl]- 2-[(2-thiophen-2-yl)-vinyl]- thiophene A 250ml, 2 neck RBF, flame dried, mag stirred, is equipped with an addition funnel and charged with 1.65g (5.7mmol) of (trans)-5-[2-(5-Pyrrolidin-1-yl-thiophen-2-yl)-vinyl]-thiophene-2-carbaldehyde. 150mL dry THF is added and mixture is stirred to dissolve. 2.0g (8.55mmol) diethyl(2-thienylmethyl)phosphonate is added to the solution. Potassium tert-butoxide (8.8mL, 1.0M soln. in THF) is then added dropwise through the addition funnel over a 30min period. The reaction is allowed to stir overnight, quenched with brine, organics are separated. Water layer extracted with DCM and the combined organics are dried over mag sulfate. Solvent

is removed by rotovap. Crude product is purified by column chromatography on silica (DCM), to afford 1.8g (85%).

^1H NMR (CDCl_3 , 500 MHz), 7.13 (d, 1H, $J = 5.5$ Hz), 6.99 (d, 1H, $J = 5.0$ Hz), 6.96 (m, 2H), 6.936 (d, 1H, $J = 5$ Hz), 6.87 (d, 1H, $J = 15.5$ Hz), 6.835 (d, 1H, $J = 5.2$ Hz), 6.73 (d, 2H, $J = 5$ Hz), 6.53 (d, 1H, $J = 15.6$ Hz), 5.59 (d, 1H, $J = 5$ Hz), 3.28 (t, 4H, $J = 5$ Hz), 2.01 (m, 4H)

(trans)-5-[2-(5-Pryolidin-1-yl-thiophen-2-yl)-vinyl]- 2-[(2-thiophen-2-yl)-vinyl]-2-carboxaldehyde]- thiophene A vacuum dried, mag stirred, 250mL RBF, is charged with 1.8g (4.87mmol) of (trans)-5-[2-(5-Pryolidin-1-yl-thiophen-2-yl)-vinyl]- 2-[(2-thiophen-2-yl)-vinyl]- thiophene. 150mL freshly distilled THF is added and stirred to dissolve. Solution is cooled to -78°C (dry-ice/acetone). n-buLi (4.26mL, 1.6M soln. In hexane), is added dropwise over a 10min period. The reaction mixture is then stirred for 2 hours. DMF (1.13mL, 14.61mmol) is added in 1 portion. Reaction is allowed to warm to RT overnight (12hrs), then quenched with brine and extracted with diethyl ether. Organics are dried over magnesium sulfate and solvent is removed in vacuo to yield 1.53g (79%) of bright red product. Product is pure by ^1H NMR and used without further purification.

^1H NMR (CDCl_3 , 500 MHz) 9.8 (s, 1H), 7.605 (d, 1H, $J = 4.5$ Hz), 7.17 (d, 1H, $J = 15.5$), 7.06 (d, 1H, $J = 5.1$ Hz), 6.95 (d, 1H, $J = 3.5$ Hz), 6.92 (d, 1H, $J = 15.6$ Hz), 6.86 (d, 1H, $J = 16.5$ Hz), 6.763 (d, 2H, $J = 3$ Hz), 6.53 (d, 1H, $J = 15.5$ Hz), 5.59 (d, 1H, $J = 5$ Hz), 3.28 (t, 4H, $J = 5$ Hz), 2.01 (m, 4H)

(trans)-5-[2-(5-Pryolidin-1-yl-thiophen-2-yl)-vinyl]- 2-[(2-thiophen-2-yl)-vinyl-2-vinyl-2-(2-dicyanomethylene-3-cyano-4,5,5-trimethyl-2,5-dihydrofuran)]- thiophene A 100ml RBF, mag stirred is equipped with a small soxhlet extractor apparatus filled with activated 4 angstrom molecular sieves. The apparatus is then charged with (trans)-5-[2-(5-Pryolidin-1-yl-thiophen-2-yl)-vinyl]- 2-[(2-thiophen-2-yl)-vinyl-2-carboxaldehyde]- thiophene 1.45g (3.65mmol), and 2-dicyanomethylene-3-cyano-4,5,5-trimethyl-2,5-dihydrofuran 0.873g (4.38mmol). To this mixture is added 40mL chloroform and triethylamine 0.1mL (0.73mmol). The mixture is then heated at reflux for 24hrs. The chloroform is then removed in Vacuo and the product purified by silica gel column chromatography (40% EtOac/DCM). .

¹H NMR (CDCl₃, 500 MHz) 7.739 (d, 1H, J = 15.5Hz), 7.335 (d, 1H, J = 3.5Hz), 7.159 (d, 1H, J = 15.5Hz), 7.03 (d, 1H, J = 4.5Hz), 6.98 (d, 1H, J = 3Hz), 6.945 (d, 1H, J = 15.5Hz), 6.8565 (d, 1H, J = 15.5Hz), 6.790 (m, 2H), 6.557 (d, 1H, J = 15.5Hz), 6.525 (d, 1H, J = 15.5Hz), 5.628 (d, 1H, J = 4Hz), 3.312 (t, 4H, J = 6.5Hz), 2.034 (m, 4H), 1.79 (s, 6H);

LRMS M/z expected = 578.77, M/z found = 578.1

λ_{max} (shimadzu UV- 1601 UV-visible spectrophotometer) = 735.5nm

β_{relative} to chloroform (780nm) = 3876+/- 281

(1300nm) = 12166

β_{HRS} (esu) P. Kaatz and D.P. Shelton = 620(+/-45) x 10⁻³⁰

β_{HRS} (esu) K.Clays and A. Persoons = 1899 (+/- 138) x 10⁻³⁰

Notes to Chapter 5

1. Kang, H.; Zhu, P.; Yang, Y.; Facchetti, A.; Marks, T. J., Self-assembled electrooptic thin films with remarkably blue-shifted optical absorption based on an x-shaped chromophore. *Journal of the American Chemical Society* **2004**, 126, (49), 15974-15975.
2. Moylan, C. R.; Ermer, S.; Lovejoy, S. M.; McComb, I. H.; Leung, D. S.; Wortmann, R.; Krdmer, P.; Twieg, R. J., (Dicyanomethylene)pyran Derivatives with C_{2v} Symmetry: An Unusual Class of Nonlinear Optical Chromophores. *J. Am. Chem. Soc.* **1996**, 118, (51), 12950-12955.
3. Oudar, J. L., Optical nonlinearities of conjugated molecules. Stilbene derivatives and highly polar aromatic compounds. *J. Chem. Phys.* **1977**, 67, (2), 446-57.
4. Materials Studio and DMol3, Accelrys: San Diego. **2002**.
5. Hammer, B.; Hansen, L. B.; No/rskov, J. K., Improved adsorption energetics within density-functional theory using revised Perdew-Burke-Ernzerhof functionals. *Physical Review B: Condensed Matter and Materials Physics* **1999**, 59, (11), 7413-7421.
6. Sim, F.; Chin, S.; Dupuis, M.; Rice, J. E., Electron correlation effects in hyperpolarizabilities of p-nitroaniline. *Journal of Physical Chemistry* **1993**, 97, (6), 1158-63.
7. Cyvin, S. J.; Rauch, J. E.; Decius, J. C., Theory of hyper-Raman effects (nonlinear inelastic light scattering). Selection rules and depolarization ratios for the second-order polarizability. *Journal of Chemical Physics* **1965**, 43, (11), 4083-95.
8. Ando, K., A Mechanistic Study of the Horner-Wadsworth-Emmons Reaction: Computational Investigation on the Reaction Pass and the Stereochemistry in the Reaction of Lithium Enolate Derived from Trimethyl Phosphonoacetate with Acetaldehyde. *Journal of Organic Chemistry* **1999**, 64, (18), 6815-6821.
9. Wang, C. W.; Dalton, L. R., A facile Synthesis of Thienylmethylphosphonates: direct conversion from thiophenes. *Tetrahedron Lett.* **2000**, 41, 617-620.
10. Miyashita, M.; Yoshikoshi, A.; Grieco, P. A., Pyridinium p-toluenesulfonate. A mild and efficient catalyst for the tetrahydropyranylation of alcohols. *Journal of Organic Chemistry* **1977**, 42, (23), 3772-4.

11. Jen, A. K. Y.; Rao, V. P.; Wong, K. Y.; Drost, K. J., Functionalized thiophenes: second-order nonlinear optical materials. *Journal of the Chemical Society, Chemical Communications* **1993**, (1), 90-2.

List of References

1. Materials Studio and DMol3, Accelrys: San Diego. **2002**.
2. Alain, V.; Fort, A.; Barzoukas, M.; Chen, C.-T.; Blanchard-Desce, M.; Marder, S. R.; Perry, J. W., The linear and non-linear optical properties of some conjugated ferrocene compounds with potent heterocyclic acceptors. *Inorg. Chim. Acta* **1996**, 242, (1-2), 43-9.
3. Albert, I. D. L.; Marks, T. J.; Ratner, M. A., Optical nonlinearities in the lowest excited triplet state of organic molecules. *Book of Abstracts, 210th ACS National Meeting, Chicago, IL, August 20-24 1995*, (Pt. 2), PHYS-213.
4. Almeida Vilson, R.; Xu, Q.; Barrios Carlos, A.; Lipson, M., Guiding and confining light in void nanostructure. *Optics letters* **2004**, 29, (11), 1209-11.
5. Ando, K., A Mechanistic Study of the Horner-Wadsworth-Emmons Reaction: Computational Investigation on the Reaction Pass and the Stereochemistry in the Reaction of Lithium Enolate Derived from Trimethyl Phosphonoacetate with Acetaldehyde. *Journal of Organic Chemistry* **1999**, 64, (18), 6815-6821.
6. Annoni, E.; Pizzotti, M.; Ugo, R.; Quici, S.; Morotti, T.; Bruschi, M.; Mussini, P., Synthesis, electronic characterisation and significant second-order non-linear optical responses of meso-tetraphenylporphyrins and their ZnII complexes carrying a push or pull group in the b pyrrolic position. *Eur. J. Inorg. Chem.* **2005**, (19), 3857-3874.
7. Ashwell, G. J., Langmuir-Blodgett films: molecular engineering of non-centrosymmetric structures for second-order nonlinear optical applications. *J. Mater. Chem.* **1999**, 9, (9), 1991-2003.
8. Ashwell, G. J.; Jackson, P. D.; Crossland, W. A., Non-centrosymmetry and second-harmonic generation in Z-type Langmuir-Blodgett films. *Nature* **1994**, 368, (6470), 438-40.
9. Ashwell, G. J.; Maxwell, A. A.; Green, A., Unconventional Langmuir-Blodgett films: alignment of an optically nonlinear dye where the donor and p-electron bridge are hydrophobic and the acceptor is hydrophilic. *J. Mater. Chem.* **2002**, 12, (8), 2192-2196.
10. Baehr-Jones, T.; Hochberg, M.; Wang, G.; Lawson, R.; Liao, Y.; Sullivan, P. A.; Dalton, L.; Jen, A. K. Y.; Scherer, A., Optical modulation and detection in slotted silicon waveguides. *Opt. Express* **2005**, 13, (14), 5216-5226.
11. Bahar, I.; Erman, B.; Fytas, G.; Steffen, W., Intramolecular Contributions to

Stretched-Exponential Relaxation Behavior in Polymers. *Macromolecules* **1994**, *27*, (18), 5200-5.

12. Bai, Y.; Song, N.; Gao, J. P.; Sun, X.; Wang, X.; Yu, G.; Wang, Z. Y., A New Approach to Highly Electrooptically Active Materials Using Cross-Linkable, Hyperbranched Chromophore-Containing Oligomers as a Macromolecular Dopant. *J. Am. Chem. Soc.* **2005**, *127*, (7), 2060-2061.

13. Bale, D. H.; Liao, Y.; Sullivan, P. A.; Luo, J.; Liao, D., B.; Jen, A. K. Y.; Reid, P. J.; Dalton, L. R., Photodegradation of Polymeric Electro-Optic Materials at Telecommunication C-band Wavelengths. *Polymeric Materials Science and Engineering* **2006**, in press.

14. Batsanov, A. S.; Bryce, M. R.; Coffin, M. A.; Green, A.; Hester, R. E.; Howard, J. A. K.; Lednev, I. K.; Martin, N.; Moore, A. J.; Moore, J. N.; Orti, E.; Sanchez, L.; Saviron, M.; Viruela, P. M.; Viruela, R.; Ye, T.-Q., Donor-p-acceptor species derived from functionalized 1,3-dithiol-2-ylidene anthracene donor units exhibiting photoinduced electron transfer properties: spectroscopic, electrochemical, x-ray crystallographic and theoretical studies. *Chem. Eur. J.* **1998**, *4*, (12), 2580-2592.

15. Boldt, P.; Eisentraeger, T.; Glania, C.; Goeldenitz, J.; Kraemer, P.; Matschiner, R.; Rase, J.; Schwesinger, R.; Wichern, J.; Wortmann, R., Guanidyl and phosphoraniminyl substituents. New electron donors in second-order nonlinear optical chromophores. *Adv. Mater.* **1996**, *8*, (8), 672-675.

16. Breitung, E. M.; Shu, C.-F.; McMahon, R. J., Thiazole and Thiophene Analogues of Donor-Acceptor Stilbenes: Molecular Hyperpolarizabilities and Structure-Property Relationships. *J. Am. Chem. Soc.* **2000**, *122*, (6), 1154-1160.

17. Briers, D.; Koeckelberghs, G.; Picard, I.; Verbiest, T.; Persoons, A.; Samyn, C., Novel chromophore-functionalized poly[2-(trifluoromethyl)adamantyl acrylate-methyl vinyl urethane]s with high poling stabilities of the nonlinear optical effect. *Macromolecular Rapid Communications* **2003**, *24*, (14), 841-846.

18. Cao, Y. W.; Chai, X. D.; Chen, S. G.; Jiang, Y. S.; Yang, W. S.; Ren, Y. Z.; Blanchard-Desce, M.; Li, T. J.; Lehn, J. M., A new series of nonlinear optical organic materials with molecular receptor: design and synthesis. *Synth. Met.* **1995**, *71*, (1-3), 1733-4.

19. Cha, S. W.; Choi, D. H.; Jin, J.-I., Unusually fast optically induced birefringence in polyoxetanes bearing 4-(N,N-diphenyl)amino-4'-nitroazobenzene chromophores. *Advanced Functional Materials* **2001**, *11*, (5), 355-360.

20. Chasse, T. L.; Sachdeva, R.; Li, Q.; Li, Z.; Petrie, R. J.; Gorman, C. B.,

Structural effects on encapsulation as probed in redox-active core dendrimer isomers. *Journal of the American Chemical Society* **2003**, *125*, (27), 8250-8254.

21. Chen, A.; Dalton, L.; Sherwood, T.; Jen, A. K.-Y.; Rabiei, P.; Steier, W.; Huang, Y.; Paloczi, G. T.; Poon, J. K. S.; Scherer, A.; Yariv, A., All-organic and organic-silicon photonic ring micro-resonators. *Proceedings of SPIE-The International Society for Optical Engineering* **2005**, 5708, (Laser Resonators and Beam Control VIII), 187-197.
22. Chen, D.; Fetterman, H. R.; Chen, A.; Steier, W. H.; Dalton, L. R.; Wang, W.; Shi, Y., Demonstration of 110 GHz electro-optic polymer modulators. *App. Phys. Lett.* **1997**, *70*, (25), 3335-3337.
23. Cyvin, S. J.; Rauch, J. E.; Decius, J. C., Theory of hyper-Raman effects (nonlinear inelastic light scattering). Selection rules and depolarization ratios for the second-order polarizability. *Journal of Chemical Physics* **1965**, *43*, (11), 4083-95.
24. Dalton, L., Nonlinear Optical Polymeric Materials: From Chromophore Design to Commerical Applications. *Adv. Polym. Sci.* **2001**, *158*, 1-86.
25. Dalton, L.; Harper, A.; Ren, A.; Wang, F.; Todorova, G.; Chen, J.; Zhang, C.; Lee, M., Polymeric Electro-optic Modulators: From Chromophore Design to Integration with Semiconductor Very Large Scale Integration Electronics and Silica Fiber Optics. *Ind. Eng. Chem. Res.* **1999**, *38*, (1), 8-33.
26. Dalton, L.; Robinson, B. H.; Jen, A.-K.; Ried, P.; Eichinger, B.; Sullivan, P. A.; Akelaitis, A. J. P.; Bale, D.; Haller, M.; Luo, J.; Liu, S.; Liao, Y.; Firestone, K. A.; Bhatambrekar, N.; Bhattacharjee, S.; Sinness, J.; Hammond, S.; Buker, N.; Snoeberger, R.; Lingwood, M.; Rommel, H.; Amend, J.; Jang, S.-H.; Chen, A.; Steier, W. H., Electro-optic coefficients of 500 pm/V and beyond for organic materials. *Proceedings of SPIE-The International Society for Optical Engineering* **2005**, 5935, (Linear and Nonlinear Optics of Organic Materials V), 593502/1-593502/12.
27. Dalton, L.; Robinson, B. H.; Jen, A.-K.; Ried, P.; Eichinger, B.; Sullivan, P. A.; Akelaitis, A. J. P.; Bale, D.; Haller, M.; Luo, J.; Liu, S.; Liao, Y.; Firestone, K. A.; Sago, A.; Bhatambrekar, N.; Bhattacharjee, S.; Sinness, J.; Hammond, S.; Buker, N.; Snoeberger, R.; Lingwood, M.; Rommel, H.; Amend, J.; Jang, S.-H.; Chen, A.; Steier, W. H., Optimizing electro-optic activity in chromophore/polymer composites and in organic chromophore glasses. *Proceedings of SPIE-The International Society for Optical Engineering* **2005**, 5990, 100-109.
28. Dalton, L. D., Nonlinear optical polymeric materials: from chromophore design to commercial applications. *Advances in Polymer Science* **2002**, *158*, (Polymers for Photonics Applications I), 1-86.

29. Dalton, L. R., Polymeric electro-optic materials: optimization of electro-optic activity, minimization of optical loss, and fine-tuning of device performance. *Opt. Eng.* **2000**, 39, (3), 589-595.
30. Dalton, L. R., Organic electro-optic materials. *Pure and Applied Chemistry* **2004**, 76, (7-8), 1421-1433.
31. Dalton, L. R.; Harper, A. W.; Ghosn, R.; Steier, W. H.; Ziari, M.; Fetterman, H.; Shi, Y.; Mustacich, R. V.; Jen, A. K. Y.; Shea, K. J., Synthesis and Processing of Improved Organic Second-Order Nonlinear Optical Materials for Applications in Photonics. *Chem. Mater.* **1995**, 7, (6), 1060-81.
32. Dalton, L. R.; Harper, A. W.; Robinson, B. H., The role of London Forces in Defining Noncentrosymmetric Order of High Dipole Moment-High Hyperpolarizability Chromophores in Electrically Poled Polymeric Thin Films. *Proc. Natl. Acad. Sci. USA* **1997**, 94, (10), 4842-4847.
33. Dalton, L. R.; Robinson, B. H., Monte Carlo Simulations of the Effect of a Poling Field on the Ordering of High Dipole Moment Organic Chromophores. *J. Phys. Chem.* **2000**, 104, 4785-4795.
34. DeRosa, M. E.; He, M.; Cites, J. S.; Garner, S. M.; Tang, Y. R., Photostability of High mb Electro-Optic Chromophores at 1550 nm. *Journal of Physical Chemistry B* **2004**, 108, (25), 8725-8730.
35. Diaz, J. L.; Dobarro, A.; Villacampa, B.; Velasco, D., Structure and Optical Properties of 2,3,7,9-Polysubstituted Carbazole Derivatives. Experimental and Theoretical Studies. *Chem. Mater.* **2001**, 13, (8), 2528-2536.
36. Diaz, J. L.; Villacampa, B.; Lopez-Calahorra, F.; Velasco, D., Experimental and Theoretical Study of a New Class of Acceptor Group in Chromophores for Nonlinear Optics: 2-Substituted 4-Methylene-4*H*-oxazol-5-ones. *Chem. Mater.* **2002**, 14, (5), 2240-2251.
37. Do, J. Y.; Park, S. K.; Ju, J.-J.; Park, S.; Lee, M.-H., Electro-optic materials: hyperbranched chromophores attached linear polyimide and dendritic polyesters. *Polym. Adv. Technol.* **2005**, 16, (2-3), 221-226.
38. Ediger, M. D., Spatially heterogeneous dynamics in supercooled liquids. *Annual Review of Physical Chemistry* **2000**, 51, 99-128.
39. Facchetti, A.; Abbotto, A.; Beverina, L.; van der Boom, M. E.; Dutta, P.; Evmenenko, G.; Marks, T. J.; Pagani, G. A., Azinium-(p-Bridge)-Pyrrole NLO-Phores: Influence of Heterocycle Acceptors on Chromophoric and Self-Assembled

Thin-Film Properties. *Chem. Mater.* **2002**, 14, (12), 4996-5005.

40. Facchetti, A.; Abbotto, A.; Beverina, L.; van der Boom, M. E.; Dutta, P.; Evmenenko, G.; Pagani, G. A.; Marks, T. J., Layer-by-layer self-assembled pyrrole-based donor-acceptor chromophores as electro-optic materials. *Chem. Mater.* **2003**, 15, (5), 1064-1072.
41. Facchetti, A.; Annoni, E.; Beverina, L.; Morone, M.; Zhu, P.; Marks, T. J.; Pagani, G. A., Very large electro-optic responses in H-bonded heteroaromatic films grown by physical vapor deposition. *Nature Materials* **2004**, 3, (12), 910-917.
42. Facchetti, A.; van der Boom, M. E.; Abbotto, A.; Beverina, L.; Marks, T. J.; Pagani, G. A., Design and Preparation of Zwitterionic Organic Thin Films: Self-Assembled Siloxane-Based, Thiophene-Spaced N-Benzylpyridinium Dicyanomethanides as Nonlinear Optical Materials. *Langmuir* **2001**, 17, (19), 5939-5942.
43. Farrell, T.; Manning, A. R.; Murphy, T. C.; Meyer-Friedrichsen, T.; Heck, J.; Asselberghs, I.; Persoons, A., Structure-property dependence of the first hyperpolarizabilities of organometallic merocyanines based on the m-vinylcarbynediiron acceptor and ferrocene donor. *Eur. J. Inorg. Chem.* **2001**, (9), 2365-2375.
44. Frechet, J. M. J.; Hawker, C. J.; Gitsov, I.; Leon, J. W., Dendrimers and hyperbranched polymers: two families of three-dimensional macromolecules with similar but clearly distinct properties. *Journal of Macromolecular Science, Pure and Applied Chemistry* **1996**, A33, (10), 1399-1425.
45. Furniss, B. S.; Hannaford, A. J.; Smith, P. W. G.; Tatchell, A. R., *Vogel's Textbook of Practical Organic Chemistry*. fifth edition ed.; Addison Wesley Longman Singapore Pte Limited: 1989.
46. Furuta, P.; Frechet, J. M. J., Controlling solubility and modulating peripheral function in dendrimer encapsulated dyes. *Journal of the American Chemical Society* **2003**, 125, (43), 13173-13181.
47. Galvan-Gonzalez, A.; Belfield, K. D.; Stegeman, G. I.; Canva, M.; Marder, S. R.; Staub, K.; Levina, G.; Twieg, R. J., Photodegradation of selected p-conjugated electrooptic chromophores. *J. Appl. Phys.* **2003**, 94, (1), 756-763.
48. Galvan-Gonzalez, A.; Stegeman, G. I.; Jen, A. K. Y.; Wu, X.; Canva, M.; Kowalczyk, A. C.; Zhang, X. Q.; Lackritz, H. S.; Marder, S.; Thayumanavan, S.; Levina, G., Photostability of electro-optic polymers possessing chromophores with efficient amino donors and cyano-containing acceptors. *J. Opt. Soc. Am. B: Opt. Phys.* **2001**, 18, (12), 1846-1853.

49. Garin, J.; Orduna, J.; Andreu, R., Tetrathiafulvalene and 1,3-dithiole-based chromophores with second-order nonlinear optical properties. *Recent Research Developments in Organic Chemistry* **2001**, 5, (Pt. 1), 77-87.
50. Garin, J.; Orduna, J.; Ruperez, J. I.; Alcalá, R.; Villacampa, B.; Sanchez, C.; Martin, N.; Segura, J. L.; Gonzalez, M., Second-order nonlinear optical properties of tetrathiafulvalene-p-(thio)barbituric acid chromophores. *Tetrahedron Lett.* **1998**, 39, (21), 3577-3580.
51. Gonzalez, M.; Segura, J. L.; Seoane, C.; Martin, N.; Garin, J.; Orduna, J.; Alcalá, R.; Villacampa, B.; Hernandez, V.; Lopez Navarrete, J. T., Tetrathiafulvalene derivatives as NLO-phores: synthesis, electrochemistry, Raman spectroscopy, theoretical calculations, and NLO properties of novel TTF-derived donor-p-acceptor dyads. *J. Org. Chem.* **2001**, 66, (26), 8872-8882.
52. Gopalan, P.; Katz, H. E.; McGee, D. J.; Erben, C.; Zielinski, T.; Bousquet, D.; Muller, D.; Grazul, J.; Olsson, Y., Star-Shaped Azo-Based Dipolar Chromophores: Design, Synthesis, Matrix Compatibility, and Electro-optic Activity. *J. Am. Chem. Soc.* **2004**, 126, (6), 1741-1747.
53. Gubbelsmans, E.; Verbiest, T.; Picard, I.; Persoons, A.; Samyn, C., Poly(phenylquinoxalines) for second-order nonlinear optical applications. *Polymer* **2005**, 46, (6), 1784-1795.
54. Haller, M.; Luo, J.; Li, H.; Kim, T.-D.; Liao, Y.; Robinson, B. H.; Dalton, L. R.; Jen, A. K.-Y., A Novel Lattice-Hardening Process To Achieve Highly Efficient and Thermally Stable Nonlinear Optical Polymers. *Macromolecules* **2004**, 37, (3), 688-690.
55. Hammer, B.; Hansen, L. B.; No/rskov, J. K., Improved adsorption energetics within density-functional theory using revised Perdew-Burke-Ernzerhof functionals. *Physical Review B: Condensed Matter and Materials Physics* **1999**, 59, (11), 7413-7421.
56. Harper, A. W.; Sun, S.; Dalton, L. R.; Garner, S. M.; Chen, A.; Kalluri, S.; Steier, W. H.; Robinson, B. H., Translating microscopic optical nonlinearity into macroscopic optical nonlinearity: The role of chromophore-chromophore electrostatic interactions. *J. Opt. Soc. Am. B* **1998**, 15, (1), 329-337.
57. He, M.; Leslie, T. M.; Sinicropi, J. A., Synthesis of Chromophores with Extremely High Electro-optic Activity. 1. Thiophene-Bridge-Based Chromophores. *Chem. Mater.* **2002**, 14, (11), 4662-4668.
58. He, M.; Leslie, T. M.; Sinicropi, J. A.; Garner, S. M.; Reed, L. D., Synthesis

of Chromophores with Extremely High Electro-optic Activities. 2. Isophorone- and Combined Isophorone-Thiophene-Based Chromophores. *Chem. Mater.* **2002**, 14, (11), 4669-4675.

59. Huang, D.; Chen, B. Polymers having pendant nonlinear optical chromophores and electro-optic devices made from them. 2003-625371 2004132960, 20030723., 2004.

60. Huang, D.; Zhang, C.; Dalton, L. R.; Weber, W. P., Synthesis and Characterization of Main-Chain NLO Oligomers and Polymer that Contain 4-Dialkylamino-4'(alkylsulfonyl)azobenzene Chromophores. *J. Polym. Sci. Part A: Polym. Chem.* **2000**, 38, 546-559.

61. Janietz, S.; Bradley, D. D. C.; Grell, M.; Giebeler, C.; Inbasekaran, M.; Woo, E. P., Electrochemical determination of the ionization potential and electron affinity of poly(9,9-dioctylfluorene). *Applied Physics Letters* **1998**, 73, (17), 2453-2455.

62. Janowska, I.; Zakrzewski, J.; Nakatani, K.; Delaire, J. A.; Palusiak, M.; Walak, M.; Scholl, H., Ferrocenyl D-p-A chromophores containing 3-dicyanomethylidene-1-indanone and 1,3-bis(dicyanomethylidene)indane acceptor groups. *J. Organomet. Chem.* **2003**, 675, (1-2), 35-41.

63. Jen, A.; Neilsen, R.; Robinson, B.; Steier, W. H.; Dalton, L., Rational design of organic electro-optic materials. *Materials Research Society Symposium Proceedings* **2002**, 708, (Organic Optoelectronic Materials, Processing and Devices), 153-160.

64. Jen, A. K. Y.; Rao, V. P.; Wong, K. Y.; Drost, K. J., Functionalized thiophenes: second-order nonlinear optical materials. *Journal of the Chemical Society, Chemical Communications* **1993**, (1), 90-2.

65. Kang, H.; Zhu, P.; Yang, Y.; Facchetti, A.; Marks, T. J., Self-assembled electrooptic thin films with remarkably blue-shifted optical absorption based on an x-shaped chromophore. *Journal of the American Chemical Society* **2004**, 126, (49), 15974-15975.

66. Katti, K. V.; Raghuraman, K.; Pillarsetty, N.; Karra, S. R.; Gulotty, R. J.; Chartier, M. A.; Langhoff, C. A., First Examples of Azaphosphanes as Efficient Electron Donors in the Chemical Architecture of Thermally Stable New Nonlinear Optical Materials. *Chem. Mater.* **2002**, 14, (6), 2436-2438.

67. Kuo, W.-J.; Hsiue, G.-H.; Jeng, R.-J., Novel Guest-Host NLO Poly(ether imide) Based on a Two-Dimensional Carbazole Chromophore with Sulfonyl Acceptors. *Macromolecules* **2001**, 34, (7), 2373-2384.

68. Lemaure, V.; Steel, M.; Beljonne, D.; Bredas, J.-L.; Cornil, J., Photoinduced Charge Generation and Recombination Dynamics in Model Donor/Acceptor Pairs for Organic Solar Cell Applications: A Full Quantum-Chemical Treatment. *Journal of the American Chemical Society* **2005**, 127, (16), 6077-6086.
69. Liang, Z.; Yang, Z.; Sun, S.-S.; Wu, B.; Dalton, L. R.; Garner, S. M.; Kalluri, S.; Chen, A.; Steier, W. H., Processible and thermally stable heterocyclic polymers for second-order nonlinear optical studies. *Chem. Mater.* **1996**, 8, (11), 2681-2685.
70. Liao, Y.; Anderson, C. A.; Sullivan, P. A.; Akelaitis, A. J. P.; Robinson, B. H.; Dalton, L. R., Electro-Optical Properties of Polymers Containing Alternating Nonlinear Optical Chromophores and Bulky Spacers. *Chemistry of Materials* **2006**, 18, (4), 1062-1067.
71. Liao, Y.; Eichinger, B. E.; Firestone, K. A.; Haller, M.; Luo, J.; Kaminsky, W.; Benedict, J. B.; Reid, P. J.; Jen, A. K. Y.; Dalton, L. R.; Robinson, B. H., Systematic study of the structure-property relationship of a series of ferrocenyl nonlinear optical chromophores. *Journal of the American Chemical Society* **2005**, 127, (8), 2758-2766.
72. Liao, Y.; Sullivan, P. A.; Akelaitis, A., Extended-bridge Polyene-Aromatic hybrid, High Beta Chromophores In University of Washington: 2006.
73. Lindsey, C. P.; Patterson, G. D., Detailed comparison of the Williams-Watts and Cole-Davidson functions. *Journal of Chemical Physics* **1980**, 73, (7), 3348-57.
74. Liu, S.; Haller, M. A.; Hong, M.; Dalton, L. R.; Jang, S.-H.; Jen, A. K.-Y., Focused Microwave-Assisted Synthesis of 2,5-Dihydrofuran Derivatives as Electron Acceptors for Highly Efficient Nonlinear Optical Chromophores. *Adv. Mater.* **2003**, 15, (7-8), 603-607.
75. Lu, D.; Marten, B.; Cao, Y.; Ringnalda, M. N.; Friesner, R. A.; Goddard, W. A., III, Ab initio predictions of large hyperpolarizability push-pull polymers: Julolidinyl-n-isoxazolone and julolidinyl-n-N,N'-diethylthiobarbituric acid. *Chem. Phys. Lett.* **1995**, 242, (6), 543-7.
76. Lu, J.; Yin, J., Synthesis and characterization of photocrosslinkable, side-chain, second-order nonlinear optical poly(ester imide)s with great film-forming ability and long-term dipole orientation stability. *J. Polym. Sci., Part A: Polym. Chem.* **2002**, 41, (2), 303-312.
77. Luo, J.; Haller, M.; Li, H.; Kim, T.-D.; Jen, A. K.-Y., Highly efficient and thermally stable electro-optic polymer from a smartly controlled crosslinking process. *Adv. Mater.* **2003**, 15, (19), 1635-1638.

78. Luo, J.; Haller, M.; Li, H.; Tang, H.-Z.; Jen, A. K.-Y.; Jakka, K.; Chou, C.-H.; Shu, C.-F., A Side-Chain Dendronized Nonlinear Optical Polyimide with Large and Thermally Stable Electrooptic Activity. *Macromolecules* **2004**, 37, (2), 248-250.
79. Luo, J.; Haller, M.; Ma, H.; Liu, S.; Kim, T.-D.; Tian, Y.; Chen, B.; Jang, S.-H.; Dalton, L. R.; Jen, A. K.-Y., Nanoscale Architectural Control and Macromolecular Engineering of Nonlinear Optical Dendrimers and Polymers for Electro-Optics. *J. Phys Chem. B.* **2004**, 108, (25), 8523-8530.
80. Luo, J.; Liu, S.; Haller, M.; Liu, L.; Ma, H.; Jen, A. K.-Y., Design, synthesis, and properties of highly efficient side-chain dendronized nonlinear optical polymers for electro-optics. *Adv. Mater.* **2002**, 14, (23), 1763-1768.
81. Luo, J.; Ma, H.; Haller, M.; Jen, A. K.-Y.; Barto, R. R., Large electro-optic activity and low optical loss derived from a highly fluorinated dendritic nonlinear optical chromophore. *Chem. Commun.* **2002**, (8), 888-889.
82. Ma, H.; Chen, B.; Sassa, T.; Dalton, L. R.; Jen, A. K.-Y., Highly Efficient and Thermally Stable Nonlinear Optical Dendrimer for Electrooptics. *J. Am. Chem. Soc.* **2001**, 123, (5), 986-987.
83. Ma, H.; Jen, A. K.-Y.; Wu, J.; Wu, X.; Liu, S., A Convenient Modular Approach of Functionalizing Aromatic Polyuquinolines for Electrooptic Devices. *Chem. Mater.* **1999**, 11, (8), 2218-2225.
84. Ma, H.; Liu, S.; Luo, J.; Suresh, S.; Liu, L.; Kang, S. H.; Haller, M.; Sassa, T.; Dalton, L. R.; Jen, A. K.-Y., Highly efficient and thermally stable electro-optical dendrimers for photonics. *Adv. Funct. Mater.* **2002**, 12, (9), 565-574.
85. Ma, H.; Luo, J.; Kang, S. H.; Wong, S.; Kang, J. W.; Jen, A. K. Y.; Barto, R.; Frank, C. W., Highly fluorinated and crosslinkable dendritic polymer for photonic applications. *Macromolecular Rapid Communications* **2004**, 25, (19), 1667-1673.
86. Ma, H.; Wu, J.; Herguth, P.; Chen, B.; Jen Alex, K.-Y., A Novel Class of High-Performance Perfluorocyclobutane-Containing Polymers for Second-Order Nonlinear Optics. *Chem. Mater.* **2000**, 12, (5), 1187-1189.
87. Mao, S. S. H.; Ra, Y.; Guo, L.; Zhang, C.; Dalton, L. R.; Chen, A.; Garner, S. M.; Steier, W. H., Progress toward Device-Quality Second-Order Nonlinear Optical Materials. 1. Influence of Composition and Processing Conditions on Nonlinearity, Temporal Stability, and Optical Loss. *Chem. Mater.* **1998**, 10, (1), 146-155.
88. Marder, S. R.; Cheng, L.-T.; Tiemann, B. G.; Friedli, A. C.; Blanchard-Desce, M.; Perry, J. W.; Skindhoj, J., Large First Hyperpolarizabilities in Push-Pull

Polyenes by Tuning of the Bond Length Alternation and Aromaticity. *Science* **1994**, 263, (5146), 511-514.

89. Marder, S. R.; Perry, J. W.; Schaefer, W. P., Synthesis of Organic Salts with large Second-Order Optical Nonlinearities. *Science* **1989**, 245, (4918), 626-628.

90. Melikian, G.; Rouessac, F. P.; Alexandre, C., Synthesis of substituted dicyanomethylendihydrofurans. *Synth. Commun.* **1995**, 25, (19), 3045-51.

91. Michelotti, F.; Nicolao, G.; Tesi, F.; Bertolotti, M., On the measurement of the electro-optic properties of poled side-chain copolymer films with a modified Teng-Man technique. *Chemical Physics* **1999**, 245, (1-3), 311-326.

92. Michelotti, F.; Toussaere, E.; Levenson, R.; Liang, J.; Zyss, J., Real-time pole and probe assessment of orientational processes in electro-optic polymers. *Applied Physics Letters* **1995**, 67, (19), 2765-7.

93. Michelotti, F.; Toussaere, E.; Levenson, R.; Liang, J.; Zyss, J., Study of the orientational relaxation dynamics in a nonlinear optical copolymer by means of a pole and probe technique. *Journal of Applied Physics* **1996**, 80, (3), 1773-1778.

94. Miyashita, M.; Yoshikoshi, A.; Grieco, P. A., Pyridinium p-toluenesulfonate. A mild and efficient catalyst for the tetrahydropyranylation of alcohols. *Journal of Organic Chemistry* **1977**, 42, (23), 3772-4.

95. Moore, A. J.; Chesney, A.; Bryce, M. R.; Batsanov, A. S.; Kelly, J. F.; Howard, J. A. K.; Perepichka, I. F.; Perepichka, D. F.; Meshulam, G.; Berkovic, G.; Kotler, Z.; Mazor, R.; Khodorkovsky, V., Synthesis, structures and nonlinear optical properties of novel D-p-A chromophores: intramolecular charge transfer from 1,3-dithiole or ferrocene moieties to polynitrofluorene or dicyanomethylene moieties through conjugated linkers. *Eur. J. Org. Chem.* **2001**, (14), 2671-2687.

96. Moylan, C. R.; Ermer, S.; Lovejoy, S. M.; McComb, I. H.; Leung, D. S.; Wortmann, R.; Krdmer, P.; Twieg, R. J., (Dicyanomethylene)pyran Derivatives with C_{2v} Symmetry: An Unusual Class of Nonlinear Optical Chromophores. *J. Am. Chem. Soc.* **1996**, 118, (51), 12950-12955.

97. Nguyen, T. T.; Salle, M.; Delaunay, J.; Riou, A.; Richomme, P.; Raimundo, J. M.; Gorgues, A.; Ledoux, I.; Dhenaut, C.; Zyss, J.; Orduna, J.; Garin, J., Functionalized polyolefinic nonlinear optic chromophores incorporating the 1,3-dithiol-2-ylidene moiety as the electron-donating part. *J. Mater. Chem.* **1998**, 8, (5), 1185-1192.

98. Nielsen, R. D.; Rommel, H. L.; Robinson, B. H., Simulation of the Loading Parameter in Organic Nonlinear Optical Materials. *J. Phys. Chem. B* **2004**, 108, (25),

8659-8667.

99. Oudar, J., Optical nonlinearities of conjugated molecules. Stilbene derivatives and highly polar aromatic compounds. *J. Chem. Phys.* **1977**, 67, (2), 446-657.
100. Oudar, J. L.; Chemla, D. S., Hyperpolarizabilities of the nitroanilines and their relations to the excited state dipole moment. *J. Chem. Phys.* **1977**, 66, (6), 2664-2668.
101. Pan, F.; Knoepfle, G.; Bosshard, C.; Follonier, S.; Spreiter, R.; Wong, M. S.; Guenter, P., Electro-optic properties of the organic salt 4-N,N-dimethylamino-4',N'-methyl-stilbazolium tosylate. *Appl. Phys. Lett.* **1996**, 69, (1), 13-15.
102. Pan, Q.; Fang, C.; Zhang, Z.; Qin, Z.; Li, F.; Gu, Q.; Wu, X.; Yu, J., Synthesis and characterization of nonlinear optical chromophores containing a-cyan with thermal stability. *Opt. Mater.* **2003**, 22, (1), 45-49.
103. Park, K. H.; Yeon, K. M.; Lee, M. Y.; Lee, S. D.; Shin, D. H.; Lee, C. J.; Kim, N., Synthesis and nonlinear optical properties of PMMA copolymers having novel benzoxazole chromophores attached with various electron-withdrawing groups. *Polymer* **1998**, 39, (26), 7061-7066.
104. Pereverzev, Y. V.; Prezhdo, O. V.; Dalton, L. R., Structural origin of the enhanced electro-optic response of dendrimer systems. *Chem. Phys. Lett.* **2003**, 373, (1,2), 207-212.
105. Prasad, P. N.; Williams, D. J., *Introduction to Nonlinear Optical Effects in Molecules and Polymers*. John Wiley and Sons: New York, 1991.
106. Rabiei, P.; Steier, W. H.; Zhang, C.; Dalton, L. R., Polymer Micro-Ring Filter and Modulators. *J. Lightwave, Technol.* **2002**, 20, (11), 1968-1975.
107. Raimundo, J.-M.; Blanchard, P.; Frere, P.; Mercier, N.; Ledoux-Rack, I.; Hierle, R.; Roncali, J., Push-pull Chromophores based on 2,2'-bi(3,4-ethylenedioxythiophene) (BEDOT) pi-conjugating spacer. *Tetrahedron Lett.* **2001**, 42, 1507-1510.
108. Raimundo, J.-M.; Blanchard, P.; Gallegro-Planas, N.; Mercier, N.; Ledoux-Rack, I.; Hierle, R.; Roncali, J., Design and Synthesis of Push-Pull Chromophores for Second-Order Nonlinear Optics Derived from Rigidified Thiophene-Based pi-Conjugating Spacers. *J. Org. Chem.* **2002**, 67, (1), 205-218.
109. Rao, V. P.; Jen, A. K. Y.; Chandrasekhar, J.; Namboothiri, I. N. N.; Rathna, A., The Important Role of Heteroaromatics in the Design of Efficient Second-Order

- Nonlinear Optical Molecules: Theoretical Investigation on Push-Pull Heteroaromatic Stilbenes. *Journal of the American Chemical Society* **1996**, 118, (49), 12443-12448.
110. Rashid, A. N.; Erny, C.; Gunter, P., Hydrogen-bond-directed orientation in nonlinear optical thin films. *Adv. Mater.* **2003**, 15, (23), 2024-2027.
111. Ray, P. C.; Leszczynski, J., Nonlinear optical properties of highly conjugated push-pull porphyrin aggregates: Role of intermolecular interaction. *Chemical Physics Letters* **2006**, 419, (4-6), 578-583.
112. Robinson, B. H.; Dalton, L. R., Monte Carlo statistical mechanical simulations of the competition of intermolecular electrostatic and poling-field interactions in defining macroscopic electro-optic activity for organic chromophore/polymer materials. *J. Phys. Chem. A* **2000**, 104, (20), 4785-4795.
113. Saadeh, H.; Wang, L.; Yu, L., A New Synthetic Approach to Novel Polymers Exhibiting Large Electrooptic Coefficients and High Thermal Stability. *Macromolecules* **2000**, 33, (5), 1570-1576.
114. Schildkraut, J. S., Determination of the electrooptic coefficient of a poled polymer film. *Applied Optics* **1990**, 29, (19), 2839-41.
115. Schwartz, H.; Mazor, R.; Khodorkovsky, V.; Shapiro, L.; Klug, J. T.; Kovalev, E.; Meshulam, G.; Berkovic, G.; Kotler, Z.; Efrima, S., Langmuir and Langmuir-Blodgett Films of NLO Active 2-(p-N-Alkyl-N-methylamino)benzylidene-1,3-indandione - p/A Curves, UV-Vis Spectra and SHG behavior. *J. Phys. Chem.* **2001**, 105, (25), 5914-5921.
116. Shi, Y.; Zhang, C.; Zhang, H.; Bechtel, J. H.; Dalton, L. R.; Robinson, B.; Steier, W. H., Low (Sub-1-Volt) Halfwave Voltage Polymeric Electro-optic Modulators Achieved by Controlling Chromophore Shape. *Science* **2000**, 288, 119-122.
117. Shuto, Y.; Amano, M., Reflection measurement technique of electro-optic coefficients in lithium niobate crystals and poled polymer films. *Journal of Applied Physics* **1995**, 77, (9), 4632-8.
118. Sim, F.; Chin, S.; Dupuis, M.; Rice, J. E., Electron correlation effects in hyperpolarizabilities of p-nitroaniline. *Journal of Physical Chemistry* **1993**, 97, (6), 1158-63.
119. Sinyukov, A. M.; Leahy, M. R.; Hayden, L. M.; Haller, M.; Luo, J.; Jen, A. K. Y.; Dalton, L. R., Resonance enhanced THz generation in electro-optic polymers near the absorption maximum. *Applied Physics Letters* **2004**, 85, (24), 5827-5829.

120. Stegeman, G. I.; Van-Gonzales, A. G.; Canva, M.; Twieg, R.; Kowalczyk, A. C.; Zhang, X. Q.; Lackritz, H. S.; Marder, S.; Thayumanavan, S.; Chan, K. P.; Jen, A. K. Y.; Wu, X., Photodegradation of various electro-optic polymer families. *MCLC S&T, Section B: Nonlinear Optics* **2000**, *25*, (1-4), 57-66.
121. Stenger-Smith, J. D.; Zarras, P.; Hollins, R. A.; Chafin, A. P.; Merwin, L. H.; Yee, R.; Lindsay, G. A.; Herman, W. N.; Gratz, R. F.; Nickel, E. G., Main-Chain Syndioregic Nonlinear Optical Polymers. II. Extended Pi Conjugated and Improved Thermal Properties. *J. Pol. Sci. Part A: Polym. Chem.* **2000**, *38*, (2824-2839).
122. Sullivan, P. A. Chapter 2: Theory Guided Design and Molecular Engineering of Organic Materials for Enhanced 2nd-Order Nonlinear Optical Properties University of Washington, Seattle, 2006.
123. Sullivan, P. A.; Akelaitis, A. J. P.; Hammond, S.; Sinnes, J.; Dalton, L., Synthetic Approaches to Nanoscale Engineering of Organic Materials for Photonics Applications. *Accounts of Chemical Research* **2006**, in preperation, invited paper.
124. Sullivan, P. A.; Akelaitis, A. J. P.; K., L. S.; McGrew, G.; Lee, S. K.; Choi, D. H.; Dalton, L. R., Novel Dendritic Chromophores for Electro-optics: Influence of Binding Mode and Attachment Flexibility on Electro-Optic Behavior. *Chem. Mater.* **2006**, *18*, 344-351.
125. Sun, S.-S.; Zhang, C.; Dalton, L. R.; Garner, S. M.; Chen, A.; Steier, W. H., 1,3-Bis(dicyanomethylidene)indane-Based Second-Order NLO Materials. *Chem. Mater.* **1996**, *8*, (11), 2539-2541.
126. Suresh, S.; Zengin, H.; Spraul, B. K.; Sassa, T.; Wada, T.; Smith, D. W., Synthesis and hyperpolarizabilities of high temperature triarylamine-polyene chromophores. *Tetrahedron Lett.* **2005**, *46*, (22), 3913-3916.
127. Teng, C. C.; Man, H. T., Simple reflection technique for measuring the electro-optic coefficient of poling polymers. *Applied Physics Letters* **1990**, *56*, (18), 1734-6.
128. Tsutsumi, N.; Morishima, M.; Sakai, W., Nonlinear Optical (NLO) Polymers. 3. NLO Polyimide with Dipole Moments Aligned Transverse to the Imide Linkage. *Macromolecules* **1998**, *31*, (22), 7764-7769.
129. Van den Broeck, K.; Verbiest, T.; Degryse, J.; Van Beylen, M.; Persoons, A.; Samyn, C., High glass transition chromophore functionalized polyimides for second-order nonlinear optical applications. *Polymer* **2001**, *42*, (8), 3315-3322.
130. van der Boom, M. E.; Zhu, P.; Evmenenko, G.; Malinsky, J. E.; Lin, W.;

Dutta, P.; Marks, T. J., Nanoscale Consecutive Self-Assembly of Thin-Film Molecular Materials for Electrooptic Switching. Chemical Streamlining and Ultrahigh Response Chromophores. *Langmuir* **2002**, 18, (9), 3704-3707.

131. Villemin, D.; Liao, L., Rapid and efficient synthesis of 2-[3-cyano-4-(2-arylidene)-5,5-dimethyl-5H-furan-2-ylidene]-malononitrile under focused microwave irradiation. *Synth. Commun.* **2001**, 31, (11), 1771-1780.

132. Wang, C. W.; Dalton, L. R., A facile Synthesis of Thienylmethylphosphonates: direct conversion from thiophenes. *Tetrahedron Lett.* **2000**, 41, 617-620.

133. Wang, F.; Harper, A. W.; Lee, M. S.; Dalton, L. R.; Zhang, H.; Chen, A.; Steier, W. H.; Marder, S. R., Progress toward Device-Quality Second-Order NLO Materials: 3. Electrooptic Activity of Polymers Containing E,E,E-[4-(N,N-Dialkylamino)-phenyl]pentadienyldiene-3-phenyl-5-isoxazolone Chromophores. *Chem. Mater.* **1999**, 11, (9), 2285-2288.

134. Wong, S.; Ma, H.; Jen, A. K.-Y.; Barto, R.; Frank, C. W., Highly Fluorinated Trifluorovinyl Aryl Ether Monomers and Perfluorocyclobutane Aromatic Ether Polymers for Optical Waveguide Applications. *Macromolecules* **2003**, 36, (21), 8001-8007.

135. Yang, Z.; Aravazhi, S.; Schneider, A.; Seiler, P.; Jazbinsek, M.; Guenter, P., Synthesis and crystal growth of stilbazolium derivatives for second-order nonlinear optics. *Adv. Funct. Mater.* **2005**, 15, (7), 1072-1076.

136. Yitzchaik, S.; Di Bella, S.; Lundquist, P. M.; Wong, G. K.; Marks, T. J., Anomalous Second-Order Nonlinear Optical Response of In-Plane Poled Glassy Polymers. Spectroscopic and Theoretical Support for the Importance of Charged Chromophore Aggregates. *J. Am. Chem. Soc.* **1997**, 119, (13), 2995-3002.

137. Yokoyama, S.; Nakahama, T.; Otomo, A.; Mashiko, S., Intermolecular Coupling Enhancement of the Molecular Hyperpolarizability in Multichromophoric Dipolar Dendrons. *J. Am. Chem. Soc.* **2000**, 122, 3174-3181.

138. Zhang, C.; Wang, C. W.; Dalton, L. R.; Zhang, H.; Steier, W. H., Progress toward Device-Quality Second-Order Nonlinear Optical Materials. 4. A Trilink High μ -Beta NLO Chromophore in Thermoset Polyurethane: A "Guest-Host" Approach to Larger Electrooptic Coefficients. *Macromolecules* **2001**, 34, 253-261.

139. Zhang, S.; Zhou, G.; Yang, Z.; Qin, A.; Wang, P.; Ye, C., Design and synthesis of low dipole moment chromophores: 2,6-disubstituted cycloheptimidazoles. *Synth. Met.* **2003**, 137, (1-3), 1545-1546.

140. Zhang, T.-G.; Zhao, Y.; Asselberghs, I.; Persoons, A.; Clays, K.; Therien, M. J., Design, Synthesis, Linear, and Nonlinear Optical Properties of Conjugated (Porphinato)zinc(II)-Based Donor-Acceptor Chromophores Featuring Nitrothiophenyl and Nitrooligothiophenyl Electron-Accepting Moieties. *Journal of the American Chemical Society* **2005**, 127, (27), 9710-9720.
141. Zheng, Q.; Yao, Z.; Cheng, J.; Shen, Y.; Lu, Z., Synthesis and nonlinear optical properties of p-(dimethylamino)benzylidene dyes containing different acceptors. *Chem. Lett.* **2000**, (12), 1426-1427.

VITA

Philip A. Sullivan was born in Austin Texas in 1976. He then moved with his family to Marion, Virginia, where he attended high school. He earned the degree of Bachelor of Science in chemistry at Montana State University, Bozeman (2001), under the direction of Prof. Cynthia K. McClure. His undergraduate research focused on new synthetic methodology for the preparation of compounds with antibiotic activity. His undergraduate thesis was entitled: "Pentacovalent Oxaphospholene Reactivity and Selectivity" Philip Sullivan began his doctoral research in the area of organic photonic materials synthesis and characterization in 2002 at the University of Washington, Seattle, under the direction of Professor Larry R. Dalton.